E C M I

Anisotropic Diffusion in Image Processing

Joachim Weickert

B.G. Teubner Stuttgart

Anisotropic Diffusion in Image Processing

Joachim Weickert

Department of Computer Science
University of Copenhagen
Copenhagen, Denmark

Dr. rer. nat. Joachim Weickert

Born in 1965 in Ludwigshafen/Germany. Studies in mathematics, physics and computer science at the University of Kaiserslautern. 1987 B.Sc. in physics and industrial mathematics. 1991 M.Sc. in industrial mathematics. 1996 Ph.D. in mathematics. Postdoctoral researcher at the Image Sciences Institute at Utrecht University from 2/96 to 3/97. Since then visiting assistant research professor at the Department of Computer Science, Copenhagen University.

The cover image shows a thresholded nonwoven fabric image which was processed by applying a coherence-enhancing anisotropic diffusion filter (see Section 5.2 for more details). The goal was to visualize the quality relevant adjacent fibre structures, so-called stripes. The displayed equations describe the basic structure of nonlinear diffusion filtering in the continuous, semidiscrete, and fully discrete setting. Their theoretical foundations are treated in Chapters 2–4.

To my parents Gerda and Norbert

Preface

Partial differential equations (PDEs) have led to an entire new field in image processing and computer vision. Hundreds of publications have appeared in the last decade, and PDE-based methods have played a central role at several conferences and workshops.

The success of these techniques is not really surprising, since PDEs have proved their usefulness in areas such as physics and engineering sciences for a very long time. In image processing and computer vision, they offer several advantages:

- Deep mathematical results with respect to well-posedness are available, such that stable algorithms can be found. PDE-based methods are one of the mathematically best-founded techniques in image processing.

- They allow a reinterpretation of several classical methods under a novel unifying framework. This includes many well-known techniques such as Gaussian convolution, median filtering, dilation or erosion.

- This understanding has also led to the discovery of new methods. They can offer more invariances than classical techniques, or describe novel ways of shape simplification, structure preserving filtering, and enhancement of coherent line-like structures.

- The PDE formulation is genuinely continuous. Thus, their approximations aim to be independent of the underlying grid and may reveal good rotational invariance.

PDE-based image processing techniques are mainly used for smoothing and restoration purposes. Many evolution equations for *restoring* images can be derived as gradient descent methods for minimizing a suitable energy functional, and the restored image is given by the steady-state of this process. Typical PDE techniques for image *smoothing* regard the original image as initial state of a parabolic (diffusion-like) process, and extract filtered versions from its temporal evolution. The whole evolution can be regarded as a so-called *scale-space*, an embedding of the original image into a family of subsequently simpler, more global representations of it. Since this introduces a hierarchy into the image structures, one can use a scale-space representation for extracting semantically important information.

One of the two goals of this book is to give an overview of the state-of-the-art of PDE-based methods for image enhancement and smoothing. Emphasis is put on a

unified description of the underlying ideas, theoretical results, numerical approximations, generalizations and applications, but also historical remarks and pointers to open questions can be found. Although being concise, this part covers a broad spectrum: it includes for instance an early Japanese scale-space axiomatic, the Mumford–Shah functional for image segmentation, continuous-scale morphology, active contour models and shock filters. Many references are given which point the reader to useful original literature for a task at hand.

The second goal of this book is to present an in-depth treatment of an interesting class of parabolic equations which may bridge the gap between scale-space and restoration ideas: nonlinear diffusion filters. Methods of this type have been proposed for the first time by Perona and Malik in 1987 [326]. In order to smooth an image and to simultaneously enhance important features such as edges, they apply a diffusion process whose diffusivity is steered by derivatives of the evolving image. These filters are difficult to analyse mathematically, as they may act locally like a backward diffusion process. This gives rise to well-posedness questions. On the other hand, nonlinear diffusion filters are frequently applied with very impressive results; so there appears the need for a theoretical foundation.

We shall develop results in this direction by investigating a general class of nonlinear diffusion processes. This class comprises linear diffusion filters as well as spatial regularizations of the Perona–Malik process, but it also allows processes which replace the scalar diffusivity by a diffusion tensor. Thus, the diffusive flux does not have to be parallel to the grey value gradient: the filters may become anisotropic. Anisotropic diffusion filters can outperform isotropic ones with respect to certain applications such as denoising of highly degraded edges or enhancing coherent flow-like images by closing interrupted one-dimensional structures. In order to establish well-posedness and scale-space properties for this class, we shall investigate existence, uniqueness, stability, maximum–minimum principles, Lyapunov functionals, and invariances. The proofs present mathematical results from the nonlinear analysis of partial differential equations.

Since digital images are always sampled on a pixel grid, it is necessary to know if the results for the continuous framework carry over to the practically relevant discrete setting. These questions are an important topic of the present book as well. A general characterization of semidiscrete and fully discrete filters, which reveal similar properties as their continuous diffusion counterparts, is presented. It leads to a semidiscrete and fully discrete scale-space theory for nonlinear diffusion processes. Mathematically, this comes down to the study of nonlinear systems of ordinary differential equations and the theory of nonnegative matrices.

Organization of the book. Image processing and computer vision are interdisciplinary areas, where researchers, practitioners and students may have a very different scientific background and differing intentions. As a consequence, I have tried to keep this book as self-contained as possible, and to include various aspects

such that it should contain interesting material for many readers. The prerequisites are kept to a minimum and can be found in standard textbooks on image processing [163], matrix analysis [407], functional analysis [9, 58, 7], ordinary differential equations [56, 412], partial differential equations [185] and their numerical aspects [293, 286]. The book is organized as follows:

Chapter 1 surveys the fundamental ideas behind PDE-based smoothing and restoration methods. This general overview sketches their theoretical properties, numerical methods, applications and generalizations. The discussed methods include linear and nonlinear diffusion filtering, coupled diffusion–reaction methods, PDE analogues of classical morphological processes, Euclidean and affine invariant curve evolutions, and total variation methods.

The subsequent three chapters explore a theoretical framework for anisotropic diffusion filtering. Chapter 2 presents a general model for the continuous setting where the diffusion tensor depends on the structure tensor (interest operator, second-moment matrix), a generalization of the Gaussian-smoothed gradient allowing a more sophisticated description of local image structure. Existence and uniqueness are discussed, and stability and an extremum principle are proved. Scale-space properties are investigated with respect to invariances and information-reducing qualities resulting from associated Lyapunov functionals.

Chapter 3 establishes conditions under which comparable well-posedness and scale-space results can be proved for the semidiscrete framework. This case takes into account the spatial discretization which is characteristic for digital images, but it keeps the scale-space idea of using a continuous scale parameter. It leads to nonlinear systems of ordinary differential equations. We shall investigate under which conditions it is possible to get consistent approximations of the continuous anisotropic filter class which satisfy the abovementioned requirements.

In practice, scale-spaces can only be calculated for a finite number of scales, though. This corresponds to the fully discrete case which is treated in Chapter 4. The investigated discrete filter class comes down to solving linear systems of equations which may arise from semi-implicit time discretizations of the semidiscrete filters. We shall see that many numerical schemes share typical features with their semidiscrete counterparts, for instance well-posedness results, extremum principles, Lyapunov functionals, and convergence to a constant steady-state. This chapter also shows how one can design efficient numerical methods which are in accordance with the fully discrete scale-space framework and which are based on an additive operator splitting (AOS).

Chapter 5 is devoted to practical topics such as filter design, examples and applications of anisotropic diffusion filtering. Specific models are proposed which are tailored towards smoothing with edge enhancement and multiscale enhancement of coherent structures. Their qualities are illustrated using images arising from computer aided quality control and medical applications, but also fingerprint im-

ages and impressionistic paintings shall be processed. The results are juxtaposed to related methods from Chapter 1.

Finally, Chapter 6 concludes the book by giving a summary and discussing possible future perspectives for nonlinear diffusion filtering.

Copenhagen, October 1997   Joachim Weickert

Contents

Chapter 1

Image smoothing and restoration by PDEs

PDE-based methods appear in a large variety of image processing and computer vision areas ranging from shape-from-shading and histogramme modification to optic flow and stereo vision.

This chapter reviews their main application, namely the smoothing and restoration of images. It is written in an informal style and refers to a large amount of original literature, where proofs and full mathematical details can be found.

The goal is to make the reader sensitive to the similarities, differences, advantages and shortcomings of these techniques, and to point out the main results and open problems in this rapidly evolving area.

For each class of methods the basic ideas are explained and their theoretical background, numerical aspects, generalizations, and applications are discussed. Many of these ideas are borrowed from physical phenomena such as wave propagation or transport of heat and mass. Nevertheless, also gas dynamics, crack propagation, grassfire flow, the study of salinity profiles in oceanography, or mechanisms of the retina and the brain are closely related to some of these approaches. Although a detailed discussion of these connections would be far beyond the scope of this work, they are mentioned wherever they appear, in order to allow the interested reader to pursue these ideas. Also many historical notes are added.

The outline of this chapter is as follows: We start with reviewing the physical ideas behind diffusion processes. This helps us to better understand the next sections which are concerned with the properties of linear and nonlinear diffusion filters in image processing. The subsequent study of image enhancement methods of diffusion–reaction type relates diffusion filters to variational image restoration techniques. After that we investigate morphological filters, a topic which looks at first glance fairly different to the diffusion approach. Nevertheless, it reveals some interesting relations when it is interpreted within a PDE framework. This becomes

especially evident when considering curvature-based morphological PDEs. Finally we shall discuss total variation image restoration techniques which permit discontinuous solutions. The last section summarizes the advantages and shortcomings of the main methods and gives an outline of the questions we are concerned with in the subsequent chapters.

1.1 Physical background of diffusion processes

Most people have an intuitive impression of diffusion as a physical process that equilibrates concentration differences without creating or destroying mass. This physical observation can be easily cast in a mathematical formulation.

The equilibration property is expressed by *Fick's law:*

$$j = -D \cdot \nabla u. \tag{1.1}$$

This equation states that a concentration gradient ∇u causes a flux j which aims to compensate for this gradient. The relation between ∇u and j is described by the *diffusion tensor D*, a positive definite symmetric matrix. The case where j and ∇u are parallel is called *isotropic.* Then we may replace the diffusion tensor by a positive scalar-valued *diffusivity g*. In the general *anisotropic* case, j and ∇u are not parallel.

The observation that diffusion does only transport mass without destroying it or creating new mass is expressed by the *continuity equation*

$$\partial_t u = -\mathrm{div}\ j \tag{1.2}$$

where t denotes the time.

If we plug in Fick's law into the continuity equation we end up with the *diffusion equation*

$$\partial_t u = \mathrm{div}\,(D \cdot \nabla u). \tag{1.3}$$

This equation appears in many physical transport processes. In the context of heat transfer it is called *heat equation.* In image processing we may identify the concentration with the grey value at a certain location. If the diffusion tensor is constant over the whole image domain, one speaks of *homogeneous* diffusion, and a space-dependent filtering is called *inhomogeneous.* Often the diffusion tensor is a function of the differential structure of the evolving image itself. Such a feedback leads to *nonlinear diffusion filters.* Diffusion which does not depend on the evolving image is called *linear.*

Sometimes the computer vision literature deviates from the preceding notations: It can happen that homogeneous filtering is named isotropic, and inhomogeneous blurring is called anisotropic, even if it uses a scalar-valued diffusivity instead of a diffusion tensor.

1.2 Linear diffusion filtering

The simplest and best investigated PDE method for smoothing images is to apply a linear diffusion process. We shall focus on the relation between linear diffusion filtering and the convolution with a Gaussian, analyse its smoothing properties for the image as well as its derivatives, and review the fundamental properties of the Gaussian scale-space induced by linear diffusion filtering. Afterwards a survey on discrete aspects is given and applications and limitations of the linear diffusion paradigm are discussed. The section is concluded by sketching two linear generalizations which can incorporate a-priori knowledge: affine Gaussian scale-space and directed diffusion processes.

1.2.1 Relations to Gaussian smoothing

Gaussian smoothing

Let a grey-scale image f be represented by a real-valued mapping $f \in L^1(\mathbb{R}^2)$. A widely-used way to smooth f is by calculating the convolution

$$(K_\sigma * f)(x) := \int_{\mathbb{R}^2} K_\sigma(x-y) \, f(y) \, dy \tag{1.4}$$

where K_σ denotes the two-dimensional Gaussian of width (standard deviation) $\sigma > 0$:

$$K_\sigma(x) := \frac{1}{2\pi\sigma^2} \cdot \exp\left(-\frac{|x|^2}{2\sigma^2}\right). \tag{1.5}$$

There are several reasons for the excellent smoothing properties of this method: First we observe that since $K_\sigma \in C^\infty(\mathbb{R}^2)$ we get $K_\sigma * f \in C^\infty(\mathbb{R}^2)$, even if f is only absolutely integrable.

Next, let us investigate the behaviour in the frequency domain. When defining the Fourier transformation $\mathcal{F}$ by

$$(\mathcal{F}f)(\omega) := \int_{\mathbb{R}^2} f(x) \, \exp(-i\langle \omega, x \rangle) \, dx \tag{1.6}$$

we obtain by the convolution theorem that

$$(\mathcal{F}(K_\sigma * f))(\omega) = (\mathcal{F}K_\sigma)(\omega) \cdot (\mathcal{F}f)(\omega). \tag{1.7}$$

Since the Fourier transform of a Gaussian is again Gaussian-shaped,

$$(\mathcal{F}K_\sigma)(\omega) = \exp\left(-\frac{|\omega|^2}{2/\sigma^2}\right), \tag{1.8}$$

we observe that (1.4) is a low-pass filter that attenuates high frequencies in a monotone way.

Interestingly, the smoothing behaviour can also be understood in the context of a PDE interpretation.

Equivalence to linear diffusion filtering

It is a classical result (cf. e.g. [331, pp. 267–271] and [185, pp. 43–56]) that for any bounded $f \in C(\mathbb{R}^2)$ the linear diffusion process

$$\partial_t u \;=\; \Delta u, \tag{1.9}$$
$$u(x,0) \;=\; f(x) \tag{1.10}$$

possesses the solution

$$u(x,t) = \begin{cases} f(x) & (t=0) \\ (K_{\sqrt{2t}} * f)(x) & (t>0). \end{cases} \tag{1.11}$$

This solution is unique, provided we restrict ourselves to functions satisfying

$$|u(x,t)| \;\leq\; M \cdot \exp\left(a|x|^2\right) \qquad (M, a > 0). \tag{1.12}$$

It depends continuously on the initial image f with respect to $\|.\|_{L^\infty(\mathbb{R}^2)}$, and it fulfils the maximum–minimum principle

$$\inf_{\mathbb{R}^2} f \;\leq\; u(x,t) \;\leq\; \sup_{\mathbb{R}^2} f \quad \text{on} \quad \mathbb{R}^2 \times [0,\infty). \tag{1.13}$$

From (1.11) we observe that the time t is related to the spatial width $\sigma = \sqrt{2t}$ of the Gaussian. Hence, smoothing structures of order σ requires to stop the diffusion process at time

$$T = \tfrac{1}{2}\sigma^2. \tag{1.14}$$

Figure 5.2 (b) and 5.3 (c) in Chapter 5 illustrate the effect of linear diffusion filtering.

Gaussian derivatives

In order to understand the structure of an image we have to analyse grey value fluctuations within a neighbourhood of each image point, that is to say, we need information about its derivatives. However, differentiation is ill-posed[1], as small perturbations in the original image can lead to arbitrarily large fluctuations in the derivatives. Hence, the need for regularization methods arises. A thorough

---

[1]A problem is called well-posed, if it has a unique solution which depends continuously on the input data and parameters. If one of these conditions is violated, it is called ill-posed.

treatment of this mathematical theory can be found in the books of Tikhonov and Arsenin [402], Louis [266] and Engl et al. [128].

One possibility to regularize is to convolve the image with a Gaussian prior to differentiation [404]. By the equality

$$\partial_{x_1}^n \partial_{x_2}^m (K_\sigma * f) \;=\; K_\sigma * (\partial_{x_1}^n \partial_{x_2}^m f) \;=\; (\partial_{x_1}^n \partial_{x_2}^m K_\sigma) * f \qquad (1.15)$$

for sufficiently smooth f, we observe that all derivatives undergo the same Gaussian smoothing process as the image itself and this process is equivalent to convolving the image with derivatives of a Gaussian.

Replacing derivatives by these *Gaussian derivatives* has a strong regularizing effect. This property has been used to stabilize ill-posed problems like deblurring images by solving the heat equation backwards in time[2] [141, 177]. Moreover, Gaussian derivatives can be combined to so-called *differential invariants*, expressions that are invariant under transformations such as rotations, for instance $|\nabla K_\sigma * u|$ or $\Delta K_\sigma * u$.

Differential invariants are useful for the detection of features such as edges, ridges, junctions, and blobs; see [256] for an overview. To illustrate this, we focus on two applications for detecting edges.

A frequently used method is the *Canny edge detector* [69]. It is based on calculating the first derivatives of the Gaussian-smoothed image. After applying sophisticated thinning and linking mechanisms (*non-maxima suppression* and *hysteresis thresholding*), edges are identified as locations where the gradient magnitude has a maximum. This method is often acknowledged to be the best linear edge detector, and it has become a standard in edge detection.

Another important edge detector is the *Marr–Hildreth operator* [278], which uses the *Laplacian-of-Gaussian (LoG)* ΔK_σ as convolution kernel. Edges of f are identified as zero-crossings of $\Delta K_\sigma * f$. This needs no further postprocessing and always gives closed contours. There are indications that LoGs and especially their approximation by *differences-of-Gaussians (DoGs)* play an important role in the visual system of mammals, see [278] and the references therein. Young developed this theory further by presenting evidence that the receptive fields in primate eyes are shaped like the sum of a Gaussian and its Laplacian [449], and Koenderink and van Doorn suggested the set of Gaussian derivatives as a general model for the visual system [242].

If one investigates the temporal evolution of the zero-crossings of an image filtered by linear diffusion, one observes an interesting phenomenon: When increasing the smoothing scale σ, no new zero-crossings are created which cannot be traced back to finer scales [439]. This evolution property is called *causality* [240]. It is

---

[2]Of course, solutions of the regularization can only approximate the solution of the original problem (if it exists). In practice, increasing the order of applied Gaussian derivatives or reducing the kernel size will finally deteriorate the results of deblurring.

closely connected to the maximum–minimum principle of certain parabolic opera-
tors [189]. Attempts to reconstruct the original image from the temporal evolution
of the zero-crossings of the Laplacian have been carried out by Hummel and Mo-
niot [190]. They concluded, however, that this is practically unstable unless very
much additional information is provided.

In the western world the evolution property of the zero-crossings was the key
investigation which has inspired Witkin to the so-called scale-space concept [439].
This shall be discussed next.

1.2.2   Scale-space properties

The general scale-space concept

It is a well-known fact that images usually contain structures at a large variety of
scales. In those cases where it is not clear in advance which is the right scale for the
depicted information it is desirable to have an image representation at multiple
scales. Moreover, by comparing the structures at different scales, one obtains a
hierarchy of image structures which eases a subsequent image interpretation.

A *scale-space* is an image representation at a continuum of scales, embedding
the image f into a family $\{T_t f | t \geq 0\}$ of gradually simplified versions of it, provided
that it fulfils certain requirements[3]. Most of these properties can be classified as
architectural, smoothing (information-reducing) or invariance requirements [12].

An important architectural assumption is *recursivity*, i.e. for $t = 0$, the scale-
space representation gives the original image f, and the filtering may be split into
a sequence of filter banks:

$$
\begin{aligned}
T_0 f &= f, &&\text{(1.16)}\\
T_{t+s} f &= T_t(T_s f) &&\forall\, s, t \geq 0. &&\text{(1.17)}
\end{aligned}
$$

This property is very often referred to as the *semigroup property*. Other architec-
tural principles comprise for instance regularity properties of T_t and local behaviour
as t tends to 0.

Smoothing properties and information reduction arise from the wish that the
transformation should not create artifacts when passing from fine to coarse rep-
resentation. Thus, at a coarse scale, we should not have additional structures
which are caused by the filtering method itself and not by underlying structures
at finer scales. This simplification property is specified by numerous authors in
different ways, using concepts such as no creation of new level curves (causality)
[240, 450, 189, 255], nonenhancement of local extrema [30, 257], decreasing number

---

[3]Recently it has also been proposed to extend the scale-space concept to *scale–imprecision
space* by taking into account the imprecision of the measurement device [171].

of local extrema [255], maximum loss of figure impression [196], Tikhonov regularization [302, 303], maximum–minimum principle [189, 328], positivity [324, 138], preservation of positivity [191, 193, 320], comparison principle [12], and Lyapunov functionals [415, 429]. Especially in the linear setting, many of these properties are equivalent or closely related; see [426] for more details.

We may regard an image as a representative of an equivalence class containing all images that depict the same object. Two images of this class differ e.g. by grey-level shifts, translations and rotations or even more complicated transformations such as affine mappings. This makes the requirement plausible that the scale-space analysis should be invariant to as many of these transformations as possible, in order to analyse only the depicted object [196, 16].

The pioneering work of Alvarez, Guichard, Lions and Morel [12] shows that every scale-space fulfilling some fairly natural architectural, information-reducing and invariance axioms is governed by a PDE with the original image as initial condition. Thus, PDEs are the suitable framework for scale-spaces.

Often these requirements are supplemented with an additional assumption which is equivalent to the superposition principle, namely *linearity:*

$$T_t(af + bg) \;=\; a\,T_t f + b\,T_t g \qquad \forall\, t \geq 0, \quad \forall\, a, b \in \mathrm{I\!R}. \qquad (1.18)$$

As we shall see below, imposing linearity restricts the scale-space idea to essentially one representative.

Gaussian scale-space

The historically first and best investigated scale-space is the *Gaussian scale-space*, which is obtained via convolution with Gaussians of increasing variance, or – equivalently – by linear diffusion filtering according to (1.9), (1.10).

Usually a 1983 paper by Witkin [439] or a 1980 report by Stansfield [392] are regarded as the first references to the linear scale-space idea. Recent work by Weickert, Ishikawa and Imiya [426, 427], however, shows that scale-space is more than 20 years older: An axiomatic derivation of 1-D Gaussian scale-space has already been presented by Taizo Iijima in a technical paper from 1959 [191] followed by a journal version in 1962 [192]. Both papers are written in Japanese.

In [192] Iijima considers an observation transformation Φ which depends on a scale parameter σ and which transforms the original image $f(x)$ into a blurred version[4] $\Phi[f(x'), x, \sigma]$. This class of blurring transformations is called *boke* (defocusing). He assumes that it has the structure

$$\Phi[f(x'), x, \sigma] = \int\limits_{-\infty}^{\infty} \phi\{f(x'), x, x', \sigma\}\, dx', \qquad (1.19)$$

---

[4]The variable x' serves as a dummy variable.

and that it should satisfy five conditions:

(I) *Linearity (with respect to multiplications):*
    If the intensity of a pattern becomes A times its original intensity, then the
    same should happen to the observed pattern:

$$\Phi[Af(x'), x, \sigma] \;=\; A\,\Phi[f(x'), x, \sigma]. \tag{1.20}$$

(II) *Translation invariance:*
    Filtering a translated image is the same as translating the filtered image:

$$\Phi[f(x'-a), x, \sigma] \;=\; \Phi[f(x'), x-a, \sigma]. \tag{1.21}$$

(III) *Scale invariance:*
    If a pattern is spatially enlarged by some factor λ, then there exists a $\sigma' = \sigma'(\sigma, \lambda)$ such that

$$\Phi[f(x'/\lambda), x, \sigma] \;=\; \Phi[f(x'), x/\lambda, \sigma']. \tag{1.22}$$

(IV) *(Generalized) semigroup property:*
    If f is observed under a parameter σ_1 and this observation is observed un-
    der a parameter σ_2, then this is equivalent to observing f under a suitable
    parameter $\sigma_3 = \sigma_3(\sigma_1, \sigma_2)$:

$$\Phi\Big[\Phi[f(x''), x', \sigma_1], x, \sigma_2\Big] \;=\; \Phi[f(x''), x, \sigma_3]. \tag{1.23}$$

(V) *Preservation of positivity:*
    If the original image is positive, then the observed image is positive as well:

$$\Phi[f(x'), x, \sigma] > 0 \qquad \forall\, f(x') > 0, \quad \forall\, \sigma > 0. \tag{1.24}$$

Under these requirements Iijima derives in a very systematic way that

$$\Phi[f(x'), x, \sigma] \;=\; \frac{1}{2\sqrt{\pi}\sigma} \int\limits_{-\infty}^{\infty} f(x')\,\exp\left(\frac{-(x-x')^2}{4\sigma^2}\right)\, dx'. \tag{1.25}$$

Thus, $\Phi[f(x'), x, \sigma]$ is just the convolution between f and a Gaussian with standard
deviation $\sigma\sqrt{2}$.

This has been the starting point of an entire world of linear scale-space research
in Japan, which is basically unknown in the western world. Japanese scale-space
theory was well-embedded in a general framework for pattern recognition, feature
extraction and object classification [195, 197, 200, 320], and many results have

been established earlier than in the western world. Apart from their historical merits, these Japanese results reveal many interesting qualities which should induce everyone who is interested in scale-space theory to have a closer look at them. More details can be found in [426, 427] as well as in some English scale-space papers by Iijima such as [195, 197]. In particular, the latter ones show that there is no justification to deny Iijima's pioneering role in linear scale-space theory because of language reasons.

Table 1.1: Overview of continuous Gaussian scale-space axiomatics (I1 = Iijima [191, 192], I2 = Iijima [193, 194], I3 = Iijima [196], O = Otsu [320], K = Koenderink [240], Y = Yuille/Poggio [450], B = Babaud et al. [30], L1 = Lindeberg [255], F1 = Florack et al. [140], A = Alvarez et al. [12], P = Pauwels et al. [324], N = Nielsen et al. [303], L2 = Lindeberg [257], F2 = Florack [138]).

	I1	I2	I3	O	K	Y	B	L1	F1	A	P	N	L2	F2
convolution kernel	•	•		•		•	•	•	•	•	•		•	•
semigroup property	•	•					•	•	•	•	•	•	•	•
locality										•				
regularity						•	•	•	•	•	•		•	•
infinetes. generator											•			
max. loss principle			•											
causality					•	•	•	•					•	
nonnegativity	•	•		•						•	•			•
Tikhonov regulariz.												•		
aver. grey level invar.			•	•			•	•		•	•			
flat kernel for $t \to \infty$						•			•					
isometry invariance		•		•		•	•	•	•	•	•	•	•	•
homogen. & isotropy					•									
separability				•					•					
scale invariance	•	•				•	•		•		•	•		•
valid for dimension	1	2	2	2	1,2	1,2	1	1	> 1	N	1,2	N	N	N

Table 1.1 presents an overview of the current Japanese and western Gaussian scale-space axiomatics (see [426, 427] for detailed explanations). All of these axiomatics use explicitly or implicitly[5] a linearity assumption. We observe that – despite the fact that many axiomatics reveal similar first principles – not two of them are identical. Each of the 14 axiomatics confirms and enhances the evidence that the others give: that Gaussian scale-space is unique within a *linear* framework.

A detailed treatment of Gaussian scale-space theory can be found in two Japanese monographs by Iijima [197, 198], as well as in English books by Lindeberg [256], Florack [139], and ter Haar Romeny [176]. A collection edited by

---

[5]Often it is assumed that the filter is a convolution integral. This is equivalent to linearity and translation invariance.

Sporring, Nielsen, Florack and Johansen [389] gives an excellent overview of the various aspects of this theory, and additional material is presented in [211]. Many relations between Gaussian scale-space and regularization theory have been elaborated by Nielsen [302], and readers who wish to analyse linear and nonlinear scale-space concepts in terms of differential and integral geometry can find a lot of material in the thesis of Salden [351].

1.2.3   Numerical aspects

The preceding theory is entirely continuous. However, in practical problems, the image is sampled at the nodes *(pixels)* of a fixed equidistant grid. Thus, the diffusion filter has to be discretized.

By virtue of the equivalence of solving the linear diffusion equation and convolving with a Gaussian, we can either approximate the convolution process or the diffusion equation.

When restricting the image to a finite domain and applying the Fast Fourier Transformation (FFT), convolution in the spatial domain can be reduced to multiplication in the frequency domain, cf. (1.7). This proceeding requires a fixed computational effort of order $N \log N$, which depends only on the pixel number N, but not on the kernel size σ. For large kernels this is faster than most spatial techniques. Especially for small kernels, however, aliasing effects in the Fourier domain may create oscillations and over- and undershoots [178].

One efficient possibility to approximate Gaussian convolution in the spatial domain consists of applying recursive filters [109, 448]. More frequently the Gaussian kernel is just sampled and truncated at some multiple of its standard deviation σ. Factorizing a higher-dimensional Gaussian into one-dimensional Gaussians reduces the computational effort to $O(N\sigma)$. Convolution with a truncated Gaussian, however, reveals the drawback that it does not preserve the semigroup property of the continuous Gaussian scale-space [255].

Lindeberg [255] has established a linear scale-space theory for the *semidiscrete*[6] case. His results are in accordance with those of Norman [312], who proposed in 1960 that the discrete analogue of the Gaussian kernel should be given in terms of modified Bessel functions of integer order. Since this scale-space family arises naturally from a semidiscretized version of the diffusion equation, it has been argued that approximating the diffusion equation should be preferred to discretizing the convolution integral [255].

Recently, interesting semidiscrete and fully discrete linear scale-space formulations have been established utilizing stochastic principles: Åström and Heyden [27] study a framework based on stationary random fields, while the theory by Salden et al. [353] exploits the relations between diffusion and Markov processes.

---

[6]By semidiscrete we mean discrete in space and continuous in time throughout this work.

Among the numerous numerical possibilities to approximate the linear diffusion equation, finite difference (FD) schemes dominate the field. Apart from some implicit approaches [166, 67, 68] allowing realizations as a recursive filter [14, 10, 451], explicit schemes are mainly used. A very efficient approximation of the Gaussian scale-space results from applying multigrid ideas. The *Gaussian pyramid* [64] has the computational complexity $O(N)$ and gives a multilevel representation at finitely many scales of different resolution. By subsequently smoothing the image with an explicit scheme for the diffusion equation and restricting the result to a coarser grid, one obtains a simplified image representation at the next coarser grid. Due to their simplicity and efficiency, pyramid decompositions have become very popular and have been integrated into commercially available hardware [70, 214]. Pyramids are not invariant under translations, however, and sometimes it is argued that they are undersampled and that the pyramid levels should be closer[7]. These are the reasons why some people regard pyramids rather as predecessors of the scale-space idea than as a numerical approximation[8].

1.2.4   Applications

Due to its equivalence to convolution with a Gaussian, linear diffusion filtering has been applied in numerous fields of image processing and computer vision. It can be found in almost every standard textbook in these fields.

Less frequent are applications which exploit the *evolution* of an image under Gaussian scale-space. This *deep structure* analysis [240] provides useful information for extracting semantic information from an image, for instance

- for finding the most relevant scales *(scale selection, focus-of-attention)*. This may be done by searching for extrema of (nonlinear) combinations of normalized Gaussian derivatives [256] or by analysing information theoretic measures such as the entropy [208, 388] or generalized entropies [390] over scales.

- for multiscale segmentation of images [172, 254, 256, 313, 408]. The idea is to identify segments at coarse scales and to link backwards to the original image in order to improve the localization.

In recent years also applications of Gaussian scale-space to stereo, optic flow and image sequences have become an active research field [139, 215, 241, 258, 259, 302, 306, 441]. Several scale-space applications are summarized in a survey paper by ter Haar Romeny [175].

---

[7]Of course, multiresolution techniques such as pyramids or discrete wavelet transforms [92, 106] are just designed to have few or no redundancies, while scale-space analysis intends to extract semantical information by tracing signals through a continuum of scales.

[8]Historically, this is incorrect: Iijima's scale-space work [191] is much older than multigrid ideas in image processing.

Interesting results arise when one studies linear scale-space on a sphere [236, 353]: while the diffusion equation remains the correct concept, Gaussian kernels are of no use anymore: appropriate kernels have to be expressed in terms of Legendre functions [236]. This and other results [12, 255] indicate that the PDE formulation of linear scale-space in terms of a diffusion equation is more natural and has a larger generalization potential than convolution with Gaussians.

1.2.5   Limitations

In spite of several properties that make linear diffusion filtering unique and easy to handle, it reveals some drawbacks as well:

(a) An obvious disadvantage of Gaussian smoothing is the fact that it does not only smooth noise, but also blurs important features such as edges and, thus, makes them harder to identify. Since Gaussian smoothing is designed to be completely uncommitted, it cannot take into account any a-priori information on structures which are worth being preserved (or even enhanced).

(b) Linear diffusion filtering dislocates edges when moving from finer to coarser scales, see e.g. Witkin [439]. So structures which are identified at a coarse scale do not give the right location and have to be traced back to the original image [439, 38, 165]. In practice, relating dislocated information obtained at different scales is difficult and bifurcations may give rise to instabilities. These coarse-to-fine tracking difficulties are generally denoted as the *correspondence problem.*

(c) Some smoothing properties of Gaussian scale-space do not carry over from the 1-D case to higher dimensions: A closed zero-crossing contour can split into two as the scale increases [450], and it is generally not true that the number of local extrema is nonincreasing, see [254, 255] for illustrative counterexamples. A deep mathematical analysis of such phenomena has been carried out by Damon [105] and Rieger [342]. It turned out that the pairwise creation of an extremum and a saddle point is not an exception, but happens generically.

Regarding (b) and (c), much efforts have been spent in order to understand the deep structure in Gaussian scale-space, for instance by analysing its *toppoints* [210]. There is some evidence that these points, where the gradient vanishes and the Hessian does not have full rank, carry essential image information [212]. Part III of the book edited by Sporring et al. [389] and the references therein give an overview of the state-of-the-art in deep structure analysis.

Due to the uniqueness of Gaussian scale-space within a linear framework we know that any modification in order to overcome the problems (a)–(c) will either

renounce linearity or some scale-space properties. We shall see that appropriate methods to avoid the shortcomings (a) and (b) are nonlinear diffusion processes, while (c) requires morphological equations [206, 207, 218].

1.2.6   Generalizations

Before we turn our attention to nonlinear processes, let us first investigate two linear modifications which have been introduced in order to address the problems (a) and (b) from the previous section.

Affine Gaussian scale-space

A straightforward generalization of Gaussian scale-space results from renouncing invariance under rotations. This leads to the *affine Gaussian scale-space*

$$u(x,t) \; := \; \int_{\mathbb{R}^2} \frac{1}{4\pi\sqrt{\det(D_t)}} \, \exp\left(-\frac{(x-y)^\top D_t^{-1}(x-y)}{4}\right) \, f(y)\,dy \qquad (1.26)$$

where $D_t := tD$, $t > 0$, and $D \in \mathbb{R}^{2\times 2}$ is symmetric positive definite[9]. For a *fixed* matrix D, calculating the convolution integral (1.26) is equivalent to solving a linear anisotropic diffusion problem with D as diffusion tensor:

$$\partial_t u \;=\; \mathrm{div}\,(D\,\nabla u), \qquad\qquad (1.27)$$
$$u(x,0) \;=\; f(x). \qquad\qquad (1.28)$$

In [427] it is shown that affine Gaussian scale-space has been axiomatically derived by Iijima in 1962 [193, 194]. He named $u(x,t)$ the *generalized figure* of f, and (1.27) the *basic equation of figure* [196]. In 1971 this concept was realized in hardware in the optical character reader ASPET/71 [199, 200]. The scale-space part has been regarded as the reason for its reliability and robustness.

In 1992 Nitzberg and Shiota [310] proposed to adapt the Gaussian kernel shape to the structure of the original image. By chosing D in (1.26) as a function of the structure tensor (cf. Section 2.2) of f, they combined nonlinear shape adaptation with linear smoothing. Later on similar ideas have been developed in [259, 443].

It should be noted that shape-adapted Gaussian smoothing with a spatially varying D is no longer equivalent to a diffusion process of type (1.27). In practice this can be experienced by the fact that shape-adaptation of Gaussian smoothing does not preserve the average grey level, while the divergence formulation ensures that this is still possible for nonuniform diffusion filtering; see Section 1.1. Also in this case the diffusion equation seems to be more general. If one wants to relate

---

[9]Isotropic Gaussian scale-space can be recovered using the unit matrix for D.

shape-adapted Gaussian smoothing to a PDE, one has to carry out sophisticated scaling limits [310].

Noniterative shape-adapted Gaussian smoothing differs from nonlinear anisotropic diffusion filtering by the fact that the latter one introduces a feedback into the process: it adapts the diffusion tensor in (1.27) to the differential structure of the filtered image instead of the original image. Such concepts will be investigated in Section 1.3.3 and in the remaining chapters of this book.

Directed diffusion

Another method for incorporating a-priori knowledge into a linear diffusion process is suggested by Illner and Neunzert [202]. Provided we are given some background information in form of a smooth image b, they show that under some technical requirements and suitable boundary conditions the classical solution u of

$$\partial_t u \ = \ b \, \Delta u - u \, \Delta b, \tag{1.29}$$
$$u(x, 0) \ = \ f(x) \tag{1.30}$$

converges to b along a path where the relative entropy with respect to b increases in a monotone way. Numerical experiments have been carried out by Giuliani [159], and an analysis in terms of nonsmooth b and weak solutions is due to Illner and Tie [203].

Such a *directed diffusion process* requires to specify an entire image as background information in advance; in many applications it would be desirable to include a priori knowledge in a less specific way, e.g. by prescribing that features within a certain contrast and scale range are considered to be semantically important and processed differently. Such demands can be satisfied by nonlinear diffusion filters.

1.3   Nonlinear diffusion filtering

Adaptive smoothing methods are based on the idea of applying a process which itself depends on local properties of the image. Although this concept is well-known in the image processing community (see [349] and the references therein for an overview), a corresponding PDE formulation was first given by Perona and Malik [326] in 1987. We shall discuss this model in detail, especially its ill-posedness aspects. This gives rise to study regularizations. These techniques can be extended to anisotropic processes which make use of an adapted diffusion tensor instead of a scalar diffusivity.

1.3.1 The Perona–Malik model

Basic idea

Perona and Malik propose a nonlinear diffusion method for avoiding the blurring and localization problems of linear diffusion filtering [326, 328]. They apply an inhomogeneous process that reduces the diffusivity at those locations which have a larger likelihood to be edges. This likelihood is measured by $|\nabla u|^2$. The Perona–Malik filter is based on the equation

$$\partial_t u = \operatorname{div}\left(g(|\nabla u|^2)\,\nabla u\right). \tag{1.31}$$

and it uses diffusivities such as

$$g(s^2) = \frac{1}{1 + s^2/\lambda^2} \qquad (\lambda > 0). \tag{1.32}$$

Although Perona and Malik name their filter anisotropic, it should be noted that – in our terminology – it would be regarded as an isotropic model, since it utilizes a scalar-valued diffusivity and not a diffusion tensor.

Interestingly, there exists a relation between (1.31) and the neural dynamics of brightness perception: In 1984 Cohen and Grossberg [94] proposed a model of the primary visual cortex with similar inhibition effects as in the Perona–Malik model.

The experiments of Perona and Malik were visually very impressive: edges remained stable over a very long time. It was demonstrated [328] that edge detection based on this process clearly outperforms the linear Canny edge detector, even without applying non-maxima suppression and hysteresis thresholding. This is due to the fact that diffusion and edge detection interact in one single process instead of being treated as two independent processes which are to be applied subsequently. Moreover, there is another reason for the impressive behaviour at edges, which we shall discuss next.

Edge enhancement

To study the behaviour of the Perona–Malik filter at edges, let us for a moment restrict ourselves to the one-dimensional case. This simplifies the notation and illustrates the main behaviour since near a straight edge a two-dimensional image approximates a function of one variable.

For the diffusivity (1.32) it follows that the *flux function* $\Phi(s) := sg(s^2)$ satisfies $\Phi'(s) \geq 0$ for $|s| \leq \lambda$, and $\Phi'(s) < 0$ for $|s| > \lambda$, see Figure 1.1. Since (1.31) can be rewritten as

$$\partial_t u = \Phi'(u_x)u_{xx}, \tag{1.33}$$

we observe that – in spite of its nonnegative diffusivity – the Perona–Malik model is of *forward parabolic type* for $|u_x| \leq \lambda$, and of *backward parabolic type* for $|u_x| > \lambda$.
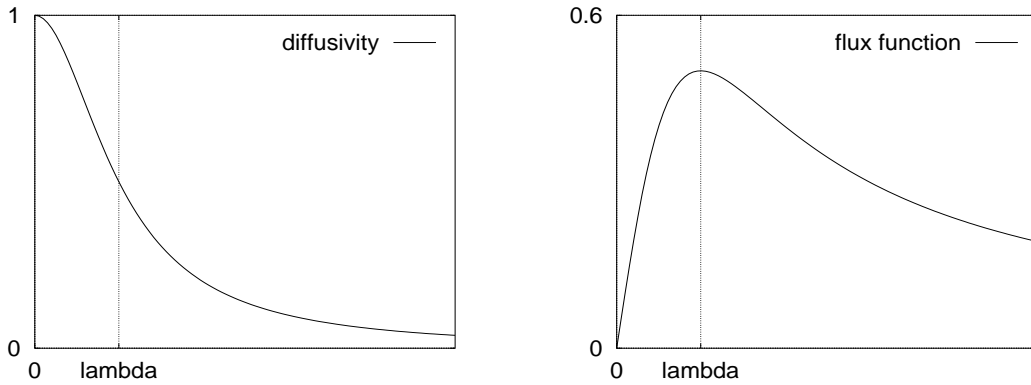
Figure 1.1: (a) LEFT: Diffusivity $g(s^2) = \frac{1}{1+s^2/\lambda^2}$. (b) RIGHT: Flux function $\Phi(s) = \frac{s}{1+s^2/\lambda^2}$.

Hence, λ plays the role of a *contrast parameter* separating forward (low contrast) from backward (high contrast) diffusion areas.

It is not hard to verify that the Perona–Malik filter increases the slope at inflection points of edges within a backward area: If there exists a sufficiently smooth solution u it satisfies

$$\partial_t(u_x^2) \;=\; 2u_x\partial_x(u_t) \;=\; 2\Phi''(u_x)u_xu_{xx}^2 + 2\Phi'(u_x)u_xu_{xxx}. \tag{1.34}$$

A location x_0 where u_x^2 is maximal at some time t is characterized by $u_xu_{xx}=0$ and $u_xu_{xxx}\leq 0$. Therefore,

$$(\partial_t(u_x^2))\,(x_0,t) \;\geq\; 0 \quad \text{for} \quad |u_x(x_0,t)| > \lambda \tag{1.35}$$

with strict inequality for $u_xu_{xxx}<0$.

In the two-dimensional case, (1.33) is replaced by [12]

$$\partial_t u \;=\; \Phi'(\nabla u)u_{\eta\eta} + g(|\nabla u|^2)u_{\xi\xi} \tag{1.36}$$

where the *gauge coordinates* ξ and η denote the directions perpendicular and parallel to ∇u, respectively. Hence, we have forward diffusion along *isophotes* (i.e. lines of constant grey value) combined with forward–backward diffusion along *flowlines* (lines of maximal grey value variation).

We observe that the forward–backward diffusion behaviour is not only restricted to the special diffusivity (1.32), it appears for all diffusivities $g(s^2)$ whose rapid decay causes non-monotone flux functions $\Phi(s) = sg(s^2)$. Overviews of several common diffusivities for the Perona–Malik model can be found in [43, 343], and a family of diffusivities with different decay rates is investigated in [36]. Rapidly decreasing diffusivities are explicitly intended in the Perona–Malik method as they

give the desirable result of blurring small fluctuations and sharpening edges. Therefore, they are the main reason for the visually impressive results of this restoration technique.

It is evident that the "optimal" value for the contrast parameter λ has to depend on the problem. Several proposals have been made to facilitate such a choice in practice, for instance adapting it to a specified quantile in the cumulative gradient histogramme [328], using statistical properties of a training set of regions which are considered as flat [444], or estimating it by means of the local image geometry [270].

Ill-posedness

Unfortunately, forward–backward equations of Perona–Malik type cause some theoretical problems. Although there is no general theory for nonlinear parabolic processes, there exist certain frameworks which allow to establish well-posedness results for a large class of equations. Let us recall three examples:

- Let $S(N)$ denote the set of symmetric $N \times N$ matrices and $\text{Hess}(u)$ the Hessian of u. Classical differential inequality techniques [411] based on the Nagumo–Westphal lemma require that the underlying nonlinear evolution equation

$$\partial_t u \;=\; F(t, x, u, \nabla u, \text{Hess}(u)) \tag{1.37}$$

  satisfies the monotony property

$$F(t, x, r, p, Y) \;\geq\; F(t, x, r, p, X) \tag{1.38}$$

  for all $X, Y \in S(2)$ where $Y - X$ is positive semidefinite.

- The same requirement is needed for applying the theory of viscosity solutions. A detailed introduction into this framework can be found in a paper by Crandall, Ishii and Lions [103].

- Let H be a Hilbert space with scalar product $(.,.)$ and $A : H \to H$. In order to apply the concept of maximal monotone operators [57] to the problem

$$\frac{du}{dt} + Au \;=\; 0, \tag{1.39}$$
$$u(0) \;=\; f \tag{1.40}$$

  one has to ensure that A is *monotone*, i.e.

$$(Au - Av, u - v) \;\geq\; 0 \qquad \forall\, u, v \in H. \tag{1.41}$$

We observe that the nonmonotone flux function of the Perona–Malik process implies that neither (1.38) is satisfied nor A defined by $Au := -\mathrm{div}\left(g(|\nabla u|^2)\,\nabla u\right)$ is monotone. Therefore, none of these frameworks is applicable to ensure well-posedness results.

One reason why people became pessimistic about the well-posedness of the Perona–Malik equation was a result by Höllig [187]. He constructed a forward–backward diffusion process which can have infinitely many solutions. Although this process was different from the Perona–Malik process, one was warned what can happen. In 1994 the general conjecture was that the Perona–Malik filter might have weak solutions, but one should neither expect uniqueness nor stability [329]. In the meantime several theoretical results are available which provide some insights into the actual degree of ill-posedness of the Perona–Malik filter.

Kawohl and Kutev [222] proved that the Perona–Malik process does not have global (weak) C^1 solutions for intial data that involve backward diffusion. The existence of local C^1 solutions remained unproven. If they exist, however, Kawohl and Kutev showed that these solutions are unique and satisfy a maximum-minimum principle. Moreover, under special assumptions on the initial data, it was possible to establish a comparison principle.

Kichenassamy [224, 225] proposed a notion of generalized solutions, which are piecewise linear and contain jumps, and he showed that an analysis of their moving and merging gives similar effects to those one can observe in practice.

Results of You et al. [446] give evidence that the Perona–Malik process is unstable with respect to perturbations of the initial image. They showed that the energy functional leading to the Perona–Malik process as steepest descent method has an infinite number of global minima which are dense in the image space. Each of these minima corresponds to a piecewise constant image, and slightly different initial images may end up in different minima for $t \to \infty$.

Interestingly, forward–backward diffusion equations of Perona–Malik type are not as unnatural as they look at first glance: besides their importance in computer vision they have been proposed as a mathematical model for heat and mass transfer in a stably stratified turbulent shear flow. Such a model is used to explain the evolution of stepwise constant temperature or salinity profiles in the ocean. Related equations also play a role in population dynamics and viscoelasiticity, see [35] and the references therein.

Numerically, the mainly observable instability is the so-called *staircasing effect*, where a sigmoid edge evolves into piecewise linear segments which are separated by jumps. It has already been observed by Posmentier in 1977 [333]. He used an equation of Perona–Malik type for numerical simulations of the salinity profiles in oceans. Starting from a smoothly increasing initial distribution he reported the creation of perturbations which led to a stepwise constant profile after some time.

In image processing, numerical studies of the staircasing effect have been carried out by Nitzberg and Shiota [310], Fröhlich and Weickert [148], and Benhamouda [36]. All results point in the same direction: the number of created plateaus depends strongly on the regularizing effect of the discretization. Finer discretizations are less regularizing and lead to more "stairs". Weickert and Benhamouda [425] showed that the regularizing effect of a standard finite difference discretization is sufficient to turn the Perona–Malik filter into a well-posed initial value problem for a nonlinear system of ordinary differential equations. Its global solution satisfies a maximum–minimum principle and converges to a constant steady-state. The theoretical framework for this analysis will be presented in Chapter 3.

There exists also a discrete explanation why staircasing is essentially the only observable instability: In 1-D, standard FD discretizations are monotonicity preserving, which guarantees that no additional oscillations occur during the evolution. This has been shown by Dzu Magaziewa [123] in the semidiscrete case and by Benhamouda [36, 425] in the fully discrete case with an explicit time discretization. Further contributions to the explanation and avoidance of staircasing can be found in [4, 36, 98, 225, 438].

Scale-space interpretation

Perona and Malik renounced the assumption of Koenderink's linear scale-space axiomatic [240] that the smoothing should treat all spatial points and scale levels equally. Instead of this, they required that region boundaries should be sharp and should coincide with the semantically meaningful boundaries at each resolution level *(immediate localization)*, and that intra-region smoothing should be preferred to inter-region smoothing *(piecewise smoothing)*. These properties are of significant practical interest, as they guarantee that structures can be detected easily and correspondence problems can be neglected. Experiments demonstrated that the Perona–Malik filter satisfies these requirements fairly well [328].

In order to establish a smoothing scale-space property for this nonlinear diffusion process, a natural way would be to prove a maximum–minimum principle, provided one knows that there exists a sufficiently smooth solution. Since the existence question used to be the bottleneck in the past, the first proof is due to Kawohl and Kutev who established an extremum principle for their local weak C^1 solution to the Perona–Malik filter [222]. Of course, this is only partly satisfying, since in scale-space theory one is interested in having an extremum principle for the entire time interval $[0, \infty)$.

Nevertheless, also other attempts to apply scale-space frameworks to the Perona–Malik process have not been more successful yet:

- Salden [350], Florack [143] and Eberly [124] proposed to carry over the linear scale-space theory to the nonlinear case by considering nonlinear diffusion

processes which result from special rescalings of the linear one. Unfortunately, the Perona–Malik filter turned out not to belong to this class [143].

- Alvarez, Guichard, Lions and Morel [12] have developed a nonlinear scale-space axiomatic which comprises the linear scale-space theory as well as nonlinear morphological processes (which we will discuss in 1.5 and 1.6). Their smoothing axiom is a monotony assumption *(comparison principle)* requiring that the scale-space is order-preserving:

$$f \leq g \quad \Longrightarrow \quad T_t f \leq T_t g \quad \forall\, t \geq 0. \tag{1.42}$$

This property is closely related to a maximum–minimum principle and to L^∞-stability of the solution [12, 261]. However, the Perona–Malik model does not fit into this framework, because its local weak solution satisfies a comparison principle only for some finite time, but not for all $t > 0$; see [222].

1.3.2   Regularized nonlinear models

It has already been mentioned that numerical schemes may provide implicit regularizations which stabilize the Perona–Malik process [425]. Hence, it has been suggested to introduce the regularization directly into the continuous equation in order to become more independent of the numerical implementation [81, 310].

Since the dynamics of the solution may critically depend on the sort of regularization, one should adjust the regularization to the desired goal of the forward–backward heat equation [35]. One can apply spatial or temporal regularization (and of course, a combination of both). Below we shall discuss three examples which illustrate the variety of possibilities and their tailoring towards a specific task.

(a) The first spatial regularization attempt is probably due to Posmentier who observed numerically the stabilizing effect of averaging the gradient within the diffusivity [333].

A mathematically sound formulation of this idea is given by Catté, Lions, Morel and Coll [81]. By replacing the diffusivity $g(|\nabla u|^2)$ of the Perona–Malik model by a Gaussian-smoothed version $g(|\nabla u_\sigma|^2)$ with $u_\sigma := K_\sigma * u$ they end up with

$$\partial_t u = \operatorname{div} \left(g(|\nabla u_\sigma|^2)\, \nabla u \right). \tag{1.43}$$

In [81] existence, uniqueness and regularity of a solution for $\sigma > 0$ have been established.

This process has been analysed and modified in many ways: Whitaker and Pizer [438] have suggested that the regularization parameter σ should be

a decreasing function in t, and Li and Chen [252] have proposed to subsequently decrease the contrast parameter λ. A detailed study of the influence of the parameters in a regularized Perona–Malik model has been carried out by Benhamouda [36]. Kačur and Mikula [217] have investigated a modification which allows to diffuse differently in different grey value ranges. Spatial regularizations of the Perona–Malik process leading to anisotropic diffusion equations have been proposed by Weickert [413, 415] and will be described in 1.3.3. Torkamani–Azar and Tait [403] suggest to replace the Gaussian convolution by the exponential filter of Shen and Castan[10] [381].

In Chapter 2 we shall see that spatial regularizations lead to well-posed scale-spaces with a large class of Lyapunov functionals which guarantee that the solution converges to a constant steady-state.

From a practical point of view, spatial regularizations offer the advantage that they make the filter insensitive to noise at scales smaller than σ. Therefore, when regarding (1.43) as an image restoration equation, it exhibits besides the contrast parameter λ an additional *noise scale σ*. This avoids a shortcoming of the genuine Perona–Malik process which misinterprets strong oscillations due to noise as edges which should be preserved or even enhanced. Examples for spatially regularized nonlinear diffusion filtering can be found in Figure 5.2 (c) and 5.4 (a),(b).

(b) P.-L. Lions proved in a private communication to Mumford that the one-dimensional process

$$\partial_t u = \partial_x \left(g(v)\, \partial_x u \right), \tag{1.44}$$
$$\partial_t v = \tfrac{1}{\tau} \left(|\partial_x u|^2 - v \right) \tag{1.45}$$

leads to a well-posed filter (cf. [329]). We observe that v is intended as a time-delay regularization of $|\partial_x u|^2$ where the parameter $\tau > 0$ determines the delay. These equations arise as a special case of the spatio-temporal regularizations of Nitzberg and Shiota [310] when neglecting any spatial regularization. Mumford conjectures that this model gives piecewise constant steady-states. In this case, the steady-state solution would solve a segmentation problem.

(c) In the context of shear flows, Barenblatt et al. [35] regularized the one-dimensional forward–backward heat equation by considering the third-order equation

$$\partial_t u = \partial_x(\Phi(u_x)) + \tau \partial_{xt}(\Psi(u_x)) \tag{1.46}$$

---

[10]This renounces invariance under rotation.

where Ψ is strictly increasing and uniformly bounded in $\mathbb{R}$, and $|\Phi'(s)| = O(\Psi'(s))$ as $s \to \pm\infty$. This regularization was physically motivated by introducing a relaxation time τ into the diffusivity.

For the corresponding initial boundary value problem with homogeneous Neumann boundary conditions they proved the existence of a unique generalized solution. They also showed that smooth solutions may become discontinuous within *finite* time, before they finally converge to a piecewise constant steady-state.

These examples demonstrate that regularization is much more than stabilizing an ill-posed process: *Regularization is modeling. Appropriately chosen regularizations create the desired filter features.* We observe that spatial regularizations are closer to scale-space ideas while temporal regularization are more related to image restoration and segmentation, since they may lead to nontrivial steady-states.

1.3.3   Anisotropic nonlinear models

All nonlinear diffusion filters that we have investigated so far utilize a scalar-valued diffusivity g which is adapted to the underlying image structure. Therefore, they are isotropic and the flux $j = -g\nabla u$ is always parallel to ∇u. Nevertheless, in certain applications it would be desirable to bias the flux towards the orientation of interesting features. These requirements cannot be satisfied by a scalar diffusivity anymore, a diffusion tensor leading to anisotropic diffusion filters has to be introduced.

First anisotropic ideas in image processing date back to Graham [167] in 1962, followed by Newman and Dirilten [300], Lev, Zucker and Rosenfeld [250], and Nagao and Matsuyama [297]. They used convolution masks that depended on the underlying image structure. Related statistical approaches were proposed by Knutsson, Wilson and Granlund [237]. These ideas have been further developed by Nitzberg and Shiota [310], Lindeberg and Gårding [259], and Yang et al. [443]. Their suggestion to use shape-adapted Gaussian masks has been discussed in Section 1.2.6.

Anisotropic diffusion filters usually apply spatial regularization strategies[11]. A general theoretical framework for spatially regularized anisotropic diffusion filters will be presented in the remaining chapters of this book.

Below we study two representatives of anisotropic diffusion processes. The first one offers advantages at noisy edges, whereas the second one is well-adapted to the processing of one-dimensional features. They are called edge-enhancing anisotropic diffusion and coherence-enhancing anisotropic diffusion, respectively.

---

[11] An exception is the time-delay regularization of Cottet and El-Ayyadi [100, 101].

(a) *Anisotropic regularization of the Perona–Malik process*

In the interior of a segment the nonlinear isotropic diffusion equation (1.43) behaves almost like the linear diffusion filter (1.9), but at edges diffusion is inhibited. Therefore, noise at edges cannot be eliminated successfully by this process. To overcome this problem, a desirable method should prefer diffusion along edges to diffusion perpendicular to them.

Anisotropic models do not only take into account the modulus of the edge detector ∇u_σ, but also its direction. To this end, we construct the orthonormal system of eigenvectors v_1, v_2 of the diffusion tensor D such that they reflect the estimated edge structure:

$$v_1 \parallel \nabla u_\sigma, \qquad v_2 \perp \nabla u_\sigma. \tag{1.47}$$

In order to prefer smoothing along the edge to smoothing across it, Weickert [415] proposed to choose the corresponding eigenvalues λ_1 and λ_2 as

$$\begin{aligned}
\lambda_1(\nabla u_\sigma) &:= g(|\nabla u_\sigma|^2), &\tag{1.48}\\
\lambda_2(\nabla u_\sigma) &:= 1. &\tag{1.49}
\end{aligned}$$

Section 5.1 presents several examples where this process is applied to test images.

In general, ∇u does not coincide with one of the eigenvectors of D as long as $\sigma > 0$. Hence, this model behaves really anisotropic. If we let the regularization parameter σ tend to 0, we end up with the isotropic Perona–Malik process.

Another anisotropic model which can be regarded as a regularization of an isotropic nonlinear diffusion filter has been described in [413].

(b) *Anisotropic models for smoothing one-dimensional objects*

A second motivation for introducing anisotropy into diffusion processes arises from the wish to process one-dimensional features such as line-like structures. To this end, Cottet and Germain [102] constructed a diffusion tensor with eigenvectors as in (1.47) and corresponding eigenvalues

$$\begin{aligned}
\lambda_1(\nabla u_\sigma) &:= 0, &\tag{1.50}\\
\lambda_2(\nabla u_\sigma) &:= \frac{\eta|\nabla u_\sigma|^2}{1 + (|\nabla u_\sigma|/\sigma)^2} & (\eta > 0). &\tag{1.51}
\end{aligned}$$

This is a process diffusing solely perpendicular to ∇u_σ. For $\sigma \to 0$, we observe that ∇u becomes an eigenvector of D with corresponding eigenvalue 0. Therefore, the process stops completely. In this sense, it is not intended as an anisotropic regularization of the Perona–Malik equation. Well-posedness

results for the Cottet–Germain filter comprise an existence proof for weak solutions.

Since the Cottet–Germain model diffuses only in one direction, it is clear that its result depends very much on the smoothing direction. For enhancing parallel line-like structures, one can improve this model when replacing $\nabla u_\sigma^\perp$ by a more robust descriptor of local orientation, the structure tensor (cf. Section 2.2). This leads to *coherence-enhancing anisotropic diffusion* [418], which shall be discussed in Section 5.2, where also many examples can be found.

1.3.4 Generalizations

Higher dimensions. It is easily seen that many of the previous results can be generalized to higher dimensions. This may be useful when considering e.g. medical image sequences from computerized tomography (CT) or magnetic resonance imaging (MRI), or when applying diffusion filters to the postprocessing of fluctuating higher-dimensional numerical data. The first three-dimensional nonlinear diffusion filters have been investigated by Gerig et al. [155] in the isotropic case and by Rambaux and Garçon [339] in the anisotropic case. A generalization of coherence-enhancing anisotropic diffusion to higher dimensions is proposed in [428], and Sánchez–Ortiz et al. [355] describe nonlinear diffusion filtering of 3-D image sequences by treating them as 4-D data sets.

More sophisticated structure descriptors. The edge detector ∇u_σ enables us to adapt the diffusion to magnitude and direction of edges, but it can neither distinguish between edges and corners nor does it give a reliable measure of local orientation. As a remedy, one can steer the smoothing process by more advanced structure descriptors such as higher-order derivatives [127] or tensor-valued expressions of first-order derivatives [414, 418]. The theoretical analysis in the present work shall comprise the second possibility. It has also been proposed to replace ∇u_σ by a Bayesian classification result in feature space [26].

Vector-valued models. Vector-valued images can arise either from devices measuring multiple physical properties or from a feature analysis of one single image. Examples for the first category are colour images, multi-spectral Landsat exposures and multi-spin echo MR images, whereas representatives of the second class are given by statistical moments or the *jet space* induced by the image itself and its partial derivatives up to a given order. Feature vectors play an important role for tasks like texture segmentation.

The simplest idea how to apply diffusion filtering to multichannel images would be to diffuse all channels separately and independently from each other. This leads to the undesirable effect that edges may be formed at different locations for each channel. In order to avoid this, one should use a common diffusivity which combines information from all channels. Such isotropic vector-valued diffusion models were studied by Gerig et al. [155, 156] and Whitaker [433, 434] in the context of medical imagery. Extensions to anisotropic vector-valued models with a common tensor-valued structure descriptor for all channels have been investigated by Weickert [422].

1.3.5   Numerical aspects

For nonlinear diffusion filtering numerous numerical methods have been applied:

Finite element techniques are described in [367, 391, 34, 216]. Bänsch and Mikula reported a significant speed-up by supplementing them with an adaptive mesh coarsening [34]. Neural network approximations to nonlinear diffusion filters are investigated by Cottet [100, 99] and Fischl and Schwartz [137]. Perona and Malik [327] propose hardware realizations by means of analogue VLSI networks with nonlinear resistors. A very detailed VLSI proposal has been developed by Gijbels et al. [158].

In [148] three schemes for a spatially regularized 1-D Perona–Malik filter are compared: a wavelet method of Petrov–Galerkin type, a pseudospectral method and a finite-difference scheme. It turned out that all results became fairly similar, when the regularization parameter σ was sufficiently large. Since the computational effort is of a comparable order of magnitude, it seems to be a matter of taste which scheme is preferred.

Most implementations of nonlinear diffusion filters are based on finite difference methods, since they are easy to handle and the pixel structure of digital images already provides a natural discretization on a fixed rectangular grid. Explicit schemes are the most simple to code and, therefore, they are used almost exclusively. Due to their local behaviour, they are well-suited for parallel architectures. Nevertheless, they suffer from the fact that fairly small time step sizes are needed in order to ensure stability. Semi-implicit schemes – which approximate the diffusivity or the diffusion tensor in an explicit way and the rest implicitly – are considered in [81]. They possess much better stability properties. A fast multigrid technique using a pyramid algorithm for the Perona–Malik filter has been studied by Acton et al. [5, 4]; see also [349] for related ideas.

While the preceding techniques are focusing on *approximating* a continuous equation, it is often desirable to have a genuinely discrete theory which guarantees that an algorithm *exactly* reveals the same qualitative properties as its continuous counterpart. Such a framework is presented in [420, 421], both for the semidiscrete

Table 1.2: Requirements for continuous, semidiscrete and fully discrete nonlinear diffusion scale-space.

requirement	continuous $u_t = \text{div}\,(D\nabla u)$ $u(t=0) = f$ $\langle D\nabla u, n\rangle = 0$	semidiscrete $\frac{du}{dt} = A(u)u$ $u(0) = f$	discrete $u^0 = f$ $u^{k+1} = Q(u^k)u^k$
smoothness	$D \in \text{C}^\infty$	A Lipschitz-continuous	Q continuous
symmetry	D symmetric	A symmetric	Q symmetric
conservation	div form; reflective b.c.	column sums are 0	column sums are 1
nonnegativity	positive semidefinite	nonnegative off-diagonals	nonnegative elements
connectivity	uniformly pos. definite	irreducible	irreducible; pos. diagonal

and for the fully discrete case. A detailed treatment of this theory can be found in Chapter 3 and 4, respectively. Table 1.2 gives an overview of the requirements which are needed in order to prove well-posedness, average grey value invariance, causality in terms of an extremum principle and Lyapunov functionals, and convergence to a constant steady-state [423].

We observe that the requirements belong to five categories: smoothness, symmetry, conservation, nonnegativity and connectivity requirements. These criteria are easy to check for many discretizations. In particular, it turns out that suitable explicit and semi-implicit finite difference discretizations of many discussed models create discrete scale-spaces. The discrete nonlinear scale-space concept has also led to the development of fast novel schemes, which are based on an *additive operator splitting (AOS)* [424, 430]. Under typical accuracy requirements, they are about 10 times more efficient than the widely used explicit schemes, and a speed-up by another order of magnitude can be achieved by a parallel implementation [431]. A general framework for AOS schemes will be presented in Section 4.4.2.

1.3.6   Applications

Nonlinear diffusion filters have been applied for postprocessing fluctuating data [269, 415], for visualizing quality-relevant features in computer aided quality control [299, 413, 418], and for enhancing textures such as fingerprints [418]. They have proved to be useful for improving subsampling [144] and line detection [156, 418], for blind image restoration [445], for scale-space based segmentation algorithms

[307, 308], for segmentation of textures [433, 437] and remotely sensed data [6, 5], and for target tracking in infrared images [65]. Most applications, however, are concerned with the filtering of medical images [26, 28, 29, 155, 244, 248, 264, 270, 308, 321, 355, 386, 393, 431, 434, 437, 444]. Some of these applications will be investigated in more detail in Chapter 5.

Besides such specific problem solutions, nonlinear diffusion filters can be found in commercial software packages such as the medical visualization tool Analyze.[12]

1.4 Methods of diffusion–reaction type

This section investigates variational frameworks, in which diffusion–reaction equations or coupled systems of them are interpreted as steepest descent minimizers of suitable energy functionals. This idea connects diffusion methods to edge detection and segmentation ideas.

Besides the variational interpretation there exist other interesting theoretical frameworks for diffusion filters such as the Markov random field and mean field annealing context [152, 153, 247, 251, 328, 387], robust statistics [41], and deterministic interactive particle models [279]. Their discussion, however, would lead us beyond the scope of this book.

1.4.1 Single diffusion–reaction equations

Nordström [311] has suggested to obtain a reconstruction u of a degraded image f by minimizing the energy functional

$$E_f(u, w) := \int_\Omega \left(\beta \cdot (u - f)^2 + w \cdot |\nabla u|^2 + \lambda^2 \cdot (w - \ln w) \right) dx. \tag{1.52}$$

The parameters β and λ are positive weights and $w : \Omega \to [0, 1]$ gives a fuzzy edge representation: in the interior of a region, w approaches 1 while at edges, w is close to 0 (as we shall see below).

The first summand of E punishes deviations of u from f *(deviation cost)*, the second term detects unsmoothness of u within each region *(stabilizing cost)*, and the last one measures the extend of edges *(edge cost)*. Cost terms of these three types are typical for variational image restoration methods.

The corresponding Euler equations to this energy functional are given by

$$0 = \beta \cdot (u - f) - \operatorname{div}(w \nabla u), \tag{1.53}$$

$$0 = \lambda^2 \cdot (1 - \tfrac{1}{w}) + |\nabla u|^2, \tag{1.54}$$

---

[12]Analyze is a registered trademark of Mayo Medical Ventures, 200 First Street SW, Rochester, MN 55905, U.S.A.

equipped with a homogeneous Neumann boundary condition for u.

Solving (1.54) for w gives

$$w = \frac{1}{1 + |\nabla u|^2/\lambda^2}. \qquad (1.55)$$

We recognize that w is identical with the Perona–Malik diffusivity $g(|\nabla u|^2)$ introduced in (1.32). Therefore, (1.53) can be regarded as the steady-state equation of

$$\partial_t u = \mathrm{div}\,(g(|\nabla u|^2)\,\nabla u) + \beta(f - u). \qquad (1.56)$$

This equation can also be obtained directly as the descent method of the functional

$$F_f(u) := \int\limits_\Omega \left(\beta \cdot (u - f)^2 \,+\, \lambda^2 \cdot \ln\left(1 + \tfrac{|\nabla u|^2}{\lambda^2}\right)\right) dx. \qquad (1.57)$$

The diffusion–reaction equation (1.56) consists of the Perona–Malik process with an additional bias term $\beta \cdot (f - u)$. One of Nordström's motivations for introducing this term was to free the user from the difficulty of specifying an appropriate stopping time for the Perona–Malik process.

However, it is evident that the Nordström model just shifts the problem of specifying a stopping time T to the problem of determining β. So it seems to be a matter of taste which formulation is preferred. People interested in image restoration usually prefer the reaction term, while for scale-space researchers it is more natural to have a constant steady-state as the simplest image representation.

Nordström's method may suffer from the same ill-posedness problems as the underlying Perona–Malik equation, and it is not hard to verify that the energy functional (1.57) is nonconvex. Therefore, it can possess numerous local minima, and the process (1.56) with f as initial condition does not necessarily converge to a global minimum. Similar difficulties may also arise in other diffusion–reaction models, where convergence results have not yet been established [152, 186].

A popular possibility to avoid these ill-posedness and convergence problems is to renounce edge-enhancing diffusivities in order to end up with (nonquadratic) convex functionals [43, 88, 110, 367, 391]. In this case the frameworks of convex optimization and monotone operators are applicable, ensuring well-posedness and stability of a standard finite-element approximation [367].

Diffusion–reaction approaches have been applied to edge detection [367, 391], to the restoration of inverse scattering images [263], to SPECT [88] and vascular reconstruction in medical imaging [102, 325], and to optic flow [368, 111] and stereo problems [343]. They can be extended to vector-valued images [369] and to corner-preserving smoothing of curves [136, 323]. Diffusion–reaction methods with constant diffusivities have also been used for local contrast normalization in images [330].

1.4.2 Coupled systems of diffusion–reaction equations

Mumford and Shah [295, 296] have proposed to obtain a segmented image u from f by minimizing the functional

$$E_f(u, K) = \beta \int_\Omega (u-f)^2 \, dx \; + \int_{\Omega \setminus K} |\nabla u|^2 \, dx \; + \; \alpha |K| \qquad (1.58)$$

with nonnegative parameters α and β. The discontinuity set K consists of the edges, and its one-dimensional Hausdorff measure $|K|$ gives the total edge length. Like the Nordström functional (1.52), this expression consists of three cost terms: the first one is the deviation cost, the second one gives the stabilizing cost, and the third one represents the edge cost.

The Mumford–Shah functional can be regarded as a continuous version of the Markov random field method of Geman and Geman [154] and the weak membrane model of Blake and Zisserman [42]. Related approaches are also used to model materials with two phases and a free interface.

The fact that (1.58) leads to a free discontinuity problem causes many challenging theoretical questions [249]. The book of Morel and Solimini [292] covers a very detailed analysis of this functional. Although the existence of a global minimizer with a closed edge set K has been established [108, 17], uniqueness is in general not true [292, pp. 197–198]. Regularity results for K in terms of (at least) C^1-arcs have recently been obtained [18, 19, 20, 48, 49, 107].

The concept of energy functionals for segmenting images offers the practical advantage that it provides a framework for comparing the quality of two segmentations. On the other hand, (1.58) exhibits also some shortcomings, e.g. the problem that sigmoid-like edges produce multiple segmentation boundaries *(over-segmentation, staircasing effect)* [377]. Another drawback results from the fact that the Mumford–Shah functional allows only singularities which are typical for minimal surfaces: Corners or T-junctions are not possible and segments meet at triple points with 120° angle [296]. In order to avoid such problems, modifications of the Mumford–Shah functional have been proposed by Shah [379]. An affine invariant generalization of (1.58) is investigated in [32, 31] and applied to affine invariant texture segmentation [31, 33], and a Mumford–Shah functional for curves can be found in [323].

Since many algorithms in image processing can be restated as versions of the Mumford–Shah functional [292] and since it is a prototype of a free discontinuity problem it is instructive to study this variational problem in more detail.

Numerical complications arise from the fact that the Mumford–Shah functional has numerous local minima. Global minimizers such as the simulated annealing method used by Geman and Geman [154] are extremely slow. Hence, one searches for fast (suboptimal) deterministic strategies, e.g. pyramidal region-growing algorithms [3, 239].

Another important class of numerical methods is based on the idea to approximate the discontinuity set K by a smooth function w, which is close to 0 near edges of u and which approximates 1 elsewhere.

We may for instance study the functional

$$F_f(u, w) := \int_\Omega \left(\beta \cdot (u - f)^2 + w^2 \cdot |\nabla u|^2 + \alpha \cdot \left(c|\nabla w|^2 + \tfrac{(1-w)^2}{4c} \right) \right) dx \qquad (1.59)$$

with a positive parameter c specifying the "edge width". Ambrosio and Tortorelli proved that this functional converges to the Mumford–Shah functional for $c \to 0$ (in the sense of Γ-convergence, see [22] for more details).

Minimizing F_f corresponds to the gradient descent equations

$$\partial_t u \;=\; \text{div}\,(w^2 \nabla u) + \beta \cdot (f - u), \qquad\qquad (1.60)$$
$$\partial_t w \;=\; c\Delta w - \tfrac{w}{\alpha}|\nabla u|^2 + \tfrac{(1-w)}{4c} \qquad\qquad (1.61)$$

with homogeneous Neumann boundary conditions. Equations of this type are investigated by Richardson and Mitter [341]. Since (1.60) resembles the Nordström process (1.56), similar problems can arise: The functional F_f is not jointly convex in u and v, so it may have many local minima and a gradient descent algorithm may get trapped in a poor local minimum. Well-posedness results for this system have not been obtained up to now, but a maximum–minimum principle and a local stability proof have been established.

Another diffusion–reaction system is studied by Shah [375, 376]. He replaces the functional (1.58) by two coupled convex energy functionals and applies gradient descent. This results in finding an equilibrium state between two competing processes. Experiments indicate that it converges to a stable solution. Proesmans et al. [337, 336] observed that this solution looks fairly blurred since the equations contain diffusion terms such as Δu. They obtained pronounced edges by replacing such a term by its Perona–Malik counterpart $\text{div}\,(g(|\nabla u|^2)\,\nabla u)$. Related equations are also studied in [398]. Of course, this approach gives rise to the same theoretical questions as (1.60), (1.61).

The system of Richardson and Mitter is used for edge detection [341]. Shah investigates diffusion–reaction systems for matching stereo images [378], while Proesmans et al. apply coupled diffusion-reaction equations to image sequence analysis, vector-valued images and stereo vision [336, 338]. Their finite difference algorithms run on a parallel transputer network.

It should also be mentioned that there exist reaction–diffusion systems which have been applied to image restoration [334, 335, 382], texture generation [406, 440] and halftoning [382], and which are not connected to Perona–Malik or Mumford–Shah ideas. They are based on Turing's pattern formation model [405].

1.5 Classic morphological processes

Morphology is an approach to image analysis based on shapes. Its mathematical formalization goes back to the group around Matheron and Serra, both working at ENS des Mines de Paris in Fontainebleau. The theory had first been developed for binary images, afterwards it was extended to grey-scale images by regarding level sets as shapes. Its applications cover biology, medical diagnostics, histology, quality control, radar and remote sensing, science of material, mineralogy, and many others.

Morphology is usually described in terms of algebraic set theory, see e.g. [280, 371, 181, 184] for an overview. Nevertheless, PDE formulations for classic morphological processes have been discovered recently by Brockett and Maragos [60], van den Boomgaard [50], Arehart et al. [25] and Alvarez et al. [12].

This section surveys the basic ideas and elementary operations of binary and grey-scale morphology, presents its PDE representations for images and curves, and summarizes the results concerning well-posedness and scale-space properties. Afterwards numerical aspects of the PDE formulation of these processes are discussed, and generalizations are sketched which comprise the morphological equivalent of Gaussian scale-space.

1.5.1 Binary and grey-scale morphology

Binary morphology considers *shapes (silhouettes)*, i.e. closed sets $X \subset \mathbb{R}^2$ whose boundaries are Jordan curves [16]. Henceforth, we identify a shape X with its characteristic function

$$\chi(x) := \begin{cases} 1 & \text{if } x \in X, \\ 0 & \text{else.} \end{cases} \tag{1.62}$$

Binary morphological operations affect only the boundary curve of the shape and, therefore, they can be viewed as curve or shape deformations.

Grey-scale morphology generalizes these ideas [274] by decomposing an image f into its level sets $\{X_a f, \ a \in \mathbb{R}\}$, where

$$X_a f := \{x \in \mathbb{R}^2, \ f(x) \geq a\}. \tag{1.63}$$

A binary morphological operation A can be extended to some grey-scale image f by defining

$$X_a(Af) := A(X_a f) \quad \forall \, a \in \mathbb{R}. \tag{1.64}$$

We observe that for this type of morphological operations only grey-level sets matter. As a consequence, they are invariant under monotone grey-level rescalings. This *morphological invariance (grey-scale invariance)* is characteristic for all methods we shall study in Section 1.5 and 1.6, except for 1.5.6 and some modifications

in 1.6.5. It is a very desirable property in all cases where brightness changes of the illumination occur or where one wants to be independent of the specific contrast range of the camera. On the other hand, for applications like edge detection or image restoration, contrast provides important information which should be taken into account. Moreover, in some cases isolines may give inadequate information about the depicted physical object boundaries.

1.5.2   Basic operations

Classic morphology analyses a shape by matching it with a so-called *structuring element*, a bounded set $B \subset \mathbb{R}^2$. Typical shapes for B are discs, squares, or ellipses.

The two basic morphological operations, *dilation* and *erosion* with a structuring element B, are defined for a grey-scale image $f \in L^\infty(\mathbb{R}^2)$ by [60]

$$\text{dilation:} \qquad (f \oplus B)(x) := \sup\{f(x-y),\ y \in B\}, \qquad (1.65)$$

$$\text{erosion:} \qquad (f \ominus B)(x) := \inf\{f(x+y),\ y \in B\}. \qquad (1.66)$$

These names can be easily motivated when considering a shape in a binary image and a disc-shaped structuring element. In this case dilation blows up its boundaries, while erosion shrinks them.

Dilation and erosion form the basis for constructing other morphological processes, for instance *opening* and *closing:*

$$\text{opening:} \qquad (f \circ B)(x) := ((f \ominus B) \oplus B)(x), \qquad (1.67)$$

$$\text{closing:} \qquad (f \bullet B)(x) := ((f \oplus B) \ominus B)(x). \qquad (1.68)$$

In the preceding shape interpretation opening smoothes the shape by breaking narrow isthmuses and eliminating small islands, while closing smoothes by eliminating small holes, fusing narrow breaks and filling gaps at the contours [181].

1.5.3   Continuous-scale morphology

Let us consider a convex structuring element tB with a scaling parameter $t > 0$. Then, calculating $u(t) = f \oplus tB$ and $u(t) = f \ominus tB$, respectively[13], can be shown to be equivalent to solving

$$\partial_t u(x,t) = \sup_{y \in B} \langle y, \nabla u(x,t) \rangle, \qquad (1.69)$$

$$\partial_t u(x,t) = \inf_{y \in B} \langle y, \nabla u(x,t) \rangle. \qquad (1.70)$$

with f as initial condition [12, 360].

---

[13]Henceforth, we frequently use the simplified notation $u(t)$ instead of $u(.,t)$

By choosing e.g. $B := \{y \in \mathbb{R}^2,\ |y| \leq 1\}$ one obtains

$$\partial_t u = |\nabla u|, \tag{1.71}$$

$$\partial_t u = -|\nabla u|. \tag{1.72}$$

The solution $u(t)$ is the dilation (resp. erosion) of f with a disc of radius t and centre 0 as structuring element. Figure 5.5 (a) presents the temporal evolution of a test image under such a continuous-scale dilation.

Connection to curve evolution

Morphological PDEs such as (1.71) or (1.72) are closely related to shape and curve evolutions. This can be illustrated by considering a smooth Jordan curve $C : [0, 2\pi] \times [0, \infty) \rightarrow \mathbb{R}^2$,

$$C(p, t) = \begin{pmatrix} x_1(p, t) \\ x_2(p, t) \end{pmatrix} \tag{1.73}$$

where p is the parametrization and t is the evolution parameter. We assume that C evolves in outer normal direction n with speed β, which may be a function of its curvature $\kappa := \frac{\det(C_p, C_{pp})}{|C_p|^3}$:

$$\partial_t C = \beta(\kappa) \cdot n, \tag{1.74}$$

$$C(p, 0) = C_0(p). \tag{1.75}$$

One can embed the curve $C(p, t)$ in an image $u(x, t)$ in such a way that C is just a level curve of u. The corresponding evolution for u is given by [319, 362, 16]

$$\partial_t u = \beta(\text{curv}(u)) \cdot |\nabla u|. \tag{1.76}$$

where the curvature of u is

$$\text{curv}(u) := \text{div} \left(\frac{\nabla u}{|\nabla u|} \right). \tag{1.77}$$

Sometimes the image evolution (1.76) is called the *Eulerian formulation* of the curve evolution (1.74), because it is written in terms of a fixed coordinate system.

We observe that (1.71) and (1.72) correspond to the simple cases $\beta = \pm 1$. Hence, they describe the curve evolutions

$$\partial_t C = \pm n. \tag{1.78}$$

This equation moves level sets in normal direction with constant speed. Such a process is also named *grassfire flow* or *prairie flow*. It is closely related to the Huygens principle for wave propagation [25]. Its importance for shape analysis in biological vision has already been pointed out in the sixties by Blum [47]. He simulated grassfire flow by a self-constructed opticomechanical device.

1.5.4 Theoretical results

Equations such as (1.78) may develop singularities and intersections even for smooth initial data. Hence, concepts of jump conditions, entropy solutions, and shocks have to be applied to this shape evolution [228].

A suitable framework for the image evolution equation (1.76) is provided by the theory of viscosity solutions [103]. The advantage of this analysis is that it allows us to treat shapes with singularities such as corners, where the classical solution concept does not apply, but a unique weak solution in the viscosity sense still exists.

It can be shown [90, 129, 103], that for an initial value

$$f \in \mathrm{BUC}(\mathbb{R}^2) := \{\varphi \in L^\infty(\mathbb{R}^2) \mid \varphi \text{ is uniformly continuous on } \mathbb{R}^2\} \qquad (1.79)$$

the equations (1.69),(1.70) possess a unique global viscosity solution $u(x,t)$ which fulfils the maximum–minimum principle

$$\inf_{\mathbb{R}^2} f \ \leq \ u(x,t) \ \leq \ \sup_{\mathbb{R}^2} f \quad \text{on} \quad \mathbb{R}^2 \times [0,\infty). \qquad (1.80)$$

Moreover, it is L^∞-stable: for two different initial images f, g the corresponding solutions $u(t)$, $v(t)$ satisfy

$$\|u(t) - v(t)\|_{L^\infty(\mathbb{R}^2)} \ \leq \ \|f - g\|_{L^\infty(\mathbb{R}^2)}. \qquad (1.81)$$

1.5.5 Scale-space properties

Brockett and Maragos [60] pointed out that the convexity of B is sufficient to ensure the semigroup property of the corresponding dilations and erosions. This establishes an important architectural scale-space property.

Similar results have been found by van den Boomgaard and Smeulders [53]. Moreover, they conjecture a causality property where singularities play a role similar to zero-crossings in Gaussian scale-space.

Jackway and Deriche [206, 207] prove a causality theorem for the dilation–erosion scale-space, which is also based on local extrema instead of zero-crossings. They establish that under erosion the number of local minima is decreasing, while dilation reduces the number of local maxima. The location of these extrema is preserved during their whole lifetime.

A complete scale-space interpretation is due to Alvarez, Guichard, Lions and Morel [12]: They prove that under three architectural assumptions (semigroup property, locality and regularity), one smoothing axiom (comparison principle) and additional invariance requirements (grey-level shift invariance, invariance under rotations and translations, morphological invariance), a two-dimensional scale-space

equation has the following form:

$$\partial_t u = |\nabla u| \, F(t, \text{curv}(u)) \qquad (1.82)$$

Clearly, dilation and erosion belong to the class (1.82), thus being good candidates for morphological scale-spaces. Indeed, in [12] it is shown that the converse is true as well: all axioms that lead to (1.82) are fulfilled.[14]

1.5.6 Generalizations

It is possible to extend morphology with a structuring element to morphology with nonflat structuring functions. In this case we have to renounce invariance under monotone grey level transformations, but we gain an interesting insight into a process which has very much in common with Gaussian scale-space.

A dilation of an image f with a structuring function $b : \mathbb{R}^2 \to \mathbb{R}$ is defined as

$$(f \oplus b)(x) \; := \; \sup_{y \in \mathbb{R}^2} \{ f(x - y) + b(y) \}. \qquad (1.83)$$

This is a generalization of definition (1.65), since one can recover dilation with a structuring element B by considering the flat structuring function

$$b(x) \; := \; \begin{cases} 0 & (x \in B), \\ -\infty & (x \notin B). \end{cases} \qquad (1.84)$$

Van den Boomgaard [50, 51] and Jackway [206] proposed to dilate an image $f(x)$ with quadratic structuring functions of type

$$b(x, t) \; = \; -\frac{|x|^2}{4t} \qquad (t > 0). \qquad (1.85)$$

It can be shown [50, 53] that the result $u(x, t)$ is a weak solution of

$$\partial_t u \; = \; |\nabla u|^2, \qquad (1.86)$$
$$u(x, 0) \; = \; f(x). \qquad (1.87)$$

The temporal evolution of a test image under this process is illustrated in Figure 5.5 (b).

In analogy to the fact that Gaussian-type functions $k(x, t) = a \exp(\frac{|x|^2}{4t})$ are the only rotationally symmetric kernels which are separable with respect to convolution, van den Boomgaard proves that the quadratic structuring functions $b(x, t)$ are the only rotationally invariant structuring functions which are separable with respect to dilation [50, 51].

---

[14]Invariance under rotations is only satisfied for a disc centered in 0 as structuring element.

A useful tool for understanding this similarity and many other analogies between morphology and linear systems theory is the *slope transform*. This generalization of the Legendre transform is the morphological equivalent of the Fourier transform. It has been discovered simultaneously by Dorst and van den Boomgaard [119] and by Maragos [275] in slightly differing formulations.

The close relation between (1.86) and Gaussian scale-space has also triggered Florack and Maas [142] to study a one-parameter family of isomorphisms of linear diffusion which reveals (1.86) as limiting case.

1.5.7   Numerical aspects

Dilations or erosions with quadratic structuring functions are separable and, thus, they can be implemented very efficiently by applying one-dimensional operations. A fast algorithm is described by van den Boomgaard [51].

For morphological operations with flat structuring elements, the situation is more complicated. Schemes for dilation or erosion which are based on *curve* evolution turn out be be difficult to handle: they require prohibitive small time steps, and suffer from the problem of coping with singularities and topological changes [319, 25, 360].

For this reason it is useful to discretize the corresponding *image* evolution equations. The widely-used *Osher–Sethian schemes* [319] are based on the idea to derive numerical methods for such equations from techniques for hyperbolic conservation laws. Overviews of these level set approaches and their various applications can be found in [372, 374].

To illustrate the basic idea with a simple example, let us restrict ourselves to the one-dimensional dilation equation $\partial_t u = |\partial_x u|$. A first-order upwind Osher–Sethian scheme for this process is given by

$$\frac{u_i^{n+1} - u_i^n}{\tau} \; = \; \sqrt{\left(\min\left(\frac{u_i^n - u_{i-1}^n}{h}, 0\right)\right)^2 + \left(\max\left(\frac{u_{i+1}^n - u_i^n}{h}, 0\right)\right)^2}, \qquad (1.88)$$

where h is the pixel size, τ is the time step size, and u_i^n denotes a discrete approximation of $u(ih, n\tau)$.

Level set methods possess two advantages over classical set-theoretic schemes for dilation/erosion [25, 360, 218, 66]:

(a) They give excellent results for non-digitally scalable structuring elements whose shapes cannot be represented correctly on a discrete grid, for instance discs or ellipses.

(b) The time t plays the role of a continuous scale parameter. Therefore, the size of a structuring element need not be multiples of the pixel size, and it is possible to get results with sub-pixel accuracy.

However, they reveal also two disadvantages:

(a) They are slower than set-theoretic morphological schemes.

(b) Dissipative effects such as blurring of discontinuities occur.

To address the first problem, speed-up techniques for shape evolution have been proposed which use only points close to the curve at every time step [8, 435, 373]. Blurring of discontinuities can be minimized by applying shock-capturing techniques such as high-order ENO[15] schemes [395, 385].

1.5.8 Applications

Continuous-scale morphology has been applied to shape-from-shading problems, gridless image halftoning, distance transformations, and skeletonization. Applications outside the field of image processing and computer vision include for instance shape offsets in CAD and path planning in robotics. Overviews and suitable references can be found in [233, 276].

1.6 Curvature-based morphological processes

Besides providing a useful reinterpretation of classic continuous-scale morphology, the PDE approach has led to the discovery of new morphological operators. These processes are curvature-based, and – although they cannot be written in conservation form – they reveal interesting relations to diffusion processes. Two important representatives of this class are mean curvature motion and its affine invariant counterpart. In this subsection we shall discuss these PDEs, possible generalizations, numerical aspects, and applications.

1.6.1 Mean-curvature filtering

In order to motivate our first curvature-based morphological PDE, let us recall that the linear diffusion equation (1.9) can be rewritten as

$$\partial_t u = \partial_{\eta\eta} u + \partial_{\xi\xi} u, \tag{1.89}$$

where the unit vectors η and ξ are parallel and perpendicular to ∇u, respectively. The first term on the right-hand side of (1.89) describes smoothing along the flowlines, while the second one smoothes along isophotes. When we want to smooth

---

[15]ENO means *essentially non-oscillatory*. By adapting the stencil for derivative approximations to the local smoothness of the solution, ENO schemes obtain both high-order accuracy in smooth regions and sharp shock transitions [183].

the image anisotropically along its isophotes, we can neglect the first term and end up with the problem

$$\partial_t u \;=\; \partial_{\xi\xi} u, \tag{1.90}$$
$$u(x,0) \;=\; f(x). \tag{1.91}$$

By straightforward calculations one verifies that (1.90) can also be written as

$$\partial_t u \;=\; \frac{u_{x_2}^2 u_{x_1 x_1} - 2 u_{x_1} u_{x_2} u_{x_1 x_2} + u_{x_1}^2 u_{x_2 x_2}}{u_{x_1}^2 + u_{x_2}^2} \tag{1.92}$$

$$\;=\; \Delta u - \frac{1}{|\nabla u|^2}\langle \nabla u, \mathrm{Hess}(u)\nabla u\rangle \tag{1.93}$$

$$\;=\; |\nabla u|\,\mathrm{curv}(u). \tag{1.94}$$

Since $\mathrm{curv}(u) = \mathrm{div}\left(\frac{\nabla u}{|\nabla u|}\right)$ is the curvature of u (mean curvature for dimensions ≥ 3), equation (1.94) is named *(mean) curvature motion (MCM)*. The corresponding curve evolution

$$\partial_t C(p,t) = \kappa(p,t) \cdot n(p,t) \tag{1.95}$$

shows that (1.90) propagates isophotes in inner normal direction with a velocity that is given by their curvature $\kappa = \frac{\det(C_p, C_{pp})}{|C_p|^3}$.

Processes of this type have first been studied by Brakke in 1978 [54]. They arise in flame propagation, crystal growth, the derivation of minimal surfaces, grid generation, and many other applications; see [372, 374] and the references therein for an overview. The importance of MCM in image processing became only recently clear: As nicely explained in a paper by Guichard and Morel [173], mean curvature motion can be regarded as the limit process when classic morphological operators such as median filtering are iteratively applied.

Figure 5.5 (c) and 5.11 (a) present examples for mean curvature filtering. Equation (1.95) is also called *geometric heat equation* or *Euclidean shortening flow*. The subsequent discussions shall clarify these names.

Intrinsic heat flow

Interestingly, there exists a further connection between linear diffusion and motion by curvature. Let $v(p,t)$ denote the *Euclidean arc-length* of $C(p,t)$, i.e.

$$v(p,t) := \int_0^p |C_\rho(\rho,t)|\, d\rho, \tag{1.96}$$

where $C_\rho := \partial_\rho C$. The Euclidean arc-length is characterized by $|C_v| = 1$. It is invariant under *Euclidean transformations*, i.e. mappings

$$x \;\rightarrow\; Rx + b \tag{1.97}$$

where $R \in \mathbb{R}^{2 \times 2}$ denotes a rotation matrix and $b \in \mathbb{R}^2$ is a translation vector. Since it is well-known from differential geometry (see e.g. [71], p. 14) that

$$\kappa(p,t) \cdot n(p,t) = \partial_{vv} C(p,t), \qquad (1.98)$$

we recognize that curvature motion can be regarded as Euclidean invariant diffusion of isophotes:

$$\partial_t C(p,t) = \partial_{vv} C(p,t). \qquad (1.99)$$

This *geometric heat equation* is intrinsic, since it is independent of the curve parametrization. However, the reader should be aware of the fact that – although this equation looks like a linear one-dimensional heat equation – it is in fact nonlinear, since the arc-length v is again a function of the curve.

Theoretical results

For the evolution of a smooth curve under its curvature, it has been shown in [188, 151, 169] that a smooth solution exists for some finite time interval $[0, T)$. A convex curve remains convex, a nonconvex one becomes convex and, for $t \to T$, the curve shrinks to a *circular point*, i.e. a point with a circle as limiting shape. Moreover, since under all flows $C_t = C_{qq}$ the Euclidean arc-length parametrization $q(p) := v(p)$ is the fastest way to shrink the Euclidean perimeter $\oint |C_p| \, dp$, equation (1.99) is called *Euclidean shortening flow* [150]. The time for shrinking a circle of radius σ to a point is given by

$$T = \tfrac{1}{2} \sigma^2. \qquad (1.100)$$

In analogy to the dilation/erosion case it can be shown that, for an initial image $f \in \mathrm{BUC}(\mathbb{R}^2)$, equation (1.90) has a unique viscosity solution which is L^∞-stable and satisfies a maximum–minimum principle [12].

Scale-space interpretation

A shape scale-space interpretation for curve evolution under Euclidean heat flow is studied by Kimia and Siddiqi [227]. It is based on results of Evans and Spruck [129]. They establish the semigroup property as architectural quality, and smoothing properties follow from the fact that the total curvature decreases. Moreover, the number of extrema and inflection points of the curvature is nonincreasing.

As an image evolution, MCM belongs to the class of morphological scale-spaces which satisfy the general axioms of Alvarez, Guichard, Lions and Morel [12], that have been mentioned in 1.5.5.

When studying the evolution of isophotes under MCM, it can be shown that, if one isophote is enclosed by another, this ordering is preserved [129, 227]. Such a *shape inclusion principle* implies in connection with (1.100) that it takes the time $T = \tfrac{1}{2} \sigma^2$ to remove all isophotes within a circle of radius σ. This shows that the

relation between temporal and spatial scale for MCM is the same as for linear diffusion filtering (cf. (1.14)).

Moreover, two level sets cannot move closer to one another than they were initially [129, 227]. Hence, contrast cannot be enhanced. This property is characteristic for all scale-spaces of the Alvarez–Guichard–Lions–Morel axiomatic and distinguishes them from nonlinear diffusion filters.

1.6.2   Affine invariant filtering

Motivation

Although Euclidean invariant smoothing methods are sufficient in many applications, there exist certain problems which also require invariance with respect to affine transformations. A *(full) affine transformation* is a mapping

$$x \;\rightarrow\; Ax + b \tag{1.101}$$

where $b \in \mathbb{R}^2$ denotes a translation vector and the matrix $A \in \mathbb{R}^{2\times2}$ is invertible. Affine transformations arise as shape distortions of planar objects when being observed from a large distance under different angles.

Affine invariant intrinsic diffusion

In analogy to the Euclidean invariant heat flow, Sapiro and Tannenbaum [362, 363] constructed an affine invariant flow by replacing the Euclidean arc-length $v(p,t)$ in (1.99) by an "arc-length" $s(p,t)$ that is invariant with respect to affine transformations with $\det(A) = 1$.

Such an affine arc-length was proposed by Blaschke [44, pp. 12–15] in 1923. It is characterized by $\det(C_s, C_{ss}){=}1$, and it can be calculated as

$$s(p,t) \;:=\; \int\limits_0^p \Big(\det \big(C_\rho(\rho,t),\, C_{\rho\rho}(\rho,t) \big) \Big)^{\frac{1}{3}} d\rho. \tag{1.102}$$

By virtue of

$$\partial_{ss} C(p,t) = \big(\kappa(p,t) \big)^{\frac{1}{3}} \cdot n(p,t) \tag{1.103}$$

we obtain the *affine invariant heat flow*

$$\partial_t C(p,t) \;=\; \big(\kappa(p,t) \big)^{\frac{1}{3}} \cdot n(p,t), \tag{1.104}$$
$$C(p,0) \;=\; C_0(p). \tag{1.105}$$

Affine invariant image evolution

When regarding the curve $C(p,t)$ as a level-line of an image $u(x,t)$, we end up with the evolution equation

$$\partial_t u \;=\; |\nabla u| \left(\mathrm{curv}(u) \right)^{\frac{1}{3}} \tag{1.106}$$

$$=\; \left(u_{x_2}^2 u_{x_1 x_1} - 2 u_{x_1} u_{x_2} u_{x_1 x_2} + u_{x_1}^2 u_{x_2 x_2} \right)^{\frac{1}{3}} \tag{1.107}$$

$$=\; |\nabla u|^{\frac{2}{3}} u_{\xi\xi}^{\frac{1}{3}}, \tag{1.108}$$

where ξ is the direction perpendicular to ∇u. The temporal evolution of an image under such an evolution resembles mean curvature motion; see Fig. 5.6(a).

Besides the name *affine invariant heat flow*, this equation is also called *affine shortening flow, affine morphological scale-space (AMSS)*, and *fundamental equation in image processing*.

This image evolution equation has been discovered independently of and simultaneously with the curve evolution approach of Sapiro and Tannenbaum by Alvarez, Guichard, Lions and Morel [12] via an axiomatic scale-space approach. After having mentioned some theoretical results, we shall briefly sketch this reasoning below.

Theoretical results

The curve evolution properties of affine invariant heat flow can be shown to be the same as in the Euclidean invariant case, with three exceptions [363]:

(a) Closed curves shrink to points with an ellipse as limiting shape (*elliptical points*).

(b) The name *affine shortening flow* reflects the fact that, under all flows $C_t = C_{qq}$, the affine arc-length parametrization $q(p) := s(p)$ is the fastest way to shrink the affine perimeter

$$L(t) \;:=\; \oint \left(\det \left(C_p(p,t), C_{pp}(p,t) \right) \right)^{\frac{1}{3}} dp. \tag{1.109}$$

(c) The time for shrinking a circle of radius σ to a point is

$$T = \tfrac{3}{4}\, \sigma^{\frac{4}{3}}. \tag{1.110}$$

For the image evolution equation (1.106) we have the same results as for MCM and dilation/erosion concerning well-posedness of a viscosity solution which satisfies a maximum–minimum principle [12].

Scale-space properties

Alvarez, Guichard, Lions and Morel [12] proved that (1.106) is unique (up to temporal rescalings) when imposing on the scale-space axioms for (1.82) an additional *affine invariance axiom*:

> *For every invertible $A \in \mathbb{R}^{2 \times 2}$ and for all $t \geq 0$, there exists a rescaled time $t'(t, A) \geq 0$, such that*

$$T_t(Af) = A(T_{t'}f) \quad \forall f \in \text{BUC}(\mathbb{R}^2). \qquad (1.111)$$

For this reason they call the AMSS equation also *fundamental equation in image analysis*. Simplifications of this axiomatic and related axioms for shape scale-spaces can be found in [16].

The scale-space reasoning of Sapiro and Tannenbaum investigates properties of the curve evolution, see [362] and the references therein. Based on results of [229, 24] they point out that the Euclidean absolute curvature decreases as well as the number of extrema and inflection points of curvature. Moreover, a shape inclusion principle holds.

1.6.3   Generalizations

In order to analyse planar shapes in a way that does not depend on their location in $\mathbb{R}^3$, one requires a multiscale analysis which is invariant under a general projective mapping

$$(x_1, x_2)^\top \ \rightarrow \ \left(\frac{a_{11}x_1 + a_{21}x_2 + a_{31}}{a_{13}x_1 + a_{23}x_2 + a_{33}}, \ \frac{a_{12}x_1 + a_{22}x_2 + a_{32}}{a_{13}x_1 + a_{23}x_2 + a_{33}} \right)^\top \qquad (1.112)$$

with $A = (a_{ij}) \in \mathbb{R}^{3 \times 3}$ and $\det A = 1$. Research in this direction has been carried out by Faugeras and Keriven [130, 131, 133], Bruckstein and Shaked [62], Olver et al. [314], and Dibos [112, 113]. It turns out that intrinsic heat-equation-like formulations for the projective group are more complicated than the Euclidean and affine invariant ones, and that there is some evidence that they do not reveal the same smoothing scale-space properties [314]. A study of heat flows which are invariant under subgroups of the projective group can be found in [314, 113].

An intrinsic heat flow for images painted on surfaces has been investigated by Kimmel [232]. It is invariant to the bending (isometric mapping) of the surface. This *geodesic curvature flow* and other evolutions, both for scalar and vector-valued images, can be regarded as steepest descent methods of energy functionals which have been proposed by Polyakov in the context of string theory [235].

Euclidean and affine invariant curve evolutions can also be modified in order to obtain area- or length-preserving equations [188, 150, 352, 366].

Recently it has been suggested to modify AMSS such that any evolution at T- or X-junctions of isophotes is inhibited [75]. Such a filtering intends to simplify the image while preserving its "semantical atoms" in the sense of Kanizsa [219].

Generalizations of MCM or AMSS to 3-D images are investigated in [91, 78, 298, 316]. In this case two principal curvatures occur. Since they can have different sign, the question arises of how to combine them to a process which simplifies arbitrary surfaces without creating singularities. In contrast to the 2-D situation, topological changes such as the splitting of conconvex structures may occur. This problem is reminiscent of the creation of new extrema in diffusion scale-spaces when going from 1-D to 2-D.

Affine scale-space axiomatics for image sequences (movies) have been established in [12, 287, 288], and possibilities to generalize the axiomatic of Alvarez, Guichard, Lions and Morel to colour images are discussed in [82].

1.6.4   Numerical aspects

Due to the equivalence between curve evolution and morphological image processing PDEs, we have three main classes of numerical methods: curve evolution schemes, set-theoretic morphological schemes and approximation schemes for the Eulerian formulation. A comparison of different methods of these classes can be found in [95].

Curve evolution schemes are investigated by Mokhtarian and Mackworth [291], Bruckstein et al. [61], Cohignac et al. [95], Merriman et al. [285], Ruuth [347], and Moisan [289]. In [61] discrete analogues of MCM and AMSS for the evolution of planar polygons are introduced. In complete analogy to the behaviour of the continuous equations, convergence to polygones, whose corners belong to circles and ellipses, respectively, is established. Related discrete curve evolutions are analysed in [135, 359]. Curve evolution schemes can reveal perfect affine invariance.

Convergent set-theoretic morphological schemes for MCM and AMSS have been proposed by Catté et al. [80, 79]. On the one hand, they are very fast and they are entirely invariant under monotone grey-scale transformations, on the other hand, it is difficult to find consistent approximations on a pixel grid which have good rotational invariance. This is essentially the same tradeoff as for circular structuring elements in classical set-theoretic morphology, cf. 1.5.7.

Most direct approximations of morphological image evolution equations are based on the Osher–Sethian schemes [319, 372, 374]. In the case of MCM or AMSS, this leads to an explicit finite difference method which approximates the spatial derivatives by central differences. Different variants of these schemes have been proposed in order to get better rotational invariance, higher stability or less dissipative effects [10, 15, 95, 267, 362]. A comparative evaluation of these approaches has been carried out by Lucido et al. [267]. Niessen et al. [305, 304] approximate

the spatial derivatives by Gaussian derivatives which are calculated in the Fourier domain.

Concerning stability one observes that all these explicit schemes can violate a discrete maximum–minimum principle and require small time steps to be experimentally stable. For AMSS an additional constraint appears: the behaviour of this equation is highly nonlocal, since affine invariance implies that circles are equivalent to ellipses of any arbitrary eccentricity. If one wants to have a good numerical approximation of affine invariance, one has to decrease the temporal step size significantly below the step size of experimental stability [16, 218]. Using Gaussian derivatives for MCM or AMSS permits larger time steps for large kernels [304], but their calculation in the Fourier domain is computationally expensive and aliasing may lead to oscillatory solutions, cf. 1.2.3.

One way to achieve unconditional L^∞-stability for MCM is to approximate $u_{\xi\xi}$ by suitable linear combinations of one-dimensional second-order derivatives along grid directions and to apply an implicit finite difference scheme [95, 13, 146]. Schemes of this type, however, renounce consistency with the original equation as well as rotational invariance: round shapes evolve into polygonal structures.

A consistent semi-implicit approximation of MCM which discretizes the first-order spatial derivatives explicitly and the second-order derivatives implicitly has been proposed by Alvarez [10]. In order to solve the resulting linear system of equations he applies symmetric Gauß–Seidel iterations.

Nicolet and Spühler [301] investigate a consistent fully implicit scheme for MCM leading to a nonlinear system of equations. It is solved by means of nonlinear Gauß–Seidel iterations. Comparing it with the explicit scheme they report a tradeoff between the larger time step size and the higher computational effort per step.

An inherent problem of all finite difference schemes for morphological image evolutions are their dissipative effects which create additional blurring of discontinuities. As a remedy, one can decompose the image into binary level sets, map them into Lipschitz-continuous images by applying a distance transformation, and run a finite difference method on them. Afterwards one extracts the processed level sets as the zero-level sets of the evolved images, and assembles the final image by superimposing all evolved level sets [75]. The natural price one has to pay for the excellent results is a fairly high computational effort.

A software package which contains implementations of MCM, AMSS and many other modern techniques such as wavelets, Mumford-Shah segmentation, and active contour models (cf. 1.6.6) is available under the name MegaWave2.[16]

---

[16]MegaWave2 has been developed by Jacques Froment and Sylvain Parrino, CEREMADE, University Paris IX, 75775 Paris Cedex 16, France. More information can be found under `http://www.ceremade.dauphine.fr`.

1.6.5   Applications

The special invariances of AMSS are useful for shape recognition tasks [12, 96, 97, 132], for corner detection [15], and for texture discrimination [265, 16]. MCM and AMSS have also been applied to denoising [305, 304] and blob detection [157, 301] in medical images and to terrain matching [268]. The potential of MCM for shape segmentation [290] has even been used for classifying chrysanthemum leaves [1].

If one aims to use these equations for image restoration one usually modifies them by multiplying them with a term that reduces smoothing at high-contrast edges [13, 364, 365, 304]; see also Fig. 5.6 (b). Adapting them to tasks such as texture enhancement requires more sophisticated and more global feature descriptors than the gradient, for instance an analysis by means of Gabor functions [72, 234]. Introducing a reaction term as in [102] allows to attract the solution to specified grey values which can be used as quantization levels [11]. Another modification results from omitting the factor $|\nabla u|$ in the mean curvature motion (1.94), see e.g. [126, 127]. This corresponds to nonlinear diffusion filters and a restoration method by total variation minimization [345] which shall be described in 1.7.2.

In order to improve images, MCM or AMSS have also been combined with other processes such as linear diffusion [13], shock filtering ([14], cf. 1.7.1) or global PDEs for histogramme enhancement [358].

Malladi and Sethian [272] propose to replace MCM by a technique in which the motion of level curves is based on either $\min(\kappa, 0)$ or $\max(\kappa, 0)$, depending on the average grey value within a certain neighbourhood. This so-called *min–max flow* produces a restored image as steady-state solution and reveals good denoising properties. Well-posedness results are not known up to now, since the theory of viscosity solutions is no longer applicable.

All these preceding modifications are at the expense of renouncing the morphological invariance of the genuine operators (and also affine invariance in the case of [364, 365, 304], unless an "affine invariant gradient" [231, 315] is used). If one wants to stay within the morphological framework one can combine different morphological processes, for instance MCM and dilation/erosion. This leads to a process which is useful for analysing components of shape [228, 230, 383, 384, 453], and which is called *entropy scale-space* or *reaction–diffusion scale-space*.

Recently Steiner et al. proposed a method for caricature-like shape exaggeration [394]. They evolved the boundary curve by means of a backward Euclidean shortening flow with a stabilizing bias term as in (1.56).

It is interesting to note that, already in 1965, Gabor – the inventor of optical holography and the so-called Gabor functions – proposed a deblurring algorithm based on combining MCM with backward smoothing along flowlines [149, 260]. This long-time forgotten method is similar to the Perona–Malik process (1.36) for large image gradients.

1.6.6   Active contour models

One of the main applications of curve evolution ideas appears in the context of *active contour models (deformable models).* 2-D versions are also called *snakes*, while 3-D active models are sometimes named *active surfaces* or *active blobs.* Active contour models can be used to search image features in an interactive way. Especially for assisting the segmentation of medical images they have become very popular [282]: The expert user gives a good initial guess of an interesting contour (organ, tumour, ...), which will be carried the rest of the way by some energy minimization. Apart from these practical merits, snake models incorporate many ideas ranging from energy minimization over curve evolution to the Perona–Malik filter and diffusion–reaction models. It is therefore not surprising that they play an important role in several generalization and unification attempts [356, 380, 452].

Explicit snakes

Kass, Witkin and Terzopoulos proposed the first active contour model in a journal paper in 1988 [221]. Their snakes can be thought of as an energy-minimizing spline, which is attracted by image features such as edges. For this reason, the energy functional consists of two parts: an internal energy fraction which controls the smoothness of the result, and an external energy term attracting the result to salient image features.

Such a snake is represented by a curve $C(s) = (x_1(s), x_2(s))^\top$ which minimizes the functional

$$E(C(s)) = \oint_{C(s)} \left(\tfrac{\alpha}{2} \, |C_s(s)|^2 + \tfrac{\beta}{2} \, |C_{ss}(s)|^2 - \gamma \, |\nabla f(C(s))|^2 \right) ds. \qquad (1.113)$$

The first summand is a membrane term causing the curve to shrink, the second one is a rigidity term which encourages a straight contour, and the third term pushes the contour to high gradients of the image f. We observe that terms 1 and 2 describe the internal energy, while the third one represents the external (image) energy. The nonnegative parameters α, β and γ serve as weights of these expressions. Since this model makes direct use of the snake contour, it is also called an explicit model.

Minimizing the functional (1.113) by steepest descent gives

$$\frac{\partial C}{\partial t} = \alpha C_{ss} - \beta C_{ssss} - \gamma \nabla(|\nabla f|^2), \qquad (1.114)$$

which can be approximated by finite differences. A 3-D version of such an active contour model is presented in [401].

Usually, the result will depend on the choice of the initial curve and a good segmentation requires an initial curve which is close to the final segment. The main

disadvantage of the preceding model is its topological rigidity: a classical explicit snake cannot split in order to segment several objects simultaneously[17]. In practice, it is also sometimes not easy to find a good balance between the parameters α, β and γ.

Implicit snakes

In 1993 some of the inherent difficulties of explicit snakes have been solved by replacing them by a so-called implicit model. It was discovered by Caselles, Catté, Coll and Dibos [73], and later on by Malladi, Sethian and Vemuri [273].

The idea behind implicit snakes is to embed the initial curve $C_0(s)$ as a zero level curve into a function $u_0 : \mathbb{R}^2 \to \mathbb{R}$, for instance by using the distance transformation. Then u_0 is evolved under a PDE which includes knowledge about the original image f:

$$\partial_t u \;=\; g(|\nabla f_\sigma|^2)\,|\nabla u|\,\left(\mathrm{div}\,\left(\frac{\nabla u}{|\nabla u|}\right) + \nu\right). \tag{1.115}$$

This evolution is stopped at some time T, when the process does hardly alter anymore, and the final contour C is extracted as the zero level curve of $u(x,T)$.

The terms in (1.115) have the following meaning:

- $|\nabla u|\,\mathrm{div}\,(\nabla u/|\nabla u|)$ is the curvature term of MCM which smoothes level sets; see (1.94).

- $\nu|\nabla u|$ describes motion in normal direction, i.e. dilation or erosion depending on the sign of ν. This so-called *balloon force* [93] is required for pushing a level set into concave regions, a compensation for the property of MCM to create convex regions.

- g is a stopping function such as the Perona–Malik diffusivity (1.32): it becomes small for large $|\nabla f_\sigma| = |\nabla K_\sigma * f|$. Hence, it slows down the snake as soon as it approaches significant edges of the original image f.

For this model Caselles et al. could prove well-posedness in the viscosity sense [73]. Whitaker and Chen developed similar implicit active contour models for 3-D images [436, 435], and Caselles and Coll investigated related approaches for image sequences [74].

An advantage of implicit snake models is their topological flexibility: The contour may split. This allows simultaneous segmentation of multiple objects. Moreover, they use essentially only one remaining parameter, the balloon force ν. On

---

[17]Recently McInerley and Terzopoulos have proposed modified explicit deformable models which allow topological changes [281, 283].

the other hand, the process does not really stop at the desired result, it only slows down, and it is difficult to interpret implicit snakes in terms of energy minimization. In order to address the initialization problem, Tek and Kimia use implicit active contours starting from randomly chosen seed points, both in 2-D [399] and in 3-D [400]. They name this technique *reaction–diffusion bubbles.*

Geodesic snakes

Geodesic snakes make a synthesis of explicit and implicit snake ideas. They have been proposed simultaneously by Caselles, Kimmel and Sapiro [76] and by Kichenassamy, Kumar, Olver, Tannenbaum and Yezzi [226]. These snakes replace the contour energy (1.113) by

$$E(C) = \oint_{C(s)} \left(\tfrac{\alpha}{2} |C_s(s)|^2 - \gamma\, g(|\nabla f_\sigma(C)|^2) \right) ds \qquad (1.116)$$

where g denotes again a Perona–Malik diffusivity of type (1.32). Under some additional assumptions they derive that minimizing (1.116) is equivalent to searching

$$\min_C \oint_{C(s)} g\big(|\nabla f_\sigma(C(s))|^2\big) |C_s(s)|\, ds. \qquad (1.117)$$

This is nothing else than finding a curve of minimal distance *(geodesic)* with respect to some image-induced metric. Embedding the initial curve as a level set of some image u_0 and applying a descent method to the corresponding Euler-Lagrange equation leads to the image evolution PDE

$$\partial_t u \;=\; |\nabla u|\, \mathrm{div}\left(g(|\nabla f_\sigma|^2)\, \frac{\nabla u}{|\nabla u|} \right). \qquad (1.118)$$

This active contour model is parameter-free, but often a speed term $\nu g(|\nabla f_\sigma|^2)|\nabla u|$ is added to achieve faster and more stable attraction to edges. A theoretical analysis of geodesic snakes concerning existence, uniqueness and stability of a viscosity solution can be found in [76, 226], and extensions to 3-D images are studied in [77, 226, 271]. Recently also an affine invariant analogue to geodesic active contours has been proposed [315]. Techniques which can be related to geodesic active contours have also been used for solving 3-D vision problems such as stereo [134] and motion analysis [322].

Self-snakes

The properties of geodesic snakes induced Sapiro to use a related technique for image enhancement [357]: he replaced $g(|\nabla f_\sigma|^2)$ in (1.118) by $g(|\nabla u_\sigma|^2)$. Then the

snake becomes a *self-snake* no longer underlying external image forces. For $\sigma = 0$ this gives

$$\partial_t u = |\nabla u| \operatorname{div}\left(g(|\nabla u|^2)\,\frac{\nabla u}{|\nabla u|}\right) \tag{1.119}$$

$$= g(|\nabla u|^2)\,u_{\xi\xi} + \nabla^\top\!\big(g(|\nabla u|^2)\big)\,\nabla u \tag{1.120}$$

with $\xi \perp \nabla u$. Although this equation cannot be cast in divergence form, we observe striking similarities with the Perona–Malik process from Section 1.3.1: the latter can be written as

$$\partial_t u = g(|\nabla u|^2)\,\Delta u + \nabla^\top\!\big(g(|\nabla u|^2)\big)\,\nabla u. \tag{1.121}$$

Thus, it cannot be excluded that a self-snake without spatial regularization reveals the same ill-posedness problems as the Perona–Malik filter [356]. For $\sigma > 0$, however, Chen, Vemuri and Wong [89] established existence and stability of a unique viscosity solution to a modified self-snake process. Their model contains a reaction term which inhibits smoothing at edges and keeps the filtered image u close to the original image f; cf. [380]. The restored image is given by the steady-state of

$$\partial_t u = |\nabla u| \operatorname{div}\left(g(|\nabla u_\sigma|^2)\,\frac{\nabla u}{|\nabla u|}\right) + \beta\,|\nabla u|\,(f-u) \qquad (\beta > 0). \tag{1.122}$$

The temporal evolution of a regularized self-snake without reaction term is depicted in Fig. 5.6(c). Generalizations of self-snakes to vector-valued images [357, 361] can be obtained using Di Zenzo's first fundamental form for colour images [114]; see also [414, 422] for related ideas.

1.7 Total variation methods

Inspired by observations from fluid dynamics where the *total variation (TV)*

$$TV(u) := \int\limits_\Omega |\nabla u|\,dx \tag{1.123}$$

plays an important role for shock calculations, one may ask if it is possible to apply related ideas to image processing. This would be useful to restore discontinuities such as edges.

Below we shall focus on two important TV-based image restoration techniques which have been pioneered by Osher and Rudin: TV-preserving methods and techniques which are TV-minimizing subject to certain constraints.[18]

---

[18]Another image enhancement method that is close in spirit is due to Eidelman, Grossmann and Friedman [125]. It maps the image grey values to gas dynamical parameters and solves the compressible Euler equations using shock-capturing total variation diminishing (TVD) techniques based on Godunov's method.

1.7.1   TV-preserving methods

In 1990 Osher and Rudin have proposed to restore blurred images by *shock filtering* [317]. These filters calculate the restored image as the steady-state solution of the problem

$$\partial_t u \;=\; -|\nabla u|\, F(\mathcal{L}(u)), \tag{1.124}$$
$$u(x,0) \;=\; f(x). \tag{1.125}$$

Here, $\operatorname{sgn}(F(u)) = \operatorname{sgn}(u)$, and $\mathcal{L}(u)$ is a second-order elliptic operator whose zero-crossings correspond to edges, e.g. the Laplacian $\mathcal{L}(u) = \Delta u$ or the second-order directional derivative $\mathcal{L}(u) = u_{\eta\eta}$ with $\eta \,\|\, \nabla u$.

By means of our knowledge from morphological processes, we recognize that this filter aims to produce a flow field that is directed from the interior of a region towards its edges where it develops shocks. Thus, the goal is to obtain a piecewise constant steady-state solution with discontinuities only at the edges of the initial image.

It has been shown that a one-dimensional version of this filter preserves the total variation and satisfies a maximum–minimum principle, both in the continuous and discrete case. For the two-dimensional case not many theoretical results are available except for a discrete maximum–minimum principle.

Recently van den Boomgaard [52] pointed out that the 1-D version of (1.124) with $F(u) := \operatorname{sgn}(u)$ arises as the PDE formulation of a classical image enhancement algorithm by Kramer and Bruckner [243]. Kramer and Bruckner proved in 1975 that their N-dimensional discrete scheme converges after a finite number of iterations to a state where each point is a local extremum.

Osher and Rudin have also proposed another TV-preserving deblurring technique [318]. It solves the linear diffusion equation backwards in time under the regularizing constraint that the total variation remains constant. This stabilization can be realized by keeping local extrema fixed during the whole evolution.

From a practical point of view, TV-preserving methods suffer from the problem that fluctuations due to noise do also create shocks. For this reason, Alvarez and Mazorra [14] replace the operator $\mathcal{L}(u) = u_{\eta\eta}$ in (1.124) by a Gaussian-smoothed version $\mathcal{L}(K_\sigma * u) = K_\sigma * u_{\eta\eta}$ and supplement the resulting equation with a noise-eliminating mean curvature process. They prove that their semi-implicit finite-difference scheme has a unique solution which satisfies a maximum–minimum principle.

1.7.2   TV-minimizing methods

Total variation is good for quantifying the simplicity of an image since it measures oscillations without unduly punishing discontinuities. For this reason, blocky

images (consisting only of a few almost piecewise constant segments) reveal very small total variation.

In order to restore noisy blocky images, Rudin, Osher and Fatemi [345] have proposed to minimize the total variation under constraints which reflect assumptions about noise.[19]

To fix ideas, let us study an example. Given an image f with additive noise of zero mean and known variance σ^2, we seek a restoration u satisfying

$$\min_u \int_\Omega |\nabla u| \, dx \tag{1.126}$$

subject to

$$\int_\Omega (u - f)^2 \, dx = \sigma^2, \tag{1.127}$$

$$\int_\Omega u \, dx = \int_\Omega f \, dx. \tag{1.128}$$

In order to solve this constrained variational problem, PDE methods can be applied: A solution of (1.126)–(1.128) verifies necessarily the Euler equation

$$\operatorname{div}\left(\frac{\nabla u}{|\nabla u|}\right) - \mu - \lambda(u - f) = 0 \tag{1.129}$$

with homogeneous Neumann boundary conditions. The (unknown) Lagrange multipliers μ and λ have to be determined in such a way that the constraints are fulfilled. Interestingly, (1.129) looks similar to the steady-state equation of the diffusion–reaction equation (1.56), but – in contrast to TV approaches – equation (1.56) is not intended to satisfy the noise constraint exactly [346]. Moreover, the divergence term in (1.129) is identical with the curvature, which relates TV-minimizing techniques to MCM.

In [345] a gradient descent method is proposed to solve (1.129). It uses an explicit finite difference scheme with central and one-sided spatial differences and adapts the Lagrange multiplier by means of the gradient projection method of Rosen.

One may also reformulate the constrained TV minimization as an unconstrained problem [83]: The penalized least square problem

$$\min_u \left(\frac{1}{2} \|u - f\|_{L^2(\Omega)}^2 + \alpha \int_\Omega |\nabla u| \, dx\right) \tag{1.130}$$

is equivalent to the constrained TV minimization, if α is related to the Lagrange multiplier λ via $\alpha = \frac{1}{\lambda}$.

---

[19]Related ideas have also been developed by Geman and Reynolds [153].

In recent years, problems of type (1.130) have attracted much interest from mathematicians working on inverse problems, optimization, or numerical analysis [2, 84, 85, 87, 115, 117, 118, 204, 205, 253, 409]. To overcome the problem that the total variation integral contains the nondifferentiable argument $|\nabla u|$, one applies regularization strategies or techniques from nonsmooth optimization. Much research is done in order to find efficient numerical methods for which convergence can be established.

TV-minimizing methods have been generalized in different ways:

- The constrained TV-minimization idea is frequently adapted to other constraints such as blur, noise with blur, or other types of noise [262, 344, 346, 116, 253, 410, 83]. Lions et al. [262] and Dobson and Santosa [115] have shown the existence of BV(Ω)-solutions for problems of this type. Recently, Chambolle and Lions [83] have extended the existence proof to noncompact operators (which comprises also the situation without blur), and they have established uniqueness.

- The tendency of TV-minimizing to create piecewise constant structures can cause undesired effects such as the creation of staircases at sigmoid-like edges [116, 83]. As a remedy, it has been proposed to minimize the L^1-norm of expressions containing also higher-order derivatives [344, 83]. Another possibility is to consider the constrained minimization of

$$B(u) \; := \; \int\limits_{\Omega} |\nabla u|^{p(|\nabla u|)} \, dx, \tag{1.131}$$

  where $p(|\nabla u|)$ decreases from 2 to 1, as $|\nabla u|$ ranges from 0 to ∞; see [46].

- TV-minimizing methods have also been used for estimating discontinuous blurring kernels such as motion or out-of-focus blur from a degraded image. This leads to TV-based blind deconvolution algorithms [86].

- They have been applied to colour images [45], where the generalized TV norm is chosen as the l^2-norm of the TV norms of the separate channels.

- Strong and Chan have identified the parameter α in (1.130) as a scale parameter [396]. By adapting α to the local image structure, they establish relations between TV-minimizing methods and nonlinear diffusion techniques [397].

Total variation methods have been applied to restoring images of military relevance [345, 346, 262, 253], to improving material from criminal and civil investigations as court evidence [344], and to enhancing pictures from confocal microscopy [409] and tomography [115, 396]. They are useful for enhancing reconstruction algorithms for inverse scattering problems [37], and the idea of L^1-norm minimization has also led to improved optic flow algorithms [245].

1.8 Conclusions and further scope of the book

Although we have seen that there exists a large variety of PDE-based scale-space and image restoration methods which offer many advantages, we have also become aware of some limitations. They shall serve as a motivation for the theory which will be explored in the subsequent chapters.

Linear diffusion and morphological scale-spaces are well-posed and have a solid axiomatic foundation. On the other hand, for some applications, they possess the undesirable property that they do not permit contrast enhancement and that they may blur and delocalize structures.

Pure restoration methods such as diffusion–reaction equations or TV-based techniques do allow contrast enhancement and lead to stable structures but can suffer from theoretical or practical problems, for instance unsolved well-posedness questions or the search for efficient minimizers of nonconvex or nondifferentiable functionals. Moreover, most image-enhancing PDE methods focus on edge detection and segmentation problems. Other interesting image restoration topics have found less attention.

For both scale-space and restoration methods many questions concerning their discrete realizations are still open: discrete scale-space results are frequently missing, minimization algorithms can get trapped in a poor local minimum, or the use of explicit schemes causes restrictive step size limitations.

The goal of the subsequent chapters is to develop a theory for nonlinear anisotropic diffusion filters which addresses some of the abovementioned shortcomings. In particular, we shall see that anisotropic nonlinear diffusion processes can share many advantages of the scale-space and the image enhancement world. A scale-space interpretation is presented which does not exclude contrast enhancement, and well-posedness results are established. Both scale-space and well-posedness properties carry over from the continuous to the semidiscrete and discrete setting. The latter comprises for instance semi-implicit techniques for which unconditional stability in the L^∞-norm is proved. The general framework, for which the results hold, includes also linear and isotropic nonlinear diffusion filters. Finally, specific anisotropic models are presented which permit applications beyond segmentation and edge enhancement tasks, for instance enhancement of coherent flow-like structures in textures.

Chapter 2

Continuous diffusion filtering

This chapter presents a general continuous model for anisotropic diffusion filters, analyses its theoretical properties and gives a scale-space interpretation. To this end, we adapt the diffusion process to the structure tensor, a well-known tool for analysing local orientation. Under fairly weak assumptions on the class of filters, it is possible to establish well-posedness and regularity results and to prove a maximum–minimum principle. Since the proof does not require any monotony assumption it applies also to contrast-enhancing diffusion processes. After sketching invariances of the resulting scale-space, we focus on analysing its smoothing properties. We shall see that, besides the extremum principle, a large class of associated Lyapunov functionals plays an important role in this context [414, 415].

2.1   Basic filter structure

Let us consider a rectangular image domain $\Omega := (0, a_1) \times (0, a_2)$ with boundary $\Gamma := \partial\Omega$ and let an image be represented by a mapping $f \in \mathrm{L}^\infty(\Omega)$. The class of anisotropic diffusion filters we are concerned with is represented by the initial boundary value problem

$$\partial_t u = \mathrm{div}\,(D\,\nabla u) \qquad \text{on} \qquad \Omega \times (0, \infty), \tag{2.1}$$

$$u(x, 0) = f(x) \qquad \text{on} \qquad \Omega, \tag{2.2}$$

$$\langle D\nabla u, \, n \rangle = 0 \qquad \text{on} \qquad \Gamma \times (0, \infty). \tag{2.3}$$

Hereby, n denotes the outer normal and $\langle ., . \rangle$ the Euclidean scalar product on $\mathrm{I\!R}^2$. In order to adapt the diffusion tensor $D \in \mathrm{I\!R}^{2\times 2}$ to the local image structure, one would usually let it depend on the edge estimator ∇u_σ (cf. 1.3.3), where

$$u_\sigma(x, t) := (K_\sigma * \tilde{u}(., t))(x) \qquad (\sigma > 0) \tag{2.4}$$

and $\tilde{u}$ denotes an extension of u from Ω to $\mathrm{I\!R}^2$, which may be obtained by mirroring at Γ (cf. [81]).

However, we shall choose a more general structure descriptor which comprises the edge detector ∇u_σ, but also allows to extract more information. This will be presented next.

2.2   The structure tensor

In order to identify features such as corners or to measure the local coherence of structures, we need methods which take into account how the orientation of the (smoothed) gradient changes within the vicinity of any investigated point.

The *structure tensor* – also called *interest operator*, *scatter matrix* or *(windowed second) moment tensor* – is an important representative of this class. Matrices of this type are useful for many different tasks, for instance for analysing flow-like textures [340, 31], corners and T-junctions [145, 182, 310, 309], shape cues [256, pp. 349–382] and spatio–temporal image sequences [209, pp. 147–153], [168, pp. 219–258]. Related approaches can also be found in [39, 40, 220]. Let us focus on some aspects which are of importance in our case.

In order to study orientations instead of directions, we have to identify gradients which differ only by their sign: they share the same orientation, but point in opposite directions. To this end, we reconsider the vector-valued structure descriptor ∇u_σ within a matrix framework. The matrix J_0 resulting from the tensor product

$$J_0(\nabla u_\sigma) := \nabla u_\sigma \otimes \nabla u_\sigma := \nabla u_\sigma \nabla u_\sigma^T \qquad (2.5)$$

has an orthonormal basis of eigenvectors v_1, v_2 with $v_1 \parallel \nabla u_\sigma$ and $v_2 \perp \nabla u_\sigma$. The corresponding eigenvalues $|\nabla u_\sigma|^2$ and 0 give just the contrast (the squared gradient) in the eigendirections.

Averaging this orientation information can be accomplished by convolving $J_0(\nabla u_\sigma)$ componentwise with a Gaussian K_ρ. This gives the structure tensor

$$J_\rho(\nabla u_\sigma) := K_\rho * (\nabla u_\sigma \otimes \nabla u_\sigma) \qquad (\rho \geq 0). \qquad (2.6)$$

It is not hard to verify that the symmetric matrix $J_\rho = \begin{pmatrix} j_{11} & j_{12} \\ j_{12} & j_{22} \end{pmatrix}$ is positive semidefinite and possesses orthonormal eigenvectors v_1, v_2 with

$$v_1 \parallel \begin{pmatrix} 2j_{12} \\ j_{22} - j_{11} + \sqrt{(j_{11}-j_{22})^2 + 4j_{12}^2} \end{pmatrix}. \qquad (2.7)$$

The corresponding eigenvalues μ_1 and μ_2 are given by

$$\mu_{1,2} = \frac{1}{2} \left(j_{11} + j_{22} \pm \sqrt{(j_{11}-j_{22})^2 + 4j_{12}^2} \right), \qquad (2.8)$$

where the $+$ sign belongs to μ_1. As they integrate the variation of the grey values within a neighbourhood of size $O(\rho)$, they describe the average contrast in the

eigendirections. Thus, the *integration scale* ρ should reflect the characteristic window size over which the orientation is to be analysed. Presmoothing in order to obtain ∇u_σ makes the structure tensor insensitive to noise and irrelevant details of scales smaller than $O(\sigma)$. The parameter σ is called *local scale* or *noise scale*.

By virtue of $\mu_1 \geq \mu_2 \geq 0$, we observe that v_1 is the orientation with the highest grey value fluctuations, and v_2 gives the preferred local orientation, the *coherence direction*. Furthermore, μ_1 and μ_2 can be used as descriptors of local structure: Constant areas are characterized by $\mu_1 = \mu_2 = 0$, straight edges give $\mu_1 \gg \mu_2 = 0$, corners can be identified by $\mu_1 \geq \mu_2 \gg 0$, and the expression

$$(\mu_1 - \mu_2)^2 = (j_{11} - j_{22})^2 + 4j_{12}^2 \qquad (2.9)$$

becomes large for anisotropic structures. It is a measure of the *local coherence*.

An example which illustrates the advantages of the structure tensor for analysing coherent patterns can be found in Figure 5.10 (d); see Section 5.2.

2.3   Theoretical results

In order to discuss well-posedness results, let us first recall some useful notations. Let $H^1(\Omega)$ be the Sobolev space of functions $u(x) \in L^2(\Omega)$ with all distributional derivatives of first order being in $L^2(\Omega)$. We equip $H^1(\Omega)$ with the norm

$$\|u\|_{H^1(\Omega)} := \left(\|u\|_{L^2(\Omega)}^2 + \sum_{i=1}^{2} \|\partial_{x_i} u\|_{L^2(\Omega)}^2 \right)^{1/2} \qquad (2.10)$$

and identify it with its dual space. Let $L^2(0, T; H^1(\Omega))$ be the space of functions u, strongly measurable on $[0, T]$ with range in $H^1(\Omega)$ (for the Lebesgue measure dt on $[0, T]$) such that

$$\|u\|_{L^2(0,T;H^1(\Omega))} := \left(\int_0^T \|u(t)\|_{H^1(\Omega)}^2 \, dt \right)^{1/2} < \infty. \qquad (2.11)$$

In a similar way, $C([0, T]; L^2(\Omega))$ is defined as the space of continuous functions $u : [0, T] \to L^2(\Omega)$ supplemented with the norm

$$\|u\|_{C([0,T];L^2(\Omega))} := \max_{[0,T]} \|u(t)\|_{L^2(\Omega)}. \qquad (2.12)$$

As usual, we denote by $C^p(X, Y)$ the set of C^p-mappings from X to Y.

Now we can give a precise formulation of the problem we are concerned with. We need the following prerequisites:

Assume that $f \in L^\infty(\Omega)$, $\rho \geq 0$, and $\sigma, T > 0$.
Let $a := \operatorname*{ess\,inf}_\Omega f$, $b := \operatorname*{ess\,sup}_\Omega f$, and consider the problem

$$\partial_t u = \operatorname{div}\left(D(J_\rho(\nabla u_\sigma))\,\nabla u\right) \qquad \text{on} \qquad \Omega \times (0, T],$$
$$u(x, 0) = f(x) \qquad \text{on} \qquad \Omega,$$
$$\langle D(J_\rho(\nabla u_\sigma))\nabla u,\, n \rangle = 0 \qquad \text{on} \qquad \Gamma \times (0, T],$$

where the diffusion tensor $D = (d_{ij})$ satisfies the following properties:

(C1) Smoothness:
  $D \in C^\infty(\mathbb{R}^{2\times 2}, \mathbb{R}^{2\times 2})$.

(C2) Symmetry:
  $d_{12}(J) = d_{21}(J)$ for all symmetric matrices $J \in \mathbb{R}^{2\times 2}$.

(C3) Uniform positive definiteness:
  For all $w \in L^\infty(\Omega, \mathbb{R}^2)$ with $|w(x)| \leq K$ on $\bar\Omega$, there exists a positive lower bound $\nu(K)$ for the eigenvalues of $D(J_\rho(w))$.

(P_c)

Under these assumptions the following theorem, which generalizes and extends results from [81, 414], can be proved.

Theorem 1 (Well-posedness,[1] regularity, extremum principle)
The problem (P_c) has a unique solution $u(x, t)$ in the distributional sense which satisfies

$$u \;\in\; C([0, T]; L^2(\Omega)) \,\cap\, L^2(0, T; H^1(\Omega)), \tag{2.13}$$
$$\partial_t u \;\in\; L^2(0, T; H^1(\Omega)). \tag{2.14}$$

Moreover, $u \in C^\infty(\bar\Omega \times (0, T])$. This solution depends continuously on f with respect to $\|\,.\,\|_{L^2(\Omega)}$, and it fulfils the extremum principle

$$a \leq u(x, t) \leq b \quad \text{on} \quad \Omega \times (0, T]. \tag{2.15}$$

---

[1] For a complete well-posedness proof one also has to establish stability with respect to perturbations of the diffusion equation. This topic will not be addressed here.

Proof:

(a) **Existence, uniqueness and regularity**

Existence, uniqueness and regularity are straightforward anisotropic extensions of the proof for the isotropic case studied by Catté, Lions, Morel and Coll [81]. Therefore, we just sketch the basic ideas of this proof.

Existence can be proved using Schauder's fixed point theorem. One considers the solution $U(w)$ of a distributional linear version of (P_c) where D depends on some function w instead of u. Then one shows that U is a weakly continuous mapping from a nonempty, convex and weakly compact subset W_0 of $W(0,T) := \left\{ w \in \mathrm{L}^2(0,T;\mathrm{H}^1(\Omega)), \frac{dw}{dt} \in \mathrm{L}^2(0,T;\mathrm{H}^1(\Omega)) \right\}$ into itself. Since $W(0,T)$ is contained in $\mathrm{L}^2(0,T;\mathrm{L}^2(\Omega))$, with compact inclusion, U reveals a fixed point $u \in W_0$, i.e. $u = U(u)$.

Smoothness follows from classical bootstrap arguments and the general theory of parabolic equations [246]. Since $u(t) \in \mathrm{H}^1(\Omega)$ for all $t > 0$, one deduces that $u(t) \in \mathrm{H}^2(\Omega)$ for all $t > 0$. By iterating, one can establish that u is a strong solution of (P_c) and $u \in \mathrm{C}^\infty((0,T] \times \bar{\Omega})$.

The basic idea of the uniqueness proof consists of using energy estimates for the difference of two solutions, such that the Gronwall–Bellman inequality can be applied. Then, uniqueness follows from the fact that both solutions start with the same initial values.

Finally an iterative linear scheme is investigated, whose solution is shown to converge in $\mathrm{C}([0,T];\mathrm{L}^2(\Omega))$ to the strong solution of (P_c).

(b) **Extremum principle**

In order to prove a maximum–minimum principle, we utilize Stampacchia's truncation method (cf. [58], p. 211).

We restrict ourselves to proving only the maximum principle. The minimum principle follows from the maximum principle when being applied to the initial datum $-f$.

Let $G \in \mathrm{C}^1(\mathbb{R})$ be a function with $G(s) = 0$ on $(-\infty, 0]$ and $0 < G'(s) \le C$ on $(0, \infty)$ for some constant C. Now, we define

$$H(s) := \int_0^s G(\sigma)\, d\sigma, \qquad s \in \mathbb{R},$$

$$\varphi(t) := \int_\Omega H(u(x,t) - b)\, dx, \qquad t \in [0,T].$$

By the Cauchy–Schwarz inequality, we have

$$\int_\Omega |G(u(x,t)-b)\, \partial_t u(x,t)|\, dx \le C \cdot \|u(t)-b\|_{\mathrm{L}^2(\Omega)} \cdot \|\partial_t u(t)\|_{\mathrm{L}^2(\Omega)}$$

and by virtue of (2.13), (2.14) we know that the right-hand side of this estimate exists. Therefore, φ is differentiable for $t > 0$, and we get

$$
\begin{aligned}
\frac{d\varphi}{dt} &= \int_\Omega G(u-b)\,\partial_t u\,dx \\[2mm]
&= \int_\Omega G(u-b)\,\operatorname{div}\left(D(J_\rho(\nabla u_\sigma))\,\nabla u\right)dx \\[2mm]
&= \int_\Gamma G(u-b)\,\underbrace{\langle D(J_\rho(\nabla u_\sigma))\,\nabla u, n\rangle}_{=0}\,dS \\[2mm]
&\quad - \int_\Omega \underbrace{G'(u-b)}_{\geq 0}\,\underbrace{\langle \nabla u, D(J_\rho(\nabla u_\sigma))\,\nabla u\rangle}_{\geq 0}\,dx \\[2mm]
&\leq \; 0. \hspace{6.5cm} (2.16)
\end{aligned}
$$

By means of $H(s) \leq \frac{C}{2}s^2$, we have

$$
0 \;\leq\; \varphi(t) \;\leq\; \int_\Omega H(u(x,t)-f(x))\,dx \;\leq\; \frac{C}{2}\,\|u(t)-f\|_{\mathrm{L}^2(\Omega)}^2. \qquad (2.17)
$$

Since $u \in \mathrm{C}([0,T];\mathrm{L}^2(\Omega))$, the right-hand side of (2.17) tends to $0 = \varphi(0)$ for $t \to 0^+$ which proves the continuity of $\varphi(t)$ in 0. Now from

$$
\varphi \in \mathrm{C}[0,T], \qquad \varphi(0) = 0, \qquad \varphi \geq 0 \quad \text{on} \quad [0,T]
$$

and (2.16), it follows that

$$
\varphi \equiv 0 \quad \text{on} \quad [0,T].
$$

Hence, for all $t \in [0,T]$, we obtain $u(x,t)-b \leq 0$ almost everywhere (a.e.) on Ω. Due to the smoothness of u for $t > 0$, we finally end up with the assertion

$$
u(x,t) \leq b \quad \text{on} \quad \bar\Omega \times (0,T].
$$

(c) **Continuous dependence on the initial image**
Let $f, h \in \mathrm{L}^\infty(\Omega)$ be two initial values and u, w the corresponding solutions. In the same way as in the uniqueness proof in [81], one shows that there exists some constant $c > 0$ such that

$$
\frac{d}{dt}\left(\|u(t)-w(t)\|_{\mathrm{L}^2(\Omega)}^2\right) \;\leq\; c \cdot \|\nabla u(t)\|_{\mathrm{L}^2(\Omega)}^2 \cdot \|u(t)-w(t)\|_{\mathrm{L}^2(\Omega)}^2.
$$

Applying the Gronwall–Bellman lemma [57, pp. 156–137] yields

$$
\|u(t)-w(t)\|_{\mathrm{L}^2(\Omega)}^2 \;\leq\; \|f-h\|_{\mathrm{L}^2(\Omega)}^2 \cdot \exp\left(c \cdot \int_0^t \|\nabla u(s)\|_{\mathrm{L}^2(\Omega)}^2\,ds\right).
$$

By means of the extremum principle we know that u is bounded on $\bar{\Omega} \times [0, T]$. Thus, ∇u_σ is also bounded, and prerequisite (C3) implies that there exists some constant $\nu = \nu(\sigma, \|f\|_{L^\infty(\Omega)}) > 0$, such that

$$
\begin{aligned}
& \int_0^t \|\nabla u(s)\|_{L^2(\Omega)}^2 \, ds \\
\leq\ & \int_0^T \|\nabla u(s)\|_{L^2(\Omega)}^2 \, ds \\
\leq\ & \frac{1}{\nu} \int_0^T \left| \int_\Omega \langle \nabla u(x, s), D(J_\rho(\nabla u_\sigma(x, s))) \nabla u(x, s) \rangle \, dx \right| ds \\
=\ & \frac{1}{\nu} \int_0^T \left| \int_\Omega u(x, s) \cdot \mathrm{div} \left(D(J_\rho(\nabla u_\sigma(x, s))) \nabla u(x, s) \right) dx \right| ds \\
\leq\ & \frac{1}{\nu} \int_0^T \|u(s)\|_{L^2(\Omega)} \|\partial_t u(s)\|_{L^2(\Omega)} \, ds \\
\leq\ & \frac{1}{\nu} \|u\|_{L^2(0,T;H^1(\Omega))} \|\partial_t u\|_{L^2(0,T;H^1(\Omega))}.
\end{aligned}
$$

By virtue of (2.13), (2.14), we know that the right-hand of this estimate exists. Now, let $\epsilon > 0$ and choose

$$
\delta\ :=\ \epsilon \cdot \exp\left(\frac{-c}{2\nu} \|u\|_{L^2(0,T;H^1(\Omega))} \|\partial_t u\|_{L^2(0,T;H^1(\Omega))} \right).
$$

Then for $\|f - h\|_{L^2(\Omega)} < \delta$, the preceding results imply

$$
\|u(t) - w(t)\|_{L^2(\Omega)} < \epsilon \qquad \forall\, t \in [0, T],
$$

which proves the continuous dependence on the initial data. $\qquad\square$

Remarks:

(a) We observe a strong smoothing effect which is characteristic for many diffusion processes: under fairly weak assumptions on the initial image ($f \in L^\infty(\Omega)$) we obtain an infinitely often differentiable solution for arbitrary small positive times. More restrictive requirements – for instance $f \in \mathrm{BUC}(\mathbb{R}^2)$ in order to apply the theory of viscosity solutions – are not necessary in our case.

(b) Moreover, our proof does not require any monotony assumption. This has the advantage that contrast-enhancing processes are permitted as well. Chapter 5 will illustrate this by presenting examples where contrast is enhanced.

(c) The continuous dependence of the solution on the initial image has significant practical impact as it ensures stability with respect to perturbations of the original image. This is of importance when considering stereo image pairs, spatio-temporal image sequences or slices from medical CT or MRI sequences, since we know that similar images remain similar after filtering.[2]

(d) The extremum principle offers the practical advantage that, if we start for instance with an image within the range $[0, 255]$, we will never obtain results with grey value such as 257. It is also closely related to smoothing scale-space properties, as we shall see in 2.4.2.

(e) The well-posedness results are essentially based on the fact that the regularization by convolution with a Gaussian allows to estimate $\|\nabla u_\sigma\|_{L^\infty(\Omega)}$ by $\|u\|_{L^\infty(\Omega)}$. This property is responsible for the uniform positive definiteness of the diffusion tensor.

2.4 Scale-space properties

Let us now investigate scale-space properties of the class (P_c) and juxtapose the results to other scale-spaces. To this end, we shall not focus on further investigations of architectural requirements like recursivity, regularity and locality, as these qualities do not distinguish nonlinear diffusion scale-spaces from other ones. We start with briefly discussing invariances. Afterwards, we turn to a more crucial task, namely the question in which sense our evolution equation – which may allow contrast enhancement – can still be considered as a smoothing, information-reducing image transformation.

2.4.1 Invariances

Let $u(x, t)$ be the unique solution of (P_c) and define the scale-space operator T_t by

$$T_t f := u(t), \qquad t \geq 0, \tag{2.18}$$

where $u(t) := u(., t)$.
The properties we discuss now illustrate that an invariance of T_t with respect to some image transformation P is characterized by the fact that T_t and P commute. Much of the terminology used below is borrowed from [12].

---

[2]This does not contradict contrast enhancement: In the case of two similar images, where one leads to contrast enhancement and the other not, the regularization damps the enhancement process in such a way that both images do not differ much after filtering.

Grey level shift invariance

Since the diffusion tensor is only a function of $J_\rho(\nabla u_\sigma)$, but not of u, we may shift the grey level range by an arbitrary constant C, and the filtered images will also be shifted by the same constant. Moreover, a constant function is not affected by diffusion filtering. Therefore, we have

$$
\begin{aligned}
T_t(0) &= 0, & (2.19)\\
T_t(f + C) &= T_t(f) + C & \forall\, t \ge 0. & (2.20)
\end{aligned}
$$

Reverse contrast invariance

From $D(J_\rho(-\nabla u_\sigma)) = D(J_\rho(\nabla u_\sigma))$, it follows that

$$
T_t(-f) = -T_t(f) \qquad \forall\, t \ge 0. \tag{2.21}
$$

This property is not fulfilled by classical morphological scale-space equations like dilation and erosion. When reversing the contrast, the role of dilation and erosion has to be exchanged as well.

Average grey level invariance

Average grey level invariance is a further property in which diffusion scale-spaces differ from morphological scale-spaces. In general, the evolution PDEs of the latter ones are not of divergence form and do not preserve the mean grey value. A constant average grey level is essential for scale-space based segmentation algorithms such as the hyperstack [307, 408]. It is also a desirable quality for applications in medical imaging where grey values measure physical qualities of the depicted object, for instance proton densities in MR images.

Proposition 1 (Conservation of average grey value).
The average grey level

$$
\mu := \frac{1}{|\Omega|} \int_\Omega f(x)\,dx \tag{2.22}
$$

is not affected by nonlinear diffusion filtering:

$$
\frac{1}{|\Omega|} \int_\Omega T_t f\,dx = \mu \qquad \forall\, t > 0. \tag{2.23}
$$

Proof:
Define $I(t) := \int_\Omega u(x,t)\,dx$ for all $t \ge 0$. Then the Cauchy–Schwarz inequality

implies

$$|I(t)-I(0)| \;=\; \left|\int_\Omega \big(u(x,t)-f(x)\big)\,dx\right| \;\le\; |\Omega|^{1/2}\,\|u(t)-f\|_{\mathrm{L}^2(\Omega)}.$$

Since $u \in \mathrm{C}([0,T];\mathrm{L}^2(\Omega))$, the preceding inequality gives the continuity of $I(t)$ in 0.

For $t > 0$, Theorem 1, the divergence theorem and the boundary conditions yield

$$\frac{dI}{dt} \;=\; \int_\Omega \partial_t u\,dx \;=\; \int_\Gamma \langle D(J_\rho(\nabla u_\sigma))\nabla u,\, n\rangle\,dS \;=\; 0.$$

Hence, $I(t)$ must be constant for all $t \ge 0$. $\qquad\qquad\qquad\qquad\qquad\Box$

Average grey level invariance may be described by commuting operators, when introducing an averaging operator $M : \mathrm{L}^1(\Omega) \to \mathrm{L}^1(\Omega)$ which maps f to a constant image with the same mean grey level:

$$(Mf)(y) := \frac{1}{|\Omega|}\int_\Omega f(x)\,dx \qquad \forall\,y \in \Omega. \tag{2.24}$$

Then Proposition 1 and grey level shift invariance imply that the order of M and T_t can be exchanged:

$$M(T_t f) = T_t(Mf) \qquad \forall\,t \ge 0. \tag{2.25}$$

When studying diffusion filtering as a pure initial value problem in the domain $\mathrm{I\!R}^2$, it also makes sense to investigate Euclidean transformations of an image. This leads us to translation and isometry invariance.

Translation invariance

Define a translation τ_h by $(\tau_h f)(x) := f(x+h)$. Then diffusion filtering fulfils

$$T_t(\tau_h f) = \tau_h(T_t f) \qquad \forall\,t \ge 0. \tag{2.26}$$

This is a consequence of the fact that the diffusion tensor depends on $J_\rho(\nabla u_\sigma)$ solely, but not explicitly on x.

Isometry invariance

Let $R \in \mathrm{I\!R}^{2\times 2}$ be an orthogonal transformation. If we apply R to f by defining $Rf(x) := f(Rx)$, then the eigenvalues of the diffusion tensor are unaltered and any eigenvector v is transformed into Rv. Thus, it makes no difference whether the orthogonal transformation is applied before or after diffusion filtering:

$$T_t(Rf) = R(T_t f) \qquad \forall\,t \ge 0. \tag{2.27}$$

2.4.2 Information-reducing properties

Nonenhancement of local extrema

Koenderink [240] required that a scale-space evolution should not create new level curves when increasing the scale parameter. If this is satisfied, iso-intensity linking through the scales is possible and a structure at a coarse scale can (in principle) be traced back to the original image *(causality)*. For this reason, he imposed that at spatial extrema with nonvanishing determinant of the Hessian isophotes in scale-space are upwards convex. He showed that this constraint can be written as

$$\text{sgn}(\partial_t u) = \text{sgn}(\Delta u). \tag{2.28}$$

A sufficient condition for the causality equation (2.28) to hold is requiring that local extrema with positive or negative definite Hessians are not enhanced: an extremum in ξ at time θ satisfies $\partial_t u > 0$ if ξ is a minimum, and $\partial_t u < 0$ if ξ is a maximum. This implication is easily seen: In the first case, for instance, the eigenvalues η_1, η_2 of the Hessian $\text{Hess}(u)$ are positive. Thus,

$$\Delta u \;=\; \text{trace}(\text{Hess}(u)) \;=\; \eta_1 + \eta_2 \;>\; 0, \tag{2.29}$$

giving immediately the causality requirement (2.28).

Nonenhancement of local extrema has first been used by Babaud et al. [30] in the context of linear diffusion filtering. However, it is also satisfied by nonlinear diffusion scale-spaces, as we shall see now.[3]

Theorem 2 (Nonenhancement of local extrema).
Let u be the unique solution of (P_c) and consider some $\theta > 0$. Suppose that $\xi \in \Omega$ is a local extremum of $u(.,\theta)$ with nonvanishing Hessian. Then,

$$\partial_t u(\xi,\theta) \;<\; 0, \qquad \text{if } \xi \text{ is a local maximum,} \tag{2.30}$$

$$\partial_t u(\xi,\theta) \;>\; 0, \qquad \text{if } \xi \text{ is a local minimum.} \tag{2.31}$$

Proof:
Let $D(J_\rho(\nabla u_\sigma)) =: (d_{ij}(J_\rho(\nabla u_\sigma)))$. Then we have

$$\partial_t u \;=\; \sum_{i=1}^{2}\sum_{j=1}^{2}\left(\partial_{x_i} d_{ij}(J_\rho(\nabla u_\sigma))\right)\partial_{x_j} u \;+\; \sum_{i=1}^{2}\sum_{j=1}^{2} d_{ij}(J_\rho(\nabla u_\sigma))\,\partial_{x_i x_j} u. \tag{2.32}$$

Since $\nabla u(\xi,\theta) = 0$ and $\partial_{x_i} d_{ij}(J_\rho(\nabla u_\sigma(\xi,\theta)))$ is bounded, the first term of the right-hand side of (2.32) vanishes in (ξ,θ).

---

[3]As in the linear diffusion case, nonenhancement of local extrema generally does not imply that their number is nonincreasing, cf. 1.2.5 and [342].

We know that the diffusion tensor $D := D(J_\rho(\nabla u_\sigma(\xi, \theta)))$ is positive definite. Hence, there exists an orthogonal matrix $S \in \mathbb{R}^{2 \times 2}$ such that

$$S^T D S = \mathrm{diag}(\lambda_1, \lambda_2) =: \Lambda$$

with λ_1, λ_2 being the positive eigenvalues of D.

Now, let us assume that (ξ, θ) is a local maximum where $H := \mathrm{Hess}(u(\xi, \theta))$ and, thus, $B := (b_{ij}) := S^T H S$ are negative definite. Then we have

$$b_{ii} < 0 \quad (i = 1, 2),$$

and by the invariance of the trace with respect to orthogonal transformations it follows that

$$
\begin{aligned}
\partial_t u(\xi, \theta) &= \mathrm{trace}\,(DH) \\
&= \mathrm{trace}\,(S^T D S\, S^T H S) \\
&= \mathrm{trace}\,(\Lambda B) \\
&= \sum_{i=1}^{2} \lambda_i\, b_{ii} \\
&< 0.
\end{aligned}
$$

If ξ is a local minimum of $u(x, \theta)$, one proceeds in the same way utilizing the positive definiteness of the Hessian. $\qquad \square$

Nonenhancement of local extrema distinguishes anisotropic diffusion from classical contrast enhancing methods such as high-frequency emphasis [163, pp. 182–183], which do violate this principle. Although possibly behaving like backward diffusion across edges, nonlinear diffusion is always in the forward region at extrema. This ensures its stability.

It should be noted that nonenhancement of local extrema is just one possibility to end up with Koenderink's causality requirement. Another way to establish causality is via the extremum principle (2.15) following Hummel's reasoning; see [189] for more details.

Lyapunov functionals and behaviour for $t \to \infty$

Since scale-spaces are intended to subsequently simplify an image, it is desirable that, for $t \to \infty$, we obtain the simplest possible image representation, namely a constant image with the same average grey value as the original one. The following theorem states that anisotropic diffusion filtering always leads to a constant steady-state. This is due to the class of Lyapunov functionals associated with the diffusion process.

Theorem 3 (Lyapunov functionals and behaviour for $t \to \infty$).
Suppose that u is the solution of (P_c) and let a, b, μ and M be defined as in (P_c), (2.22) and (2.24), respectively. Then the following properties are valid:

(a) (Lyapunov functionals)
  For all $r \in C^2[a, b]$ with $r'' \geq 0$ on $[a, b]$, the function

$$V(t) := \Phi(u(t)) := \int_\Omega r(u(x, t))\, dx \tag{2.33}$$

  is a Lyapunov functional:

  (i) $\Phi(u(t)) \geq \Phi(Mf)$ for all $t \geq 0$.

  (ii) $V \in C[0, \infty) \cap C^1(0, \infty)$ and $V'(t) \leq 0$ for all $t > 0$.

  Moreover, if $r'' > 0$ on $[a, b]$, then $V(t) = \Phi(u(t))$ is a strict Lyapunov functional:

  (iii) $\Phi(u(t)) = \Phi(Mf) \iff \begin{cases} u(t) = Mf & \text{on } \bar{\Omega} & \text{(if } t > 0) \\ u(t) = Mf & \text{a.e. on } \Omega & \text{(if } t = 0) \end{cases}$

  (iv)   If $t > 0$, then $V'(t) = 0$ if and only if $u(t) = Mf$ on $\bar{\Omega}$.

  (v) $V(0) = V(T) \quad$ for $T > 0 \quad \iff \begin{cases} f = Mf & \text{a.e. on } \Omega & \text{and} \\ u(t) = Mf & \text{on } \bar{\Omega} \times (0, T] \end{cases}$

(b) (Convergence)

  (i) $\lim\limits_{t \to \infty} \|u(t) - Mf\|_{L^p(\Omega)} = 0 \quad$ for $\quad p \in [1, \infty)$.

  (ii)   In the 1D case, the convergence $\lim\limits_{t \to \infty} u(x, t) = \mu$ is uniform on $\bar{\Omega}$.

Proof:

(a) (i) Since $r \in C^2[a, b]$ with $r'' \geq 0$ on $[a, b]$, we know that r is convex on $[a, b]$. Using the average grey level invariance and Jensen's inequality we obtain, for all $t \geq 0$,

$$\begin{aligned}
\Phi(Mf) &= \int_\Omega r\left(\frac{1}{|\Omega|} \int_\Omega u(x, t)\, dx\right) dy \\
&\leq \int_\Omega \left(\frac{1}{|\Omega|} \int_\Omega r(u(x, t))\, dx\right) dy \\
&= \int_\Omega r(u(x, t))\, dx \\
&= \Phi(u(t)). \tag{2.34}
\end{aligned}$$

(ii) Let us start by proving the continuity of $V(t)$ in 0. Thanks to the maximum–minimum principle, we may choose a constant

$$L := \max_{s \in [a,b]} |r'(s)|$$

such that for all $t > 0$, the Lipschitz condition

$$|r(u(x,t)) - r(f(x))| \leq L\,|u(x,t) - f(x)|$$

is verified a.e. on Ω. From this and the Cauchy–Schwarz inequality, we get

$$
\begin{aligned}
|V(t) - V(0)| &\leq |\Omega|^{1/2}\,\|r(u(t)) - r(f)\|_{L^2(\Omega)} \\
&\leq |\Omega|^{1/2}\,L\,\|u(t) - f\|_{L^2(\Omega)},
\end{aligned}
$$

and by virtue of $u \in C([0,T]; L^2(\Omega))$, the limit $t \to 0^+$ gives the announced continuity in 0.

By Theorem 1 and the boundedness of r' on $[a,b]$, we know that V is differentiable for $t > 0$ and $V'(t) = \int_\Omega r'(u)\,u_t\,dx$. Thus, the divergence theorem yields

$$
\begin{aligned}
V'(t) &= \int_\Omega r'(u)\,\mathrm{div}\,(D(J_\rho(\nabla u_\sigma))\nabla u)\,dx \\
&= \int_\Gamma r'(u)\,\underbrace{\langle D(J_\rho(\nabla u_\sigma))\nabla u, n\rangle}_{=0}\,dS \\
&\quad - \int_\Omega \underbrace{r''(u)}_{\geq 0}\,\underbrace{\langle \nabla u, D(J_\rho(\nabla u_\sigma))\nabla u\rangle}_{\geq 0}\,dx \\
&\leq 0.
\end{aligned}
$$

(iii) Let $\Phi(u(t)) = \Phi(Mf)$.

If $t > 0$, then $u(t)$ is continuous in $\bar{\Omega}$. Let us now show that equality in the estimate (2.34) implies that $u(t) = \mathrm{const.}$ on $\bar{\Omega}$. To this end, assume that u is not constant on $\bar{\Omega}$. Then, by the continuity of u, there exists a partition $\Omega = \Omega_1 \cup \Omega_2$ with $|\Omega_1|, |\Omega_2| \in (0, |\Omega|)$ and

$$\alpha := \frac{1}{|\Omega_1|}\int_{\Omega_1} u\,dx \neq \frac{1}{|\Omega_2|}\int_{\Omega_2} u\,dx =: \beta.$$

From $r'' > 0$ on $[a,b]$ it follows that r is strictly convex on $[a,b]$ and

$$r\left(\frac{1}{|\Omega|}\int_\Omega u\,dx\right) = r\left(\frac{|\Omega_1|}{|\Omega|}\alpha + \frac{|\Omega_2|}{|\Omega|}\beta\right)$$

$$< \quad \frac{|\Omega_1|}{|\Omega|} r(\alpha) + \frac{|\Omega_1|}{|\Omega|} r(\beta)$$

$$\leq \quad \frac{1}{|\Omega|} \int_{\Omega_1} r(u) \, dx + \frac{1}{|\Omega|} \int_{\Omega_2} r(u) \, dx$$

$$= \quad \frac{1}{|\Omega|} \int_{\Omega} r(u) \, dx.$$

If we utilize this result in the estimate (2.34) we observe that, for $t > 0$, $\Phi(u(t)) = \Phi(Mf)$ implies that $u(t) = $ const. on $\bar{\Omega}$. Thanks to the average grey value invariance we finally obtain $u(t) = Mf$ on $\bar{\Omega}$.

So let us turn to the case $t = 0$. From (i) and (ii), we conclude that $\Phi(u(\theta)) = \Phi(Mf)$ for all $\theta > 0$. Thus, we have $u(\theta) = Mf$ for all $\theta > 0$. For $\theta > 0$, the Cauchy–Schwarz inequality gives

$$\int_{\Omega} |u(x, \theta) - \mu| \, dx \leq |\Omega|^{1/2} \|u(\theta) - Mf\|_{\mathrm{L}^2(\Omega)} = 0.$$

Since $u \in \mathrm{C}([0, T]; \mathrm{L}^2(\Omega))$, the limit $\theta \to 0^+$ finally yields $u(0) = Mf$ a.e. on Ω.

Conversely, it is obvious that $u(t) = Mf$ (a.e.) on Ω implies $\Phi(u(t)) = \Phi(Mf)$.

(iv) Let $t > 0$ and $V'(t) = 0$. Then from

$$0 = V'(t) = -\int_{\Omega} \underbrace{r''(u(x, t))}_{>0} \langle \nabla u(x, t), D(J_\rho(\nabla u_\sigma(x, t)))\nabla u(x, t) \rangle \, dx$$

and the smoothness of u we obtain

$$\langle \nabla u, D(J_\rho(\nabla u_\sigma))\nabla u \rangle = 0 \quad \text{on } \bar{\Omega}.$$

By the uniform boundedness of D, there exists some constant $\nu > 0$, such that

$$\nu |\nabla u|^2 \leq \langle \nabla u, D(J_\rho(\nabla u_\sigma))\nabla u \rangle \quad \text{on } \bar{\Omega} \times (0, \infty).$$

Thus, we have $\nabla u(x, t) = 0$ a.e. on Ω. Due to the continuity of ∇u, this yields $u(x, t) = $ const. for all $x \in \Omega$, and the average grey level invariance finally gives $u(x, t) = \mu$ on Ω.

Conversely, let $u(x, t) = \mu$ on Ω. Then,

$$V'(t) = -\int_{\Omega} r''(u) \langle \nabla u, D(J_\rho(\nabla u_\sigma))\nabla u \rangle \, dx = 0.$$

(v) Suppose that $V(T) = V(0)$. Since V is decreasing, we have

$$V(t) = \text{const.} \qquad \text{on } [0, T].$$

Let $\epsilon > 0$. Then for any $t \in [\epsilon, T]$, we have $V'(t) = 0$, and part (iv) implies that $u(t) = Mf$ on Ω. Now, the Cauchy–Schwarz inequality gives

$$\int_\Omega |f - Mf| \, dx \;\leq\; |\Omega|^{1/2} \, \|f - u(t)\|_{\mathrm{L}^2(\Omega)}.$$

As $u \in \mathrm{C}([0, T]; \mathrm{L}^2(\Omega))$, the limit $t \to 0^+$ yields $f = Mf$ a.e. on Ω. Conversely, if $u(t) = Mf$ (a.e.) on Ω holds for all $t \in [0, T]$, it is evident that $V(0) = V(T)$.

(b) (i) By the grey level shift invariance we know that $v := u - Mf$ satisfies the diffusion equation as well. We multiply this equation by v, integrate, and use the divergence theorem to obtain

$$\int_\Omega v v_t \, dx \;=\; -\int_\Omega \langle \nabla v, D(J_\rho(\nabla v_\sigma)) \nabla v \rangle \, dx.$$

Since ∇v_σ is bounded, we find some $\nu > 0$ such that

$$\frac{1}{2} \frac{d}{dt} \left(\|v\|_{\mathrm{L}^2(\Omega)}^2 \right) \;\leq\; -\nu \, \|\nabla v\|_{\mathrm{L}^2(\Omega)}^2.$$

For $t > 0$, there exists some x_0 with $v(x_0) = 0$. Therefore, Poincaré's inequality (cf. [9, p. 122]) may be applied giving

$$\|v\|_{\mathrm{L}^2(\Omega)}^2 \;\leq\; C_0 \, \|\nabla v\|_{\mathrm{L}^2(\Omega)}^2$$

with some constant $C_0 = C_0(\Omega) > 0$. This yields

$$\frac{d}{dt} \|v\|_{\mathrm{L}^2(\Omega)}^2 \;\leq\; -2\nu \, C_0 \, \|v\|_{\mathrm{L}^2(\Omega)}^2$$

and hence the exponential decay of $\|v\|_{\mathrm{L}^2(\Omega)}$ to 0.

By the maximum principle, we know that $\|v(t)\|_{\mathrm{L}^\infty(\Omega)}$ is bounded by $\|f - Mf\|_{\mathrm{L}^\infty(\Omega)}$. Thus, for $q \in \mathbb{N}$, $q \geq 2$, we get

$$\|v(t)\|_{L^q(\Omega)}^q \;\leq\; \|f - Mf\|_{\mathrm{L}^\infty(\Omega)}^{q-2} \cdot \|v(t)\|_{\mathrm{L}^2(\Omega)}^2 \;\to\; 0,$$

and Hölder's inequality gives, for $1 \leq p < q < \infty$,

$$\|v(t)\|_{L^p(\Omega)} \;\leq\; |\Omega|^{(1/p)-(1/q)} \cdot \|v(t)\|_{L^q(\Omega)} \;\to\; 0.$$

This proves the assertion.

(ii) To prove uniform convergence in the one-dimensional setting, we can generalize and adapt methods from [202] to our case.

Let $\Omega = (0, a)$. From part (a) we know that $V(t) := \int_0^a u^2(x, t)\, dx$ is nonincreasing and bounded from below. Thus, the sequence $(V(i))_{i \in \mathbb{N}}$ converges.

Since $V \in \mathrm{C}[0, \infty) \cap \mathrm{C}^1(0, \infty)$ the mean value theorem implies

$$\exists\, t_i \in (i,\, i+1): \qquad V'(t_i) \;=\; V(i+1) - V(i).$$

Thus, $(t_i)_{i \in \mathbb{N}} \to \infty$ and from the convergence of $(V(i))_{i \in \mathbb{N}}$ it follows that

$$V'(t_i) \to 0. \tag{2.35}$$

Thanks to the uniform positive definiteness of D there exists some $\nu > 0$ such that, for $t > 0$,

$$
\begin{aligned}
V'(t) \;&=\; -2 \int_0^a u_x^2\, D(J_\rho(\partial_x u_\sigma))\, dx \\[6pt]
&\leq\; -2\nu \int_0^a u_x^2\, dx \\[6pt]
&\leq\; 0.
\end{aligned}
\tag{2.36}
$$

Equations (2.35) and (2.36) yield

$$\|u_x(t_i)\|_{\mathrm{L}^2(\Omega)} \to 0.$$

Hence, $u(t_i)$ is a bounded sequence in $\mathrm{H}^1(0, a)$. By virtue of the Rellich–Kondrachov theorem [7, p. 144] we know that the embedding from $\mathrm{H}^1(0, a)$ into $\mathrm{C}^{0,\alpha}[0, a]$, the space of Hölder-continuous functions on $[0, a]$ [7, pp. 9–12], is compact for $\alpha \in (0, \tfrac{1}{2})$. Therefore, there exists a subsequence $(t_{i_j}) \to \infty$ and some $\bar{u}$ with

$$u(t_{i_j}) \to \bar{u} \quad \text{in} \quad \mathrm{C}^{0,\alpha}[0, a].$$

This also gives $u(t_{i_j}) \to \bar{u}$ in $\mathrm{L}^2(0, a)$. Since we already know from (b)(i) that $u(t_{i_j}) \to Mf$ in $\mathrm{L}^2(0, a)$, it follows that $\bar{u} = Mf$. Hence,

$$\lim_{j \to \infty} \|u(t_{i_j}) - Mf\|_{\mathrm{L}^\infty(\Omega)} = 0. \tag{2.37}$$

Part (a) tells us that $\|u(t) - Mf\|_{\mathrm{L}^p(\Omega)}^p$ is a Lyapunov function for $p \geq 2$. Thus,

$$\|u(t) - Mf\|_{\mathrm{L}^\infty(\Omega)} = \lim_{p \to \infty} \|u(t) - Mf\|_{\mathrm{L}^p(\Omega)}$$

is also nonincreasing. Therefore, $\lim_{t\to\infty} \|u(t) - Mf\|_{\mathrm{L}^\infty(\Omega)}$ exists and from (2.37) we conclude that

$$\lim_{t\to\infty} \|u(t) - Mf\|_{\mathrm{L}^\infty(\Omega)} = 0.$$

The smoothness of u establishes finally that the convergence

$$\lim_{t\to\infty} u(x, t) = \mu$$

is uniform on $\bar{\Omega}$.   □

Since the class (P_c) does not forbid contrast enhancement it admits processes where forward diffusion has to compete with backward diffusion. Theorem 3 is of importance as it states that the regularization by convolving with K_σ tames the backward diffusion in such a way that forward diffusion wins in the long run. Moreover, the competition evolves in a certain direction all the time: although backward diffusion may be locally superior, the global result – denoted by the Lyapunov functional – becomes permanently better for forward diffusion.

Let us have a closer look at what might be the meaning of this global result in the context of image processing. Considering the Lyapunov functions associated with $r(s) := |s|^p$, $r(s) := (s - \mu)^{2n}$ and $r(s) := s \ln s$, respectively, the preceding theorem gives the following corollary.

Corollary 1 (Special Lyapunov functionals).
Let u be the solution of (P_c) and a and μ be defined as in (P_c) and (2.22). Then the following functions are decreasing for $t \in [0, \infty)$:

(a) $\|u(t)\|_{\mathrm{L}^p(\Omega)}$ *for all $p \geq 2$.*

(b) $M_{2n}[u(t)] \;:=\; \dfrac{1}{|\Omega|} \displaystyle\int_\Omega (u(x,t) - \mu)^{2n}\, dx$ *for all $n \in \mathbb{N}$.*

(c) $H[u(t)] \;:=\; \displaystyle\int_\Omega u(x,t)\, \ln(u(x,t))\, dx,$ *if $a > 0$.*

Corollary 1 offers multiple possibilities of how to interpret nonlinear anisotropic diffusion filtering as a smoothing transformation.

As a special case of (a) it follows that the energy $\|u(t)\|^2_{\mathrm{L}^2(\Omega)}$ is reduced by diffusion.

Part (b) gives a probabilistic interpretation of anisotropic diffusion filtering. Consider the intensity in an image f as a random variable Z_f with distribution

$F_f(z)$, i.e. $F_f(z)$ is the probability that an arbitrary grey value Z_f of f does not exceed z. By the average grey level invariance, μ is equal to the expected value

$$EZ_{u(t)} := \int_{\mathbb{R}} z \, dF_{u(t)}(z), \qquad (2.38)$$

and it follows that $M_{2n}[u(t)]$ is just the even central moment

$$\int_{\mathbb{R}} \left(z - EZ_{u(t)}\right)^{2n} dF_{u(t)}(z). \qquad (2.39)$$

The second central moment (the variance) characterizes the spread of the intensity about its mean. It is a common tool for constructing measures for the relative smoothness of the intensity distribution. The fourth moment is frequently used to describe the relative flatness of the grey value distribution. Higher moments are more difficult to interpret, although they do provide important information for tasks like texture discrimination [163, pp. 414–415]. All decreasing even moments demonstrate that the image becomes smoother during diffusion filtering. Hence, local effects such as edge enhancement, which object to increase central moments, are overcompensated by smoothing in other areas.

If we choose another probabilistic model of images, then part (c) characterizes the information-theoretical side of our scale-space. Provided the initial image f is strictly positive on Ω, we may regard it also as a two-dimensional density.[4] Then,

$$S[u(t)] := -\int_{\Omega} u(x,t) \ln(u(x,t)) \, dx \qquad (2.40)$$

is called the *entropy* of $u(t)$, a measure of uncertainty and missing information [63]. Since anisotropic diffusion filters increase the entropy the corresponding scale-space embeds the genuine image f into a family of subsequently likelier versions of it which contain less information. Moreover, for $t \to \infty$, the process reaches the state with the lowest possible information, namely a constant image. This information-reducing property indicates that anisotropic diffusion might be generally useful in the context of image compression. In particular, it helps to explain the success of nonlinear diffusion filtering as a preprocessing step for subsampling as observed in [144]. The interpretation of the entropy in terms of Lyapunov functionals carries also over to generalized entropies; see [390] for more details.

From all the previous considerations, we recognize that, in spite of possible contrast-enhancing properties, anisotropic diffusion does really simplify the original image in a steady way.

Let us finally point out another interpretation of the Lyapunov functionals. In a classic scale-space representation, the time t plays the role of the scale parameter. By increasing t, one transforms the image from a local to a more global

---

[4]Without loss of generality we omit the normalization.

representation. We have seen in Chapter 1 that, for linear diffusion scale-spaces and morphological scale-spaces, it is possible to associate with the evolution time a corresponding spatial scale.

In the nonlinear diffusion case, however, the situation is more complicated. Since the smoothing is nonuniform, one can only define an average measure for the globality of the representation. This can be achieved by taking some Lyapunov function $\Phi(u(t))$ and investigating the expression

$$\Psi(u(t)) \ := \ \frac{\Phi(f) - \Phi(u(t))}{\Phi(f) - \Phi(Mf)}. \tag{2.41}$$

We observe that $\Psi(t)$ increases from 0 to 1. It gives the average globality of $u(t)$ and its value can be used to measure the distance of $u(t)$ from the initial state f and the final state Mf. Prescribing a certain value for Ψ provides us with an a-posteriori criterion for the stopping time of the nonlinear diffusion process. Experiments in this direction can be found in [431, 308].

Chapter 3

Semidiscrete diffusion filtering

The goal of this chapter is to study a semidiscrete framework for diffusion scale-spaces where the image is sampled on a finite grid and the scale parameter is continuous. This leads to a system of nonlinear ordinary differential equations (ODEs). We shall investigate conditions under which one can establish similar properties as in the continuous setting concerning well-posedness, extremum principles, average grey level invariance, Lyapunov functions, and convergence to a constant steady-state. Afterwards we shall discuss whether it is possible to obtain such filters from spatial discretizations of the continuous models that have been investigated in Chapter 2. We will see that there exists a finite stencil on which a difference approximation of the spatial derivatives are in accordance with the semidiscrete scale-space framework.

3.1   The general model

A discrete image can be regarded as a vector $f \in \mathbb{R}^N$, $N \geq 2$, whose components f_j, $j = 1,...,N$ represent the grey values at each pixel. We denote the index set $\{1, ..., N\}$ by J. In order to specify the requirements for our semidiscrete filter class we first recall a useful definition of irreducible matrices [407, pp. 18–20].

Definition 1 (Irreducibility). *A matrix $A = (a_{ij}) \in \mathbb{R}^{N \times N}$ is called irreducible if for any $i, j \in J$ there exist $k_0,...,k_r \in J$ with $k_0 = i$ and $k_r = j$ such that $a_{k_p k_{p+1}} \neq 0$ for $p = 0,...,r-1$.*

The semidiscrete problem class (P_s) we are concerned with is defined in the following way:

Let $f \in \mathbb{R}^N$. Find a function $u \in C^1([0, \infty), \mathbb{R}^N)$ which satisfies an initial value problem of type

$$\frac{du}{dt} = A(u)\, u,$$
$$u(0) = f,$$

where $A = (a_{ij})$ has the following properties:

(S1) Lipschitz-continuity of $A \in C(\mathbb{R}^N, \mathbb{R}^{N \times N})$ for every bounded subset of $\mathbb{R}^N$,

(S2) symmetry: $\qquad\qquad a_{ij}(u) = a_{ji}(u) \quad \forall\, i, j \in J, \quad \forall\, u \in \mathbb{R}^N,$

(S3) vanishing row sums: $\quad \sum_{j \in J} a_{ij}(u) = 0 \quad \forall\, i \in J, \quad \forall\, u \in \mathbb{R}^N,$

(S4) nonnegative off-diagonals: $\quad a_{ij}(u) \geq 0 \quad \forall\, i \neq j, \quad \forall\, u \in \mathbb{R}^N,$

(S5) irreducibility for all $u \in \mathbb{R}^N$.

(P_s)

Not all of these requirements are necessary for every theoretical result below. (S1) is needed for well-posedness, the proof of a maximum–minimum principle involves (S3) and (S4), while average grey value invariance uses (S2) and (S3). The existence of Lyapunov functions can be established by means of (S2)–(S4), and strict Lyapunov functions and the convergence to a constant steady-state require (S5) in addition to (S2)–(S4).

This indicates that these properties reveal some interesting parallels to the continuous setting from Chapter 2: In both cases we need smoothness assumptions to ensure well-posedness; (S2) and (S3) correspond to the specific structure of the divergence expression with a symmetric diffusion tensor D, while (S4) and (S5) play a similar role as the nonnegativity of the eigenvalues of D and its uniform positive definiteness, respectively.

3.2   Theoretical results

Before we can establish scale-space results, it is of importance to ensure the existence of a unique solution. This is done in the theorem below which also states the continuous dependence of the solution and a maximum–minimum principle.

Theorem 4 (Well-posedness, extremum principle).
For every $T > 0$ the problem (P_s) has a unique solution $u(t) \in \mathrm{C}^1([0, T], \mathbb{R}^N)$.
This solution depends continuously on the initial value and the right-hand side of
the ODE system, and it satisfies the extremum principle

$$a \;\le\; u_i(t) \;\le\; b \qquad \forall\, i \in J, \quad \forall\, t \in [0, T], \tag{3.1}$$

where

$$a := \min_{j \in J} f_j, \tag{3.2}$$

$$b := \max_{j \in J} f_j. \tag{3.3}$$

Proof:

(a) **Local existence and uniqueness**

Local existence and uniqueness are proved by showing that our problem
satisfies the requirements of the Picard–Lindelöf theorem [432, p. 59].

Let $t_0 := 0$ and $\beta > 0$. Evidently, $\phi(t, u) := \psi(u) := A(u)\,u$ is continuous on

$$B_0 := [0, T] \times \left\{ u \in \mathbb{R}^N \;\middle|\; \|u\|_\infty \le \|f\|_\infty + \beta \right\},$$

since it is a composition of continuous functions. Moreover, by the compact-
ness of B_0 there exists some $c > 0$ with

$$\|\phi(t, u)\|_\infty \le c \qquad \forall\, (t, u) \in B_0.$$

In order to prove existence and uniqueness of a solution of (P_s) in

$$R_0 := \left\{ (t, u) \;\middle|\; t \in [t_0, t_0 + \min(\tfrac{\beta}{c}, T)], \; \|u - f\|_\infty \le \beta \right\} \subset B_0$$

we have to show that $\phi(t, u)$ satisfies a global Lipschitz condition on R_0 with
respect to u. However, this follows directly from the fact that A is Lipschitz-
continuous on $\{u \in \mathbb{R}^N \mid \|u - f\|_\infty \le \beta\}$.

(b) **Maximum–minimum principle**

We prove only the maximum principle, since the proof for the minimum
principle is analogous.

Assume that the problem (P_s) has a unique solution on $[0, \theta]$. First we show
that the derivative of the largest component of $u(t)$ is nonpositive for every

$t \in [0, \theta]$. Let $u_k(\vartheta) := \max_{j \in J} u_j(\vartheta)$ for some arbitrary $\vartheta \in [0, \theta]$. If we keep this k fixed we obtain, for $t = \vartheta$,

$$
\begin{aligned}
\frac{du_k}{dt} &= \sum_{j \in J} a_{kj}(u)\, u_j \\
&= a_{kk}(u)\, u_k + \sum_{j \in J \setminus \{k\}} \underbrace{a_{kj}(u)}_{\geq 0}\, \underbrace{u_j}_{\leq u_k} \\
&\leq u_k \cdot \sum_{j \in J} a_{kj}(u) \\
&\stackrel{(S4)}{=} 0.
\end{aligned}
\tag{3.4}
$$

Let us now prove that this implies a maximum principle (cf. [201]). Let $\varepsilon > 0$ and set

$$
u_\varepsilon(t) := u(t) - \begin{pmatrix} \varepsilon t \\ \vdots \\ \varepsilon t \end{pmatrix}.
$$

Moreover, let $P := \{ p \in J \mid u_{\varepsilon p}(0) = \max_{j \in J} u_{\varepsilon j}(0) \}$. Then, by (3.4),

$$
\left(\frac{du_{\varepsilon p}}{dt} \right)(0) = \underbrace{\left(\frac{du_p}{dt} \right)(0)}_{\leq 0} - \varepsilon \; < \; 0 \qquad \forall\, p \in P.
\tag{3.5}
$$

By means of

$$
\max_{i \in J \setminus P} u_{\varepsilon i}(0) \; < \; \max_{j \in J} u_{\varepsilon j}(0),
$$

and the continuity of u there exists some $t_1 \in (0, \theta)$ such that

$$
\max_{i \in J \setminus P} u_{\varepsilon i}(t) \; < \; \max_{j \in J} u_{\varepsilon j}(0) \qquad \forall\, t \in [0, t_1).
\tag{3.6}
$$

Next, let us consider some $p \in P$. Due to (3.5) and the smoothness of u we may find a $\vartheta_p \in (0, \theta)$ with

$$
\left(\frac{du_{\varepsilon p}}{dt} \right)(t) \; < \; 0 \qquad \forall\, t \in [0, \vartheta_p).
$$

Thus, we have

$$
u_{\varepsilon p}(t) \; < \; u_{\varepsilon p}(0) \qquad \forall\, t \in (0, \vartheta_p)
$$

and, for $t_2 := \min_{p \in P} \vartheta_p$, it follows that

$$
\max_{p \in P} u_{\varepsilon p}(t) \; < \; \max_{j \in J} u_{\varepsilon j}(0) \qquad \forall\, t \in (0, t_2).
\tag{3.7}
$$

Hence, for $t_0 := \min(t_1, t_2)$, the estimates (3.6) and (3.7) give

$$\max_{j \in J} u_{\varepsilon j}(t) < \max_{j \in J} u_{\varepsilon j}(0) \qquad \forall\, t \in (0, t_0). \tag{3.8}$$

Now we prove that this estimate can be extended to the case $t \in (0, \theta)$. To this end, assume the opposite is true. Then, by virtue of the intermediate value theorem, there exists some t_3 which is the smallest time in $(0, \theta)$ such that

$$\max_{j \in J} u_{\varepsilon j}(t_3) = \max_{j \in J} u_{\varepsilon j}(0).$$

Let $u_{\varepsilon k} := \max_{j \in J} u_{\varepsilon j}(t_3)$. Then the minimality of t_3 yields

$$u_{\varepsilon k}(t) < u_{\varepsilon k}(t_3) \qquad \forall\, t \in (0, t_3), \tag{3.9}$$

and inequality (3.4) gives

$$\left(\frac{du_{\varepsilon k}}{dt}\right)(t_3) = \underbrace{\left(\frac{du_k}{dt}\right)(t_3)}_{\leq 0} - \varepsilon < 0.$$

Due to the continuity of $\frac{du}{dt}$ there exists some $t_4 \in (0, t_3)$ with

$$\left(\frac{du_{\varepsilon k}}{dt}\right)(t) < 0 \qquad \forall\, t \in (t_4, t_3]. \tag{3.10}$$

The mean value theorem, however, implies that we find a $t_5 \in (t_4, t_3)$ with

$$\left(\frac{du_{\varepsilon k}}{dt}\right)(t_5) = \frac{u_{\varepsilon k}(t_3) - u_{\varepsilon k}(t_4)}{t_3 - t_4} \overset{(3.9)}{>} 0,$$

which contradicts (3.10). Hence, (3.8) must be valid on the entire interval $(0, \theta)$.

Together with $u = \lim_{\varepsilon \to 0} u_\varepsilon$ and the continuity of u this yields the announced maximum principle

$$\max_{j \in J} u_j(t) \leq \max_{j \in J} u_j(0) \qquad \forall\, t \in [0, \theta].$$

(c) **Global existence and uniqueness**

Global existence and uniqueness follow from local existence and uniqueness when being combined with the extremum principle.

Using the notations and results from (a), we know that the problem (P_s) has a unique solution $u(t)$ for $t \in [t_0, t_0 + \min(\frac{\beta}{c}, T)]$.

Now let $t_1 := t_0 + \min(\frac{\beta}{c}, T)$, $g := u(t_1)$, and consider the problem

$$\begin{aligned}
\frac{du}{dt} &= A(u)\,u, \\
u(t_1) &= g.
\end{aligned}$$

Clearly, $\phi(t, u) = A(u)u$ is continuous on

$$B_1 := [0, T] \times \left\{ u \in \mathrm{I\!R}^N \;\middle|\; \|u\|_\infty \le \|g\|_\infty + \beta \right\},$$

and by the extremum principle we know that $B_1 \subset B_0$. Hence,

$$\|\phi(t, u)\|_\infty \le c \qquad \forall\,(t, u) \in B_1.$$

with the same c as in (a). Using the same considerations as in (a) one shows that ϕ is Lipschitz-continuous on

$$R_1 := \left\{ (t, u) \;\middle|\; t \in [t_1, t_1 + \min(\tfrac{\beta}{c}, T)],\; \|u - g\|_\infty \le \beta \right\}.$$

Hence, the considered problem has a unique solution on $[t_1, t_1 + \min(\frac{\beta}{c}, T)]$. Therefore, (P_s) reveals a unique solution on $[0, \min(\frac{2\beta}{c}, T)]$, and, by iterating this reasoning, the existence of a unique solution can be extended to the entire interval $[0, T]$. As a consequence, the extremum principle is valid on $[0, T]$ as well.

(d) **Continuous dependence**

Let $u(t)$ be the solution of

$$\begin{aligned}
\frac{du}{dt} &= \phi(t, u), \\
u(0) &= f
\end{aligned}$$

for $t \in [0, T]$ and $\phi(u, t) = \psi(u) = A(u)u$. In order to show that $u(t)$ depends continuously on the initial data and the right-hand side of the ODE system, it is sufficient to prove that $\phi(t, u)$ is continuous, and that there exists some $\alpha > 0$ such that $\phi(t, u)$ satisfies a global Lipschitz condition on

$$S_\alpha := \left\{ (t, v) \;\middle|\; t \in [0, T],\; \|v - u\|_\infty \le \alpha \right\}.$$

with respect to its second argument. In this case the results in [412, p. 93] ensure that for every $\varepsilon > 0$ there exists a $\delta > 0$ such that the solution $\tilde{u}$ of the perturbed problem

$$\begin{aligned}
\frac{d\tilde{u}}{dt} &= \tilde{\phi}(t, \tilde{u}), \\
\tilde{u}(0) &= \tilde{f}
\end{aligned}$$

with continuous $\tilde{\phi}$ and

$$\|\tilde{f} - f\|_\infty < \delta,$$
$$\|\tilde{\phi}(t, v) - \phi(t, v)\|_\infty < \delta \quad \text{for} \quad \|v - u\|_\infty < \alpha$$

exists in $[0, T]$ and satisfies the inequality

$$\|\tilde{u}(t) - u(t)\|_\infty < \varepsilon.$$

Similar to the the local existence and uniqueness proof, the global Lipschitz condition on S_α follows direcly from the fact that A is Lipschitz-continuous on $\{v \in \mathbb{R}^N \mid \|v - u\|_\infty \leq \alpha\}$. $\qquad\square$

3.3   Scale-space properties

It is evident that properties such as grey level shift invariance or reverse contrast invariance are automatically satisfied by every consistent semidiscrete approximation of the continuous filter class (P_c). On the other hand, translation invariance only makes sense for translations in grid direction with multiples of the grid size, and isometry invariance is satisfied for consistent schemes up to an discretization error. So let us focus on average grey level invariance now.

Proposition 2 (Conservation of average grey value).
The average grey level

$$\mu := \frac{1}{N} \sum_{j \in J} f_j \tag{3.11}$$

is not affected by the semidiscrete diffusion filter:

$$\frac{1}{N} \sum_{j \in J} u_j(t) = \mu \qquad \forall \, t \geq 0. \tag{3.12}$$

Proof:
By virtue of (S2) and (S3) we have $\sum\limits_{j \in J} a_{jk}(u) = 0$ for all $k \in J$. Thus, for $t \geq 0$,

$$\sum_{j \in J} \frac{du_j}{dt} = \sum_{j \in J} \sum_{k \in J} a_{jk}(u) \, u_k = \sum_{k \in J} \Big(\sum_{j \in J} a_{jk}(u) \Big) u_k = 0,$$

which shows that $\sum\limits_{j \in J} u_j(t)$ is constant on $[0, \infty)$ and concludes the proof. $\qquad\square$

This property is in complete accordance with the result for the continuous filter class.

Similar to the continuous setting, it is possible to find a large class of Lyapunov functions which establish smoothing scale-space properties and ensure that the image tends to a constant steady-state with the same average grey level as the initial image.

Theorem 5 (Lyapunov functions and behaviour for $t \to \infty$).
Let $u(t)$ be the solution of (P_s), let a, b, and μ be defined as in (3.2), (3.3), and (3.11), respectively, and let $c := (\mu, \mu, ..., \mu)^\top \in \mathbb{R}^N$.
Then the following properties are valid:

(a) (Lyapunov functions)
  For all $r \in \mathrm{C}^1[a, b]$ with increasing r' on $[a, b]$, the function

$$V(t) := \Phi(u(t)) := \sum_{i \in J} r(u_i(t))$$

  is a Lyapunov function:

  (i) $\Phi(u) \geq \Phi(c)$ for all $t \geq 0$.

  (ii) $V \in \mathrm{C}^1[0, \infty)$ and $V'(t) \leq 0$ for all $t \geq 0$.

  Moreover, if r' is strictly increasing on $[a, b]$, then $V(t) = \Phi(u(t))$ is a strict Lyapunov function:

  (iii) $\Phi(u) = \Phi(c) \quad \Longleftrightarrow \quad u = c$

  (iv) $V'(t) = 0 \quad \Longleftrightarrow \quad u = c$

(b) (Convergence)
  $\lim\limits_{t \to \infty} u(t) = c.$

Proof:

(a)   (i) Since r' is increasing on $[a, b]$ we know that r is convex on $[a, b]$. Average grey level invariance and this convexity yield, for all $t \geq 0$,

$$
\begin{aligned}
\Phi(c) &= \sum_{i=1}^{N} r\left(\sum_{j=1}^{N} \frac{1}{N} u_j\right) \\
&\leq \sum_{i=1}^{N} \left(\frac{1}{N} \sum_{j=1}^{N} r(u_j)\right) \\
&= \sum_{j=1}^{N} r(u_j) \\
&= \Phi(u). \qquad\qquad (3.13)
\end{aligned}
$$

(ii) Since $u \in \mathrm{C}^1([0, \infty), \mathrm{I\!R}^N)$ and $r \in \mathrm{C}^1[a, b]$, it follows that $V \in \mathrm{C}^1[0, \infty)$. Using the prerequisites (S2) and (S3) we get

$$
\begin{aligned}
V'(t) \;&=\; \sum_{i=1}^{N} \frac{du_i}{dt}\, r'(u_i) \\[2mm]
&\overset{(S3)}{=}\; \sum_{i=1}^{N} \sum_{j=1}^{N} a_{ij}(u)\,(u_j - u_i)\, r'(u_i) \\[2mm]
&=\; \sum_{i=1}^{N} \left(\sum_{j=i+1}^{N} + \sum_{j=1}^{i-1} \right) a_{ij}(u)\,(u_j - u_i)\, r'(u_i) \\[2mm]
&=\; \sum_{i=1}^{N} \sum_{k=1}^{N-i} a_{i,i+k}(u)\,(u_{i+k} - u_i)\, r'(u_i) \\[2mm]
&\;+ \sum_{i=1}^{N} \sum_{k=1}^{N-i} a_{i+k,i}(u)\,(u_i - u_{i+k})\, r'(u_{i+k}) \\[2mm]
&\overset{(S2)}{=}\; \sum_{i=1}^{N} \sum_{k=1}^{N-i} a_{i,i+k}(u)\,(u_{i+k} - u_i) \left(r'(u_i) - r'(u_{i+k}) \right). \quad (3.14)
\end{aligned}
$$

Since r' is increasing, we always have

$$
(u_{i+k} - u_i) \left(r'(u_i) - r'(u_{i+k}) \right) \;\leq\; 0.
$$

With this and (S4), equation (3.14) implies that $V'(t) \leq 0$ for $t \geq 0$.

(iii) Let us first prove that equality in the estimate (3.13) implies that all components of u are equal.

To this end, suppose that $u_{i_0} := \min_i u_i < \max_j u_j =: u_{j_0}$ and let

$$
\eta \;:=\; \sum_{\substack{j=1 \\ j \neq j_0}}^{N} \frac{\frac{1}{N} u_j}{1 - \frac{1}{N}}.
$$

Then, $\eta < u_{j_0}$. Since r' is strictly increasing on $[a, b]$, we know that r is strictly convex. Hence, we get

$$
\begin{aligned}
r\left(\sum_{i=1}^{N} \frac{1}{N} u_j \right) \;&=\; r\left(\frac{1}{N} u_{j_0} + \left(1 - \frac{1}{N}\right) \eta \right) \\[2mm]
&<\; \frac{1}{N} r(u_{j_0}) + \left(1 - \frac{1}{N}\right) r(\eta) \\[2mm]
&\leq\; \frac{1}{N} r(u_{j_0}) + \sum_{\substack{j=1 \\ j \neq j_0}}^{N} \frac{1}{N} r(u_j) \\[2mm]
&=\; \sum_{j=1}^{N} \frac{1}{N} r(u_j).
\end{aligned}
$$

This shows that equality in (3.13) implies that $u_1 = ... = u_N$. By virtue of the grey level shift invariance we conclude that $u = c$.

Conversely, it is trivial that $\Phi(u) = \Phi(c)$ for $u = c$.

(iv) Let $V'(t) = 0$. From (3.14) we have

$$0 \;=\; V'(t) \;=\; \sum_{i=1}^{N} \sum_{k=1}^{N-i} \underbrace{a_{i,i+k}(u) \, (u_{i+k}-u_i) \, \big(r'(u_i)-r'(u_{i+k})\big)}_{\leq 0},$$

and by virtue of the symmetry of $A(u)$ it follows that

$$a_{ij}(u) \, (u_j-u_i) \, \big(r'(u_i)-r'(u_j)\big) \;=\; 0 \qquad \forall\, i, j \in J. \tag{3.15}$$

Now consider two arbitrary $i_0, j_0 \in J$. The irreducibility of $A(u)$ implies that there exist $k_0,...,k_r \in J$ with $k_0 = i_0$, $k_r = j_0$, and

$$a_{k_p k_{p+1}}(u) \neq 0, \qquad p = 0, ..., r-1.$$

As r' is strictly increasing we have, for $p = 0,...,r-1$,

$$(u_{k_p} - u_{k_{p+1}}) \, \big(r'(u_{k_{p+1}})-r'(u_{k_p})\big) \;=\; 0 \quad \Longleftrightarrow \quad u_{k_p} = u_{k_{p+1}}.$$

From this and (3.15) we get

$$u_{i_0} = u_{k_0} = u_{k_1} = ... = u_{k_r} = u_{j_0}.$$

Since i_0 and j_0 are arbitrary, we obtain $u_i = \text{const.}$ for all $i \in J$, and the average grey level invariance gives $u = c$. This proves the first implication.

Conversely, let $u_i = \text{const.}$ for all $i \in J$. Then from the representation (3.14) we immediately conclude that $V'(t) = 0$.

(b) The convergence proof is based on classical Lyapunov reasonings, see e.g. [180] for an introduction to these techniques.

Consider the Lyapunov function $V(t) := \Phi(u(t)) := |u(t)-c|^2$, which results from the choice $r(s) := (s-\mu)^2$. Since $V(t)$ is decreasing and bounded from below by 0, we know that $\lim_{t\to\infty} V(t) =: \eta$ exists and $\eta \geq 0$.

Now assume that $\eta > 0$.

Since $|u(t)-c|$ is bounded from above by $\alpha := |f-c|$ we have

$$|u(t)-c| \leq \alpha \qquad \forall\, t \geq 0. \tag{3.16}$$

By virtue of $\Phi(x) = |x-c|^2$ we know that, for $\beta \in (0, \sqrt{\eta})$,

$$\Phi(x) < \eta \qquad \forall\, x \in \mathbb{R}^N, \quad |x-c| < \beta.$$

Let w.l.o.g. $\beta < \alpha$. Since $\Phi(u(t)) \geq \eta$ we conclude that

$$|u(t) - c| \geq \beta \qquad \forall\, t \geq 0. \qquad (3.17)$$

So from (3.16) and (3.17) we have

$$u(t) \in \{x \in \mathbb{R}^N \mid \beta \leq |x - c| \leq \alpha\} =: S \qquad \forall\, t \geq 0.$$

By (a)(ii),(iv), the compactness of S, and $\beta > 0$ there exists some $M > 0$ such that

$$V'(t) \leq -M \qquad \forall\, t \geq 0.$$

Therefore, it follows

$$V(t) \;=\; V(0) + \int_0^t V'(\theta)\, d\theta \;\leq\; V(0) - tM$$

which implies $\lim\limits_{t\to\infty} V(t) = -\infty$ and, thus, contradicts (a)(i).

Hence the assumption $\eta > \rho$ is wrong and we must have $\eta = \rho$.

According to (a)(iii) this yields $\lim\limits_{t\to\infty} u(t) = c$. □

As in the continuous case, we can consider the Lyapunov functions associated with $r(s) := |s|^p$, $r(s) := (s - \mu)^{2n}$ and $r(s) := s \ln s$, respectively, and obtain the following corollary.

Corollary 2 (Special Lyapunov functions).
Let u be the solution of (P_s) and a and μ be defined as in (3.2) and (3.11). Then the following functions are decreasing for $t \in [0, \infty)$:

(a)　$\|u(t)\|_p$　*for all $p \geq 2$.*

(b)　$M_{2n}[u(t)] \;:=\; \frac{1}{N} \sum\limits_{j=1}^{N} (u_j(t) - \mu)^{2n}$　*for all $n \in \mathbb{N}$.*

(c)　$H[u(t)] \;:=\; \sum\limits_{j=1}^{N} u_j(t)\, \ln(u_j(t)),$　*if $a > 0$.*

Since all p-norms $(p \geq 2)$ and all central moments are decreasing, while the discrete entropy

$$S[u(t)] \;:=\; -\sum_{j=1}^{N} u_j(t)\, \ln(u_j(t)) \qquad (3.18)$$

is increasing with respect to t, we observe that the semidiscrete setting reveals smoothing scale-space properties which are closely related to the continuous case.

3.4   Relation to continuous models

In this section we investigate whether it is possible to use spatial discretizations of the continuous filter class (P_c) in order to construct semidiscrete diffusion models satisfying (S1)–(S5). First we shall verify that this is easily done for isotropic models. In the anisotropic case, however, the mixed derivative terms make it more difficult to ensure nonnegative off-diagonal elements. A constructive existence proof is presented showing that for a sufficiently large stencil it is always possible to find such a nonnegative discretization. This concept is illustrated by investigating the situation on a (3×3)-stencil in detail.

3.4.1   Isotropic case

Let the rectangle $\Omega = (0, a_1) \times (0, a_2)$ be discretized by a grid of $N = n_1 \cdot n_2$ pixels such that a pixel (i, j) with $1 \leq i \leq n_1$ and $1 \leq j \leq n_2$ represents the location (x_i, y_j) where

$$x_i \quad := \quad (i - \tfrac{1}{2})\, h_1, \tag{3.19}$$

$$y_j \quad := \quad (j - \tfrac{1}{2})\, h_2, \tag{3.20}$$

and the grid sizes h_1, h_2 are given by $h_1 := a_1/n_1$ and $h_2 := a_2/n_2$, respectively.

These pixels can be numbered by means of an arbitrary bijection

$$p : \quad \{1, ..., n_1\} \times \{1, ..., n_2\} \quad \rightarrow \quad \{1, ..., N\}. \tag{3.21}$$

Thus, pixel (i, j) is represented by a single index $p(i, j)$.

Let us now verify that a standard FD space discretization of an isotropic variant of (P_c) leads to a semidiscrete filter satisfying the requirements (S1)–(S5). To this end, we may replace the diffusion tensor $D(J_\rho(\nabla u_\sigma))$ by some scalar-valued function $g(J_\rho(\nabla u_\sigma))$. The structure tensor requires the calculations of convolutions with ∇K_σ and K_ρ, respectively. In the spatially discrete case this comes down to specific vector–matrix multiplications. For this reason, we may approximate the structure tensor by some matrix $H(u) = (h_{ij}(u))$ where $H \in C^\infty(\mathbb{R}^N, \mathbb{R}^{2\times2})$.

Next, consider some pixel $k = p(i, j)$. Then a consistent spatial discretization of the isotropic diffusion equation with homogeneous Neumann boundary conditions can be written as

$$\frac{du_k}{dt} \;=\; \sum_{n=1}^{2} \sum_{l \in \mathcal{N}_n(k)} \frac{g_l + g_k}{2h_l^2}\, (u_l - u_k), \tag{3.22}$$

where $\mathcal{N}_n(k)$ consists of the one or two neighbours of pixel k along the n-th coordinate axis (boundary pixels have only one neighbour) and $g_k := g\left((H(u))_k\right)$.

In vector–matrix notation (3.22) becomes

$$\frac{du}{dt} \;=\; A(u)\, u, \tag{3.23}$$

where the matrix $A(u) = (a_{kl}(u))_{kl}$ is given by

$$a_{kl} := \begin{cases} \frac{g_k+g_l}{2h_n^2} & (l \in \mathcal{N}_n(k)), \\ -\sum\limits_{n=1}^{2}\sum\limits_{l\in\mathcal{N}_n(k)} \frac{g_k+g_l}{2h_n^2} & (l = k), \\ 0 & (\text{else}). \end{cases} \qquad (3.24)$$

Let us now verify that (S1)–(S5) are fulfilled.

Since $H \in C^\infty(\mathbb{R}^N, \mathbb{R}^{2\times2})$ and $g \in C^\infty(\mathbb{R}^{2\times2})$, we have $A \in C^\infty(\mathbb{R}^N, \mathbb{R}^{N\times N})$. This proves (S1).

The symmetry of A follows directly from (3.24) and the symmetry of the neighbourhood relation:

$$l \in \mathcal{N}_n(k) \iff k \in \mathcal{N}_n(l).$$

By the construction of A it is also evident that all row sums vanish, i.e. (S3) is satisfied. Moreover, since g is positive, it follows that $a_{kl} \geq 0$ for all $k \neq l$ and, thus, (S4) holds.

In order to show that A is irreducible, let us consider two arbitrary pixels k and l. Then we have to find $k_0,...,k_r \in J$ with $k_0 = k$ and $k_r = l$ such that $a_{k_q k_{q+1}} \neq 0$ for $q = 0,...,r-1$. If $k = l$, we already know from (3.24) that $a_{kk} < 0$. In this case we have the trivial path $k = k_0 = k_r = l$. For $k \neq l$, we may choose any arbitrary path $k_0,...,k_r$, such that k_q and k_{q+1} are neighbours for $q = 0,...,r-1$. Then,

$$a_{k_q k_{q+1}} = \frac{g_{k_q} + g_{k_{q+1}}}{2h_n^2} > 0$$

for some $n \in \{1, 2\}$. This proves (S5).

Remarks:

(a) We observe that (S1)–(S5) are properties which are valid for all arbitrary pixel numberings.

(b) The filter class (P_c) is not the only family which leads to semidiscrete filters satisfying (S1)–(S5). Interestingly, a semidiscrete version of the Perona–Malik filter – which is to a certain degree ill-posed in the continuous setting (cf. 1.3.1) – also satisfies (S1)–(S5) and, thus, reveals all the discussed well-posedness and scale-space properties [425]. This is due to the fact that the extremum principle limits the modulus of discrete gradient approximations. Hence, the spatial discretization implicitly causes a regularization. These results are also in accordance with a recent paper by Pollak et al. [332]. They study an image evolution under an ODE system with a discontinuous right hand side, which has some interesting relations to the limit case of a semidiscrete Perona–Malik model. They also report stable behaviour of their process.

3.4.2 Anisotropic case

If one wishes to transfer the results from the isotropic case to the general aniso-
tropic setting the main difficulty arises from the fact that, due to the mixed deriva-
tive expressions, it is not obvious how to ensure (S4), the nonnegativity of all off-
diagonal elements of $A(u)$. The theorem below states that this is always possible
for a sufficiently large stencil.

Theorem 6 (Existence of a nonnegative discretization).
*Let $D \in \mathbb{R}^{2 \times 2}$ be symmetric positive definite with a spectral condition number
κ. Then there exists some $m(\kappa) \in \mathbb{N}$ such that $\mathrm{div}\,(D\,\nabla u)$ reveals a second-order
nonnegative FD discretization on a $(2m+1) \times (2m+1)$-stencil.*

Proof:
Let us consider some $m \in \mathbb{N}$ and the corresponding $(2m+1) \times (2m+1)$-stencil. The
"boundary pixels" of this stencil define $4m$ principal orientations $\beta_i \in (-\frac{\pi}{2}, \frac{\pi}{2}]$,
$i = -2m+1, ..., 2m$ according to

$$\beta_i := \begin{cases} \arctan\left(\frac{ih_2}{mh_1}\right) & (|i| \leq m), \\ \mathrm{arccot}\left(\frac{(2m-i)h_1}{mh_2}\right) & (m < i \leq 2m), \\ \mathrm{arccot}\left(\frac{(i-2m)h_1}{mh_2}\right) & (-2m+1 \leq i < -m). \end{cases}$$

Now let $J_m := \{1, ..., 2m-1\}$ and define a partition of $(-\frac{\pi}{2}, \frac{\pi}{2}]$ into $4m-2$ subin-
tervals I_i, $|i| \in J_m$:

$$(-\tfrac{\pi}{2}, \tfrac{\pi}{2}] = \bigcup_{i=-2m+1}^{-1} \underbrace{(\theta_i, \theta_{i+1}]}_{=:I_i} \cup \bigcup_{i=1}^{2m-1} \underbrace{(\theta_{i-1}, \theta_i]}_{=:I_i},$$

where

$$\theta_i := \begin{cases} 0 & (i = 0), \\ \frac{1}{2}\arctan\left(\frac{2}{\cot\beta_i - \tan\beta_{i+1}}\right) & (i \in \{1, ..., 2m-2\},\ \beta_i + \beta_{i+1} < \frac{\pi}{2}), \\ \frac{\pi}{4} & (i \in \{1, ..., 2m-2\},\ \beta_i + \beta_{i+1} = \frac{\pi}{2}), \\ \frac{\pi}{2} + \frac{1}{2}\arctan\left(\frac{2}{\cot\beta_i - \tan\beta_{i+1}}\right) & (i \in \{1, ..., 2m-2\},\ \beta_i + \beta_{i+1} > \frac{\pi}{2}), \\ \frac{\pi}{2} & (i = 2m-1), \end{cases}$$

and

$$\theta_i := -\theta_{-i} \qquad (i \in \{-2m+1, ..., -1\}).$$

It is not hard to verify that $\beta_i \in I_i$ for $|i| \in J_m$.

Let $\lambda_1 \geq \lambda_2 > 0$ be the eigenvalues of D with corresponding eigenvectors
$(\cos\psi, \sin\psi)^\top$ and $(-\sin\psi, \cos\psi)^\top$, where $\psi \in (-\frac{\pi}{2}, \frac{\pi}{2}]$. Now we show that for
a suitable m there exists a stencil direction β_k, $|k| \in J_m$ such that the splitting

$$\mathrm{div}\,(D\,\nabla u) \;=\; \partial_{e_{\beta_0}}\left(\alpha_0\,\partial_{e_{\beta_0}}u\right) + \partial_{e_{\beta_k}}\left(\alpha_k\,\partial_{e_{\beta_k}}u\right) + \partial_{e_{\beta_{2m}}}\left(\alpha_{2m}\,\partial_{e_{\beta_{2m}}}u\right) \qquad (3.25)$$

with $e_{\beta_i} := (\cos\beta_i, \sin\beta_i)^\top$ reveals nonnegative "directional diffusivities" α_0, α_k, α_{2m} along the stencil orientations β_0, β_k, β_{2m}. This can be done by proving the following properties:

(a) Let $\psi \in I_k$ and $D = \begin{pmatrix} a & b \\ b & c \end{pmatrix}$. Then a nonnegative splitting of type (3.25) is possible if

$$\min\left(a - b\cot\beta_k,\ c - b\tan\beta_k\right) \geq 0. \qquad (3.26)$$

(b) Inequality (3.26) is satisfied for

$$\frac{\lambda_1}{\lambda_2} \leq \min\left(\cot(\rho_k-\beta_k)\tan\rho_k,\ \cot(\beta_k-\eta_k)\cot\eta_k\right) =: \kappa_{k,m} \qquad (3.27)$$

with

$$\rho_k := \begin{cases} \theta_k & (|k| \in \{1,...,2m-2\}), \\ \frac{1}{2}(\theta_k + \beta_k) & (|k| = 2m-1), \end{cases}$$

$$\eta_k := \begin{cases} \frac{1}{2}\beta_k & (|k| = 1), \\ \theta_{k-1} & (|k| \in \{2,...,2m-1\}). \end{cases}$$

(c) $\lim\limits_{m\to\infty}\left(\min\limits_{|i|\in J_m}\kappa_{i,m}\right) = \infty.$

Once these assertions are proved a nonnegative second-order discretization of (3.25) arises in a natural way, as we shall see at the end of this chapter. So let us now verify (a)–(c).

(a) In order to use subsequent indices, let $\varphi_0 := 0$, $\varphi_1 := \beta_k$ where $\psi \in I_k$, and $\varphi_2 := \frac{\pi}{2}$. Furthermore, let $\gamma_0 := \alpha_0$, $\gamma_1 := \alpha_k$, and $\gamma_2 := \alpha_{2m}$. Then (3.25) requires that

$$\mathrm{div}\left(\begin{pmatrix} a & b \\ b & c \end{pmatrix}\nabla u\right) = \sum_{i=0}^{2}\frac{\partial}{\partial e_{\varphi_i}}\left(\gamma_i\frac{\partial u}{\partial e_{\varphi_i}}\right)$$

$$= \frac{\partial}{\partial x}\sum_{i=0}^{2}\cos\varphi_i\Big(\gamma_i(u_x\cos\varphi_i + u_y\sin\varphi_i)\Big)$$

$$+ \frac{\partial}{\partial y}\sum_{i=0}^{2}\sin\varphi_i\Big(\gamma_i(u_x\cos\varphi_i + u_y\sin\varphi_i)\Big)$$

$$= \mathrm{div}\left(\begin{pmatrix} \sum_{i=0}^{2}\gamma_i\cos^2\varphi_i & \sum_{i=0}^{2}\gamma_i\sin\varphi_i\cos\varphi_i \\ \sum_{i=0}^{2}\gamma_i\sin\varphi_i\cos\varphi_i & \sum_{i=0}^{2}\gamma_i\sin^2\varphi_i \end{pmatrix}\nabla u\right).$$

By comparing the coefficients and using the definition of φ_0, φ_1 and φ_2 we obtain the linear system

$$\begin{pmatrix} 1 & \cos^2\beta_k & 0 \\ 0 & \sin\beta_k\cos\beta_k & 0 \\ 0 & \sin^2\beta_k & 1 \end{pmatrix}\begin{pmatrix} \gamma_0 \\ \gamma_1 \\ \gamma_2 \end{pmatrix} = \begin{pmatrix} a \\ b \\ c \end{pmatrix}$$

which has the unique solution

$$\gamma_0 \;=\; a - b \cot \beta_k, \tag{3.28}$$

$$\gamma_1 \;=\; \frac{b}{\sin \beta_k \cos \beta_k}, \tag{3.29}$$

$$\gamma_2 \;=\; c - b \tan \beta_k. \tag{3.30}$$

From the structure of the eigenvalues and eigenvectors of D it is easily seen that

$$b = (\lambda_1 - \lambda_2) \sin \psi \cos \psi.$$

Now, $\lambda_1 - \lambda_2 \geq 0$, and since $\psi, \beta_k \in I_k$ we conclude that ψ and β_k belong to the same quadrant. Thus, γ_1 is always nonnegative. In order to satisfy the nonnegativity of γ_0 and γ_2 we need that

$$\min\left(a - b \cot \beta_k, \; c - b \tan \beta_k\right) \;\geq\; 0.$$

(b) Let $\frac{\lambda_1}{\lambda_2} \leq \kappa_{k,m}$ and consider the case $0 < \beta_k < \frac{\pi}{2}$. By defining

$$B(\varphi) \;:=\; \cos^2\varphi - \sin \varphi \cos \varphi \cot \beta_k,$$
$$C(\varphi) \;:=\; \sin^2\varphi + \sin \varphi \cos \varphi \cot \beta_k$$

we get

$$\frac{\lambda_1}{\lambda_2} \;\leq\; \cot(\rho_k - \beta_k) \tan \rho_k \;=\; -\frac{C(\rho_k)}{B(\rho_k)} \;=\; \min_{\varphi \in (\beta_k, \theta_k)} \left(-\frac{C(\varphi)}{B(\varphi)}\right).$$

Since $B(\varphi) < 0$ on $(\beta_k, \frac{\pi}{2})$ we have

$$\lambda_1 B(\varphi) + \lambda_2 C(\varphi) \;\geq\; 0 \qquad \forall\, \varphi \in (\beta_k, \theta_k). \tag{3.31}$$

Because of

$$B(\varphi) \geq 0 \qquad \forall\, \varphi \in [-\tfrac{\pi}{2}, \beta_k],$$
$$C(\varphi) \geq 0 \qquad \forall\, \varphi \in [0, \tfrac{\pi}{2}],$$

and the continuity of $B(\varphi)$ and $C(\varphi)$ we may extend (3.31) to the entire interval $I_k = (\theta_{k-1}, \theta_k]$. In particular, since $\psi \in I_k$, we have

$$\begin{aligned}
0 \;&\leq\; \lambda_1 B(\psi) + \lambda_2 C(\psi) \\
&=\; (\lambda_1 \cos^2\psi + \lambda_2 \sin^2\psi) - (\lambda_1 - \lambda_2) \sin \psi \cos \psi \cot \beta_k.
\end{aligned}$$

By the representation

$$\begin{aligned}
\begin{pmatrix} a & b \\ b & c \end{pmatrix} &= \begin{pmatrix} \cos \psi & -\sin \psi \\ \sin \psi & \cos \psi \end{pmatrix} \begin{pmatrix} \lambda_1 & 0 \\ 0 & \lambda_2 \end{pmatrix} \begin{pmatrix} \cos \psi & \sin \psi \\ -\sin \psi & \cos \psi \end{pmatrix} \\
&= \begin{pmatrix} \lambda_1 \cos^2\psi + \lambda_2 \sin^2\psi & (\lambda_1 - \lambda_2) \sin \psi \cos \psi \\ (\lambda_1 - \lambda_2) \sin \psi \cos \psi & \lambda_1 \sin^2\psi + \lambda_2 \cos^2\psi \end{pmatrix}
\end{aligned}$$

we recognize that this is just the desired condition

$$a - b \cot \beta_k \geq 0. \tag{3.32}$$

For the case $-\frac{\pi}{2} < \beta_k < 0$ a similar reasoning can be applied leading also to (3.32).

In an analogous way one verifies that

$$\frac{\lambda_1}{\lambda_2} \leq \cot(\beta_k - \eta_k) \cot \eta_k \qquad \Longrightarrow \qquad c - b \tan \beta_k \geq 0.$$

(c) Let us first consider the case $1 \leq i \leq 2m-2$. Then, $\rho_i = \theta_i$, and the definition of θ_i implies that

$$\cot \rho_i - \tan \rho_i = \cot \beta_i - \tan \beta_{i+1}.$$

Solving for $\cot \rho_i$ and $\tan \rho_i$, respectively, yields

$$\cot \rho_i = \frac{1}{2} \left(\cot \beta_i - \tan \beta_{i+1} + \sqrt{(\cot \beta_i - \tan \beta_{i+1})^2 + 4} \right),$$

$$\tan \rho_i = \frac{1}{2} \left(-\cot \beta_i + \tan \beta_{i+1} + \sqrt{(\cot \beta_i - \tan \beta_{i+1})^2 + 4} \right).$$

By means of these results we obtain

$$\cot(\rho_i - \beta_i) \tan \rho_i = \frac{\cot \beta_i + \tan \rho_i}{\cot \beta_i - \cot \rho_i} = 1 + \frac{2}{\sqrt{\frac{(\cot \beta_i + \tan \beta_{i+1})^2}{(\cot \beta_i - \tan \beta_{i+1})^2 + 4}} - 1}.$$

Let us now assume that $1 \leq i \leq m-1$. Then we have

$$\tan \beta_{i+1} = \frac{(i+1) h_2}{m h_1},$$

$$\cot \beta_i = \frac{m h_1}{i h_2}.$$

This gives

$$\frac{(\cot \beta_i + \tan \beta_{i+1})^2}{(\cot \beta_i - \tan \beta_{i+1})^2 + 4} = \frac{1}{1 - \frac{4m^2 i}{\left(m^2 \frac{h_1}{h_2} + i(i+1) \frac{h_2}{h_1} \right)^2}} =: \frac{1}{1 - g_m(i)} =: f_m(i).$$

For $m > \frac{1}{2} \frac{h_2}{h_1}$ the function $g_m(x)$ is bounded and attains its global maximum in

$$x_m := -\frac{1}{6} + \frac{1}{6} \sqrt{1 + 12 \, m^2 \frac{h_1^2}{h_2^2}}.$$

Thus, for $1 \leq i \leq m-1$,

$$g_m(i) \ \leq \ g_m(x_m) \ \rightarrow \ 0^+ \quad \text{for} \quad m \rightarrow \infty,$$

which yields

$$f_m(i) \ \leq \ \frac{1}{1 - g_m(x_m)} \ \rightarrow \ 1^+ \quad \text{for} \quad m \rightarrow \infty.$$

This gives

$$\min_{1 \leq i \leq m-1} \Big(\cot(\rho_i - \beta_i) \tan \rho_i \Big) \ \geq \ 1 + \frac{2}{\sqrt{f_m(x_m)} - 1} \ \rightarrow \ \infty \quad \text{for} \quad m \rightarrow \infty.$$

For $m \leq i \leq 2m-2$ similar calculations show that by means of

$$\tan \beta_{i+1} \ = \ \frac{m h_2}{(2m-i-1) \, h_1},$$

$$\cot \beta_i \ = \ \frac{(2m-i) \, h_1}{m h_2}$$

one obtains

$$\min_{m \leq i \leq 2m-2} \Big(\cot(\rho_i - \beta_i) \tan \rho_i \Big) \ \rightarrow \ \infty \quad \text{for} \quad m \rightarrow \infty.$$

For $i = 2m-1$ we have

$$\begin{aligned}
\cot \Big(\rho_{2m-1} - \beta_{2m-1} \Big) \tan \rho_{2m-1} \ &= \ \cot \left(\frac{\pi}{4} - \frac{\beta_{2m-1}}{2} \right) \tan \left(\frac{\pi}{4} + \frac{\beta_{2m-1}}{2} \right) \\
&= \ \tan^2 \left(\frac{\pi}{4} + \frac{\beta_{2m-1}}{2} \right) \\
&\rightarrow \ \infty \quad \text{for} \quad m \rightarrow \infty.
\end{aligned}$$

It is not hard to verify that for $-2m + 1 \leq i \leq -1$ the preceding results carry over. Hence,

$$\lim_{m \rightarrow \infty} \left(\min_{|i| \in J_m} \Big(\cot(\rho_i - \beta_i) \tan \rho_i \Big) \right) \ = \ \infty. \tag{3.33}$$

Now, in a similar way as above, one establishes that

$$\lim_{m \rightarrow \infty} \left(\min_{|i| \in J_m} \Big(\cot(\beta_i - \eta_i) \cot \eta_i \Big) \right) \ = \ \infty. \tag{3.34}$$

From (3.33) and (3.34) we finally end up with the assertion

$$\lim_{m \rightarrow \infty} \Big(\min_{|i| \in J_m} \kappa_{i,m} \Big) \ = \ \infty.$$

$\square$

Remarks:

(a) We observe that the preceding existence proof is constructive. Moreover, only three directions are sufficient to guarantee a nonnegative directional splitting. Thus, unless m is very small, most of the stencil coefficients can be set to zero.

(b) Especially for large m, a $(2m{+}1){\times}(2m{+}1)$-stencil reveals much more directions than those $4m$ that are induced by the $8m$ "boundary pixels". Therefore, even if we use only 3 directions, we may expect to find stricter estimates than those given in the proof. These estimates might be improved further by admitting more than 3 directions.

(c) For a specified diffusion tensor function D it is possible to give a-priori estimates for the required stencil size: using the extremum principle it is not hard to show that

$$|\nabla u_\sigma(x,t)| \;=\; |(\nabla K_\sigma {*} u)(x,t)| \;\leq\; \frac{4\,\|f\|_{\mathrm{L}^\infty(\Omega)}}{\sqrt{2\pi}\,\sigma} \quad \text{on} \quad \bar\Omega \times (0,\infty),$$

where the notations from Chapter 2 have been used. Thanks to the uniform positive definiteness of D there exists an upper limit for the spectral condition number of D. This condition limit can be used to fix a suitable stencil size.

(d) The existence of a nonnegative directional splitting distinguishes the filter class (P_c) from morphological anisotropic equations such as mean curvature motion. In this case it has been proved that it is impossible to find a nonnegative directional splitting on a finite stencil [13]. As a remedy, Crandall and Lions [104] propose to study a convergent sequence of regularizations which can be approximated on a finite stencil.

   Let us now illustrate the ideas in the proof of Theorem 6 by applying them to a practical example: We want to find a nonnegative spatial discretization of $\operatorname{div}(D\nabla u)$ on a $(3{\times}3)$-stencil, where

$$D = \begin{pmatrix} a & b \\ b & c \end{pmatrix}$$

and a, b and c may be functions of $J_\rho(\nabla u_\sigma)$.

   Since $m = 1$ we have a partition of $(-\frac{\pi}{2}, \frac{\pi}{2}]$ into $4m{-}2 = 2$ subintervals:

$$\left(-\tfrac{\pi}{2}, \tfrac{\pi}{2}\right] \;=\; \left(-\tfrac{\pi}{2}, 0\right] \cup \left(0, \tfrac{\pi}{2}\right] \;=:\; I_{-1} \cup I_1.$$

I_{-1} and I_1 belong to the grid angles

$$\begin{aligned}
\beta_{-1} &= \arctan\left(-\frac{h_2}{h_1}\right), \\
\beta_1 &= \arctan\left(\frac{h_2}{h_1}\right) =: \beta.
\end{aligned}$$

First we focus on the case $\psi \in I_1$ where $(\cos\psi, \sin\psi)$ denotes the eigenvector to the larger eigenvalue λ_1 of D. With the notations from the proof of Theorem 6 we obtain

$$\begin{aligned}
\theta_1 &= \frac{\pi}{2}, \\
\rho_1 &= \frac{\theta_1 + \beta_1}{2} = \frac{\pi}{4} + \frac{\beta}{2}, \\
\eta_1 &= \frac{\beta}{2}.
\end{aligned}$$

Therefore, we get

$$\begin{aligned}
\cot(\rho_1 - \beta_1)\tan\rho_1 &= \cot\left(\frac{\pi}{4} - \frac{\beta}{2}\right)\tan\left(\frac{\pi}{4} + \frac{\beta}{2}\right) = \frac{1 + \sin\beta}{1 - \sin\beta}, \\
\cot(\beta_1 - \eta_1)\cot\eta_1 &= \cot^2\left(\frac{\beta}{2}\right) = \frac{1 + \cos\beta}{1 - \cos\beta},
\end{aligned}$$

which restricts the upper condition number for a nonnegative discretization with $\psi \in I_1$ to

$$\kappa_{1,1} := \min\left(\frac{1 + \sin\beta}{1 - \sin\beta}, \frac{1 + \cos\beta}{1 - \cos\beta}\right). \tag{3.35}$$

Thanks to the symmetry we obtain the same condition restriction for $\psi \in I_{-1}$. These bounds on the condition number attain their maximal value for $h_1 = h_2$. In this case $\beta = \frac{\pi}{4}$ gives

$$\kappa_{1,1} = \kappa_{-1,1} = \frac{1 + \frac{1}{2}\sqrt{2}}{1 - \frac{1}{2}\sqrt{2}} = 3 + 2\sqrt{2} \approx 5.8284. \tag{3.36}$$

By virtue of (3.28)–(3.30) we obtain as expressions for the directional diffusivities

$$\begin{aligned}
\alpha_{-1} &= \left(|b| - b\right) \cdot \frac{h_1^2 + h_2^2}{2h_1 h_2}, \\
\alpha_0 &= a - |b| \cdot \frac{h_1}{h_2}, \\
\alpha_1 &= \left(|b| + b\right) \cdot \frac{h_1^2 + h_2^2}{2h_1 h_2}, \\
\alpha_2 &= c - |b| \cdot \frac{h_2}{h_1}.
\end{aligned}$$

This induces in a natural way the following second-order discretization for div $(D\nabla u)$:

$\dfrac{\|b_{i-1,j+1}\|-b_{i-1,j+1}}{4h_1h_2}$ $+\dfrac{\|b_{i,j}\|-b_{i,j}}{4h_1h_2}$	$\dfrac{c_{i,j+1}+c_{i,j}}{2h_2^2} - \dfrac{\|b_{i,j+1}\|+\|b_{i,j}\|}{2h_1h_2}$	$\dfrac{\|b_{i+1,j+1}\|+b_{i+1,j+1}}{4h_1h_2}$ $+\dfrac{\|b_{i,j}\|+b_{i,j}}{4h_1h_2}$
$\dfrac{a_{i-1,j}+a_{i,j}}{2h_1^2}$ $-\dfrac{\|b_{i-1,j}\|+\|b_{i,j}\|}{2h_1h_2}$	$-\dfrac{a_{i-1,j}+2a_{i,j}+a_{i+1,j}}{2h_1^2}$ $-\dfrac{\|b_{i-1,j+1}\|-b_{i-1,j+1}+\|b_{i+1,j+1}\|+b_{i+1,j+1}}{4h_1h_2}$ $-\dfrac{\|b_{i-1,j-1}\|+b_{i-1,j-1}+\|b_{i+1,j-1}\|-b_{i+1,j-1}}{4h_1h_2}$ $+\dfrac{\|b_{i-1,j}\|+\|b_{i+1,j}\|+\|b_{i,j-1}\|+\|b_{i,j+1}\|+2\|b_{i,j}\|}{2h_1h_2}$ $-\dfrac{c_{i,j-1}+2c_{i,j}+c_{i,j+1}}{2h_2^2}$	$\dfrac{a_{i+1,j}+a_{i,j}}{2h_1^2}$ $-\dfrac{\|b_{i+1,j}\|+\|b_{i,j}\|}{2h_1h_2}$
$\dfrac{\|b_{i-1,j-1}\|+b_{i-1,j-1}}{4h_1h_2}$ $+\dfrac{\|b_{i,j}\|+b_{i,j}}{4h_1h_2}$	$\dfrac{c_{i,j-1}+c_{i,j}}{2h_2^2} - \dfrac{\|b_{i,j-1}\|+\|b_{i,j}\|}{2h_1h_2}$	$\dfrac{\|b_{i+1,j-1}\|-b_{i+1,j-1}}{4h_1h_2}$ $+\dfrac{\|b_{i,j}\|-b_{i,j}}{4h_1h_2}$

All nonvanishing entries of the p-th row of $A(u)$ are represented in this stencil, where $p(i,j)$ is the index of some inner pixel (i,j). Thus, for instance, the upper left stencil entry gives the element $(p(i,j),\, p(i-1,j+1))$ of $A(u)$. The other notations should be clear from the context as well, e.g. $b_{i,j}$ denotes a finite difference approximation of $b(J_\rho(\nabla u_\sigma))$ at some grid point (x_i, y_j).

The problem of finding nonnegative difference approximations to elliptic expressions with mixed derivatives has a long history; see e.g. [294, 120, 170]. Usually it is studied for the expression

$$a(x,y)\,\partial_{xx}u + 2b(x,y)\,\partial_{xy}u + c(x,y)\,\partial_{yy}u.$$

The approach presented here extends these results to

$$\partial_x\Big(a(x,y)\,\partial_x u\Big) + \partial_x\Big(b(x,y)\,\partial_y u\Big) + \partial_y\Big(b(x,y)\,\partial_x u\Big) + \partial_y\Big(c(x,y)\,\partial_y u\Big)$$

and establishes the relation between the condition number of $\begin{pmatrix} a & b \\ b & c \end{pmatrix}$ and the nonnegativity of the difference operator. Recently Kocan described an interesting alternative to obtain upper bounds for the stencil size as a function of the condition number [238]. His derivation is based on the diophantine problem of approximating irrationals by rational numbers.

Chapter 4

Discrete diffusion filtering

This chapter presents a discrete class of diffusion processes for which one can establish similar properties as in the semidiscrete case concerning existence, uniqueness, continuous dependence of the solution on the initial image, maximum-minimum principle, average grey level invariance, Lyapunov sequences and convergence to a constant steady-state. We shall see that this class comprises α-semi-implicit discretizations of the semidiscrete filter class (P_s) as well as certain variants of them which are based on an additive operator splitting.

4.1 The general model

As in Chapter 3 we regard a discrete image as a vector $f \in \mathbb{R}^N$, $N \geq 2$, and denote the index set $\{1, ..., N\}$ by J. We consider the following discrete filter class (P_d):

Let $f \in \mathbb{R}^N$. Calculate a sequence $(u^{(k)})_{k \in \mathbb{N}_0}$ of processed versions of f by means of

$$
\begin{aligned}
u^{(0)} &= f, \\
u^{(k+1)} &= Q(u^{(k)}) \, u^{(k)}, \qquad \forall \, k \in \mathbb{N}_0,
\end{aligned}
$$

where $Q = (q_{ij})$ has the following properties:

(D1) continuity in its argument: $\qquad Q \in \mathrm{C}(\mathbb{R}^N, \mathbb{R}^{N \times N})$,

(D2) symmetry: $\qquad q_{ij}(v) = q_{ji}(v) \quad \forall \, i, j \in J, \quad \forall \, v \in \mathbb{R}^N$,

(D3) unit row sum: $\qquad \sum_{j \in J} q_{ij}(v) = 1 \quad \forall \, i \in J, \quad \forall \, v \in \mathbb{R}^N$,

(D4) nonnegativity: $\qquad q_{ij}(v) \geq 0 \quad \forall \, i, j \in J, \quad \forall \, v \in \mathbb{R}^N$,

(D5) irreducibility for all $v \in \mathbb{R}^N$,

(D6) positive diagonal: $\qquad q_{ii}(v) > 0 \quad \forall \, i \in J, \quad \forall \, v \in \mathbb{R}^N$.

(P_d)

Remarks:

(a) Although the basic idea behind scale-spaces is to have a continuous scale parameter, it is evident that fully discrete results are of importance since, in practice, scale-space evolutions are evaluated exclusively at a finite number of scales.

(b) The requirements (D1)–(D5) have a similar meaning as their semidiscrete counterparts (S1)–(S5). Indeed, (D1) immediately gives well-posedness results, while the proof of the extremum principle requires (D3) and (D4), and average grey value invariance is based on (D2) and (D3). The existence of Lyapunov sequences is a consequence of (D2)–(D4), strict Lyapunov sequences need (D5) and (D6) in addition to (D2)–(D4), and the convergence to a constant steady-state utilizes (D2)–(D5).

(c) Nonnegative matrices $Q = (q_{ij}) \in \mathbb{R}^{N \times N}$ satisfying $\sum_{j \in J} q_{ij} = 1$ for all $i \in J$ are also called *stochastic matrices*. Moreover, if Q is stochastic and $\sum_{i \in J} q_{ij} = 1$ for all $j \in J$, then Q is *doubly stochastic*. This indicates that our discrete diffusion processes are related to the theory of Markov chains [370, 223].

4.2   Theoretical results

It is obvious that for a fixed filter belonging to the class (P_d) every initial image $f \in \mathbb{R}^N$ generates a unique sequence $(u^{(k)})_{k \in \mathbb{N}_0}$. Moreover, by means of (D1) we know that, for every finite k, $u^{(k)}$ depends continuously on f. Therefore, let us now prove a maximum–minimum principle.

Proposition 3 (Extremum principle).
Let $f \in \mathbb{R}^N$ and let $(u^{(k)})_{k \in \mathbb{N}_0}$ be the sequence of filtered images according to (P_d). Then,

$$a \; \leq \; u_i^{(k)} \; \leq \; b \qquad \forall \, i \in J, \quad \forall \, k \in \mathbb{N}_0, \tag{4.1}$$

where

$$a := \min_{j \in J} f_j, \tag{4.2}$$
$$b := \max_{j \in J} f_j. \tag{4.3}$$

Proof:
The maximum–minimum principle follows directly from the fact that, for all $i \in J$ and $k \in \mathbb{N}_0$, the following inequalities hold:

(i) $\quad u_i^{(k+1)} \; = \; \sum_{j \in J} q_{ij}(u^{(k)}) u_j^{(k)} \; \overset{(D4)}{\leq} \; \max_{m \in J} u_m^{(k)} \sum_{j \in J} q_{ij}(u^{(k)}) \; \overset{(D3)}{=} \; \max_{m \in J} u_m^{(k)}.$

(ii) $\quad u_i^{(k+1)} \; = \; \sum_{j \in J} q_{ij}(u^{(k)}) u_j^{(k)} \;\overset{(D4)}{\geq}\; \min_{m \in J} u_m^{(k)} \sum_{j \in J} q_{ij}(u^{(k)}) \;\overset{(D3)}{=}\; \min_{m \in J} u_m^{(k)}.$

$\qquad\qquad\qquad\qquad\qquad\qquad\qquad\qquad\qquad\qquad\qquad\qquad\qquad\qquad\qquad$ $\square$

4.3 Scale-space properties

All statements from Chapter 3 with respect to invariances are valid in the discrete framework as well. Below we focus on proving average grey level invariance.

Proposition 4 (Conservation of average grey value).
The average grey level

$$\mu \; := \; \frac{1}{N} \sum_{j \in J} f_j \tag{4.4}$$

is not affected by the discrete diffusion filter:

$$\frac{1}{N} \sum_{j \in J} u_j^{(k)} = \mu \qquad \forall\, k \in \mathbb{N}_0. \tag{4.5}$$

Proof:
By virtue of (D2) and (D3) we have $\sum_{i \in J} q_{ij}(u^{(k)}) = 1$ for all $j \in J$ and $k \in \mathbb{N}_0$. This so-called *redistribution property* [164] ensures that, for all $k \in \mathbb{N}_0$,

$$\sum_{i \in J} u_i^{(k+1)} \; = \; \sum_{i \in J} \sum_{j \in J} q_{ij}(u^{(k)}) u_j^{(k)} \; = \; \sum_{j \in J} \Big(\sum_{i \in J} q_{ij}(u^{(k)}) \Big) u_j^{(k)} \; = \; \sum_{j \in J} u_j^{(k)},$$

which proves the proposition. $\hfill\square$

As one might expect, the class (P_d) allows an interpretation as a transformation which is smoothing in terms of Lyapunov sequences. These functions ensure that $u^{(k)}$ converges to a constant image as $k \to \infty$. However, we need less regularity than in the semidiscrete case: The convex function r, which generates the Lyapunov sequences, needs only to be continuous, but no more differentiable.

Theorem 7 (Lyapunov sequences and behaviour for $k \to \infty$).
Assume that $(u^{(k)})_{k \in \mathbb{N}_0}$ satisfies the requirements of (P_d), let a, b, and μ be defined as in (4.2), (4.3), and (4.4), respectively, and let $c := (\mu, \mu, ..., \mu)^\top \in \mathbb{R}^N$. Then the following properties are fulfilled:

(a) (Lyapunov sequences)
For all convex $r \in \mathrm{C}[a, b]$ the sequence

$$V^{(k)} := \Phi(u^{(k)}) := \sum_{i \in J} r(u_i^{(k)}), \qquad k \in \mathbb{N}_0$$

is a Lyapunov sequence:

(i) $\Phi(u^{(k)}) \geq \Phi(c) \quad \forall \, k \in \mathbb{N}_0$

(ii) $V^{(k+1)} - V^{(k)} \leq 0 \quad \forall \, k \in \mathbb{N}_0$

Moreover, if r is strictly convex, then $V^{(k)} = \Phi(u^{(k)})$ is a strict Lyapunov sequence:

(iii) $\Phi(u^{(k)}) = \Phi(c) \quad \Longleftrightarrow \quad u^{(k)} = c$

(iv) $V^{(k+1)} - V^{(k)} = 0 \quad \Longleftrightarrow \quad u^{(k)} = c$

(b) (Convergence)
   $\lim\limits_{k \to \infty} u^{(k)} = c.$

Proof:

(a)   (i) Average grey level invariance and the convexity of r give

$$
\begin{aligned}
\Phi(c) &= \sum_{i=1}^{N} r \left(\sum_{j=1}^{N} \frac{1}{N} u_j^{(k)} \right) \\
&\leq \sum_{i=1}^{N} \left(\frac{1}{N} \sum_{j=1}^{N} r(u_j^{(k)}) \right) \\
&= \sum_{j=1}^{N} r(u_j^{(k)}) \\
&= \Phi(u^{(k)}).
\end{aligned}
\tag{4.6}
$$

(ii) For $i, j \in J$ we define

$$
a_{ij}(u^{(k)}) := \begin{cases} q_{ij}(u^{(k)}) - 1 & (i = j) \\ q_{ij}(u^{(k)}) & (i \neq j). \end{cases}
\tag{4.7}
$$

Using the convexity of r, the preceding definition, and the prerequisites (D2) and (D3) we obtain

$$
\begin{aligned}
V^{(k+1)} - V^{(k)} &= \sum_{i=1}^{N} \left(r \left(\sum_{j=1}^{N} q_{ij}(u^{(k)}) \, u_j^{(k)} \right) - r(u_i^{(k)}) \right) \\
&\stackrel{\text{conv.}}{\leq} \sum_{i=1}^{N} \left(\sum_{j=1}^{N} q_{ij}(u^{(k)}) \, r(u_j^{(k)}) - r(u_i^{(k)}) \right) \\
&\stackrel{(4.7)}{=} \sum_{i=1}^{N} \sum_{j=1}^{N} a_{ij}(u^{(k)}) \, r(u_j^{(k)}) \\
&\stackrel{(D3)}{=} \sum_{i=1}^{N} \sum_{j=1}^{N} a_{ij}(u^{(k)}) \left(r(u_j^{(k)}) - r(u_i^{(k)}) \right)
\end{aligned}
$$

$$= \sum_{i=1}^{N} \sum_{m=1}^{N-i} a_{i+m,i}(u^{(k)}) \left(r(u_i^{(k)}) - r(u_{i+m}^{(k)}) \right)$$

$$+ \sum_{i=1}^{N} \sum_{m=1}^{N-i} a_{i,i+m}(u^{(k)}) \left(r(u_{i+m}^{(k)}) - r(u_i^{(k)}) \right)$$

$$\stackrel{(D2)}{=} 0. \tag{4.8}$$

(iii) This part of the proof can be shown in exactly the same manner as in the semidiscrete case (Chapter 3, Theorem 5): Equality in the estimate (4.6) holds due to the strict convexity of r if and only if $u^{(k)} = c$.

(iv) In order to verify the first implication, let us start with a proof that $V^{(k+1)} = V^{(k)}$ implies $u_1^{(k)} = ... = u_N^{(k)}$. To this end, assume that $u^{(k)}$ is not constant:

$$u_{i_0}^{(k)} := \min_{i \in J} u_i^{(k)} < \max_{j \in J} u_j^{(k)} =: u_{j_0}^{(k)}.$$

Then, by the irreducibility of $Q(u^{(k)})$, we find $l_0, ..., l_r \in J$ with $l_0 = i_0$, $l_r = j_0$ and $q_{l_p l_{p+1}} \neq 0$ for $p = 0, ..., r-1$. Hence, there exists some $p_0 \in \{0, ..., r-1\}$ such that $n := l_{p_0}$, $m := l_{p_0+1}$, $q_{nm}(u^{(k)}) \neq 0$, and $u_m^{(k)} \neq u_n^{(k)}$. Moreover, the nonnegativity of $Q(u^{(k)})$ gives $q_{nm}(u^{(k)}) > 0$, and by (D6) we have $q_{nn}(u^{(k)}) > 0$. Together with the strict convexity of r these properties lead to

$$r \left(\sum_{j=1}^{N} q_{nj}(u^{(k)}) u_j^{(k)} \right)$$

$$= r \left(\sum_{\substack{j=1 \\ j \neq n,m}}^{N} q_{nj}(u^{(k)}) u_j^{(k)} + q_{nn}(u^{(k)}) u_n^{(k)} + q_{nm}(u^{(k)}) u_m^{(k)} \right)$$

$$< \sum_{\substack{j=1 \\ j \neq n,m}}^{N} q_{nj}(u^{(k)}) r(u_j^{(k)}) + q_{nn}(u^{(k)}) r(u_n^{(k)}) + q_{nm}(u^{(k)}) r(u_m^{(k)})$$

$$= \sum_{j=1}^{N} q_{nj}(u^{(k)}) r(u_j^{(k)}).$$

If we combine this with the results in (4.8), we obtain

$$V^{(k+1)} - V^{(k)} = \sum_{\substack{i=1 \\ i \neq n}}^{N} \left(r \left(\sum_{j=1}^{N} q_{ij}(u^{(k)}) u_j^{(k)} \right) - r(u_i^{(k)}) \right)$$

$$+ r \left(\sum_{j=1}^{N} q_{nj}(u^{(k)}) u_j^{(k)} \right) - r(u_n^{(k)})$$

$$< \quad \sum_{i=1}^{N} \left(\sum_{j=1}^{N} q_{ij}(u^{(k)}) \, r(u_j^{(k)}) - r(u_i^{(k)}) \right)$$

$$\overset{(4.8)}{=} \quad 0.$$

This establishes that $V^{(k+1)} = V^{(k)}$ implies $u_1^{(k)} = ... = u_N^{(k)}$. Then, by virtue of the grey value invariance, we conclude that $u^{(k)} = c$.

Conversely, let $u^{(k)} = c$. By means of prerequisite (D3) we obtain

$$V^{(k+1)} - V^{(k)} \;=\; \sum_{i=1}^{N} r \left(\sum_{j=1}^{N} q_{ij}(u^{(k)}) \mu \right) - \sum_{i=1}^{N} r(\mu) \;=\; 0.$$

(c) In order to prove convergence to a constant steady-state, we can argue exactly in the same way as in the semidiscrete case if we replace Lyapunov functions by Lyapunov sequences and integrals by sums. See Chapter 3, Theorem 5 for more details. □

In analogy to the semidiscrete case the preceding theorem comprises many Lyapunov functions which demonstrate the information-reducing qualities of our filter class. Choosing the convex functions $r(s) := |s|^p$, $r(s) := (s-\mu)^{2n}$ and $r(s) := s \ln s$, we immediately obtain the following corollary.

Corollary 3 (Special Lyapunov sequences).
Let $(u^{(k)})_{k \in \mathbb{N}_0}$ be a diffusion sequence according to (P_d), and let a and μ be defined as in (4.2) and (4.4). Then the following functions are decreasing in k:

(a) $\|u^{(k)}\|_p \quad$ *for all $p \geq 1$.*

(b) $M_{2n}[u^{(k)}] \;:=\; \frac{1}{N} \sum_{j=1}^{N} (u_j^{(k)} - \mu)^{2n} \quad$ *for all $n \in \mathbb{N}$.*

(c) $H[u^{(k)}] \;:=\; \sum_{j=1}^{N} u_j^{(k)} \ln(u_j^{(k)}), \quad$ *if $a > 0$.*

An interpretation of these results in terms of decreasing energy, decreasing central moments and increasing entropy is evident.

4.4 Relation to semidiscrete models

4.4.1 Semi-implicit schemes

Let us now investigate in which sense our discrete filter class covers in a natural way time discretizations of semidiscrete filters. To this end, we regard $u^{(k)}$ as an

approximation of the solution u of (P_s) at time $t = k\tau$, where τ denotes the time step size. We consider a finite difference scheme with two time levels where the operator A – which depends nonlinearly on u – is evaluated in an explicit way, while the linear remainder is discretized in an α-implicit manner. Such schemes are called α-*semi-implicit*. They reveal the advantage that the linear implicit part ensures good stability properties, while the explicit evaluation of the nonlinear terms avoids the necessity to solve nonlinear systems of equations. The theorem below states that this class of schemes is covered by the discrete framework, for which we have established scale-space results.

Theorem 8 (Scale-space interpretation for α-semi-implicit schemes).
Let $\alpha \in [0,1]$, $\tau > 0$, and let $A = (a_{ij}) : \mathbb{R}^N \to \mathbb{R}^{N \times N}$ satisfy the requirements (S1)–(S5) of section 3.1. Then the α-semi-implicit scheme

$$\frac{u^{(k+1)} - u^{(k)}}{\tau} \;=\; A(u^{(k)})\left(\alpha u^{(k+1)} + (1-\alpha)u^{(k)}\right) \tag{4.9}$$

fulfils the prerequisites (D1)–(D6) for discrete diffusion models provided that

$$\tau \;\leq\; \frac{1}{(1-\alpha)\, \max\limits_{i \in J} |a_{ii}(u^{(k)})|} \tag{4.10}$$

for $\alpha \in (0,1)$. In the explicit case ($\alpha=0$) the properties (D1)–(D6) hold for

$$\tau \;<\; \frac{1}{\max\limits_{i \in J} |a_{ii}(u^{(k)})|}, \tag{4.11}$$

and the semi-implicit case ($\alpha=1$) satisfies (D1)–(D6) unconditionally.

Proof: Let

$$
\begin{aligned}
B(u^{(k)}) &:= (b_{ij}(u^{(k)})) \;:=\; I - \alpha\tau A(u^{(k)}), \\
C(u^{(k)}) &:= (c_{ij}(u^{(k)})) \;:=\; I + (1-\alpha)\tau A(u^{(k)}),
\end{aligned}
$$

where $I \in \mathbb{R}^N$ denotes the unit matrix. Since (4.9) can be written as

$$B(u^{(k)})\, u^{(k+1)} \;=\; C(u^{(k)})\, u^{(k)}$$

we first have to show that $B(u^{(k)})$ is invertible for all $u^{(k)} \in \mathbb{R}^N$. Henceforth, the argument $u^{(k)}$ is suppressed frequently since the considerations below are valid for all $u^{(k)} \in \mathbb{R}^N$.

If $\alpha = 0$, then $B = I$ and hence invertible. Now assume that $\alpha > 0$. Then B is strictly diagonally dominant, since

$$b_{ii} \;=\; 1 - \alpha\tau a_{ii} \;\overset{(S3)}{=}\; 1 + \alpha\tau \sum_{\substack{j \in J \\ j \neq i}} a_{ij} \;>\; \alpha\tau \sum_{\substack{j \in J \\ j \neq i}} a_{ij} \;\overset{(S4)}{=}\; \sum_{\substack{j \in J \\ j \neq i}} |b_{ij}| \qquad \forall\, i \in J.$$

This also shows that $b_{ii} > 0$ for all $i \in J$, and by the structure of the off-diagonal elements of B we observe that the irreducibility of A implies the irreducibility of B. Thanks to the fact that B is irreducibly diagonally dominant, $b_{ij} \leq 0$ for all $i \neq j$, and $b_{ii} > 0$ for all $i \in J$, we know from [407, p. 85] that $B^{-1} =: H =: (h_{ij})$ exists and $h_{ij} > 0$ for all $i, j \in J$. Thus, $Q := (q_{ij}) := B^{-1}C$ exists and by (S1) it follows that $Q \in C(\mathbb{R}^N, \mathbb{R}^{N \times N})$. This proves (D1).

The requirement (D2) is not hard to satisfy: Since B^{-1} and C are symmetric and reveal the same set of eigenvectors – namely those of A – it follows that $Q = B^{-1}C$ is symmetric as well.

Let us now verify (D3). By means of (S3) we obtain

$$\sum_{j \in J} b_{ij} = 1 = \sum_{j \in J} c_{ij} \qquad \forall\, i \in J. \tag{4.12}$$

Let $v := (1, ..., 1)^\top \in \mathbb{R}^N$. Then (4.12) is equivalent to

$$Bv = v = Cv, \tag{4.13}$$

and the invertibility of B gives

$$v = B^{-1}v = Hv. \tag{4.14}$$

Therefore, from

$$Qv \;=\; HCv \;\overset{(4.13)}{=}\; Hv \;\overset{(4.14)}{=}\; v$$

we conclude that $\sum_{j \in J} q_{ij} = 1$ for all $i \in J$. This proves (D3).

In order to show that (D4) is fulfilled, we first check the nonnegativity of C. For $i \neq j$ we have

$$c_{ij} \;=\; (1-\alpha)\tau a_{ij} \;\overset{(S4)}{\geq}\; 0.$$

The diagonal entries yield

$$c_{ii} \;=\; 1 + (1-\alpha)\tau a_{ii}.$$

If $\alpha = 1$ we have $c_{ii} = 1$ for all $i \in J$. For $0 \leq \alpha < 1$, however, nonnegativity of C is not automatically guaranteed: Using (S3)–(S5) we obtain

$$a_{ii} \;\overset{(S3)}{=}\; -\sum_{\substack{j \in J \\ j \neq i}} a_{ij} \;\overset{(S4),(S5)}{<}\; 0 \qquad \forall\, i \in J. \tag{4.15}$$

Hence, $C(u^{(k)})$ is nonnegative if

$$\tau \;\leq\; \frac{1}{(1-\alpha)\,\max\limits_{i \in J} |a_{ii}(u^{(k)})|} \;=:\; \tau_\alpha(u^{(k)}).$$

Since H is nonnegative, we know that the nonnegativity of C implies the nonnegativity of $Q = HC$.

Now we want to prove (D5). If $\alpha = 1$, then $C = I$, and by the positivity of H we have $q_{ij} > 0$ for all $i, j \in J$. Thus, Q is irreducible.

Next let us consider the case $0 < \alpha < 1$ and $\tau \leq \tau_\alpha(u^{(k)})$. Then we know that C is nonnegative. Using this information, the positivity of H, the symmetry of C, and (4.12) we obtain

$$q_{ij} \;=\; \sum_{k \in J} h_{ik} c_{kj} \;\geq\; \underbrace{\min_{k \in J} h_{ik}}_{>0} \cdot \underbrace{\sum_{k \in J} c_{kj}}_{=1} \;>\; 0 \qquad \forall\, i, j \in J,$$

which establishes the irreducibility of Q.

Finally, for $\alpha = 0$, we have $Q = C$. For $i, j \in J$ with $i \neq j$ we know that $a_{ij}(u^{(k)}) > 0$ implies $c_{ij}(u^{(k)}) > 0$. Now for

$$\tau \;<\; \frac{1}{\max\limits_{i \in J} |a_{ii}(u^{(k)})|}$$

it follows that $c_{ii}(u^{(k)}) > 0$ for all $i \in J$ and, thus, the irreducibility of $A(u^{(k)})$ carries over to $Q(u^{(k)})$.

In all the abovementioned cases the time step size restrictions for ensuring irreducibility imply that all diagonal elements of $Q(u^{(k)})$ are positive. This establishes (D6). $\qquad\qquad\qquad\qquad\qquad\qquad\qquad\qquad\qquad\qquad\qquad\qquad\square$

Remarks:

(a) We have seen that the discrete filter class (P_d) – although at first glance looking like a pure explicit discretization – covers the α-semi-implicit case as well. Explicit two-level schemes are comprised by the choice $\alpha = 0$. Equation (4.11) shows that they reveal the most prohibitive time step size restrictions.

(b) The conditions (4.10) and (4.11) can be satisfied by means of an a-priori estimate. Since the semi-implicit scheme fulfils (D1)–(D6) we know by Theorem 3 that the solution obeys an extremum principle. This means that $u^{(k)}$ belongs to the compact set $\{v \in \mathbb{R}^N \mid \|v\|_\infty \leq \|f\|_\infty\}$ for all $k \in \mathbb{N}_0$. By $A \in C(\mathbb{R}^N, \mathbb{R}^{N \times N})$ it follows that

$$K_f := \max\left\{ |a_{ii}(v)| \;\middle|\; i \in J,\; v \in \mathbb{R}^N,\; \|v\|_\infty \leq \|f\|_\infty \right\}$$

exists, and (4.15) shows that $K_f > 0$. Thus, choosing

$$\tau \;\leq\; \frac{1}{(1-\alpha)\, K_f}$$

ensures that (4.10) is always satisfied, and

$$\tau \; < \; \frac{1}{K_f}$$

guarantees that (4.11) holds.

(c) If $\alpha > 0$, a large linear system of equations has to be solved. Its system matrix is symmetric, diagonally dominant, and positive definite. Usually, it is also sparse: For instance, if it results from a finite difference discretization on a $(2p+1) \times (2p+1)$-stencil it contains at most $4p^2 + 4p + 1$ nonvanishing entries per row. One should not expect, however, that in the i-th row these entries can be found within the positions $[i, i-2p^2-2p]$ to $[i, i+2p^2+2p]$. In general, the matrix reveals a much larger bandwidth.

Applying standard direct algorithms such as Gaussian elimination would destroy the zeros within the band and would lead to an immense storage and computation effort. Modifications in order to reduce these problems [122] are quite difficult to implement.

Iterative algorithms appear to be better suited. Classical methods such as Gauß–Seidel or SOR [447] are easy to code, they do not need additional storage, and their convergence can be guaranteed for the special structure of A. Unfortunately, they converge rather slowly. Faster iterative methods such as preconditioned conjugate gradient algorithms [348] need significantly more storage, which can become prohibitive for large images. A typical problem of iterative methods is that their convergence slows down for larger τ, since this increases the condition number of the system matrix. Multigrid methods [59, 179] are one possibility to circumvent these difficulties; another possibility will be studied in Section 4.4.2.

(d) For $\alpha = 1$ we obtain semi-implicit schemes which do not suffer from time step size restrictions. In spite of the fact that the nonlinearity is discretized in an explicit way they are absolutely stable in the maximum norm, and they inherit the scale-space properties from the semidiscrete setting regardless of the step size. Compared to explicit schemes, this advantage usually overcompensates for the additional effort of resolving a linear system.

(e) By the explicit discretization of the nonlinear operator A it follows that all schemes in the preceding theorem are of first order in time. This should not give rise to concern, since in image processing one is in general more interested in maintaining qualitative properties such as maximum principles or invariances rather than having an accurate approximation of the continuous equation. However, if one insists in second-order schemes, one may for

instance use the predictor–corrector approach by Douglas and Jones [121]:

$$\frac{u^{(k+1/2)} - u^{(k)}}{\tau/2} = A(u^{(k)})\, u^{(k+1/2)},$$

$$\frac{u^{(k+1)} - u^{(k)}}{\tau} = A(u^{(k+1/2)}) \left(\tfrac{1}{2}u^{(k+1)} + \tfrac{1}{2}u^{(k)}\right).$$

This scheme satisfies the properties (D1)–(D6) for $\tau \le 2/K_f$.

(f) The assumptions (S1)–(S5) are sufficient conditions for the α-semi-implicit scheme to fulfil (D1)–(D6), but they are not necessary. Nonnegativity of $Q(u^{(k)})$ may also be achieved using spatial discretizations where $A(u^{(k)})$ has negative off-diagonal elements (see [55] for examples).

4.4.2 AOS schemes

We have seen that, for $\alpha > 0$, the preceding α-semi-implicit schemes require to solve a linear system with the system matrix $(I - \alpha\tau A(u^{(k)}))$. Since this can be numerically expensive, it would be nice to have an efficient alternative. Suppose we know a splitting

$$A(u^{(k)}) = \sum_{l=1}^{m} A_l(u^{(k)}), \tag{4.16}$$

such that the m linear systems with system matrices $(I - m\alpha\tau A_l(u^{(k)}))$, $l = 1,...,m$ can be solved more efficiently. Then it is advantageous to study instead of the α-semi-implicit scheme

$$u^{(k+1)} = \left(I - \alpha\tau \sum_{l=1}^{m} A_l(u^{(k)})\right)^{-1} \left(I + (1-\alpha)\tau \sum_{l=1}^{m} A_l(u^{(k)})\right) u^{(k)} \tag{4.17}$$

its *additive operator splitting (AOS)* variant [424]

$$u^{(k+1)} = \frac{1}{m} \sum_{l=1}^{m} \left(I - \alpha m\tau A_l(u^{(k)})\right)^{-1} \left(I + (1-\alpha)m\tau A_l(u^{(k)})\right) u^{(k)}. \tag{4.18}$$

By means of a Taylor expansion one can verify that, although both schemes are not identical, they have the same approximation order in space and time. Hence, from a numerical viewpoint, they are both consistent approximations to the semidiscrete ODE system from (P_s).

The following theorem clarifies the conditions under which AOS schemes create discrete scale-spaces.

Theorem 9 (Scale-space interpretation for AOS schemes).
Let $\alpha \in (0,1]$, $\tau > 0$, and let $A_l = (a_{ijl})_{ij} : \mathbb{R}^N \to \mathbb{R}^{N \times N}$, $l = 1,...,m$ satisfy the requirements (S1)–(S4) of section 3.1. Moreover, assume that $A(u) = \sum_{l=1}^{m} A_l(u)$ is irreducible for all $u \in \mathbb{R}^N$, and that for each A_l there exists a permutation matrix $P_l \in \mathbb{R}^{N \times N}$ such that $P_l A_l P_l^T$ is block diagonal and irreducible within each block. Then the following holds:

For $\alpha \in (0,1)$, the AOS scheme (4.18) fulfils the prerequisites (D1)–(D6) of discrete diffusion scale-spaces provided that

$$\tau \; < \; \frac{1}{(1-\alpha)\, m \, \max\limits_{i,l} |a_{iil}(u^{(k)})|}. \tag{4.19}$$

In the semi-implicit case ($\alpha = 1$), the properties (D1)–(D6) are unconditionally satisfied.

Proof: The reasoning is similar to the proof of Theorem 8. Let

$$B_l(u^{(k)}) \; := \; (b_{ijl}(u^{(k)}))_{ij} \; := \; I - \alpha m \tau A_l(u^{(k)}),$$
$$C_l(u^{(k)}) \; := \; (c_{ijl}(u^{(k)}))_{ij} \; := \; I + (1-\alpha) m \tau A_l(u^{(k)}).$$

B_l is invertible because of its strict diagonal dominance:

$$b_{iil} \; \overset{(S3)}{=} \; 1 + \alpha m \tau \sum_{\substack{j \in J \\ j \neq i}} a_{ijl} \; > \; \alpha m \tau \sum_{\substack{j \in J \\ j \neq i}} a_{ijl} \; \overset{(S4)}{=} \; \sum_{\substack{j \in J \\ j \neq i}} |b_{ijl}| \qquad \forall\, i \in J.$$

Since $A_l(u)$ is continuous in u by virtue of (S1), it follows that

$$Q(u) \; := \; \frac{1}{m} \sum_{l=1}^{m} B_l^{-1}(u)\, C_l(u)$$

is also continuous in u. This proves (D1).

The symmetry property (D2) of Q results directly from the fact that B_l^{-1} and C_l are symmetric and share their eigenvectors with those of A_l.

In the same way as in the proof of Theorem 8 one shows that $B_l^{-1} C_l$ has only unit row sums for all l. Thus, the row sums of Q are 1 as well, and (D3) is satisfied.

To verify (D4), we utilize that B_l is strictly diagonally dominant, $b_{iil} > 0$ for all i, and $b_{ijl} \leq 0$ for $i \neq j$. Under these circumstances it follows from [284, p. 192] that $H_l := B_l^{-1}$ is nonnegative in all components. Thus, a sufficient condition for proving (D4) is to ensure that C_l is nonnegative for all l. For $i \neq j$ we have

$$c_{ijl} \; = \; (1-\alpha) m \tau a_{ijl} \; \overset{(S4)}{\geq} \; 0.$$

The diagonal entries yield

$$c_{iil} = 1 + (1-\alpha)m\tau a_{iil}.$$

If $\alpha = 1$ we have $c_{ii} = 1$ for all $i \in J$. For $0 < \alpha < 1$, however, nonnegativity of C is not automatically guaranteed: Since A_l satisfies (S3) and (S4), we know that $a_{iil} \leq 0$, for all i. Moreover, by (4.15) it follows that for every i there exists an l with $a_{iil} < 0$. Thus, requiring

$$\tau < \frac{1}{(1-\alpha)\, m\, \max\limits_{i,l} |a_{iil}(u^{(k)})|} =: \tau_\alpha\big(u^{(k)}\big)$$

guarantees that

$$c_{iil} > 0 \qquad \forall\, i \in J, \qquad \forall\, l = 1, ..., m. \tag{4.20}$$

Next we prove (D5), the irreducibility of Q. Suppose that $a_{i_0 j_0} \neq 0$ for some $i_0, j_0 \in J$. Then there exists an $l_0 \in \{1, ..., m\}$ such that $a_{i_0 j_0 l_0} \neq 0$. Denoting B_l^{-1} by $H_l = (h_{ijl})_{ij}$, we show now that $a_{i_0 j_0 l_0} \neq 0$ implies $h_{i_0 j_0 l_0} > 0$.

This can be seen as follows: There exist permutation matrices P_l, $l = 1, ..., m$ such that $P_l B_l P_l^T$ is block diagonal. Each block is irreducible and strictly diagonally dominant with a positive diagonal and nonpositive off-diagonals. Thus, a theorem by Varga [407, p. 85] ensures that the inverse of each block contains only positive elements. As a consequence, $a_{i_0 j_0 l_0} \neq 0$ implies $h_{i_0 j_0 l_0} > 0$.

Together with (4.20) this yields

$$q_{i_0 j_0} = \frac{1}{m}\left(\sum_{(l,n)\neq(l_0,j_0)} \underbrace{h_{i_0 nl}}_{\geq 0}\, \underbrace{c_{nj_0 l}}_{\geq 0} + \underbrace{h_{i_0 j_0 l_0}}_{>0}\, \underbrace{c_{j_0 j_0 l_0}}_{>0} \right) > 0.$$

Recapitulating, this means that, for $\tau < \tau_\alpha(u^{(k)})$,

$$a_{i_0 j_0} \neq 0 \quad \Longrightarrow \quad q_{i_0 j_0} > 0. \tag{4.21}$$

Thus, the irreducibility of A carries over to Q, and (D5) is proved.

Moreover, (4.21) also proves (D6): By virtue of (4.15) we have $a_{ii} < 0$ for all $i \in J$. Therefore, Q must have a positive diagonal. $\qquad\square$

Remarks:

(a) In analogy to the unsplit α-semi-implicit schemes, the case $\alpha = 1$ is especially interesting, because no time step size restriction occurs. Again, it is also possible to construct a predictor–corrector scheme of Douglas–Jones type [121] within the AOS framework:

$$u^{(k+1/2)} = \frac{1}{m}\sum_{l=1}^{m}\left(I - \tfrac{1}{2}m\tau A_l(u^{(k)})\right)^{-1} u^{(k)},$$

$$u^{(k+1)} = \frac{1}{m}\sum_{l=1}^{m}\left(I - \tfrac{1}{2}m\tau A_l(u^{(k+1/2)})\right)^{-1}\left(I + \tfrac{1}{2}m\tau A_l(u^{(k+1/2)})\right) u^{(k)}.$$

It satisfies (D1)–(D6) for $\tau < 2/K_f$, where K_f is determined by the a-priori estimate

$$K_f := m \, \max \left\{ |a_{iil}(v)| \, \Big| \, i \in J, \, l \in \{1, ..., m\}, \, v \in \mathbb{R}^N, \, \|v\|_\infty \le \|f\|_\infty \right\}.$$

However, the AOS–Douglas–Jones scheme is only first order accurate in time.

(b) The fact that AOS schemes use an *additive* splitting ensures that all coordinate axes are treated in exactly the same manner. This is in contrast to the various conventional splitting techniques from the literature [120, 277, 286, 354, 442]. They are *multiplicative* splittings. A typical representative is

$$u^{(k+1)} \; = \; \prod_{l=1}^m \left(I - \tau A_l(u^{(k)}) \right)^{-1} u^{(k)}.$$

Since in the general nonlinear case the split operators A_l, $l = 1,..., m$ do not commute, the result of multiplicative splittings will depend on the order of the operators. In practice, this means that these schemes produce different results if the image is rotated by 90 degrees. Moreover, most multiplicative splittings lead to a nonsymmetric matrix $Q(u^{(k)})$. This violates requirement (D2) for discrete scale-spaces.

(c) The result $u^{(k+1)}$ of an AOS scheme can be regarded as the average of m filters of type

$$v_l^{(k+1)} := \left(I - \alpha m \tau A_l(u^{(k)}) \right)^{-1} \left(I + (1-\alpha) m \tau A_l(u^{(k)}) \right) u^{(k)} \qquad (l = 1, ..., m).$$

Since $v_l^{(k+1)}$, $l = 1,...,m$ can be calculated independently from each other, it is possible to distribute their computation to different processors of a parallel machine.

(d) AOS schemes with $\alpha = 1$ have been presented in [424, 430] as efficient discretizations of the isotropic nonlinear diffusion filter of Catté et al. [81]. In Section 1.3.2 we have seen that this filter is based on the PDE

$$\partial_t u = \text{div} \left(g(|\nabla u_\sigma|^2) \, \nabla u \right).$$

In this case, a natural operator splitting $A = \sum_{l=1}^m A_l$ results from a decomposition of the divergence expression into one-dimensional terms of type

$$\partial_{x_l} (g(|\nabla u_\sigma|^2) \, \partial_{x_l} u) \qquad (l = 1, ..., m).$$

This separation is very efficient: There exist permutation matrices P_l (pixel orderings) such that $P_l A_l P_l^T$ is block diagonal and each block is diagonally dominant and tridiagonal. Hence, the corresponding linear systems can be

solved in linear effort by means of a simple Gaussian algorithm. The resulting forward substitution and backward elimination can be regarded as a recursive filter.

A parallel implementation assigning these tridiagonal subsystems to different processors is described in [431]. The denoising of a medical 3-D ultrasound data set with $138 \times 208 \times 138$ voxels on an SGI Power Challenge XL with eight 195 MHz R10000 processors was possible in less than 1 minute.

(e) The idea to base AOS schemes on decompositions into one-dimensional operators can also be generalized to anisotropic diffusion filters: Consider for instance the discretization on a (3×3)-stencil at the end of Section 3.4.2. If it fulfils (S1)–(S5), then a splitting of such a 2-D filter into 4 one-dimensional diffusion processes acting along the 4 stencil directions satisfies all prerequisites of Theorem 9.

Chapter 5

Examples and applications

The scale-space theory from Chapters 2–4 also covers methods such as linear or nonlinear isotropic diffusion filtering, for which many interesting applications have already been mentioned in Chapter 1. Therefore, the goal of the present chapter is to show that a generalization to anisotropic models with diffusion tensors depending on the structure tensor offers novel properties and application fields. Thus, we focus mainly on these anisotropic techniques and juxtapose the results to other methods. In order to demonstrate the flexibility of anisotropic diffusion filtering, we shall pursue two different objectives:

- smoothing with simultaneous edge-enhancement,

- smoothing with enhancement of coherent flow-like textures.

All calculations for diffusion filtering are performed using semi-implicit FD schemes with time steps $\Delta t \in [2, 5]$. In order to compare anisotropic diffusion to other methods, morphological scale-spaces and modifications of them have been discretized as well. For MCM and AMSS this is achieved by means of explicit FD schemes (cf. 1.6.4) with $\Delta t := 0.1$ and $\Delta t := 0.01$, respectively. Dilation with a flat structuring element is approximated by an Osher-Sethian scheme of type (1.88) with $\Delta t := 0.5$, and dilation with a quadratic structuring function is performed in a noniterative way using van den Boomgaard's algorithm from [51]. On an HP 9000/889 workstation it takes less than 0.3 CPU seconds to calculate one nonlinear diffusion step for a 256×256 image, and MCM, AMSS or dilation with a disc require approximately 0.06 seconds per iteration. Typical dilations with a quadratic structuring function take less than 0.3 seconds.

5.1   Edge-enhancing diffusion

5.1.1   Filter design

In accordance with the notations in 2.2, let μ_1, μ_2 with $\mu_1 \geq \mu_2$ be the eigenvalues of the structure tensor J_ρ, and v_1, v_2 the corresponding orthonormal eigenvectors. Since the diffusion tensor should reflect the local image structure it ought to be chosen in such a way that it reveals the same set of eigenvectors v_1, v_2 as J_ρ. The choice of the corresponding eigenvalues λ_1, λ_2 depends on the desired goal of the filter.

If one wants to smooth preferably within each region and aims to inhibit diffusion across edges, then one can reduce the diffusivity λ_1 perpendicular to edges the more the higher the contrast μ_1 is, see 1.3.3 and [415]. This behaviour may be accomplished by the following choice ($m \in \mathbb{N}$, $C_m > 0$, $\lambda > 0$):

$$\lambda_1(\mu_1) \ := \ g(\mu_1), \tag{5.1}$$

$$\lambda_2 \ := \ 1 \tag{5.2}$$

with

$$g(s) \ := \ \begin{cases} 1 & (s \leq 0) \\ 1 - \exp\left(\frac{-C_m}{(s/\lambda)^m}\right) & (s > 0). \end{cases} \tag{5.3}$$

This exponentially decreasing function is chosen in order to fulfil the smoothness requirement stated in (P_c), cf. 2.3. Since ∇u_σ remains bounded on $\Omega \times [0, \infty)$ and $\mu_1 = |\nabla u_\sigma|^2$, we know that the uniform positive definiteness of D is automatically satisfied by this filter.

The constant C_m is calculated in such a way that the flux $\Phi(s) = sg(s)$ is increasing for $s \in [0, \lambda]$ and decreasing for $s \in (\lambda, \infty)$. Thus, the preceding filter strategy can be regarded as an anisotropic regularization of the Perona–Malik model.

The choice $m := 4$ (which implies $C_4 = 3.31488$) gives visually good results and is used exclusively in the examples below. Since in this section we are only interested in edge-enhancing diffusion we may set the integration scale ρ of the structure tensor equal to 0. Applications which require nonvanishing integration scales shall be studied in section 5.2.

5.1.2   Applications

Figure 5.1 illustrates that anisotropic diffusion filtering is still capable of possessing the contrast-enhancing properties of the Perona–Malik filter (provided the regularization parameter σ is not too large). It depicts the temporal evolution of a
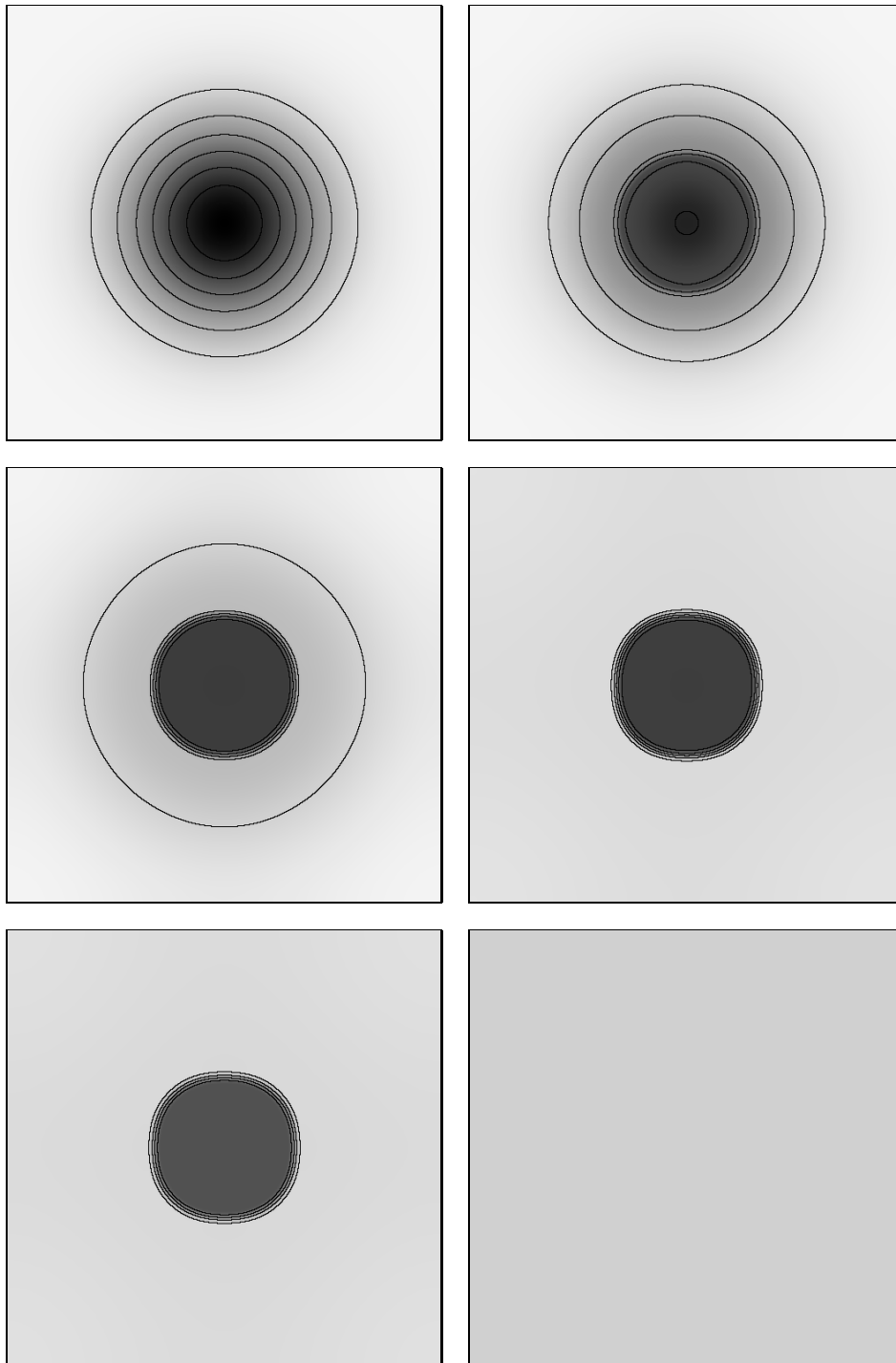
Figure 5.1: Anisotropic diffusion filtering of a Gaussian-type function, $\Omega = (0, 256)^2$, $\lambda = 3.6$, $\sigma = 2$. From top left to bottom right: $t = 0$, 125, 625, 3125, 15625, 78125.

Gaussian-like function and its isolines.[1] It can be observed that two regions with almost constant grey value evolve which are separated by a fairly steep edge. Edge enhancement is caused by the fact that, due to the rapidly decreasing diffusivity, smoothing within each region is strongly preferred to diffusion between the two adjacent regions. The edge location remains stable over a very long time interval. This indicates that, in practice, the determination of a suitable stopping time is not a critical problem. After the process of contrast enhancement is concluded, the steepness of edges decreases very slowly until the gradient reaches a value where no backward diffusion is possible anymore. Then the image converges quickly towards a constant image.

Let us now compare the denoising properties of different diffusion filters. Figure 5.2(a) consists of a triangle and a rectangle with 70 % of all pixels being completely degraded by noise. This image is taken from the software package MegaWave. Test images of this type have been used to study the behaviour of filters such as [13, 15, 16, 99, 102]. In Fig. 5.2(b) we observe that linear diffusion filtering is capable of removing all noise, but we have to pay a price: the image becomes completely blurred. Besides the fact that edges get smoothed so that they are harder to identify, the correspondence problem appears: edges become dislocated. Thus, once they are identified at a coarse scale, they have to be traced back in order to find their true location, a theoretically and practically rather difficult problem.

Fig. 5.2(c) shows the effect when applying the isotropic nonlinear diffusion equation [81]

$$\partial_t u = \text{div}\left(g(|\nabla u_\sigma|^2)\nabla u\right) \tag{5.4}$$

with g as in (5.3). Since edges are hardly affected by this process, nonlinear isotropic diffusion does not lead to correspondence problems which are characteristic for linear filtering. On the other hand, the drastically reduced diffusivity at edges is also responsible for the drawback that noise at edges is preserved.

Figure 5.2(d) demonstrates that nonlinear anisotropic filtering shares the advantages of both methods. It combines the good noise eliminating properties of linear diffusion with the stable edge structure of nonlinear isotropic filtering. Due to the permitted smoothing along edges, however, corners get more rounded than in the nonlinear isotropic case.

The scale-space behaviour of different PDE-based methods is juxtaposed in Figures 5.3–5.6, where an MRI slice of a human head is processed [414, 423].

---

[1]Except for Figs. 5.1, 5.3–5.6, where contrast enhancement is to be demonstrated, all images in the present work are depicted in such a way that the lowest value is black and the highest one appears white. They reveal a range within the interval $[0, 255]$ and all pixels have unit length in both directions.
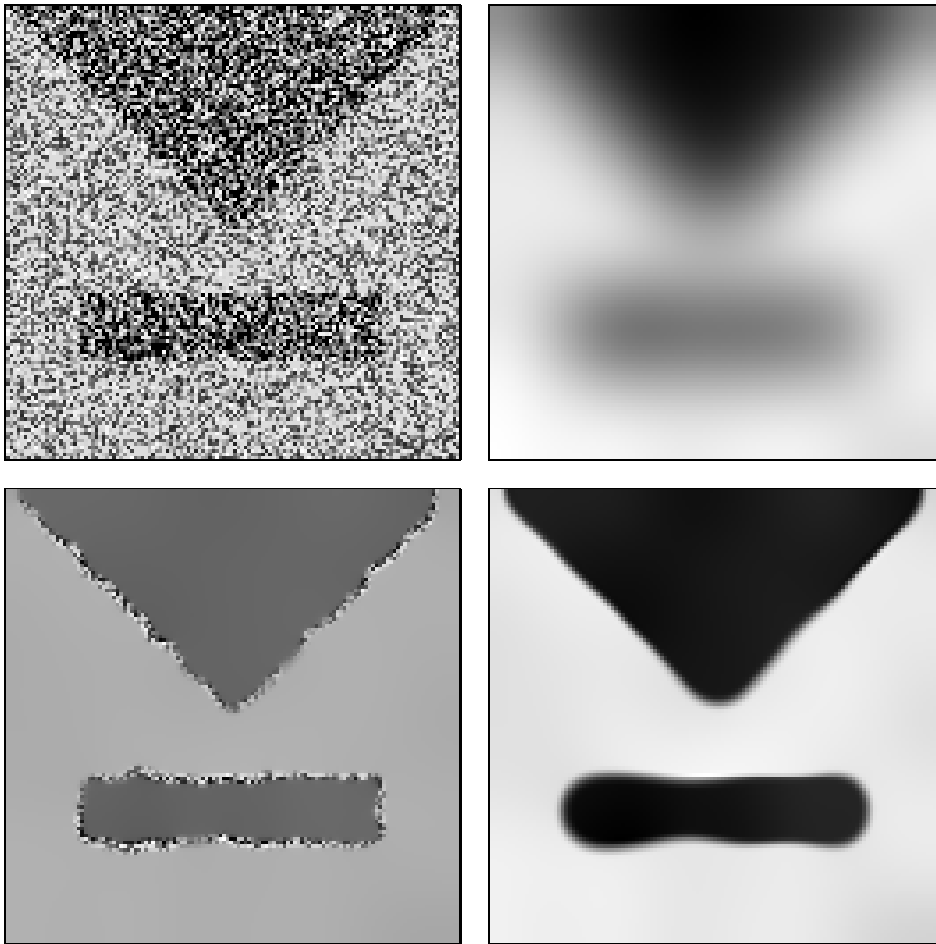
Figure 5.2: Restoration properties of diffusion filters. (a) TOP LEFT: Test image, $\Omega = (0, 128)^2$. (b) TOP RIGHT: Linear diffusion, $t = 80$. (c) BOTTOM LEFT: Nonlinear isotropic diffusion, $\lambda = 3.5$, $\sigma = 3$, $t = 80$. (d) BOTTOM RIGHT: Nonlinear anisotropic diffusion, $\lambda = 3.5$, $\sigma = 3$, $t = 80$.

Again we observe that linear diffusion (Fig. 5.3(a)) does not only blur all structures in an equal amount but also dislocates them more and more with increasing scale.

A first step to reduce these problems is to adapt the diffusivity to the gradient of the initial image f [147]. Fig. 5.3(b) shows the evolution under

$$\partial_t u = \operatorname{div}\left(g(|\nabla f|^2)\, \nabla u\right), \tag{5.5}$$

where a diffusivity of type [88]

$$g(|\nabla f|^2) := \frac{1}{\sqrt{1 + |\nabla f|^2/\lambda^2}} \qquad (\lambda > 0). \qquad (5.6)$$

is used. Compared with homogeneous linear diffusion, edges remain better localized and their blurring is reduced. On the other hand, for large t the filtered image reveals some artifacts which reflect the differential structure of the initial image.

A natural idea to reduce the artifacts of inhomogeneous linear diffusion filtering would be to introduce a feedback in the process by adapting the diffusivity g to the gradient of the actual image $u(x, t)$ instead of the original image $f(x)$. This leads to the nonlinear diffusion equation [326]

$$\partial_t u = \operatorname{div}\left(g(|\nabla u|^2)\,\nabla u\right). \qquad (5.7)$$

Figure 5.3(c) shows how such a nonlinear feedback is useful to increase the edge localization in a significant way: Structures remain well-localized as long as they can be recognized. Also blurring at edges is reduced very much. The absolute contrast at edges, however, becomes smaller.

The latter problem can be avoided using a diffusivity which decreases faster than (5.6) and leads to a nonmonotone flux function. This is illustrated in Figure 5.4(a) where the regularized isotropic nonlinear diffusion filter (5.4) with the diffusivity (5.3) is applied. At the chin we observe that this equation is indeed capable of enhancing edges. All structures are extremely well-localized and the results are segmentation-like. On the other hand, also small structures exist over a long range of scales if they differ from their vicinity by a sufficiently large contrast. One can try to make this filter faster and more insensitive to small-size structures by increasing the regularizing Gaussian kernel size σ (cf. Fig. 5.4(b)), but this also leads to stronger blurring of large structures, and it is no longer possible to enhance the contour of the entire head.

Anisotropic nonlinear diffusion (Fig. 5.4(c)) permits diffusion along edges and inhibits smoothing across them. As in Figure 5.2(d), this causes a stronger rounding of structures, which can be seen at the nose. A positive consequence of this slight shrinking effect is the fact that small or elongated and thin structures are better eliminated than in the isotropic case. Thus, we recognize that most of the depicted "segments" coincide with semantically correct objects that one would expect at these scales. Finally the image turns into a silhouette of the head, before it converges to a constant image.

The tendency to produce piecewise almost constant regions indicates that diffusion scale-spaces with nonmonotone flux are ideal preprocessing tools for segmentation. Unlike diffusion–reaction models aiming to yield *one* segmentation-like result for $t \to \infty$ (cf. 1.4), the temporal evolution of these models generates a

complete *hierarchical family* of segmentation-like images. The contrast-enhancing quality distinguishes nonlinear diffusion filters from most other scale-spaces. It should be noted that contrast enhancement is a local phenomenon which cannot be replaced by simple global rescalings of the grey value range. Therefore, it is generally not possible to obtain similar segmentation-like results by just rescaling the grey values from a scale-space which is only contrast-reducing.

The contrast and noise parameters λ and σ give the user the liberty to adapt nonlinear diffusion scale-spaces to the desired purpose in order to reward interesting features with a longer lifetime. Suitable values for them should result in a natural way from the specific problem. In this sense, the time t is rather a parameter of importance, with respect to the specified task, than a descriptor of spatial scale. The traditional opinion that the evolution parameter t of scale-spaces should be related to the spatial scale reflects the assumption that a scale-space analysis should be uncommitted. Nonlinear diffusion filtering renounces this requirement by allowing to incorporate a-priori information (e.g. about the contrast of semantically important structures) into the evolution process. The basic idea of scale-spaces, however, is maintained: to provide a family of subsequently simplified versions of the original image, which gives a hierarchy of structures and allows to extract the relevant information from a certain scale.

Besides these specific features of nonlinear diffusion scale-spaces it should be mentioned that, due to the homogeneous Neumann boundary condition and the divergence form, both linear and nonlinear diffusion filters preserve the average grey level of the image.

This is not true for the morphological filters and their modifications which are depicted in Fig. 5.5 and 5.6.

Figure 5.5(a) and (b) show the result under continuous-scale dilation with a flat disc-shaped structuring element and a quadratic structuring function, respectively. From Section 1.5.3 and 1.5.6 we know that their evolution equations are given by

$$\partial_t u \;=\; |\nabla u|, \tag{5.8}$$

for the disc, and by

$$\partial_t u \;=\; |\nabla u|^2 \tag{5.9}$$

for the quadratic structuring function. In both cases the number of local maxima is decreasing, and maxima keep their location in scale-space until they disappear [206, 207]. The fact that the maximum with the largest grey value will dominate at the end shows that these processes can be sensitive to noise (maxima might be caused by noise), and that they usually do not preserve the average grey level. It is not very difficult to guess the shape of the structuring function from the scale-space evolution.
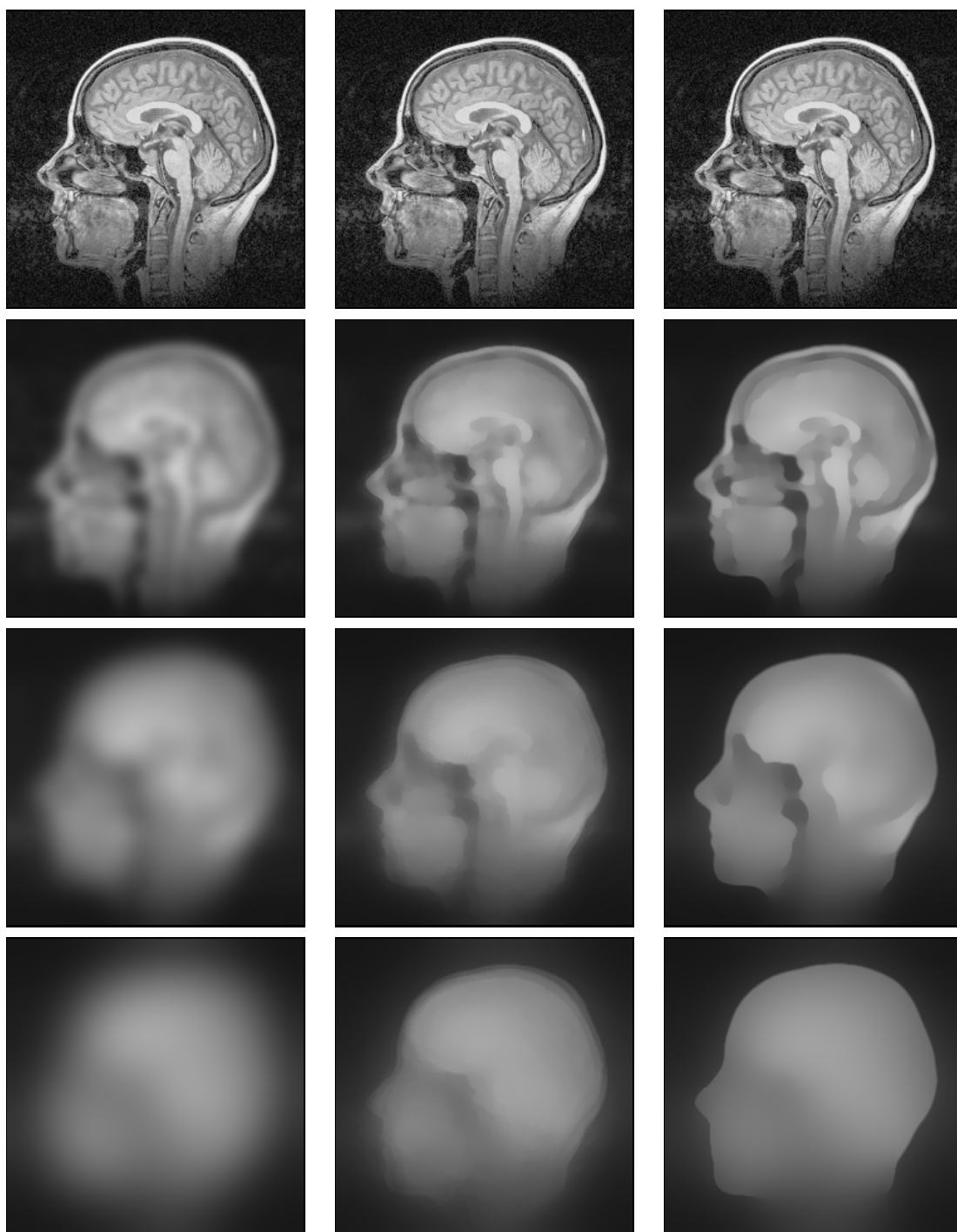
Figure 5.3: Evolution of an MRI slice under different PDEs. Top: Original image, $\Omega = (0, 236)^2$. (a) Left Column: Linear diffusion, top to bottom: $t = 0$, 12.5, 50, 200. (b) Middle Column: Inhomogeneous linear diffusion ($\lambda = 8$), $t = 0$, 70, 200, 600. (c) Right Column: Nonlinear isotropic diffusion with the Charbonnier diffusivity ($\lambda = 3$), $t = 0$, 70, 150, 400.
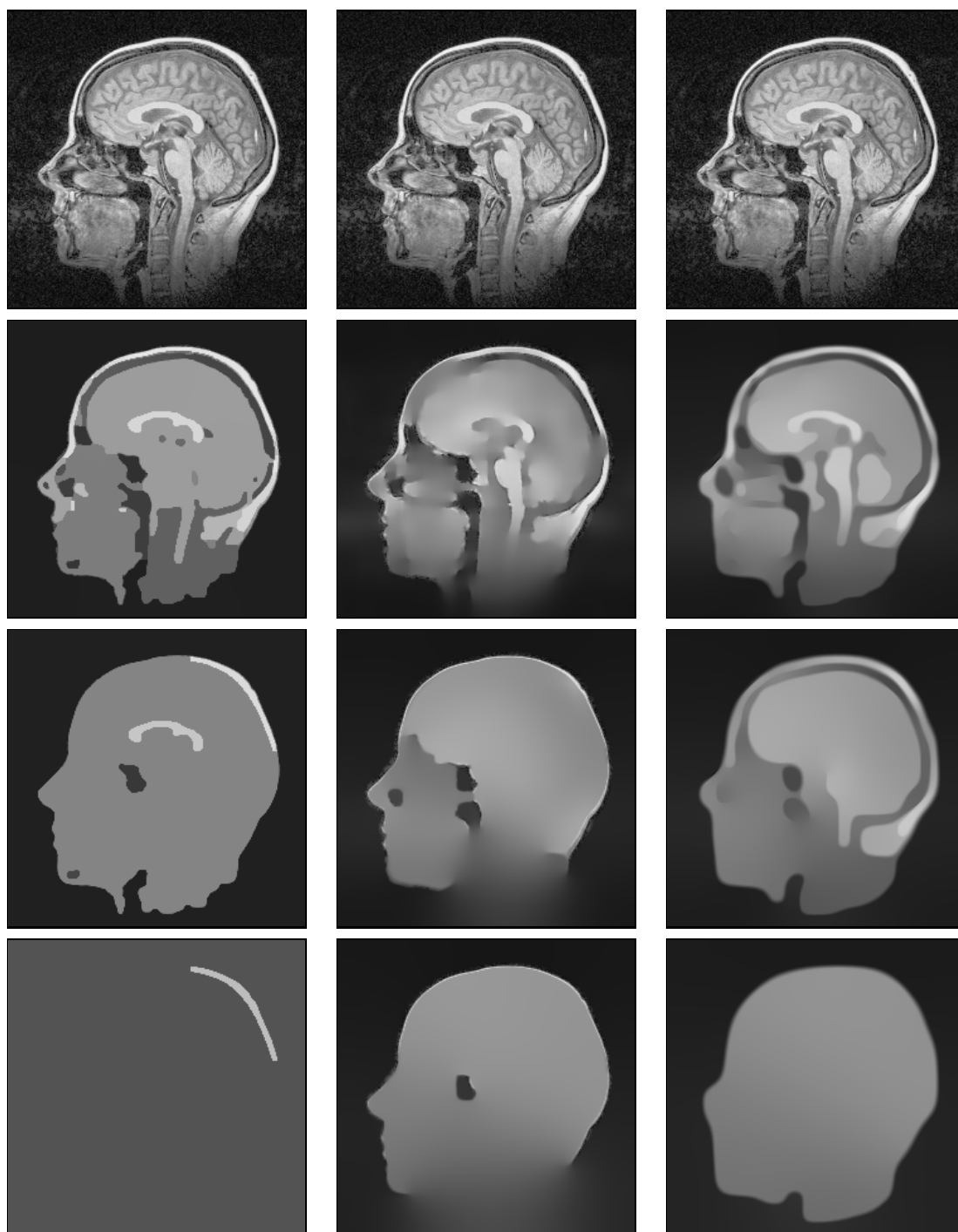
Figure 5.4: Evolution of an MRI slice under different PDEs. Top: Original image, $\Omega = (0, 236)^2$. (A) Left Column: Isotropic nonlinear diffusion ($\lambda = 3$, $\sigma = 1$), $t = 0$, 25000, 500000, 7000000. (B) Middle Column: Isotropic nonlinear diffusion ($\lambda = 3$, $\sigma = 4$), $t = 0$, 40, 400, 1500. (C) Right Column: Edge-enhancing anisotropic diffusion ($\lambda = 3$, $\sigma = 1$), $t = 0$, 250, 875, 3000.
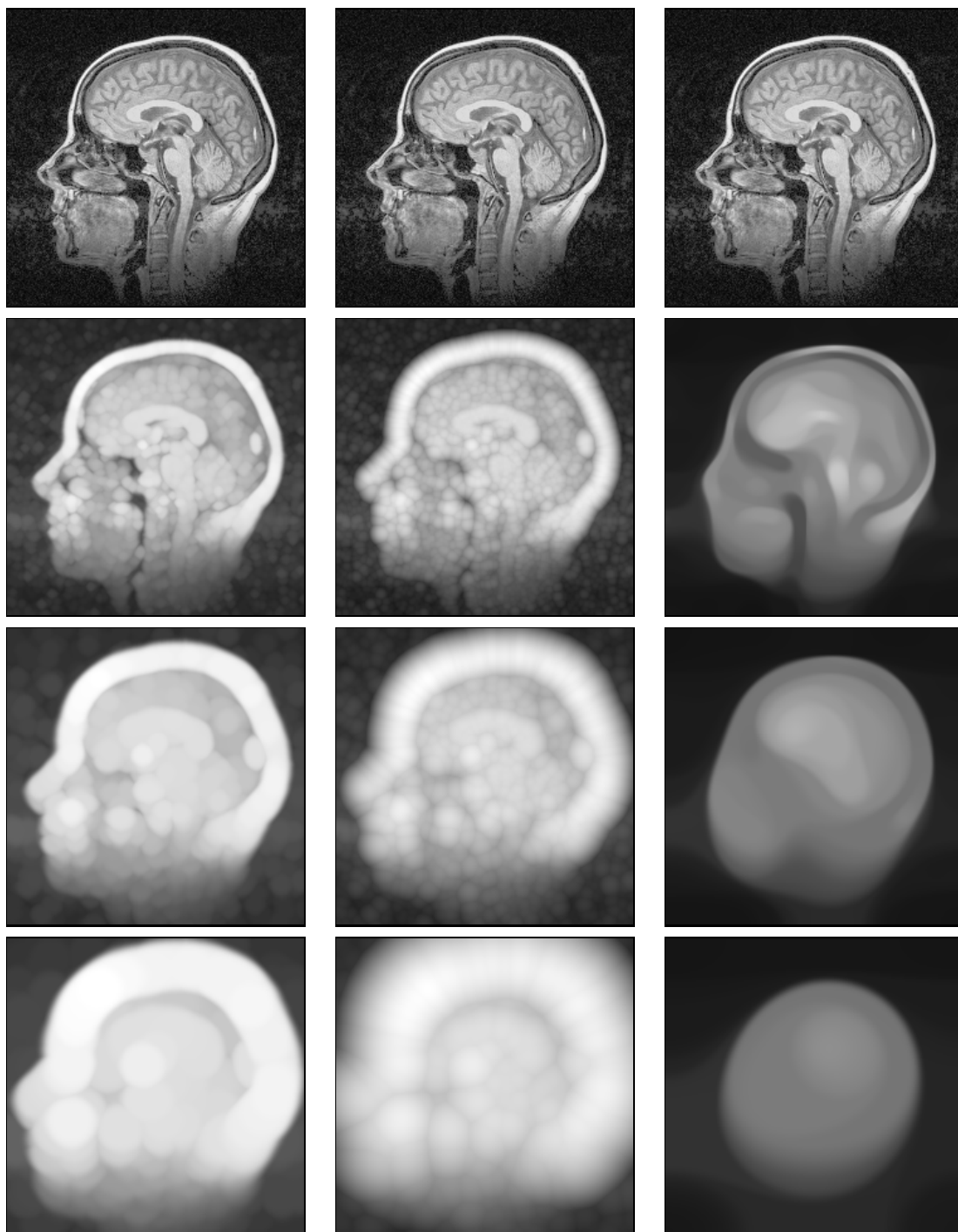
Figure 5.5: Evolution of an MRI slice under different PDEs. TOP: Original image, $\Omega = (0, 236)^2$. (A) LEFT COLUMN: Dilation with a disc, $t = 0$, 4, 10, 20. (B) MIDDLE COLUMN: Dilation with a quadratic structuring function, $t = 0$, 0.25, 1, 4. (C) RIGHT COLUMN: Mean curvature motion, $t = 0$, 70, 275, 1275.
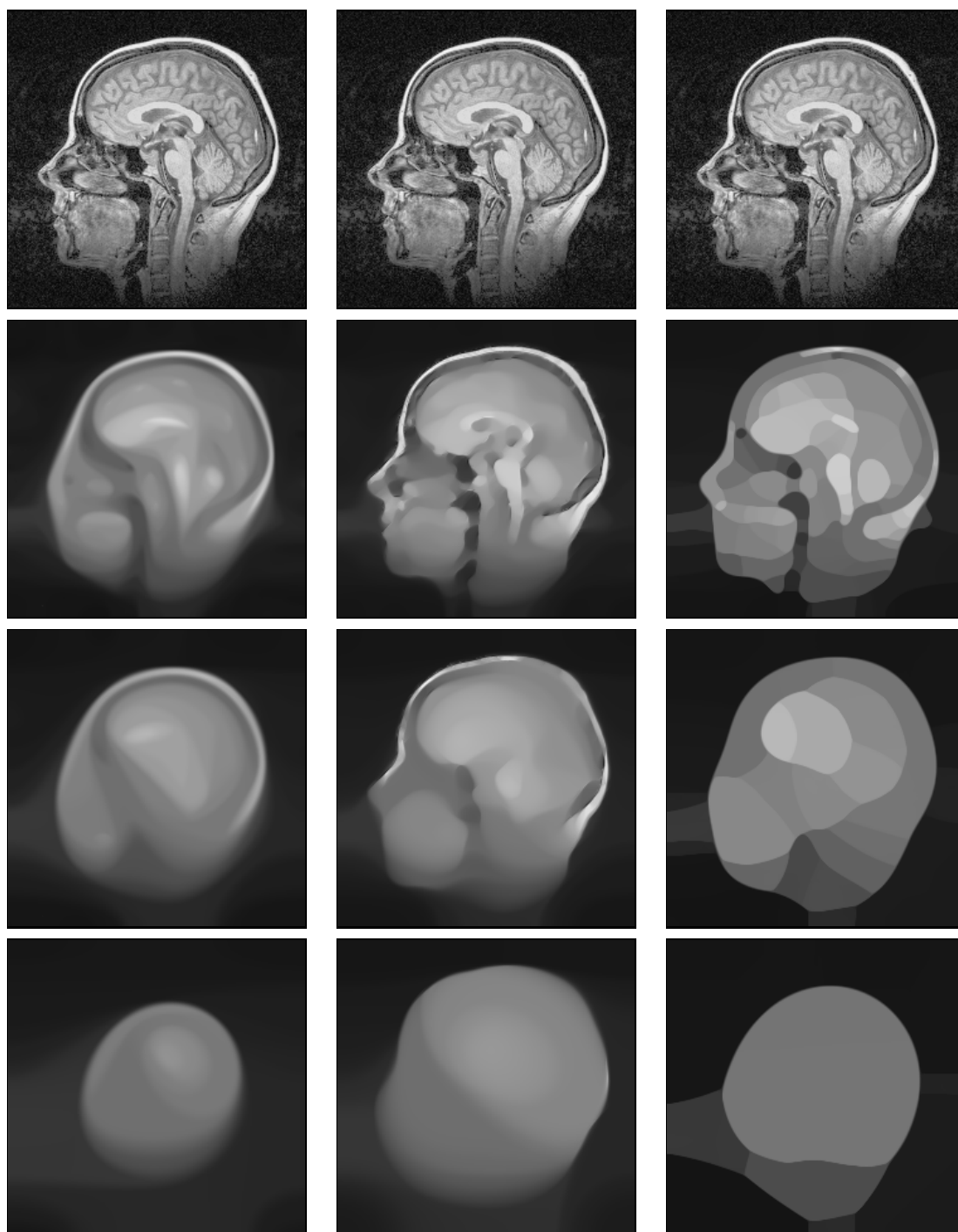
Figure 5.6: Evolution of an MRI slice under different PDEs. TOP: Original image, $\Omega = (0, 236)^2$. (A) LEFT COLUMN: Affine morphological scale-space, $t = 0, 20,$ 50, 140. (B) MIDDLE COLUMN: Modified mean curvature motion ($\lambda = 3$, $\sigma = 1$), $t = 0, 100, 350, 1500$. (C) RIGHT COLUMN: Self-snakes ($\lambda = 3$, $\sigma = 1$), $t = 0,$ 600, 5000, 40000.

A completely different morphological evolution is given by the mean curvature motion (1.90) depicted in Fig. 5.5(c). Since MCM shrinks level lines with a velocity that is proportional to their curvature, low-curved object boundaries are less affected by this process, while high-curved structures (e.g. the nose) exhibit roundings at an earlier stage. This also explains its excellent noise elimination qualities. After some time, however, the head looks almost like a ball. This is in accordance with the theory which predicts convergence of all closed level lines to circular points.

A similar behaviour can be observed for the affine invariant morphological scale-space (1.108) shown in Fig. 5.6(a). Since it takes the time $T = \frac{3}{4} s^{\frac{4}{3}}$ to remove all isolines within a circle of radius s – in contrast to $T = \frac{1}{2} s^2$ for MCM – we see that, for a comparable elimination of small structure, the shrinking effect of large structures is stronger for AMSS than for MCM. Thus, the correspondence problem is more severe than for MCM. Nevertheless, the advantage of having affine invariance may counterbalance the correspondence problem in certain applications. Since the AMSS involves no additional parameters and offers more invariances than other scale-spaces, it is ideal for uncommitted image analysis and shape recognition. Both MCM and AMSS give significantly sharper edges than linear diffusion filtering, but they are not designed to act contrast-enhancing.

One possibility to reduce the correspondence problem of morphological scale-spaces is to attenuate the curve evolution at high-contrast edges. This is at the expense of withdrawing morphology in terms of invariance under monotone grey-scale transformations.

One possibility is to use the damping function *outside* the divergence expression. Processes of this type are studied in [13, 364, 365, 304]. As a simple prototype for this idea, let us investigate the modified MCM

$$\partial_t u \;=\; g(|\nabla u_\sigma|^2)\,|\nabla u|\operatorname{div}\left(\frac{\nabla u}{|\nabla u|}\right) \tag{5.10}$$

with $g(|\nabla u_\sigma|^2)$ as in (1.32). The corresponding evolution is depicted in Fig. 5.6(b). We observe that structures remain much better localized than in the original MCM. On the other hand, the experiments give evidence that this process is probably not contrast-enhancing, see e.g. the chin. As a consequence, the results appear less segmentation-like than those for nonlinear diffusion filtering.

Using $g(|\nabla u_\sigma|^2)$ *inside* the divergence expression leads to

$$\partial_t u \;=\; |\nabla u|\operatorname{div}\left(g(|\nabla u_\sigma|^2)\,\frac{\nabla u}{|\nabla u|}\right). \tag{5.11}$$

In Section 1.6.6 we have seen that processes of this type are called self-snakes [357]. Since they differ from isotropic nonlinear diffusion filters by the $|\nabla u|$ terms inside and outside the divergence expression, they will not preserve the average
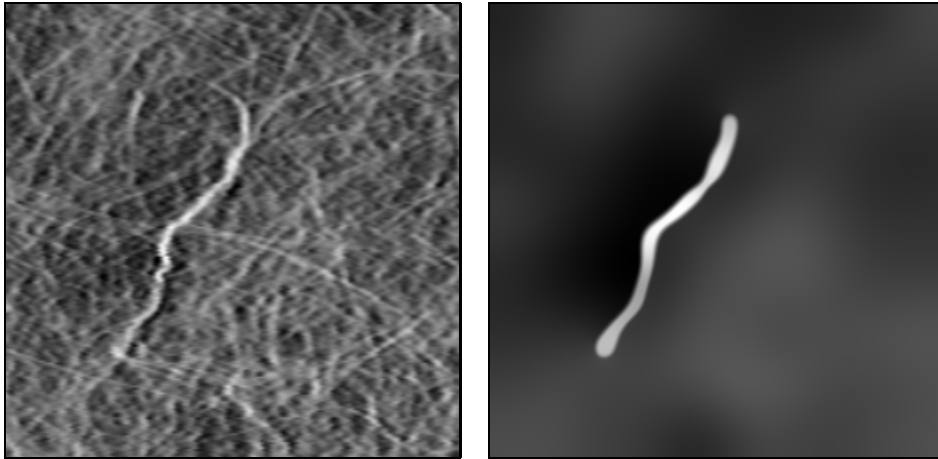
Figure 5.7: Preprocessing of a fabric image. (a) LEFT: Fabric, $\Omega = (0, 257)^2$. (b) RIGHT: Anisotropic diffusion, $\lambda = 4$, $\sigma = 2$, $t = 240$.

grey value. The evolution in Fig. 5.6(c) indicates that $g(|\nabla u_\sigma|^2)$ gives similar edge-enhancing effects as in a nonlinear diffusion filter, but one can observe a stronger tendency to create circular structures. This behaviour which resembles MCM is not surprising if one compares (1.120) with (1.121).

Let us now study two applications of nonlinear diffusion filtering in computer aided quality control (CAQ): the grading of fabrics and wood surfaces (see also [413]).

The quality of a fabric is determined by two criteria, namely clouds and stripes. Clouds result from isotropic inhomogeneities of the density distribution, whereas stripes are an anisotropic phenomenon caused by adjacent fibres pointing in the same direction. Anisotropic diffusion filters are capable of visualizing both quality-relevant features simultaneously (Fig. 5.7). For a suitable parameter choice, they perform isotropic smoothing at clouds and diffuse in an anisotropic way along fibres in order to enhance them. However, if one wants to visualize both features separately, one can use a fast pyramid algorithm based on linear diffusion filtering for the clouds [417], whereas stripes can be enhanced by a special nonlinear diffusion filter which is designed for closing interrupted lines and which shall be discussed in Section 5.2.

For furniture production it is of importance to classify the quality of wood surfaces. If one aims to automize this evaluation, one has to process the image in such a way that quality relevant features become better visible und unimportant structures disappear. Fig. 5.8(a) depicts a wood surface possessing one defect. To visualize this defect, equation (5.4) can be applied with good success (Fig. 5.8(b)).

Figure 5.8: Defect detection in wood. (a) LEFT: Wood surface, $\Omega = (0, 256)^2$. (b) RIGHT: Isotropic nonlinear diffusion, $\lambda = 4$, $\sigma = 2$, $t = 2000$.

In [413] it is demonstrated how a modified anisotropic diffusion process yields even more accurate results with less roundings at the corners.

Fig. 5.9(a) gives an example for possible medical applications of nonlinear diffusion filtering as a preprocessing tool for segmentation (see also [415] for another example). It depicts an MRI slice of the human head. For detecting Alzheimer's disease one is interested in determining the ratio between the ventricle areas, which are given by the two white longitudinal objects in the centre, and the entire head area.

In order to make the diagnosis more objective and reliable, it is intended to automize this feature extraction step by a segmentation algorithm. Figure 5.9(c) shows a segmentation according to the following simplification of the Mumford–Shah functional (1.58):

$$E_f(u, K) = \int_\Omega (u - f)^2 \, dx \, + \, \alpha |K|. \tag{5.12}$$

It has been obtained by a MegaWave programme using a hierarchical region growing algorithm due to Koepfler et al. [239]. As is seen in Fig. 5.9(d), one gets a better segmentation when processing the original image slightly by means of nonlinear diffusion filtering (Fig. 5.9(b)) prior to segmenting it.
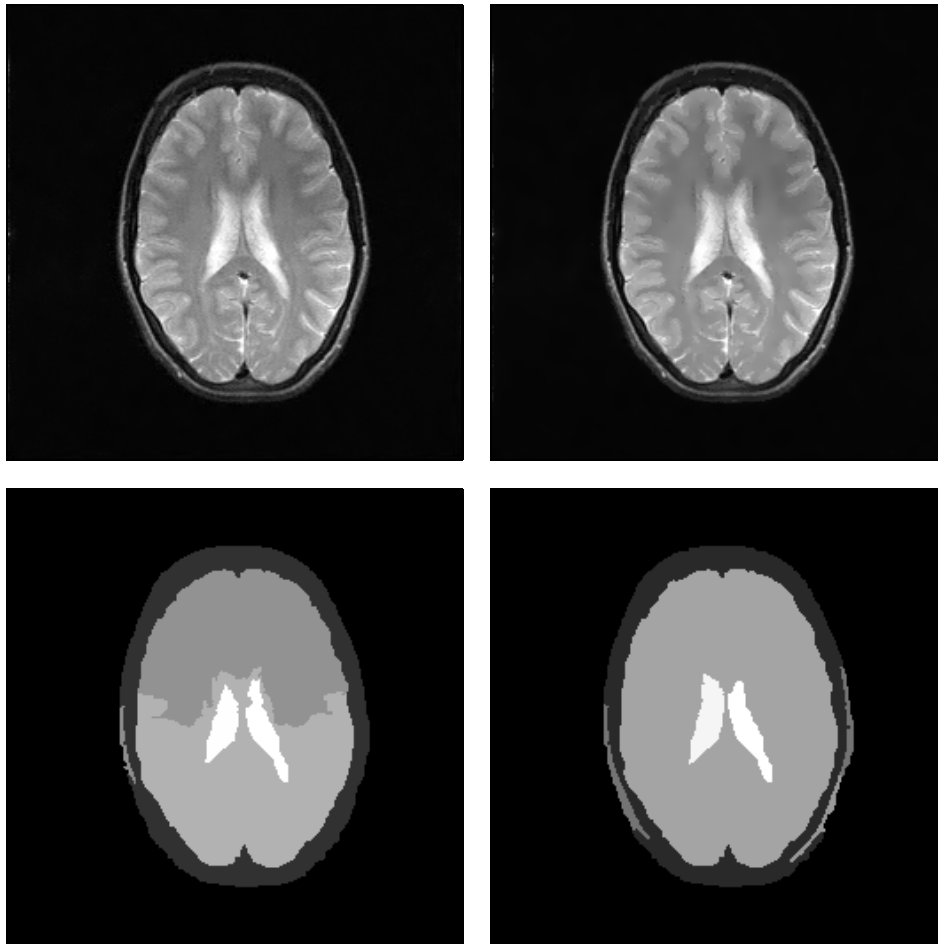
Figure 5.9: Preprocessing of an MRI slice. (a) TOP LEFT: Head, $\Omega = (0, 256)^2$. (b) TOP RIGHT: Diffusion-filtered, $\lambda = 5$, $\sigma = 0.1$, $t = 2.5$. (c) BOTTOM LEFT: Segmented original image, $\alpha = 8192$. (d) BOTTOM RIGHT: Segmented filtered image, $\alpha = 8192$.

5.2 Coherence-enhancing diffusion

5.2.1 Filter design

In this section we shall investigate how the structure tensor information can be used to design anisotropic diffusion scale-spaces which enhance the coherence of flow-like textures [418]. This requires a nonvanishing integration scale ρ.

Let again μ_1, μ_2 with $\mu_1 \geq \mu_2$ be the eigenvalues of J_ρ, and v_1, v_2 the corresponding orthonormal eigenvectors. As in 5.1 the diffusion tensor $D(J_\rho(\nabla u_\sigma))$ ought to possess the same set of eigenvectors as $J_\rho(\nabla u_\sigma)$.

If one wants to enhance coherent structures, one should smooth preferably
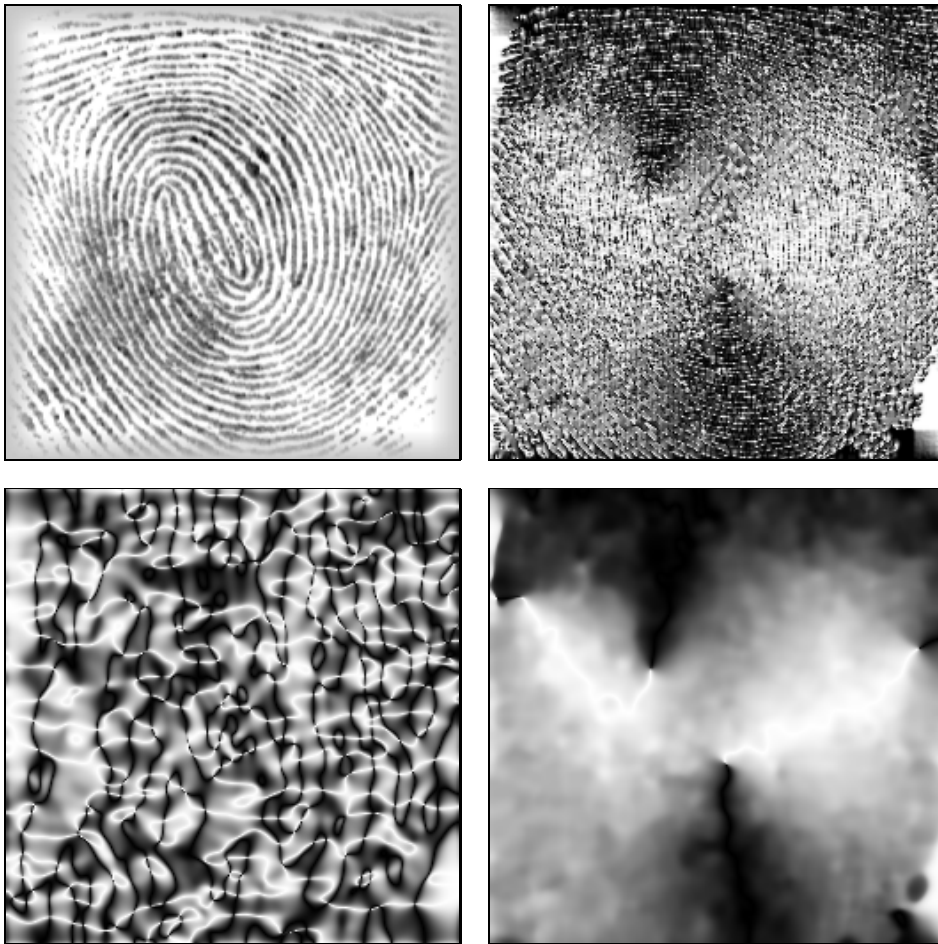
Figure 5.10: Local orientation in a fingerprint image. (a) TOP LEFT: Original fingerprint, $\Omega = (0, 256)^2$. (b) TOP RIGHT: Orientation of smoothed gradient, $\sigma = 0.5$. (c) BOTTOM LEFT: Orientation of smoothed gradient, $\sigma = 5$. (d) BOTTOM RIGHT: Structure tensor orientation, $\sigma = 0.5$, $\rho = 4$.

along the coherence direction v_2 with a diffusivity λ_2 which increases with respect to the coherence $(\mu_1 - \mu_2)^2$. This may be achieved by the following choice for the eigenvalues of the diffusion tensor ($C > 0$, $m \in \mathbb{N}$):

$$
\begin{aligned}
\lambda_1 &:= \alpha, \\
\lambda_2 &:= \begin{cases} \alpha & \text{if } \mu_1 = \mu_2, \\ \alpha + (1-\alpha)\exp\left(\frac{-C}{(\mu_1 - \mu_2)^{2m}}\right) & \text{else,} \end{cases}
\end{aligned}
$$

where the exponential function was chosen to ensure the smoothness of D and the
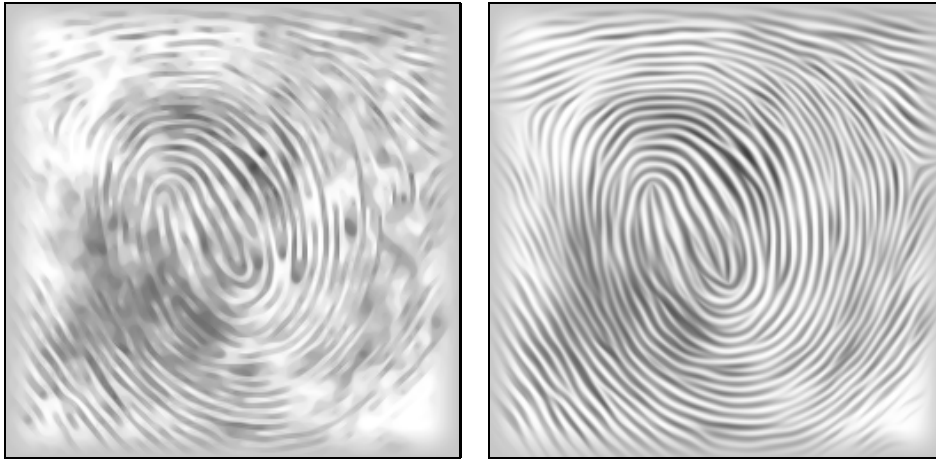
Figure 5.11: Anisotropic equations applied to the fingerprint image. (a) LEFT: Mean-curvature motion, $t = 5$. (b) RIGHT: Coherence-enhancing anisotropic diffusion, $\sigma = 0.5$, $\rho = 4$, $t = 20$.

small positive parameter $\alpha \in (0, 1)$ keeps $D(J_\rho(\nabla u_\sigma))$ uniformly positive definite.[2]

All examples below are calculated using $C := 1$, $m := 1$, and $\alpha := 0.001$.

5.2.2 Applications

Figure 5.10 illustrates the advantages of local orientation analysis by means of the structure tensor. In order to detect the local orientation of the fingerprint depicted in Fig. 5.10(a), the gradient orientation of a slightly smoothed image has been calculated (Fig. 5.10(b)). Horizontally oriented structures appear black, while vertical structures are represented in white. We observe very high fluctuations in the local orientation. When applying a larger smoothing kernel it is clear that adjacent gradients having the same orientation but opposite direction cancel out. Therefore, the results in (c) are much worse than in (b). The structure tensor, however, averages the gradient orientation instead of its direction. This is the reason for the reliable estimates of local orientation that can be obtained with this method (Fig. 5.10(d)).

To illustrate how the result of anisotropic PDE methods depends on the direction in which they smooth, let us recall the example of mean curvature motion (cf. 1.6.1):

$$\partial_t u \;=\; u_{\xi\xi} \;=\; |\nabla u|\, \mathrm{curv}(u) \tag{5.13}$$

with ξ being the direction perpendicular to ∇u. Since MCM smoothes by propagating level lines in inner normal direction we recognize that its smoothing di-

---

[2]Evidently, filters of this type are not regularizations of the Perona–Malik process: the limit $\sigma \to 0$, $\rho \to 0$ leads to a linear diffusion process with constant diffusivity α.
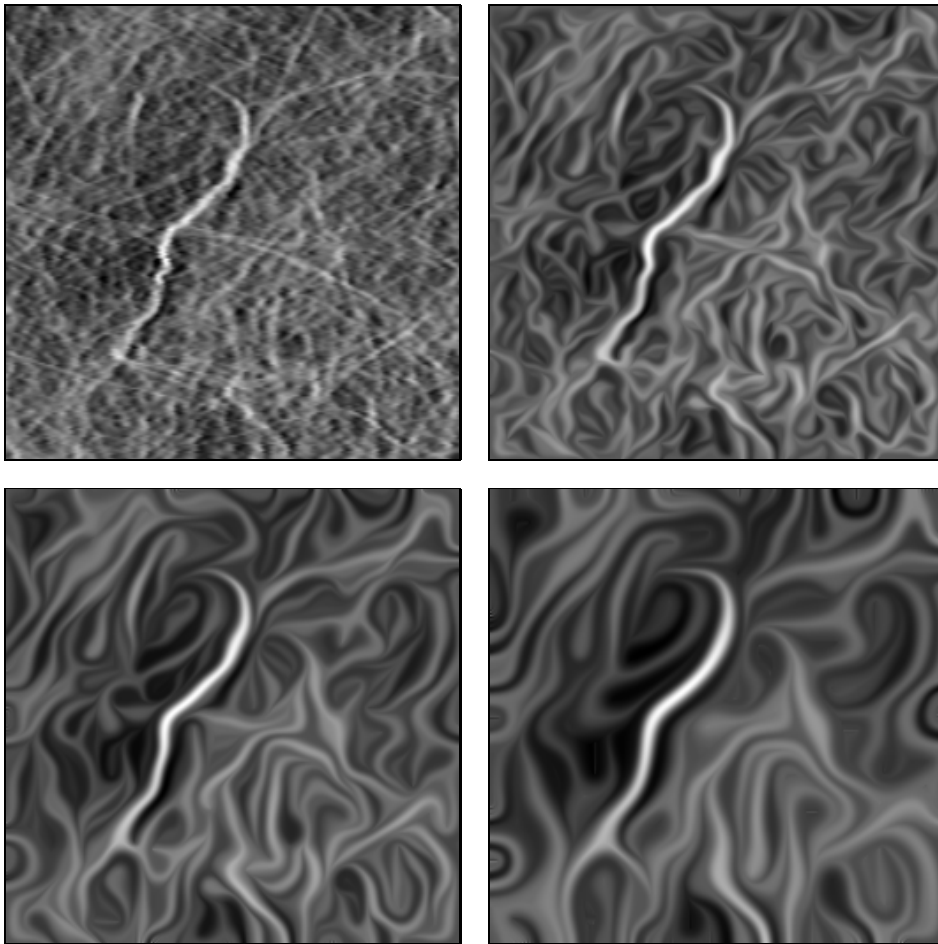
Figure 5.12: Scale-space behaviour of coherence-enhancing diffusion ($\sigma = 0.5$, $\rho = 2$). (a) TOP LEFT: Original fabric image, $\Omega = (0, 257)^2$. (b) TOP RIGHT: $t = 20$. (c) BOTTOM LEFT: $t = 120$. (d) BOTTOM RIGHT: $t = 640$.

rection depends exclusively on ∇u. Thus, although this method is in a complete anisotropic spirit, we should not expect it to be capable of closing interrupted line-like structures. The results in Fig. 5.11(a) confirm this impression.

The proposed anisotropic diffusion filter, however, biases the diffusive flux towards the coherence orientation v_2 and is therefore well-suited for closing interrupted lines in coherent flow-like textures, see Fig. 5.11(b). Due to its reduced diffusivity at noncoherent structures, the locations of the semantically important singularities in the fingerprint remain the same. This is an important prerequisite that any image processing method has to satisfy if it is to be applied to fingerprint analysis.
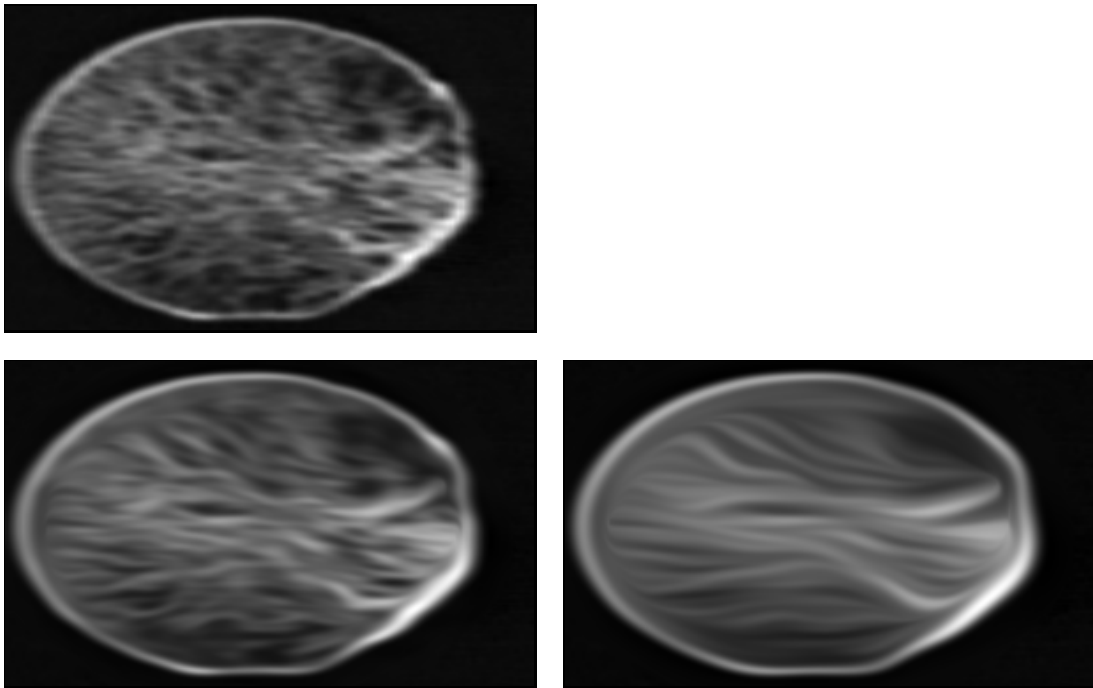
Figure 5.13: (A) TOP: High resolution slipring CT scan of a femural bone, $\Omega = (0, 300) \times (0, 186)$. (B) BOTTOM LEFT: Filtered by coherence-enhancing anisotropic diffusion, $\sigma = 0.5$, $\rho = 6$, $t = 16$. (C) BOTTOM RIGHT: Dito with $t = 128$.

Figure 5.12 depicts the scale-space behaviour of coherence-enhancing anisotropic diffusion applied to the fabric image from Fig. 5.7. The temporal behaviour of this diffusion filter seems to be appropriate for visualizing coherent fibre agglomerations (stripes) at different scales, a difficult problem for the automatic grading of nonwovens [299].

Figure 5.13 illustrates the potential of CED for medical applications. It depicts a human bone. Its internal structure has a distinctive texture through the presence of tiny elongated bony structural elements, the *trabeculae*. There is evidence that the trabecular formation is for a great deal determined by the external load. For this reason the trabecular structure constitutes an important clinical parameter in orthopedics. Examples are the control of recovery after surgical procedures, such as the placement or removal of metal implants, quantifying the rate of progression of rheumatism and osteoporosis, the determination of left-right deviations of symmetry in the load or establishing optimal load corrections by physiotherapy. From Figure 5.13(b),(c) we observe that CED is capable of enhancing the trabecular structures in order to ease their subsequent orientation analysis.
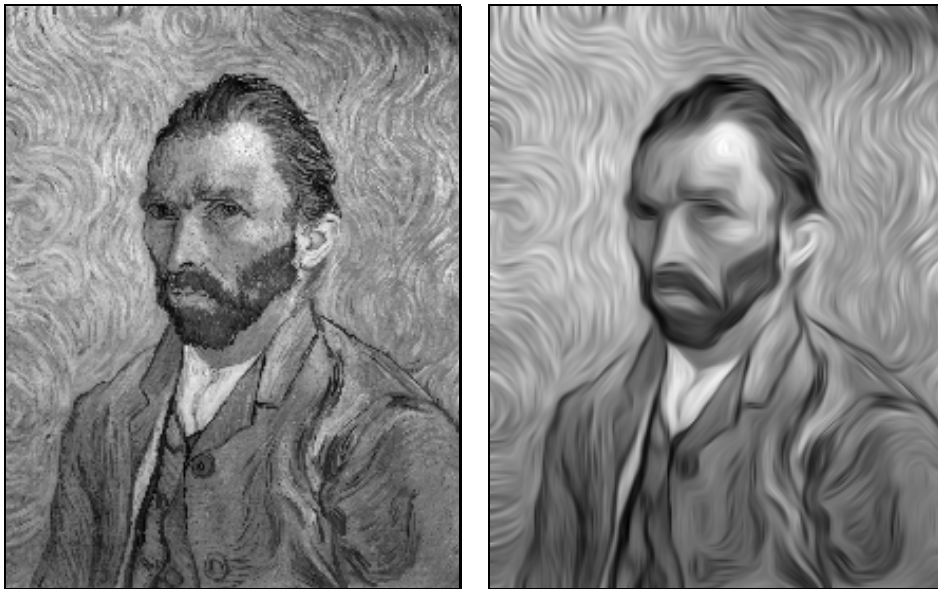
Figure 5.14: Image restoration using coherence-enhancing anisotropic diffusion. (a) LEFT: "Selfportrait" by van Gogh (Saint-Rémy, 1889; Paris, Museé d'Orsay), $\Omega = (0, 215) \times (0, 275)$. (b) RIGHT: Filtered, $\sigma = 0.5$, $\rho = 4$, $t = 6$.

Let us now investigate the impact of coherence-enhancing diffusion on images, which are not typical texture images, but still reveal a flow-like character. To this end, we shall process impressionistic paintings by Vincent van Gogh.

Fig. 5.14 shows the restoration properties of coherence-enhancing anisotropic diffusion when being applied to a selfportrait of the artist [161]. We observe that the diffusion filter can close interrupted lines and enhance the flow-like character which is typical for van Gogh paintings.

The next painting we are concerned with is called "Road with Cypress and Star" [162, 429]. It is depicted in Fig. 5.15. In order to demonstrate the influence of the integration scale ρ, all filter parameters are fixed except for ρ. Fig. 5.15(b) shows that a value for ρ which is too small does not lead to the visually dominant coherence orientation and creates structures with a lot of undesired fluctuations. Increasing the value for ρ improves the image significantly (Fig. 5.15(c)). Interestingly, a further increasing of ρ does hardly alter this result (Fig. 5.15(d)), which indicates that this van Gogh painting possesses a uniform "texture scale" reflecting the characteristic painting style of the artist.

In a last example the temporal evolution of flow-like images is illustrated by virtue of the "Starry Night" painting in Fig. 5.16 [160, 419]. Due to the established
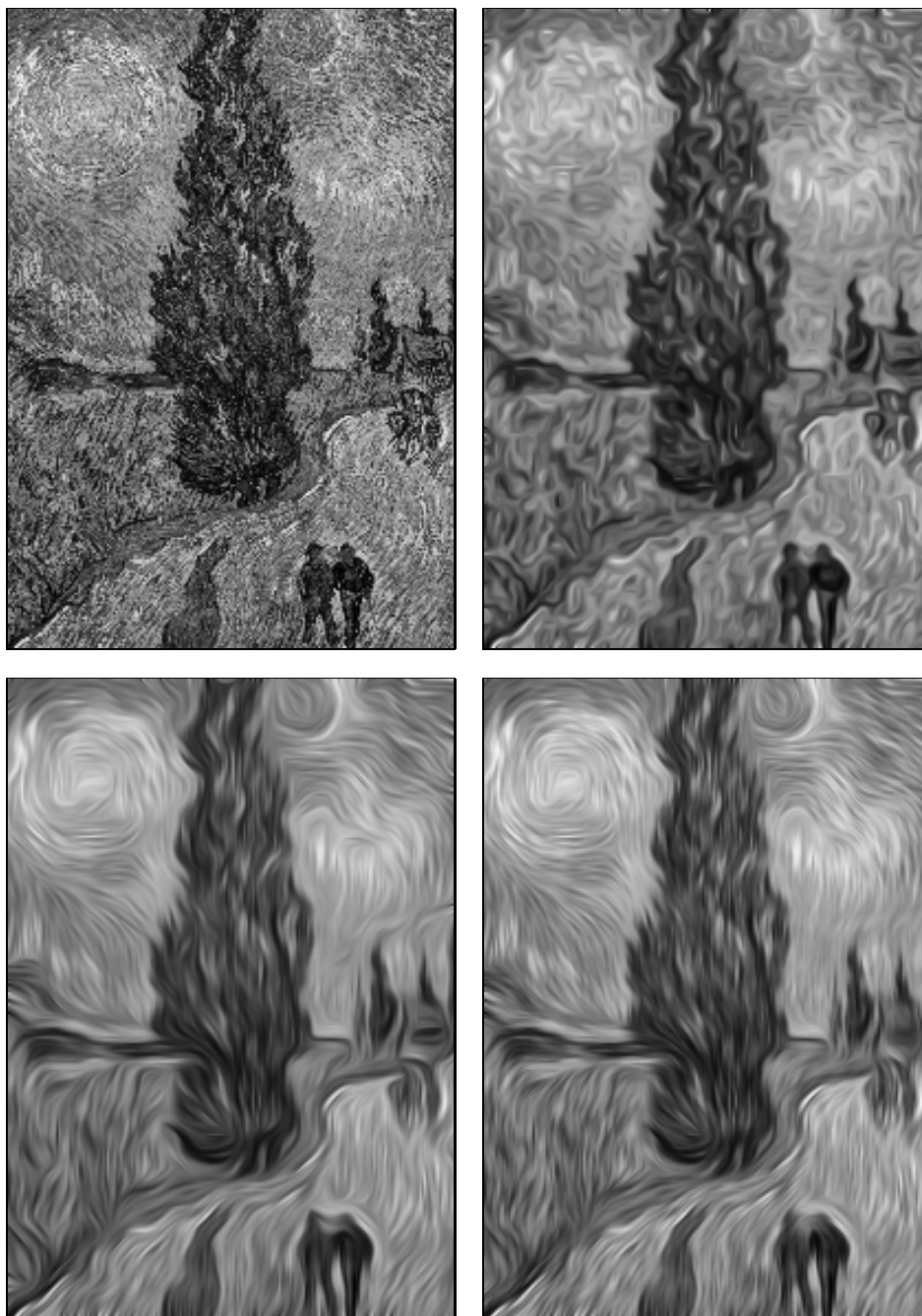
Figure 5.15: Impact of the integration scale on coherence-enhancing anisotropic diffusion ($\sigma = 0.5$, $t = 8$). (a) TOP LEFT: "Road with Cypress and Star" by van Gogh (Auvers-sur-Oise, 1890; Otterlo, Rijksmuseum Kröller–Müller), $\Omega = (0, 203) \times (0, 290)$. (b) TOP RIGHT: Filtered with $\rho = 1$. (c) BOTTOM LEFT: $\rho = 4$. (d) BOTTOM RIGHT: $\rho = 6$.
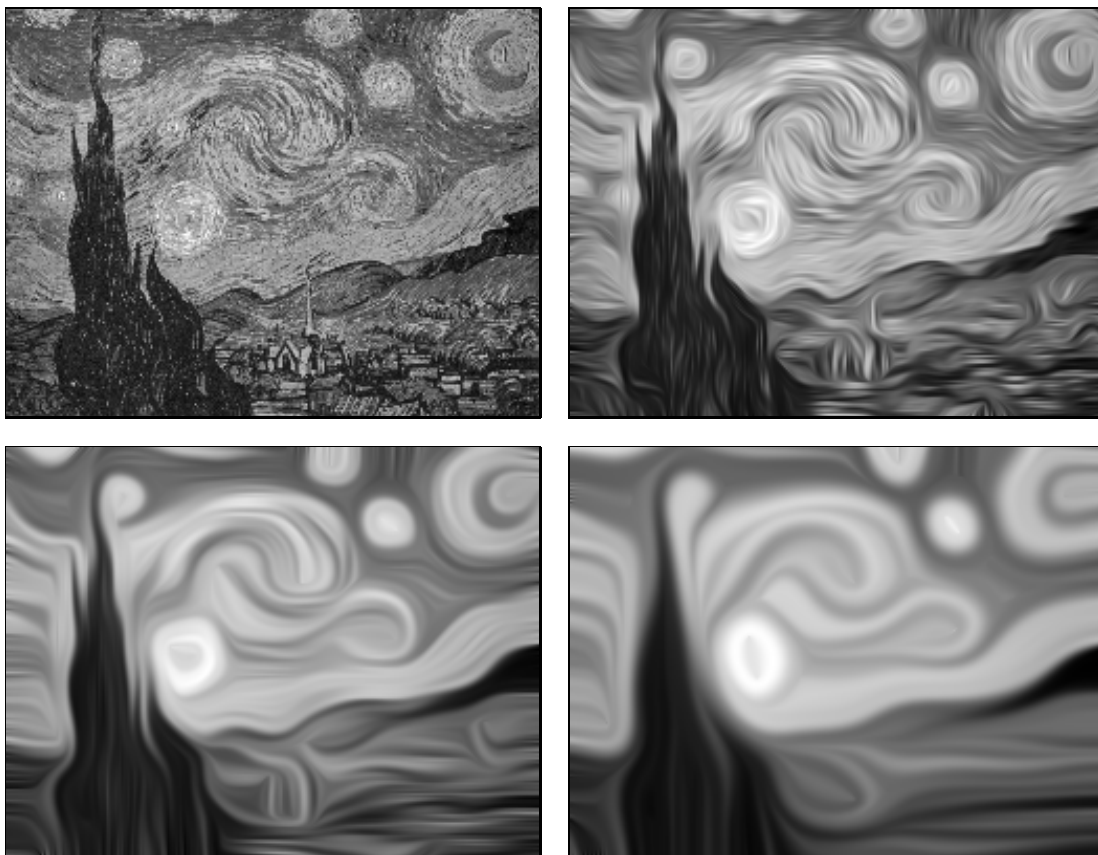
Figure 5.16: Scale-space properties of coherence-enhancing anisotropic diffusion ($\sigma = 0.5$, $\rho = 4$). (a) TOP LEFT: "Starry Night" by van Gogh (Saint-Rémy, 1889; New York, The Museum of Modern Art), $\Omega = (0, 255) \times (0, 199)$. (b) TOP RIGHT: $t = 8$. (c) BOTTOM LEFT: $t = 64$. (d) BOTTOM RIGHT: $t = 512$.

scale-space properties, the image becomes gradually simpler in many aspects, before it finally will tend to its simplest representation, a constant image with the same average grey value as the original one. The flow-like character, however, is maintained for a very long time.[3]

---

[3]Results for AMSS filtering of this image can be found in [305].

Chapter 6

Conclusions and perspectives

While Chapter 1 has given a general overview of PDE-based smoothing and restoration methods, the goal of Chapters 2–5 has been to present a scale-space framework for nonlinear diffusion filtering which does not require any monotony assumption (comparison principle). We have seen that, besides the fact that many global smoothing scale-space properties are maintained, new possibilities with respect to image restoration appear.

Rather than deducing a unique equation from first principles we have analysed well-posedness and scale-space properties of a general family of regularized anisotropic diffusion filters. Existence and uniqueness results, continuous dependence of the solution on the initial image, maximum–minimum principles, invariances, Lyapunov functionals, and convergence to a constant steady-state have been established.

The large class of Lyapunov functionals permits to regard these filters in many ways as simplifying, information-reducing transformations. These global smoothing properties do not contradict seemingly opposite local effects such as edge enhancement. For this reason it is possible to design scale-spaces with restoration properties giving segmentation-like results.

Prerequisites have been stated under which one can prove well-posedness and scale-space results in the continuous, semidiscrete and discrete setting. Each of these frameworks is self-contained and does not require the others. On the other hand, the prerequisites in all three settings reveal many similarities and, as a consequence, representatives of the semidiscrete class can be obtained by suitable spatial discretizations of the continuous class, while representatives of the discrete class may arise from time discretizations of semidiscrete filters.

The degree of freedom within the proposed class of filters can be used to tailor the filters towards specific restoration tasks. Therefore, these scale-spaces do not need to be uncommitted; they give the user the liberty to incorporate a-priori knowledge, for instance concerning size and contrast of especially interesting features.

The analysed class comprises linear diffusion filtering and the nonlinear iso-tropic model of Catté et al. [81] and Whitaker and Pizer [438], but also novel approaches have been proposed: The use of diffusion tensors instead of scalar-valued diffusivities puts us in a position to design real anisotropic diffusion processes which may reveal advantages at noisy edges. Last but not least, the fact that these filters are steered by the structure tensor instead of the regularized gradient allows to adapt them to more sophisticated tasks such as the enhancement of coherent flow-like structures.

In view of these results, anisotropic diffusion deserves to be regarded as much more than an ad-hoc strategy for transforming a degraded image into a more pleasant looking one. It is a flexible and mathematically sound class of methods which ties the advantages of two worlds: scale-space analysis and image restoration.

It is clear, however, that nonlinear diffusion filtering is a young field which has certainly not reached its final state yet. Thus, we can expect a lot of new results in the near future. Some of its future developments, however, are likely to consist of straightforward extensions of topics presented in this text:

- While the theory and the examples in the present book focus on 2-D grey-scale images, it is evident that most of its results can easily be generalized to higher dimensions and vector-valued images. The need for such extensions grows with the rapid progress in the development of faster computers, the general availability of affordable colour scanners and printers, and the wish to integrate information from different channels. Some of the references in Chapter 1 point in directions how this can be accomplished.

- The various possibilities to include semilocal or global information constitute another future perspective. This could lead to specifically tuned filters for topics such as perceptual grouping. Coherence-enhancing anisotropic diffusion is only a first step in this direction. New filter models might arise using other structure descriptors than the (regularized) gradient or the structure tensor. Interesting candidates could be wavelets, Gabor filters, or steerable filters.

- In contrast to the linear diffusion case, the relation between structures at different scales has rarely been exploited in the nonlinear context. Although this problem is less severe, since the avoidance of correspondence problems was one of the key motivations to study nonlinear scale-spaces, it would certainly be useful to better understand the deep structure in nonlinear diffusion processes. The scale-space stack of these filters appears to be well-suited to extract semantically important information with respect to a specified task. This field offers a lot of challenging mathematical questions.

- Most people working in computer vision do not have a specific knowledge on numerical methods for PDEs. As a consequence, the most widely-used numerical methods for nonlinear diffusion filtering are still the simple, but inefficient explicit (Euler forward) schemes. Novel, more time-critical application areas could be explored by applying implicit schemes, splitting and multigrid techniques, or grid adaptation strategies. In this context it would be helpful to have software packages, where different nonlinear diffusion filters are implemented in an efficient way, and which are easy to use for everyone.

- The price one has to pay for the flexibility of nonlinear diffusion filtering is the specification of some parameters. Since these parameters have a rather natural meaning, this is not a very difficult problem for someone with experience in computer vision. Somebody with another primary interest, for instance a physician who wants to denoise ultrasound images, may be frightened by this perspective. Thus, more research on finding some guidelines for automatic parameter determination for a task at hand would encourage also people without a specific image processing background to apply nonlinear diffusion filters. Several useful suggestions for parameter adaptation can already be found in [328, 36, 431, 270, 444].

- There are not yet many studies which explore the potential of nonlinear diffusion filtering when being combined with other image processing techniques. Especially combinations with concepts such as data compression, segmentation algorithms, tomographic reconstruction techniques, or neural networks for learning a-priori information might lead to novel application areas for these techniques.

Thus, there still remains a lot of work to be done. It would be nice if this book has inspired its readers to contribute to the solution of some of the remaining open problems.

Bibliography

[1] S. Abbasi, F. Mokhtarian, J. Kittler, *Reliable classification of chrysanthemum leaves through curvature scale space*, B. ter Haar Romeny, L. Florack, J. Koenderink, M. Viergever (Eds.), Scale-space theory in computer vision, Lecture Notes in Computer Science, Vol. 1252, Springer, Berlin, 284–295, 1997.

[2] R. Acar, C.R. Vogel *Analysis of bounded variation penalty methods for ill-posed problems*, Inverse Problems, Vol. 10, 1217–1229, 1994.

[3] A. Ackah–Miezan, A. Gagalowicz, *Discrete models for energy-minimizing segmentation*, Proc. Fourth Int. Conf. on Computer Vision (ICCV '93, Berlin, May 11–14, 1993), IEEE Computer Society Press, Los Alamitos, 200–207, 1993.

[4] S.T. Acton, *Edge enhancement of infrared imagery by way of the anisotropic diffusion pyramid*, Proc. IEEE Int. Conf. Image Processing (ICIP–96, Lausanne, Sept. 16–19, 1996), Vol. 1, 865–868, 1996.

[5] S.T. Acton, A.C. Bovik, M.M. Crawford, *Anisotropic diffusion pyramids for image segmentation*, Proc. IEEE Int. Conf. Image Processing (ICIP–94, Austin, Nov. 13–16, 1994), Vol. 3, IEEE Computer Society Press, Los Alamitos, 478–482, 1994.

[6] S.T. Acton, M.M. Crawford, *A mean field solution to anisotropic edge detection of remotely sensed data*, Proc. 12th Int. Geoscience and Remote Sensing Symposium (IGARSS '92, Houston, May 26–29, 1992), Vol. 2, 845–847, 1992.

[7] R.A. Adams, *Sobolev spaces*, Academic Press, New York, 1975.

[8] D. Adalsteinsson, J.A. Sethian, *A fast level set method for propagating interfaces*, J. Comput. Phys., Vol. 118, 269–277, 1995.

[9] H.W. Alt, *Lineare Funktionalanalysis*, Springer, Berlin, 1992.

[10] L. Alvarez, *Images and PDE's*, M.-O. Berger, R. Deriche, I. Herlin, J. Jaffré, J.-M. Morel (Eds.), ICAOS '96: Images, wavelets and PDEs, Lecture Notes in Control and Information Sciences, Vol. 219, Springer, London, 3–14, 1996.

[11] L. Alvarez, J. Esclarin, *Image quantization using reaction–diffusion equations*, SIAM J. Appl. Math., Vol. 57, 153–175, 1997.

[12] L. Alvarez, F. Guichard, P.-L. Lions, J.-M. Morel, *Axioms and fundamental equations in image processing*, Arch. Rational Mech. Anal., Vol. 123, 199–257, 1993.

[13] L. Alvarez, P.-L. Lions, J.-M. Morel, *Image selective smoothing and edge detection by nonlinear diffusion. II*, SIAM J. Numer. Anal., Vol. 29, 845–866, 1992.

[14] L. Alvarez, L. Mazorra, *Signal and image restoration using shock filters and anisotropic diffusion*, SIAM J. Numer. Anal., Vol. 31, 590–605, 1994.

[15] L. Alvarez, F. Morales, *Affine morphological multiscale analysis of corners and multiple junctions*, Report No. 9402, Departamento de Informática y Sistemas, Universidad de Las Palmas, Campus Universitario de Tafira, 35017 Las Palmas, Spain, 1994; to appear in Int. J. Comput. Vision.

[16] L. Alvarez, J.-M. Morel, *Formalization and computational aspects of image analysis*, Acta Numerica, 1–59, 1994.

[17] L. Ambrosio, *A compactness theorem for a special class of functions of bounded variations*, Boll. Un. Math. Ital., Vol. 3-B, 857–881, 1990.

[18] L. Ambrosio, N. Fusco, D. Pallara, *Partial regularity of free discontinuity sets II*, Preprint CV-GMT-96040106, Math. Dept., Scuola Normale Superiore, Piazza dei Cavalieri, 56126 Pisa, Italy, 1995; submitted to Annali della Scuola Normale Superiore di Pisa.

[19] L. Ambrosio, N. Fusco, D. Pallara, *Higher regularity of solutions of free discontinuity problems*, Preprint CV-GMT-96040107, Math. Dept., Scuola Normale Superiore, Piazza dei Cavalieri, 56126 Pisa, Italy, 1995.

[20] L. Ambrosio, D. Pallara, *Partial regularity of free discontinuity sets I*, Preprint CV-GMT-96040105, Math. Dept., Scuola Normale Superiore, Piazza dei Cavalieri, 56126 Pisa, Italy, 1995; submitted to Annali della Scuola Normale Superiore di Pisa.

[21] L. Ambrosio, V. Tortorelli, *On the approximation of functionals depending on jumps by elliptic functionals*, Comm. Pure Appl. Math., Vol. 43, 999–1036, 1990.

[22] L. Ambrosio, V. Tortorelli, *Approximation of functionals depending on jumps by elliptic functionals via Γ-convergence*, Boll. Un. Math. Ital., Vol. 7, 105–123, 1992.

[23] S. Angenent, *Parabolic equations on curves and surfaces. Part I. Curves with p-integrable curvature*, Annals of Mathematics, Vol. 132, 451–483, 1990.

[24] S. Angenent, *Parabolic equations on curves and surfaces. Part II. Intersections, blowup, and generalized solutions*, Annals of Mathematics, Vol. 133, 171–215, 1991.

[25] A.B. Arehart, L. Vincent, B.B. Kimia, *Mathematical morphology: The Hamilton–Jacobi connection*, Proc. Fourth Int. Conf. on Computer Vision (ICCV '93, Berlin, May 11–14, 1993), IEEE Computer Society Press, Los Alamitos, 215–219, 1993.

[26] S.R. Arridge, A. Simmons, *Multi-spectral probabilistic diffusion using Bayesian classification*, B. ter Haar Romeny, L. Florack, J. Koenderink, M. Viergever (Eds.), Scale-space theory in computer vision, Lecture Notes in Computer Science, Vol. 1252, Springer, Berlin, 224–235, 1997.

[27] K. Åström, A. Heyden, *Stochastic analysis of image acquisition and scale-space smoothing*, J. Sporring, M. Nielsen, L. Florack, P. Johansen (Eds.), Gaussian scale-space theory, Kluwer, Dordrecht, 129–136, 1997.

[28] I. Bajla, I. Holländer, *Geometry-driven diffusion smoothing of the MR brain images using a novel variable conductance*, Proc. 18th Annual Int. Conf. of the IEEE Engineering in Medicine and Biology Soc. (EMB '96, Amsterdam, Oct. 31 – Nov. 3, 1996), CD-ROM document N21.

[29] I. Bajla, M. Marušiak, M. Šrámek, *Anisotropic filtering of MRI data based upon image gradient histogram*, D. Chetverikov, W.G. Kropatsch (Eds.), Computer analysis of images and patterns, Lecture Notes in Computer Science, Vol. 719, Springer, Berlin, 90–97, 1993.

[30] J. Babaud, A.P. Witkin, M. Baudin, R.O. Duda, *Uniqueness of the Gaussian kernel for scale space filtering*, IEEE Trans. Pattern Anal. Mach. Intell., Vol. 8, 26–33, 1986.

[31] C. Ballester Nicolau, *An affine invariant model for image segmentation: Mathematical analysis and applications*, Ph.D. thesis, University of Illes Baleares, Palma de Mallorca, Spain, 1995.

[32] C. Ballester, V. Caselles, M. González, *Affine invariant segmentation by variational method*, SIAM J. Appl. Math., Vol. 56, 294–325, 1996.

[33] C. Ballester, M. González, *Texture segmentation by variational methods*, M.-O. Berger, R. Deriche, I. Herlin, J. Jaffré, J.-M. Morel (Eds.), ICAOS '96: Images, wavelets and PDEs, Lecture Notes in Control and Information Sciences, Vol. 219, Springer, London, 187–193, 1996.

[34] E. Bänsch, K. Mikula, *A coarsening finite element strategy in image selective smoothing*, Preprint No. 18/1996, Faculty of Mathematics, University of Freiburg, Hebelstr. 27, 79104 Freiburg, Germany, 1996; to appear in Computation and Visualization in Science.

[35] G.I. Barenblatt, M. Bertsch, R. Dal Passo, M. Ughi, *A degenerate pseudoparabolic regularization of a nonlinear forward–backward heat equation arising in the theory of heat and mass exchange in stably stratified turbulent shear flow*, SIAM J. Math. Anal., Vol. 24, 1414–1439, 1993.

[36] B. Benhamouda, *Parameter adaptation for nonlinear diffusion in image processing*, master thesis, Dept. of Mathematics, University of Kaiserslautern, P.O. Box 3049, 67653 Kaiserslautern, Germany, 1994.

[37] P.M. van den Berg, R.E. Kleinman, *A total variation enhanced modified gradient algorithm for profile reconstruction*, Physics Express Letters, Inverse Problems, Vol. 11, pp. L5–L10, 1995.

[38] F. Bergholm, *Edge focusing*, IEEE Trans. Pattern Anal. Mach. Intell., Vol. 9, 726–741, 1987.

[39] J. Bigün, G.H. Granlund, *Optimal orientation detection of linear symmetry*, Proc. First Int. Conf. on Computer Vision (ICCV '87, London, June 8–11, 1987), IEEE Computer Society Press, Washington, 433–438, 1987.

[40] J. Bigün, G.H. Granlund, J. Wiklund, *Multidimensional orientation estimation with applications to texture analysis and optical flow*, IEEE Trans. Pattern Anal. Mach. Intell., Vol. 13, 775–790, 1991.

[41] M.J. Black, G. Sapiro, D. Marimont, D. Heeger, *Robust anisotropic diffusion: connections between robust statistics, line processing, and anisotropic diffusion*, B. ter Haar Romeny, L. Florack, J. Koenderink, M. Viergever (Eds.), Scale-space theory in computer vision, Lecture Notes in Computer Science, Vol. 1252, Springer, Berlin, 323–326, 1997.

[42] A. Blake, A. Zisserman, *Visual reconstruction*, MIT Press, Cambridge (Mass.), 1987.

[43] L. Blanc–Féraud, P. Charbonnier, G. Aubert, M. Barlaud, *Nonlinear image processing: modelling and fast algorithm for regularization with edge detection*, Proc. IEEE Int. Conf. Image Processing (ICIP–95, Washington, Oct. 22–25, 1995), Vol. 1, 474–477, 1995.

[44] W. Blaschke, *Vorlesungen über Differentialgeometrie II*, Springer, Berlin, 1923.

[45] P. Blomgren, T.F. Chan, *Color TV: total variation methods for restoration of vector valued images*, CAM Report 96-5, Dept. of Mathematics, Univ. of California, Los Angeles, CA 90024, U.S.A., 1996; to appear in IEEE Trans. Image Proc.

[46] P. Blomgren, T.F. Chan, P. Mulet, *Extensions to total variation denoising*, F.T. Luk (Ed.), Advanced signal processing: algorithms, architectures, and implementations VII, SPIE Vol. 3162, 1997, to appear.

[47] H. Blum, *A transformation for extracting new descriptors of shape*, W. Wathen–Dunn (Ed.), Models for the perception of speech and visual form, M.I.T. Press, Cambridge, 362–380, 1967.

[48] A. Bonnet, *Charactérisation des minima globaux de la fonctionelle du Mumford–Shah en segmentation d'images*, C. R. Acad. Sci. Paris, t. 321, Série I, 1121–1126, 1995.

[49] A. Bonnet, *Sur la régularité des bords des minima de la fonctionelle de Mumford–Shah*, C. R. Acad. Sci. Paris, t. 321, Série I, 1275–1279, 1995.

[50] R. van den Boomgaard, *Mathematical morphology: Extensions towards computer vision*, Ph.D. thesis, University of Amsterdam, The Netherlands, 1992.

[51] R. van den Boomgaard, *The morphological equivalent of the Gauss convolution*, Nieuw Archief Voor Wiskunde, Vierde Serie, Deel 10, 219–236, 1992.

[52] R. van den Boomgaard, *Morphology*, oral presentation, Ph.D. School on Classical Scale-Space Theory, Copenhagen, May 10–13, 1996.

[53] R. van den Boomgaard, A. Smeulders, *The morphological structure of images: The differential equations of morphological scale-space*, IEEE Trans. Pattern Anal. Mach. Intell., Vol. 16, 1101–1113, 1994.

[54] K.A. Brakke, *The motion of a surface by its mean curvature*, Princeton University Press, Princeton, 1978.

[55] J.H. Bramble, B.E. Hubbard, *New monotone type approximations for elliptic problems*, Math. Comp., Vol. 18, 349–367, 1964.

[56] F. Brauer, J.A. Nohel, *Ordinary differential equations: A first course*, Benjamin, New York, 1967.

[57] H. Brezis, *Opérateurs maximaux monotones et semi-groupes de contractions dans les espaces de Hilbert*, North Holland, Amsterdam, 1973.

[58] H. Brezis, *Analyse fonctionelle*, Masson, Paris, 1992.

[59] W.L. Briggs, *A multigrid tutorial*, SIAM, Philadelphia, 1987.

[60] R.W. Brockett, P. Maragos, *Evolution equations for continuous-scale morphological filtering*, IEEE Trans. Signal Processing, Vol. 42, 3377–3386, 1994.

[61] A.M. Bruckstein, G. Sapiro, D. Shaked, *Evolution of planar polygons*, Int. J. Pattern Recogn. Artif. Intell., Vol. 9, 991–1014, 1995.

[62] A.M. Bruckstein, D. Shaked, *On projective invariant smoothing and evolution of planar curves and polygons*, J. Math. Imag. Vision, Vol. 7, 225–240, 1997.

[63] B. Buck, V. Macaulay (Eds.), *Maximum entropy in action*, Clarendon, Oxford, 1991.

[64] P.J. Burt, *Fast filter transforms for image processing*, Computer Graphics and Image Processing, Vol. 16, 20–51, 1981.

[65] M. Burton, S. Acton, *Target tracking using the anisotropic diffusion pyramid*, Proc. IEEE Southwest Symposium on Image Analysis and Interpetation (SSIAI '96, San Antonio, April 8–9, 1996).

[66] M.A. Butt, P. Maragos, *Comparison of multiscale morphology approaches: PDE implemented via curve evolution versus Chamfer distance transform*, P. Maragos, R.W. Schafer, M.A. Butt (Eds.), Mathematical morphology and its applications to image and signal processing, Kluwer, Boston, 31–40, 1996.

[67] L.D. Cai, *Some notes on repeated averaging smoothing*, J. Kittler (Ed.), Pattern Recognition, Lecture Notes in Computer Science, Vol. 301, Springer, Berlin, 597–605, 1988.

[68] L.D. Cai, *A "small leakage" model for diffusion smoothing of image data*, Proc. 11th Int. Joint Conf. on Artificial Intelligence (IJCAI '89, Detroit, Aug. 20–25, 1989), Vol. 2, 1585–1590, 1989.

[69] J. Canny, *A computational approach to edge detection*, IEEE Trans. Pattern Anal. Mach. Intell., Vol. 8, 679–698, 1986.

[70] V. Cantoni, M. Ferretti, *Pyramidal architectures for computer vision*, Plenum Press, New York, 1994.

[71] M.P. do Carmo, *Differentialgeometrie von Kurven und Flächen*, Vieweg, Braunschweig, 1983.

[72] R. Carmona, S. Zhong, *Adaptive image smoothing respecting feature directions*, Preprint, Dept. of Civil Engineering, Princeton University, Princeton, NJ 08544–5263, U.S.A., 1996; submitted to IEEE Trans. Image Proc.

[73] V. Caselles, F. Catté, T. Coll, F. Dibos, *A geometric model for active contours in image processing*, Numer. Math., Vol. 66, 1–31, 1993.

[74] V. Caselles, B. Coll, *Snakes in movement*, SIAM J. Numer. Anal., Vol. 33, 2445–2456, 1996.

[75] V. Caselles, B. Coll, J.-M. Morel, *Scale-space versus topographic map for natural images*, B. ter Haar Romeny, L. Florack, J. Koenderink, M. Viergever (Eds.), Scale-space theory in computer vision, Lecture Notes in Computer Science, Vol. 1252, Springer, Berlin, 29–49, 1997.

[76] V. Caselles, R. Kimmel, G. Sapiro, *Geodesic active contours*, Int. J. Comput. Vision., Vol. 22, 61–79, 1997.

[77] V. Caselles, R. Kimmel, G. Sapiro, C. Sbert, *Minimal surfaces: a geometric three dimensional segmentation approach*, Numer. Math., Vol. 77, 423–451, 1997.

[78] V. Caselles, C. Sbert, *What is the best causal scale-space for 3-D images?*, SIAM J. Appl. Math., Vol. 56, 1199–1246, 1996.

[79] F. Catté, *Convergence of iterated affine and morphological filters by nonlinear semi-group theory*, M.-O. Berger, R. Deriche, I. Herlin, J. Jaffré, J.-M. Morel (Eds.), ICAOS '96: Images, wavelets and PDEs, Lecture Notes in Control and Information Sciences, Vol. 219, Springer, London, 125–133, 1996.

[80] F. Catté, F. Dibos, G. Koepfler, *A morphological scheme for mean curvature motion and applications to anisotropic diffusion and motion of level sets*, SIAM J. Numer. Anal., Vol. 32, 1895–1909, 1995.

[81] F. Catté, P.-L. Lions, J.-M. Morel, T. Coll, *Image selective smoothing and edge detection by nonlinear diffusion*, SIAM J. Numer. Anal., Vol. 29, 182–193, 1992.

[82] A. Chambolle, *Partial differential equations and image processing*, Proc. IEEE Int. Conf. Image Processing (ICIP–94, Austin, Nov. 13–16, 1994), Vol. 1, IEEE Computer Society Press, Los Alamitos, 16–20, 1994.

[83] A. Chambolle, P.-L. Lions, *Image recovery via total variation minimization and related problems*, Numer. Math., Vol. 76, 167–188, 1997.

[84] R.H. Chan, T.F. Chan, C.K. Wong, *Cosine transform based preconditioners for total variation minimization problems in image processing*, S. Margenov, P. Vassilevski (Eds.), Proc. Second IMACS Symposium on Iterative Methods, IMACS Press, 311–329, 1995.

[85] T.F. Chan, G.H. Golub, P. Mulet, *A nonlinear primal–dual method for total-variation based image restoration*, M.-O. Berger, R. Deriche, I. Herlin, J. Jaffré, J.-M. Morel (Eds.), ICAOS '96: Images, wavelets and PDEs, Lecture Notes in Control and Information Sciences, Vol. 219, Springer, London, 241–252, 1996.

[86] T.F. Chan, C.K. Wong, *Total variation blind deconvolution*, CAM Report 96-45, Dept. of Mathematics, Univ. of California, Los Angeles, CA 90024, U.S.A., 1996; to appear in IEEE Trans. Image Proc.

[87] T.F. Chan, H.M. Zhou, R.H. Chan, *Continuation method for total variation minimizing problems in image processing*, F.T. Luk (Ed.), Advanced signal processing algorithms, SPIE Vol. 2563, 314–325, 1995.

[88] P. Charbonnier, L. Blanc–Féraud, G. Aubert, M. Barlaud, *Two deterministic half-quadratic regularization algorithms for computed imaging*, Proc. IEEE Int. Conf. Image Processing (ICIP–94, Austin, Nov. 13–16, 1994), Vol. 2, IEEE Computer Society Press, Los Alamitos, 168–172, 1994.

[89] Y. Chen, B.C. Vemuri, L. Wang, *Image denoising and segmentation via nonlinear diffusion*, Report UF-CISE-TR97-015, CISE Dept., University of Florida, Gainesville, FL 32611, U.S.A., 1997; submitted to SIAM J. Appl. Math.

[90] Y.-G. Chen, Y. Giga, S. Goto, *Uniqueness and existence of viscosity solutions of generalized mean curvature flow equations*, J. Differential Geometry, Vol. 33, 749–786, 1991.

[91] D.L. Chopp, *Computing minimal surfaces via level set curvature flow*, Ph.D. thesis LBL-30685, Physics Division, Lawrence Berkeley Laboratory, University of California, Berkeley, CA 94720, U.S.A., 1991 (see also J. Comput. Phys., Vol. 106, 77–91, 1993).

[92] C.K. Chui, *Wavelets: A tutorial in theory and applications*, Academic Press, New York, 1992.

[93] L.D. Cohen, *On active contour models and balloons*, CVGIP: Image Understanding, Vol. 53, 211–218, 1991.

[94] M.A. Cohen, S. Grossberg, *Neural dynamics of brightness perception: Features, boundaries, diffusion and resonance*, Perception and Psychophysics, Vol. 36, 428–456, 1984.

[95] T. Cohignac, F. Eve, F. Guichard, C. Lopez, J.-M. Morel, *Numerical analysis of the fundamental equation of image processing*, Preprint No. 9254, CEREMADE, Université Paris IX – Dauphine, Place du Maréchal de Lattre de Tassigny, 75775 Paris Cedex 16, France, 1992.

[96] T. Cohignac, C. Lopez, J.M. Morel, *Integral and local affine invariant parameter and application to shape recognition*, Proc. 12th Int. Conf. Pattern Recognition (ICPR 12, Jerusalem, Oct. 9–13, 1994), Vol. A, IEEE Computer Society Press, Los Alamitos, 164–168, 1994.

[97] T. Cohignac, J-.M. Morel, *Scale-space and affine invariant recognition of occluded shapes*, L.I. Rudin, S.K. Bramble (Eds.), Investigative and trial image processing, SPIE Vol. 2567, 214–222, 1995.

[98] G. Cong, S.D. Ma, *Nonlinear diffusion for early vision*, Proc. 13th Int. Conf. Pattern Recognition (ICPR 13, Vienna, Aug. 25–30, 1996), Vol. A, 403–406, 1996.

[99] G.-H. Cottet, *Diffusion approximation on neural networks and applications for image processing*, F. Hodnett (Ed.), Proc. Sixth European Conf. on Mathematics in Industry, Teubner, Stuttgart, 3–9, 1992.

[100] G.-H. Cottet, *Neural networks: Continuous approach and applications to image processing*, J. Biological Systems, Vol. 3, 1131–1139, 1995.

[101] G.-H. Cottet, M. El Ayyadi, *Nonlinear PDE operators with memory terms for image processing*, Proc. IEEE Int. Conf. Image Processing (ICIP–96, Lausanne, Sept. 16–19, 1996), Vol. 1, 481–483, 1996.

[102] G.-H. Cottet, L. Germain, *Image processing through reaction combined with nonlinear diffusion*, Math. Comp., Vol. 61, 659–673, 1993.

[103] M.G. Crandall, I. Ishii, P.-L. Lions, *User's guide to viscosity solutions of second order partial differential equations*, Bull. Am. Math. Soc., Vol. 27, 1–67, 1992.

[104] M.G. Crandall, P.-L. Lions, *Convergent difference schemes for nonlinear parabolic equations and mean curvature motion*, Numer. Math., Vol. 75, 17–41, 1996.

[105] J. Damon, *Local Morse theory for solutions to the heat equation and Gaussian blurring*, J. Differential Equations, Vol. 115, 368–401, 1995.

[106] I. Daubechies, *Ten lectures on wavelets*, SIAM, Philadelphia, 1992.

[107] G. David, C^1-*arcs for minimizers of the Mumford–Shah functional*, SIAM J. Appl. Math., Vol. 56, 783–888, 1996.

[108] E. De Giorgi, M. Carriero, A. Leaci, *Existence theorem for a minimum problem with a free discontinuity set*, Arch. Rat. Mech. Anal., Vol. 108, 195–218, 1989.

[109] R. Deriche, *Recursively implementing the Gaussian and its derivatives*, V. Srinivasan, Ong S.H., Ang Y.H. (Eds.), Proc. Second Int. Singapore Conf. on Image Proc. (Singapore, Sept. 7–11, 1992), 263–267, 1992.

[110] R. Deriche, O. Faugeras, *Les EDP en traitement des images et vision par ordinateur*, Traitement du Signal, Vol. 13, No. 6, 1997.

[111] R. Deriche, P. Kornprobst, G. Aubert, *Optical-flow estimation while preserving its discontinuities: A variational approach*, Proc. Second Asian Conf. Computer Vision (ACCV '95, Singapore, December 5–8, 1995), Vol. 2, 290–295, 1995.

[112] F. Dibos, *Analyse multiéchelle invariante par transformations projectives*, C. R. Acad. Sci. Paris, t. 320, Série I, 917–921, 1995.

[113] F. Dibos, *Projective invariant multiscale analysis*, Proc. IEEE Int. Conf. Image Processing (ICIP–96, Lausanne, Sept. 16–19, 1996), Vol. 1, 485–488, 1996.

[114] S. Di Zenzo, *A note on the gradient of a multi-image*, Computer Vision, Graphics, and Image Processing, Vol. 33, 116–125, 1986.

[115] D.C. Dobson, F. Santosa, *An image enhancement technique for electrical impedance tomography*, Inverse Problems, Vol. 10, 317–334, 1994.

[116] D.C. Dobson, F. Santosa, *Recovery of blocky images from noisy and blurred data*, SIAM J. Appl. Math., Vol. 56, 1181–1198, 1996.

[117] D. Dobson, O. Scherzer, *Analysis of regularized total variation penalty methods for denoising*, Inverse Problems, Vol. 12, 601–617, 1996.

[118] D.C. Dobson, C.R. Vogel, *Convergence of an iterative method for total variation denoising*, Preprint, Dept. of Mathematical Sciences, Montana State University, Bozeman, MT 59717-0240, U.S.A., 1995; SIAM J. Numer. Anal., to appear.

[119] L. Dorst, R. van den Boomgaard, *Morphological signal processing and the slope transform*, Signal Processing, Vol. 38, 79–98, 1994.

[120] J. Douglas, J.E. Gunn, *A general formulation of alternating direction methods. Part I. Parabolic and hyperbolic problems*, Numer. Math., Vol. 6, 428–453, 1964.

[121] J. Douglas, B.F. Jones, *On predictor–corrector methods for non-linear parabolic differential equations*, J. Soc. Ind. Appl. Math., Vol. 11, 195–204, 1963.

[122] I.S. Duff, A.M. Erisman, J.K. Reid, *Direct methods for sparse systems*, Clarendon, Oxford, 1986.

[123] S.K. Dzhu Magazieva, *Numerical study of a partial differential equation*, U.S.S.R. Comput. Maths. Math. Phys., Vol. 23, No. 4, 45–49, 1983.

[124] D. Eberly, *A differential geometric approach to anisotropic diffusion*, B.M. ter Haar Romeny (Ed.), Geometry-driven diffusion in computer vision, Kluwer, Dordrecht, 371–391, 1994.

[125] S. Eidelman, W. Grossmann, A. Friedman, *Nonlinear signal processing using integration of fluid dynamics equations*, A.G. Tescher (Ed.): Applications of digital image processing XIV, SPIE Vol. 1567, 439–450, 1991.

[126] A.I. El-Fallah, G.E. Ford, *Nonlinear adaptive image filtering based on inhomogeneous diffusion and differential geometry*, S.A. Rajala, R.L. Stevenson (Eds.), Image and video processing II, SPIE Vol. 2182, 49–63, 1994.

[127] A.I. El-Fallah, G.E. Ford, *The evolution of mean curvature in image filtering*, Proc. IEEE Int. Conf. Image Processing (ICIP–94, Austin, Nov. 13–16, 1994), Vol. 1, IEEE Computer Society Press, Los Alamitos, 298–302, 1994.

[128] H.W. Engl, M. Hanke, A. Neubauer, *Regularization of inverse problems*, Kluwer, Dordrecht, 1996.

[129] L.C. Evans, J. Spruck, *Motion of level sets by mean curvature I.*, J. Differential Geometry, Vol. 33, 635–681, 1991.

[130] O. Faugeras, *Sur l'évolution de courbes simples du plan projectif réel*, C. R. Acad. Sci. Paris, t. 317, Série I, 565–570, 1993.

[131] O. Faugeras, *Cartan's moving frame method and its application to the geometry and evolution of curves in the Euclidean, affine and projective planes*, J.L. Mundy, A. Zisserman, D. Forsyth (Eds.), Applications of invariance in computer vision, Lecture Notes in Computer Science, Vol. 825, Springer, Berlin, 11–46, 1994.

[132] O. Faugeras, R. Keriven, *Scale-spaces and affine curvature*, W. Chenke, R. Mohr (Eds.), Proc. Workshop on Geometrical Modelling and Invariants for Computer Vision (Xi'an, April 27–30, 1995), Xidian University Press, Xi'an, 1995.

[133] O. Faugeras, R. Keriven, *On projective plane curve evolution*, M.-O. Berger, R. Deriche, I. Herlin, J. Jaffré, J.-M. Morel (Eds.), ICAOS '96: Images, wavelets and PDEs, Lecture Notes in Control and Information Sciences, Vol. 219, Springer, London, 66–73, 1996.

[134] O. Faugeras, R. Keriven, *Level set methods and the stereo problem*, B. ter Haar Romeny, L. Florack, J. Koenderink, M. Viergever (Eds.), Scale-space theory in computer vision, Lecture Notes in Computer Science, Vol. 1252, Springer, Berlin, 272–283, 1997.

[135] S. Fejes, A. Rosenfeld, *Discrete active models and applications*, Pattern Recognition, Vol. 30, 817–835, 1997.

[136] P. Fiddelaers, E.J. Pauwels, L.J. Van Gool, *Geometry-driven curve evolution*, J.-O. Eklundh (Ed.), Computer Vision – ECCV '94, Lecture Notes in Computer Science, Vol. 800, Springer, Berlin, 427–432, 1994.

[137] B. Fischl, E.L. Schwartz, *Adaptive nonlinear filtering for nonlinear diffusion approximation in image processing*, Proc. 13th Int. Conf. Pattern Recognition (ICPR 13, Vienna, Aug. 25–30, 1996), Vol. D, 276–280, 1996.

[138] L.M.J. Florack, *Data, models, and images*, Proc. 1996 IEEE Int. Conf. Image Processing (ICIP–96, Lausanne, Sept. 16–19, 1996), Vol. I, 469–472, 1996.

[139] L.M.J. Florack, *Image structure*, Kluwer, Dordrecht, 1997.

[140] L.M.J. Florack, B.M. ter Haar Romeny, J.J. Koenderink, M.A. Viergever, *Scale and the differential structure of images*, Image Vision Comput., Vol. 10, 376–388, 1992.

[141] L.M.J. Florack, B.M. ter Haar Romeny, J.J. Koenderink, M.A. Viergever, *The Gaussian scale-space paradigm and the multiscale local jet*, Int. J. Comput. Vision, Vol. 18, 61–75, 1996.

[142] L. Florack, R. Maas, *Pseudo-linear scale-space theory: towards the integration of linear and morphological scale-space paradigms*, Technical Report UU-CS-1997-25, Dept. of Computer Science, Padualaan 14, 3584 CH Utrecht, The Netherlands, 1997.

[143] L.M.J. Florack, A.H. Salden, B.M. ter Haar Romeny, J.J. Koenderink, M.A. Viergever, *Nonlinear scale-space*, Image Vision Comput., Vol. 13, 279–294, 1995.

[144] G.E. Ford, R.R. Estes, H. Chen, *Scale-space analysis for image sampling and interpolation*, Proc. IEEE Int. Conf. Acoustics, Speech and Signal Processing (ICASSP–92, San Francisco, March 23–26, 1992), Vol. 3, 165–168, 1992.

[145] M.A. Förstner, E. Gülch, *A fast operator for detection and precise location of distinct points, corners and centres of circular features*, Proc. ISPRS Intercommission Conf. on Fast Processing of Photogrammetric Data (Interlaken, June 2–4, 1987), 281–305, 1987.

[146] T. Franke, H. Neumann, R. Seydel, *Anisotropic diffusion based on mean curvature motion: A computational study*, B. Jähne, P. Geißler, H. Haußecker, F. Hering (Eds.), Mustererkennung 1996, Springer, Berlin, 47–54, 1996.

[147] D.S. Fritsch, *A medial description of greyscale image structure by gradient-limited diffusion*, R.A. Robb (Ed.), Visualization in biomedical computing '92, SPIE Vol. 1808, 105–117, 1992.

[148] J. Fröhlich, J. Weickert, *Image processing using a wavelet algorithm for nonlinear diffusion*, Report No. 104, Laboratory of Technomathematics, University of Kaiserslautern, P.O. Box 3049, 67653 Kaiserslautern, Germany, 1994.

[149] D. Gabor, *Information theory in electron microscopy*, Laboratory Investigation, Vol. 14, 801–807, 1965.

[150] M. Gage, *On area-preserving evolution equation for plane curves*, Contemp. Math., Vol. 23, 51–62, 1986.

[151] M. Gage, R.S. Hamilton, *The heat equation shrinking convex plane curves*, J. Differential Geometry, Vol. 23, 69–96, 1986.

[152] D. Geiger, A. Yuille, *A common framework for image segmentation*, Int. J. Comput. Vision, Vol. 6, 227–243, 1991.

[153] D. Geman, G. Reynolds, *Constrained restoration and the recovery of discontinuities*, IEEE Trans. Pattern Anal. Mach. Intell., Vol. 14, 367–383, 1992.

[154] S. Geman, D. Geman, *Stochastic relaxation, Gibbs distributions, and the Bayesian restoration of images*, IEEE Trans. Pattern Anal. Mach. Intell., Vol. 6, 721–741, 1984.

[155] G. Gerig, O. Kübler, R. Kikinis, F.A. Jolesz, *Nonlinear anisotropic filtering of MRI data*, IEEE Trans. Medical Imaging, Vol. 11, 221–232, 1992.

[156] G. Gerig, G. Székely, *Finding line structures by multi-valued nonlinear diffusion of feature maps*, Report, Communication Technology Laboratory, Image Science Division, ETH–Zentrum, 8092 Zürich, Switzerland, 1993.

[157] G. Gerig, G. Székely, G. Israel, M. Berger, *Detection and characterization of unsharp blobs by curve evolution*, Y. Bizais, C. Barillot, R. Di Paola (Eds.), Information Processing in Medical Imaging, Kluwer, Dordrecht, 165–176, 1995.

[158] T. Gijbels, P. Six, L. Van Gool, F. Catthoor, H. De Man, A. Oosterlinck, *A VLSI-architecture for parallel non-linear diffusion with applications in vision*, Proc. IEEE Workshop on VLSI Signal Processing, Vol. 7, 398–407, 1994.

[159] D. Giuiliani, *Directed diffusion equations and edge detection*, master thesis, Dept. of Mathematics, University of Kaiserslautern, P.O. Box 3049, 67653 Kaiserslautern, Germany, 1991.

[160] V. van Gogh, *Starry night*, Saint-Rémy, 1889. New York, The Museum of Modern Art.

[161] V. van Gogh, *Selfportrait*, Saint-Rémy, 1889. Paris, Museé d'Orsay.

[162] V. van Gogh, *Road with cypress and star*, Auvers-sur-Oise, 1890. Otterlo, Rijksmuseum Kröller–Müller.

[163] R.C. Gonzalez, P. Wintz, *Digital image processing*, Addison–Wesley, Reading, 1987.

[164] R. Gorenflo, *Conservative difference schemes for diffusion problems*, Preprint No. 39, FB Mathematik, FU Berlin, Arnimallee 2–6, W-1000 Berlin 33, Germany, 1977.

[165] A. Goshtasby, *On edge focusing*, Image Vision Comput., Vol. 12, 247–256, 1994.

[166] A.R. Gourlay, *Implicit convolution*, Image Vision Comput., Vol. 3, 15–23, 1985.

[167] R. Graham, *Snow removal: A noise-stripping process for TV signals*, IRE Trans. Information Theory, Vol. 8, 129–144, 1962.

[168] G.H. Granlund, H. Knutsson, *Signal processing for computer vision*, Kluwer, Dordrecht, 1995.

[169] M. Grayson, *The heat equation shrinks embedded plane curves to round points*, J. Differential Geometry, Vol. 26, 285–314, 1987.

[170] D. Greenspan, P.C. Jain, *On non-negative difference analogues of elliptic differential equations*, J. Franklin Inst., Vol. 279, 360–365, 1965.

[171] L.D. Griffin, *Scale-imprecision space*, Image Vision Comput., Vol. 15, 369–398, 1997.

[172] L.D. Griffin, A.C.F. Colchester, G.P. Robinson, *Scale and segmentation of grey-level images using maximum gradient paths*, Image Vision Comput., Vol. 10, 389–402, 1992.

[173] F. Guichard, J.-M. Morel, *Partial differential equations and image iterative filtering*, Preprint No. 9535, CEREMADE, Université Paris IX – Dauphine, Place du Maréchal de Lattre de Tassigny, 75775 Paris Cedex 16, France, 1995; to appear in I.S. Duff, G.A. Watson (Eds.), The state of the art in numerical analysis, Oxford University Press.

[174] B.M. ter Haar Romeny (Ed.), *Geometry-driven diffusion in computer vision*, Kluwer, Dordrecht, 1994.

[175] B.M. ter Haar Romeny, *Applications of scale-space theory*, J. Sporring, M. Nielsen, L. Florack, P. Johansen (Eds.), Gaussian scale-space theory, Kluwer, Dordrecht, 3–19, 1997.

[176] B.M. ter Haar Romeny, *Front-end vision and multiscale image analysis: Introduction to scale-space theory*, Kluwer, Dordrecht, in preparation.

[177] B.M. ter Haar Romeny, L.M.J. Florack, M. de Swart, J. Wilting, M.A. Viergever, *Deblurring Gaussian blur*, F.L. Bookstein, J.S. Duncan, N. Lange, D.C. Wilson (Eds.), Mathematical methods in medical imaging III, SPIE Vol. 2299, 139–148, 1994.

[178] B.M. ter Haar Romeny, W.J. Niessen, J. Wilting, L.M.J. Florack, *Differential structure of images: accuracy of representation*, Proc. IEEE Int. Conf. Image Processing (ICIP–94, Austin, Nov. 13–16, 1994), Vol. 1, IEEE Computer Society Press, Los Alamitos, 21–25, 1994.

[179] W. Hackbusch, *Multigrid methods and applications*, Springer, New York, 1985.

[180] W. Hahn, *Theorie und Anwendung der direkten Methode von Ljapunov*, Springer, Berlin, 1959.

[181] R.M. Haralick, S.R. Sternberg, X. Zhuang, *Image analysis using mathematical morphology*, IEEE Trans. Pattern Anal. Mach. Intell., Vol. 9, 532–550, 1987.

[182] C.G. Harris, M. Stephens, *A combined corner and edge detector*, Proc. Fouth Alvey Vision Conf. (AVC 88, Manchester, Aug. 31 – Sept. 2, 1988), 147–152, 1988.

[183] A. Harten, B. Enquist, S. Osher, S. Chakravarthy, *Uniformly high order accurrate essentially non-oscillatory schemes, III*, J. Comput. Phys., Vol. 71, 231–303, 1987.

[184] H.J.A.M. Heijmans, *Mathematical morphology: A modern approach in image processing based on algebra and geometry*, SIAM Review, Vol. 37, 1–36, 1995.

[185] G. Hellwig, *Partial differential equations*, Teubner, Stuttgart, 1977.

[186] G. Hewer, C. Kenney, B.S. Manjunath, *Variational image segmentation using boundary functions*, Report No. 9607, ECE Dept., University of California, Santa Barbara, CA 93106, U.S.A., 1996; submitted to IEEE Trans. Image Proc.

[187] K. Höllig, *Existence of infinitely many solutions for a forward–backward heat equation*, Trans. Amer. Math. Soc., Vol. 278, 299–316, 1983.

[188] G. Huisken, *Flow by mean curvature of convex surfaces into spheres*, J. Differential Geometry, Vol. 20, 237–266, 1984.

[189] R.A. Hummel, *Representations based on zero-crossings in scale space*, Proc. IEEE Comp. Soc. Conf. Computer Vision and Pattern Recognition (CVPR '86, Miami Beach, June 22–26, 1986), IEEE Computer Society Press, Washington, 204–209, 1986.

[190] R. Hummel, R. Moniot, *Reconstructions from zero-crossings in scale space*, IEEE Trans. Acoustics, Speech and Signal Processing, Vol. 37, 2111–2130, 1989.

[191] T. Iijima, *Basic theory of pattern observation*, Papers of Technical Group on Automata and Automatic Control, IECE, Japan, Dec. 1959 (in Japanese).

[192] T. Iijima, *Basic theory on normalization of a pattern (for the case of a typical one-dimensional pattern)*, Bulletin of the Electrotechnical Laboratory, Vol. 26, 368–388, 1962 (in Japanese).

[193] T. Iijima, *Observation theory of two-dimensional visual patterns*, Papers of Technical Group on Automata and Automatic Control, IECE, Japan, Oct. 1962 (in Japanese).

[194] T. Iijima, *Basic theory on normalization of two-dimensional visual pattern*, Studies on Information and Control, Pattern Recognition Issue, IECE, Japan, No. 1, 15–22, 1963 (in Japanese).

[195] T. Iijima, *Theory of pattern recognition*, Electronics and Communications in Japan, 123–134, Nov. 1963 (in English).

[196] T. Iijima, *Basic equation of figure and observational transformation*, Systems, Computers, Controls, Vol. 2, No. 4, 70–77, 1971 (in English).

[197] T. Iijima, *Pattern recognition*, Corona-sha, 1973 (in Japanese).

[198] T. Iijima, *Theory of pattern recognition*, Series of Basic Information Technology, Vol. 6, Morishita Publishing, 1989 (in Japanese).

[199] T. Iijima, H. Genchi, K. Mori, *A theoretical study of pattern identification by matching method*, Proc. First USA–Japan Computer Conference (Tokyo, Oct. 3–5, 1972), 42–48, 1972 (in English).

[200] T. Iijima, H. Genchi, K. Mori, *A theory of character recognition by pattern matching method*, Proc. First Int. Joint Conf. Pattern Recognition (IJCPR 1, Washington, Oct. 1973), 50–56, 1973 (in English).

[201] R. Illner, *Global existence for two-velocity models of the Boltzmann equation*, Math. Meth. Appl. Sci., Vol. 1, 187–193, 1979.

[202] R. Illner, H. Neunzert, *Relative entropy maximization and directed diffusion equations*, Math. Meth. Appl. Sci., Vol. 16, 545–554, 1993.

[203] R. Illner, J. Tie, *On directed diffusion with measurable background*, Math. Meth. Appl. Sci., Vol. 16, 681–690, 1993.

[204] K. Ito, K. Kunisch, *Augmented Lagrangian methods for nonsmooth, convex optimization in Hilbert spaces*, Preprint No. 409/1994, Fachbereich Mathematik (3), Technische Universität Berlin, Straße des 17. Juni 136, 10623 Berlin, Germany, 1994.

[205] K. Ito, K. Kunisch, *An active set strategy for image restoration based on the augmented Lagrangian formulation*, Preprint No. 410/1994, Fachbereich Mathematik (3), Technische Universität Berlin, Straße des 17. Juni 136, 10623 Berlin, Germany, 1994.

[206] P.T. Jackway, *Morphological scale-space*, Proc. 11th Int. Conf. Pattern Recognition (ICPR 11, The Hague, Aug. 30 – Sept. 3, 1992), Vol. C, 252–255, 1992.

[207] P.T. Jackway, M. Deriche, *Scale-space properties of the multiscale morphological dilation–erosion*, IEEE Trans. Pattern Anal. Mach. Intell., Vol. 18, 38–51, 1996.

[208] M. Jägersand, *Saliency maps and attention selection in scale and spatial coordinates: an information theoretic approach*, Proc. Fifth Int. Conf. on Computer Vision (ICCV '95, Cambridge, June 20–23, 1995), IEEE Computer Society Press, Los Alamitos, 195–202, 1995.

[209] B. Jähne, *Spatio-temporal image processing*, Lecture Notes in Computer Science, Vol. 751, Springer, Berlin, 1993.

[210] P. Johansen, *On the classification of toppoints in scale-space*, J. Math. Imag. Vision, Vol. 4, 57–67, 1994.

[211] P. Johansen (Ed.), *Proceedings of the workshop on Gaussian scale-space theory*, Report DIKU 96/19, Dept. of Computer Science, University of Copenhagen, Universitetsparken 1, 2100 Copenhagen, Denmark, 1996.

[212] P. Johansen, S. Skelboe, K. Grue, J.D. Andersen, *Representing signals by their toppoints in scale space*, Proc. Eighth Int. Conf. Pattern Recognition (ICPR 8, Paris, Oct. 27–31, 1986), 215–217, 1986.

[213] F. John, *Partial differential equations*, Springer, New York, 1978.

[214] J.-M. Jolion, A. Rosenfeld, *A pyramid framework for early vision*, Kluwer, Dordrecht, 1994.

[215] D.G. Jones, J. Malik, *A computational framework for determining stereo correspondence from a set of linear spatial filters*, G. Sandini (Ed.), Computer vision – ECCV '92, Lecture Notes in Computer Science, Vol. 588, Springer, Berlin, 395–410, 1992.

[216] J. Kačur, K. Mikula, *Solution of nonlinear diffusion appearing in image smoothing and edge detection*, Appl. Num. Math., Vol. 17, 47–59, 1995.

[217] J. Kačur, K. Mikula, *Slowed anisotropic diffusion*, B. ter Haar Romeny, L. Florack, J. Koenderink, M. Viergever (Eds.), Scale-space theory in computer vision, Lecture Notes in Computer Science, Vol. 1252, Springer, Berlin, 357–360, 1997.

[218] H.-W. Kafitz, *Morphologische Differentialgleichungen in der Bildverarbeitung*, diploma thesis, Dept. of Mathematics, University of Kaiserslautern, P.O. Box 3049, 67653 Kaiserslautern, Germany, 1996.

[219] G. Kanizsa, *Organization in vision*, Praeger, New York, 1979.

[220] M. Kass, A. Witkin, *Analyzing oriented patterns*, Computer Vision, Graphics, and Image Processing, Vol. 37, 362–385, 1987.

[221] M. Kass, A. Witkin, D. Terzopoulos, *Snakes: Active contour models*, Int. J. Comput. Vision, Vol. 1, 321–331, 1988.

[222] B. Kawohl, N. Kutev, *Maximum and comparison principles for anisotropic diffusion*, Preprint, Mathematical Institute, University of Cologne, 50923 Cologne, Germany, 1997.

[223] J.G. Kemeny, J.L. Snell, *Finite Markov chains*, D. Van Nostrand, Princeton, 1960.

[224] S. Kichenassamy, *Nonlinear diffusions and hyperbolic smoothing for edge enhancement*, M.-O. Berger, R. Deriche, I. Herlin, J. Jaffré, J.-M. Morel (Eds.), ICAOS '96: Images, Wavelets and PDEs, Lecture Notes in Control and Information Sciences, Vol. 219, Springer, London, 119–124, 1996.

[225] S. Kichenassamy, *The Perona–Malik paradox*, SIAM J. Appl. Math., to appear.

[226] S. Kichenassamy, A. Kumar, P. Olver, A. Tannenbaum, A. Yezzi, *Conformal curvature flows: from phase transitions to active vision*, Arch. Rat. Mech. Anal., Vol. 134, 275–301, 1996.

[227] B.B. Kimia, K. Siddiqi, *Geometric heat equation and non-linear diffusion of shapes and images*, Computer Vision and Image Understanding, Vol. 64, 305–322, 1996.

[228] B.B. Kimia, A. Tannenbaum, S.W. Zucker, *Toward a computational theory of shape: An overview*, O. Faugeras (Ed.), Computer Vision – ECCV '90, Lecture Notes in Computer Science, Vol. 427, Springer, Berlin, 402–407, 1990.

[229] B.B. Kimia, A. Tannenbaum, S.W. Zucker, *On the evolution of curves via a function of curvature. I. The classical case*, J. Math. Anal. Appl., Vol. 163, 438–458, 1992.

[230] B. Kimia, A. Tannenbaum, S.Zucker, *Shapes, shocks, and deformations I: The components of two-dimensional shape and the reaction–diffusion space*, Int. J. Comput. Vision, Vol. 15, 189–224, 1995.

[231] R. Kimmel, *Affine differential signatures for gray level images of planar shape*, Proc. 13th Int. Conf. Pattern Recognition (ICPR 13, Vienna, Aug. 25–30, 1996), Vol. A, 45–49, 1996.

[232] R. Kimmel, *Intrinsic scale-space for images on surfaces: The geodesic curvature flow*, B. ter Haar Romeny, L. Florack, J. Koenderink, M. Viergever (Eds.), Scale-space theory in computer vision, Lecture Notes in Computer Science, Vol. 1252, Springer, Berlin, 212–223, 1997.

[233] R. Kimmel, N. Kiryati, A.M. Bruckstein, *Analyzing and synthesizing images by evolving curves with the Osher-Sethian method*, Int. J. Comput. Vision, Vol. 24, 37–56, 1997.

[234] R. Kimmel, N. Sochen, R. Malladi, *On the geometry of texture*, Preprint LBNL-39640, Lawrence Berkeley National Laboratory, University of California, Berkeley, CA 94720, U.S.A., 1996.

[235] R. Kimmel, N. Sochen, R. Malladi, *Images as embedding maps and minimal surfaces: Movies, color, and volumetric medical images*, Proc. IEEE Comp. Soc. Conf. Computer Vision and Pattern Recognition (CVPR '97, San Juan, June 17–19, 1997), IEEE Computer Society Press, Los Alamitos, 350–355, 1997.

[236] G. Kin, M. Sato, *Scale space filtering on spherical pattern*, Proc. 11th Int. Conf. Pattern Recognition (ICPR 11, The Hague, Aug. 30 – Sept. 3, 1992), Vol. C, 638–641, 1992.

[237] H.E. Knutsson, R. Wilson, G.H. Granlund, *Anisotropic nonstationary image estimation and its applications: Part I – Restoration of noisy images*, IEEE Trans. Comm., Vol. 31, 388–397, 1983.

[238] M. Kocan, *Approximation of viscosity solutions of elliptic partial differential equations on minimal grids*, Numer. Math., Vol. 72, 73–92, 1996.

[239] G. Koepfler, C. Lopez, J.-M. Morel, *A multiscale algorithm for image segmentation by variational method*, SIAM J. Numer. Anal., Vol. 31, 282–299, 1994.

[240] J.J. Koenderink, *The structure of images*, Biol. Cybern., Vol. 50, 363–370, 1984.

[241] J.J. Koenderink, *Scale-time*, Biol. Cybern., Vol. 58, 159–162, 1988.

[242] J.J. Koenderink, A.J. van Doorn, *Representation of local geometry in the visual system*, Biol. Cybern., Vol. 55, 367–375, 1987.

[243] H.P. Kramer, J.B. Bruckner, *Iterations of a non-linear transformation for enhancement of digital images*, Pattern Recognition, Vol. 7, 53–58, 1975.

[244] K. Krissian, G. Malandain, N. Ayache, *Directional anisotropic diffusion applied to segmentation of vessels in 3D images*, B. ter Haar Romeny, L. Florack, J. Koenderink, M. Viergever (Eds.), Scale-space theory in computer vision, Lecture Notes in Computer Science, Vol. 1252, Springer, Berlin, 345–348, 1997.

[245] A. Kumar, A.R. Tannenbaum, G.J. Balas, *Optic flow: a curve evolution approach*, IEEE Trans. Image Proc., Vol. 5, 598–610, 1996.

[246] O.A. Ladyženskaja, V.A. Solonnikov, N.N. Ural'ceva, *Linear and quasilinear equations of parabolic type*, American Mathematical Society, Providence, 1968.

[247] D.S. Lalush, *The relationship between diffusion filtering and Gibbs smoothing*, personal note, Dept. of Biomedical Engineering, University of North Carolina, Chapel Hill, NC 27599, U.S.A., 1994.

[248] C. Lamberti, M. Sitta, F. Sgallari, *Improvements to the anisotropic diffusion model for 2-D echo image processing*, Proc. Annual Int. Conf. of the IEEE Engineering in Medicine and Biology Society, Vol. 14, 1872–1873, 1992.

[249] A. Leaci, S. Solimini, *Variational problems with a free discontinuity set*, B.M. ter Haar Romeny (Ed.), Geometry-driven diffusion in computer vision, Kluwer, Dordrecht, 147–154, 1994.

[250] A. Lev, S. Zucker, A. Rosenfeld, *Iterative enhancement of noisy images*, IEEE Trans. Systems, Man and Cybernetics, Vol. 7, 435–442, 1977.

[251] S.Z. Li, *On discontinuity-adaptive smoothness priors in computer vision*, IEEE Trans. Pattern Anal. Mach. Intell., Vol. 17, 576–586, 1995.

[252] X. Li, T. Chen, *Nonlinear diffusion with multiple edginess thresholds*, Pattern Recognition, Vol. 27, 1029–1037, 1994.

[253] Y. Li, F. Santosa, *A computational algorithm for minimizing total variation in image enhancement*, IEEE Trans. Image Proc., Vol. 5, 987–995, 1996.

[254] L.M. Lifshitz, S.M. Pizer, *A multiresolution hierarchical approach to image segmentation based on intensity extrema*, IEEE Trans. Pattern Anal. Mach. Intell., Vol. 12, 529–540, 1990.

[255] T. Lindeberg, *Scale-space for discrete signals*, IEEE Trans. Pattern Anal. Mach. Intell., Vol. 12, 234–254, 1990.

[256] T. Lindeberg, *Scale-space theory in computer vision*, Kluwer, Boston, 1994.

[257] T. Lindeberg, *On the axiomatic foundations of linear scale-space*, J. Sporring, M. Nielsen, L. Florack, P. Johansen (Eds.), Gaussian scale-space theory, Kluwer, Dordrecht, 75–97, 1997.

[258] T. Lindeberg, D. Fagerström, *Scale-space with causal time direction*, B. Buxton, R. Cipolla (Eds.), Computer vision – ECCV '96, Volume I, Lecture Notes in Computer Science, Vol. 1064, Springer, Berlin, 229–240, 1996.

[259] T. Lindeberg, J. Gårding, *Shape-adapted smoothing in estimation of 3-D depth cues from affine distortions of local 2-D brightness structure*, Image Vision Comput., Vol. 15, 415–434, 1997.

[260] M. Lindenbaum, M. Fischer, A. Bruckstein, *On Gabor's contribution to image enhancement*, Pattern Recognition, Vol. 27, 1–8, 1994.

[261] P.-L. Lions, *Axiomatic derivation of image processing models*, Math. Mod. Meth. Appl. Sci., Vol. 4, 467–475, 1994.

[262] P.-L. Lions, S. Osher, L.I. Rudin, *Denoising and deblurring images using constrained nonlinear partial differential equations*, Preprint, Cognitech, Inc., 2800 – 28 St., Suite 101, Santa Monica, CA 90405, U.S.A., 1993.

[263] P. Lobel, L. Blanc-Féraud, C. Pichot, M. Barlaud, *A new regularization scheme for inverse scattering*, Inverse Problems, Vol. 13, 403–410, 1997.

[264] M.H. Loew, J. Rosenman, J. Chen, *A clinical tool for enhancement of portal images*, M.H. Loew (Ed.), Image processing, SPIE Vol. 2167, 543–550, 1994.

[265] C. Lopez, J.-M. Morel, *Axiomatization of shape analysis and applications to texture hyper-discrimination*, Proc. IEEE Comp. Soc. Conf. Computer Vision and Pattern Recognition (CVPR '93, New York, June 15–17, 1993), IEEE Computer Society Press, Los Alamitos, 646–647, 1993.

[266] A.K. Louis, *Inverse und schlecht gestellte Probleme*, Teubner, Stuttgart, 1989.

[267] L. Lucido, R. Deriche, L. Alvarez, V. Rigaud, *Sur quelques schémas numériques de résolution d'équations aux dérivées partielles pour le traitement d'images*, Report No. 3192, ROBOTVIS, INRIA, 2004 route des Lucioles, BP 93, 06902 Sophia–Antipolis Cedex, France, 1997.

[268] L. Lucido, J. Opderbecke, V. Rigaud, R. Deriche, Z. Zhang, *An integrated multiscale approach for terrain referenced underwater navigation*, Proc. IEEE Int. Conf. Image Processing (ICIP–96, Lausanne, Sept. 16–19, 1996), Vol. 2, 633–636, 1996.

[269] A. Lukschin, H. Neunzert, J. Struckmeier, *Interim report of the project DPH 6473/91 – Coupling of Navier-Stokes and Boltzmann regions*, Internal Report, Laboratory of Technomathematics, Kaiserslautern, 1993.

[270] D.-S. Luo, M.A. King, S. Glick, *Local geometry variable conductance diffusion for post-reconstruction filtering*, IEEE Trans. Nuclear Sci., Vol. 41, 2800–2806, 1994.

[271] R. Malladi, R. Kimmel, D. Adalsteinsson, G. Sapiro, V. Caselles, J.A. Sethian, *A geometric approach to segmentation and analysis of 3D medical images*, Proc. IEEE Workshop on Mathematical Models in Biomedical Image Analysis (MMBIA '96, San Francisco, June 21–22, 1996), IEEE Computer Society Press, Los Alamitos, 244–252, 1996.

[272] R. Malladi, J.A. Sethian, *Image processing: flows under min/max curvature and mean curvature*, Graphical Models and Image Processing, Vol. 58, 127–141, 1996.

[273] R. Malladi, J.A. Sethian, B.C. Vemuri, *Shape modeling with front propagation: A level set approach*, IEEE Trans. Pattern Anal. Mach. Intell., Vol. 17, 158–175, 1995.

[274] P. Maragos, *A representation theory for morphological image and signal processing*, IEEE Trans. Pattern Anal. Mach. Intell., Vol. 11, 586–599, 1989.

[275] P. Maragos, *Morphological systems: Slope transforms and max–min difference and differential equations*, Signal Processing, Vol. 38, 57–77, 1994.

[276] P. Maragos, *Differential morphology and image processing*, IEEE Trans. Image Proc., Vol. 5, 922–937, 1996.

[277] G.I. Marchuk, *Splitting and alternating direction methods*, P.G. Ciarlet, J.-L. Lions (Eds.), Handbook of numerical analysis, Vol. I, 197–462, 1990.

[278] D. Marr, E. Hildreth, *Theory of edge detection*, Proc. R. Soc. London Ser. B, Vol. 207, 187–217, 1980.

[279] J.L. Marroquin, *Deterministic interactive particle models for image processing and computer graphics*, CVGIP: Graphical Models and Image Processing, Vol. 55, 408–417, 1993.

[280] G. Matheron, *Random sets and integral geometry*, Wiley, New York, 1975.

[281] T. McInerney, D. Terzopoulos, *Topologically adaptable snakes*, Proc. Fifth Int. Conf. on Computer Vision (ICCV '95, Cambridge, June 20–23, 1995), IEEE Computer Society Press, Los Alamitos, 840–845, 1995.

[282] T. McInerney, D. Terzopoulos, *Deformable models in medical image analysis: A survey*, Medical Image Analysis, Vol. 1, 91–108, 1996.

[283] T. McInerney, D. Terzopoulos, *Medical image segmentation using topologically adaptable surfaces*, J. Troccaz, E. Grimson, R. Mösges (Eds.), CVRMed–MRCAS '97, Lecture Notes in Computer Science, Vol. 1205, Springer, Berlin, 23–32, 1997.

[284] T. Meis, U. Marcowitz, *Numerische Behandlung partieller Differentialgleichungen*, Springer, Berlin, 1978.

[285] B. Merriman, J. Bence, S. Osher, *Motion of multiple junctions: a level set approach*, J. Comput. Phys., Vol. 112, 334–363, 1994.

[286] A.R. Mitchell, D.F. Griffiths, *The finite difference method in partial differential equations*, Wiley, Chichester, 1980.

[287] L. Moisan, *Analyse multiéchelle de films pour la reconstruction du relief*, C. R. Acad. Sci. Paris, t. 320, Série I, 279–284, 1995.

[288] L. Moisan, *Perspective invariant movie analysis for depth recovery*, L.I. Rudin, S.K. Bramble (Eds.), Investigative and trial image processing, SPIE Vol. 2567, 84–94, 1995.

[289] L. Moisan, *Affine plane curve evolution: a fully consistent scheme*, Preprint No. 9628, CEREMADE, Université Paris IX – Dauphine, Place du Maréchal de Lattre de Tassigny, 75775 Paris Cedex 16, France, 1996.

[290] F. Mokhtarian, *Multi-scale contour segmentation*, B. ter Haar Romeny, L. Florack, J. Koenderink, M. Viergever (Eds.), Scale-space theory in computer vision, Lecture Notes in Computer Science, Vol. 1252, Springer, Berlin, 296–307, 1997.

[291] F. Mokhtarian, A.K. Mackworth, *A theory of multiscale, curvature-based shape representation for planar curves*, IEEE Trans. Pattern Anal. Mach. Intell., Vol. 14, 789–805, 1992.

[292] J.-M. Morel, S. Solimini, *Variational methods in image segmentation*, Birkhäuser, Boston, 1994.

[293] K.W. Morton, D.F. Mayers, *Numerical solution of partial differential equations*, Cambridge University Press, Cambridge, 1994.

[294] T.S. Motzkin, W. Wasow, *On the approximation of linear elliptic differential equations by difference equations with positive coefficients*, J. Mathematics and Physics, Vol. 31, 253–259, 1952.

[295] D. Mumford, J. Shah, *Boundary detection by minimizing functionals, I*, Proc. IEEE Comp. Soc. Conf. Computer Vision and Pattern Recognition (CVPR '85, San Francisco, June 19–23, 1985), IEEE Computer Society Press, Washington, 22–26, 1985.

[296] D. Mumford, J. Shah, *Optimal approximations by piecewise smooth functions and associated variational problems*, Comm. Pure Appl. Math., Vol. 42, 577–685, 1989.

[297] M. Nagao, T. Matsuyama, *Edge preserving smoothing*, Computer Graphics and Image Processing, Vol. 9, 394–407, 1979.

[298] P. Neskovic, B.B. Kimia, *Three-dimensional shape representation from curvature dependent surface evolution*, Proc. IEEE Int. Conf. Image Processing (ICIP–94, Austin, Nov. 13–16, 1994), Vol. 1, IEEE Computer Society Press, Los Alamitos, 6–10, 1994.

[299] H. Neunzert, B. Claus, K. Rjasanowa, R. Rösch, J. Weickert, *Mathematische Werkzeuge in der Bildverarbeitung zur Qualitätsbeurteilung von Oberflächen*, K.-H. Hoffmann, W. Jäger, T. Lohmann, H. Schunck (Eds.), Mathematik – Schlüsseltechnologie für die Zukunft, Springer, Berlin, 449–462, 1997.

[300] T.G. Newman, H. Dirilten, *A nonlinear transformation for digital picture processing*, IEEE Trans. Computers, Vol. 22, 869–873, 1973.

[301] E. Nicolet, M. Spühler, *Charakterisierung von unscharfen blobförmigen 3-D Strukturen*, diploma thesis, Communication Technology Laboratory, Image Science Division, ETH–Zentrum, 8092 Zürich, Switzerland, 1996.

[302] M. Nielsen, *From paradigm to algorithms in computer vision*, Ph.D. thesis, Report DIKU 95/8, Dept. of Computer Science, University of Copenhagen, Universitetsparken 1, 2100 Copenhagen, Denmark, 1995.

[303] M. Nielsen, L. Florack, R. Deriche, *Regularization, scale-space and edge detection filters*, J. Math. Imag. Vision, Vol. 7, 291–307, 1997.

[304] W.J. Niessen, B.M. ter Haar Romeny, L.M.J. Florack, M.A. Viergever, *A general framework for geometry-driven evolution equations*, Int. J. Comput. Vision, Vol. 21, 187–205, 1997.

[305] W.J. Niessen, B.M. ter Haar Romeny, M.A. Viergever, *Numerical analysis of geometry-driven diffusion equations*, B.M. ter Haar Romeny (Ed.), Geometry-driven diffusion in computer vision, Kluwer, Dordrecht, 392–410, 1994.

[306] W.J. Niessen, R. Maas, *Multiscale optic flow and stereo*, J. Sporring, M. Nielsen, L. Florack, P. Johansen (Eds.), Gaussian scale-space theory, Kluwer, Dordrecht, 31–42, 1997.

[307] W.J. Niessen, K.L. Vincken, J. Weickert, M.A. Viergever, *Nonlinear multiscale representations for image segmentation*, Computer Vision and Image Understanding, Vol. 66, 233–245, 1997.

[308] W.J. Niessen, K.L. Vincken, J. Weickert, M.A. Viergever, *Three-dimensional MR brain segmentation*, Proc. Sixth Int. Conf. on Computer Vision (ICCV '98, Bombay, Jan. 4–7, 1998), in press.

[309] M. Nitzberg, D. Mumford, T. Shiota, *Filtering, segmentation and depth*, Lecture Notes in Computer Science, Vol. 662, Springer, Berlin, 1993.

[310] M. Nitzberg, T. Shiota, *Nonlinear image filtering with edge and corner enhancement*, IEEE Trans. Pattern Anal. Mach. Intell., Vol. 14, 826–833, 1992.

[311] N. Nordström, *Biased anisotropic diffusion - a unified regularization and diffusion approach to edge detection*, Image Vision Comput., Vol. 8, 318–327, 1990.

[312] E. Norman, *A discrete analogue of the Weierstrass transform*, Proc. Amer. Math. Soc., Vol. 11, 596–604, 1960.

[313] O.F. Olsen, *Multiscale watershed segmentation*, J. Sporring, M. Nielsen, L. Florack, P. Johansen (Eds.), Gaussian scale-space theory, Kluwer, Dordrecht, 191–200, 1997.

[314] P.J. Olver, G. Sapiro, A. Tannenbaum, *Classification and uniqueness of invariant geometric flows*, C. R. Acad. Sci. Paris, t. 319, Série I, 339–344, 1994.

[315] P.J. Olver, G. Sapiro, A. Tannenbaum, *Affine invariant detection: edges, active contours, and segments*, Proc. IEEE Comp. Soc. Conf. Computer Vision and Pattern Recognition (CVPR '96, San Francisco, June 18–20, 1996), IEEE Computer Society Press, Los Alamitos, 520–525, 1996.

[316] P.J. Olver, G. Sapiro, A. Tannenbaum, *Invariant geometric evolutions of surfaces and volumetric smoothing*, SIAM J. Appl. Math., Vol. 57, 176–194, 1997.

[317] S. Osher, L. Rudin, *Feature-oriented image enhancement using shock filters*, SIAM J. Numer. Anal., Vol. 27, 919–949, 1990.

[318] S. Osher, L. Rudin, *Shocks and other nonlinear filtering applied to image processing*, A.G. Tescher (Ed.): Applications of digital image processing XIV, SPIE Vol. 1567, 414–431, 1991.

[319] S. Osher, J.A. Sethian, *Fronts propagating with curvature-dependent speed: Algorithms based on Hamilton–Jacobi formulations*, J. Comput. Phys., Vol. 79, 12–49, 1988.

[320] N. Otsu, *Mathematical studies on feature extraction in pattern recognition*, Ph.D. thesis, Report No. 818, Electrotechnical Laboratory, 1-1-4, Umezono, Sakura-mura, Niihari-gun, Ibaraki, Japan, 1981 (in Japanese).

[321] K. Ottenberg, *Model-based extraction of geometric structure from digital images*, Ph.D. thesis, Utrecht University, The Netherlands, 1993.

[322] N. Paragios, R. Deriche, *A PDE-based level-set approach for detection and tracking of moving objects*, Proc. Sixth Int. Conf. on Computer Vision (ICCV '98, Bombay, Jan. 4–7, 1998), in press.

[323] E.J. Pauwels, P. Fiddelaers, L.J. Van Gool, *Enhancement of planar shape through optimization of functionals for curves*, IEEE Trans. Pattern Anal. Mach. Intell., Vol. 17, 1101–1105, 1995.

[324] E.J. Pauwels, L.J. Van Gool, P. Fiddelaers, T. Moons, *An extended class of scale-invariant and recursive scale space filters*, IEEE Trans. Pattern Anal. Mach. Intell., Vol. 17, 691–701, 1995.

[325] E. Payot, R. Guillemaud, Y. Trousset, F. Preteux, *An adaptive and constrained model for 3D X-ray vascular reconstruction*, P. Grangeat, J.-L. Amans (Eds.), Three-dimensional image reconstruction in radiation and nuclear medicine, Kluwer, Dordrecht, 47–57, 1996.

[326] P. Perona, J. Malik, *Scale space and edge detection using anisotropic diffusion*, Proc. IEEE Comp. Soc. Workshop on Computer Vision (Miami Beach, Nov. 30 – Dec. 2, 1987), IEEE Computer Society Press, Washington, 16–22, 1987.

[327] P. Perona, J. Malik, *A network for multiscale image segmentation*, Proc. IEEE Int. Symp. Circuits and Systems (ISCAS–88, Espoo, June 7–9, 1988), 2565–2568, 1988.

[328] P. Perona, J. Malik, *Scale space and edge detection using anisotropic diffusion*, IEEE Trans. Pattern Anal. Mach. Intell., Vol. 12, 629–639, 1990.

[329] P. Perona, T. Shiota, J. Malik, *Anisotropic diffusion*, B.M. ter Haar Romeny (Ed.), Geometry-driven diffusion in computer vision, Kluwer, Dordrecht, 72–92, 1994.

[330] P. Perona, M. Tartagni, *Diffusion networks for on-chip image contrast normalization*, Proc. IEEE Int. Conf. Image Processing (ICIP–94, Austin, Nov. 13–16, 1994), Vol. 1, IEEE Computer Society Press, Los Alamitos, 1–5, 1994.

[331] I.G. Petrowski, *Vorlesungen über partielle Differentialgleichungen*, Teubner, Leipzig, 1955.

[332] I. Pollak, A.S. Willsky, H. Krim, *Scale space analysis by stabilized inverse diffusion equations*, B. ter Haar Romeny, L. Florack, J. Koenderink, M. Viergever (Eds.), Scale-space theory in computer vision, Lecture Notes in Computer Science, Vol. 1252, Springer, Berlin, 200–211, 1997.

[333] E.S. Posmentier, *The generation of salinity finestructure by vertical diffusion*, J. Phys. Oceanogr., Vol. 7, 298–300, 1977.

[334] C.B. Price, P. Wambacq, A. Oosterlinck, *Applications of reaction–diffusion equations to image processing*, IEE Third Int. Conf. Image Processing and its Applications (Warwick, 18–20 July 1989), IEE, London, 49–53, 1989.

[335] C.B. Price, P. Wambacq, A. Oosterlinck, *Computing with reaction–diffusion systems: applications in image processing*, D. Roose et al. (Eds.), Continuation and bifurcations: Numerical techniques and applications, Kluwer, 379–387, 1990.

[336] M. Proesmans, E.J. Pauwels, L.J. Van Gool, *Coupled geometry-driven diffusion equations for low-level vision*, B.M. ter Haar Romeny (Ed.), Geometry-driven diffusion in computer vision, Kluwer, Dordrecht, 191–228, 1994.

[337] M. Proesmans, E.J. Pauwels, L.J. Van Gool, T. Moons, A. Oosterlinck, *Image enhancement using non-linear diffusion*, Proc. IEEE Comp. Soc. Conf. Computer Vision and Pattern Recognition (CVPR '93, New York, June 15–17, 1993), IEEE Computer Society Press, Los Alamitos, 680–681, 1993.

[338] M. Proesmans, L. Van Gool, E. Pauwels, A. Oosterlinck, *Determination of optical flow and its discontinuities using non-linear diffusion*, J.-O. Eklundh (Ed.), Computer Vision – ECCV '94, Lecture Notes in Computer Science, Vol. 801, Springer, Berlin, 295–304, 1994.

[339] I. Rambaux, P. Garçon, *Nonlinear anisotropic diffusion filtering of 3D images*, project work, Département Génie Mathématique, INSA de Rouen and Laboratory of Technomathematics, University of Kaiserslautern, 1994.

[340] A.R. Rao, B.G. Schunck, *Computing oriented texture fields*, CVGIP: Graphical Models and Image Processing, Vol. 53, 157–185, 1991.

[341] T. Richardson, S. Mitter, *Approximation, computation, and distortion in the variational formulation*, B.M. ter Haar Romeny (Ed.), Geometry-driven diffusion in computer vision, Kluwer, Dordrecht, 169–190, 1994.

[342] J.H. Rieger, *Generic evolution of edges on families of diffused greyvalue surfaces*, J. Math. Imag. Vision, Vol. 5, 207–217, 1995.

[343] L. Robert, R. Deriche, *Dense depth map reconstruction: A minimization and regularization approach which preserves discontinuities*, B. Buxton, R. Cipolla (Eds.), Computer vision – ECCV '96, Volume I, Lecture Notes in Computer Science, Vol. 1064, Springer, Berlin, 439–451, 1996.

[344] L.I. Rudin, S. Osher, *Total variation based image restoration with free local constraints*, Proc. IEEE Int. Conf. Image Processing (ICIP–94, Austin, Nov. 13–16, 1994), Vol. 1, IEEE Computer Society Press, Los Alamitos, 31–35, 1994.

[345] L.I. Rudin, S. Osher, E. Fatemi, *Nonlinear total variation based noise removal algorithms*, Physica D, Vol. 60, 259–268, 1992.

[346] L.I. Rudin, S. Osher, C. Fu, *Total variation based restoration of noisy, blurred images*, Preprint, Cognitech, Inc., 2800 – 28 St., Suite 101, Santa Monica, CA 90405, U.S.A., 1992.

[347] S.J. Ruuth, *An algorithm for generating motion by mean curvature*, M.-O. Berger, R. Deriche, I. Herlin, J. Jaffré, J.-M. Morel (Eds.), ICAOS '96: Images, wavelets and PDEs, Lecture Notes in Control and Information Sciences, Vol. 219, Springer, London, 82–91, 1996.

[348] Y. Saad, *Iterative methods for sparse linear systems*, PWS Publishing, Boston, 1996.

[349] P. Saint-Marc, J.S. Chen, G. Medioni, *Adaptive smoothing: a general tool for early vision*, IEEE Trans. Pattern Anal. Mach. Intell., Vol. 13, 514–529, 1990.

[350] A.H. Salden, *The nonlinear rescaling process*, Report 3DCV 92-28, 3D Computer Vision, AZU, Room E.02.222, Heidelberglaan 100, 3584 CX Utrecht, The Netherlands, 1992.

[351] A.H. Salden, *Dynamic scale-space paradigms*, Ph.D. thesis, Utrecht University, The Netherlands, 1996.

[352] A.H. Salden, B.M. ter Haar Romeny, M.A. Viergever, *Image structure generating normalised geometric scale spaces*, Proc. Int. Conf. Volume Image Processing (VIP '93, Utrecht, June 2–4, 1993), 141–143, 1993.

[353] A.H. Salden, B.M. ter Haar Romeny, M.A. Viergever, *Linear scale-space theory from physical principles*, J. Math. Imag. Vision, to appear.

[354] A.A. Samarskij, *Theorie der Differenzenverfahren*, Geest & Portig, Leipzig, 1984.

[355] G.I. Sánchez–Ortiz, D. Rueckert, P. Burger, *Knowledge-based anisotropic diffusion of vector-valued 4-dimensional cardiac MR images*, R.B. Fisher, E. Trucco (Eds.), Proc. Seventh British Machine Vision Conference (BMVC 1996, Edinburgh, Sept. 9–12, 1996), BMVA Press.

[356] G. Sapiro, *From active contours to anisotropic diffusion: connections between basic PDEs in image processing*, Proc. IEEE Int. Conf. Image Processing (ICIP–96, Lausanne, Sept. 16–19, 1996), Vol. 1, 477–480, 1996.

[357] G. Sapiro, *Vector (self) snakes: a geometric framework for color, texture and multiscale image segmentation*, Proc. IEEE Int. Conf. Image Processing (ICIP–96, Lausanne, Sept. 16–19, 1996), Vol. 1, 817–820, 1996.

[358] G. Sapiro, V. Caselles, *Histogram modification via differential equations*, J. Differential Equations, Vol 135, 238–268, 1997.

[359] G. Sapiro, A. Cohen, A.M. Bruckstein, *A subdivision scheme for continuous-scale B-splines and affine-invariant progressive smoothing*, J. Math. Imag. Vision, Vol. 7, 23–40, 1997.

[360] G. Sapiro, R. Kimmel, D. Shaked, B.B. Kimia, A.M. Bruckstein, *Implementing continuous-scale morphology via curve evolution*, Pattern Recognition, Vol. 26, 1363–1372, 1993.

[361] G. Sapiro, D.L. Ringach, *Anisotropic diffusion of multivalued images with applications to color filtering*, IEEE Trans. Image Proc., Vol. 5, 1582–1586, 1996.

[362] G. Sapiro, A. Tannenbaum, *Affine invariant scale-space*, Int. J. Comput. Vision, Vol. 11, 25–44, 1993.

[363] G. Sapiro, A. Tannenbaum, *On affine plane curve evolution*, J. Funct. Anal., Vol. 119, 79–120, 1994.

[364] G. Sapiro, A. Tannenbaum, *Edge preserving geometric smoothing of MRI data*, Technical Report, Dept. of Electical Engineering, University of Minnesota, Minneapolis, MN 55455, U.S.A., 1994; submitted to IEEE Trans. Medical Imaging.

[365] G. Sapiro, A. Tannenbaum, Y.-L. You, M. Kaveh, *Experiments on geometric image enhancement*, Proc. IEEE Int. Conf. Image Processing (ICIP–94, Austin, Nov. 13–16, 1994), Vol. 2, IEEE Computer Society Press, Los Alamitos, 472–476, 1994.

[366] G. Sapiro, A. Tannenbaum, *Area and length preserving geometric invariant scale-spaces*, IEEE Trans. Pattern Anal. Mach. Intell., Vol. 17, 67–72, 1995.

[367] C. Schnörr, *Unique reconstruction of piecewise smooth images by minimizing strictly convex non-quadratic functionals*, J. Math. Imag. Vision, Vol. 4, 189–198, 1994.

[368] C. Schnörr, *Segmentation of visual motion by minimizing convex non-quadratic function-als*, Proc. 12th Int. Conf. Pattern Recognition (ICPR 12, Jerusalem, Oct. 9–13, 1994), Vol. A, IEEE Computer Society Press, Los Alamitos, 661–663, 1994.

[369] C. Schnörr, *Convex variational segmentation of multi-channel images*, M.-O. Berger, R. Deriche, I. Herlin, J. Jaffré, J.-M. Morel (Eds.), ICAOS '96: Images, wavelets and PDEs, Lecture Notes in Control and Information Sciences, Vol. 219, Springer, London, 201–207, 1996.

[370] E. Seneta, *Non-negative matrices and Markov chains*, Springer, New York, 1981.

[371] J. Serra, *Image analysis and mathematical morphology*, Academic Press, London, 1982.

[372] J.A. Sethian, *Level set methods*, Cambridge University Press, Cambridge, 1996.

[373] J.A. Sethian, *A fast marching level set method for monotonically advancing fronts*, Proc. Nat. Acad. Sci., Vol. 93, 1591–1595, 1996.

[374] J.A. Sethian, *A review of the theory, algorithms, and applications of level set methods for propagating interfaces*, Acta Numerica, 309–395, 1996.

[375] J. Shah, *Segmentation by nonlinear diffusion*, Proc. IEEE Comp. Soc. Conf. on Computer Vision and Pattern Recognition (CVPR '91, Maui, June 3–6, 1992), IEEE Computer Society Press, Los Alamitos, 202–207, 1991.

[376] J. Shah, *Segmentation by nonlinear diffusion, II*, Proc. IEEE Comp. Soc. Conf. Computer Vision and Pattern Recognition (CVPR '92, Champaign, June 15–18, 1992), IEEE Computer Society Press, Los Alamitos, 644–647, 1992.

[377] J. Shah, *Properties of energy-minimizing segmentations*, SIAM J. Control and Optimization, Vol. 30, 99–111, 1992.

[378] J. Shah, *A nonlinear diffusion model for discontinuous disparity and half-occlusions in stereo*, Proc. IEEE Comp. Soc. Conf. Computer Vision and Pattern Recognition (CVPR '93, New York, June 15–17, 1993), IEEE Computer Society Press, Los Alamitos, 34–40, 1993.

[379] J. Shah, *Piecewise smooth approximations of functions*, Calc. Var., Vol. 2, 315–328, 1994.

[380] J. Shah, *A common framework for curve evolution, segmentation and anisotropic diffusion*, Proc. IEEE Comp. Soc. Conf. Computer Vision and Pattern Recognition (CVPR '96, San Francisco, June 18–20, 1996), IEEE Computer Society Press, Los Alamitos, 136–142, 1996.

[381] J. Shen, S. Castan, *An optimal linear operator for step edge detection*, Graphical Models and Image Processing, Vol. 54, 112–133, 1992.

[382] A. Sherstinsky, R.W. Picard, *M-lattice: From morphogenesis to image processing*, IEEE Trans. Image Proc., Vol. 5, 1137–1150, 1996.

[383] K. Siddiqi, B.B. Kimia, *Parts of visual form: computational aspects*, IEEE Trans. Pattern Anal. Mach. Intell., Vol. 17, 239–251, 1995.

[384] K. Siddiqi, B.B. Kimia, *A shock grammar for recognition*, Proc. IEEE Comp. Soc. Conf. Computer Vision and Pattern Recognition (CVPR '96, San Francisco, June 18–20, 1996), IEEE Computer Society Press, Los Alamitos, 507–513, 1996.

[385] K. Siddiqi, B.B. Kimia, C.-W. Shu, *Geometric shock-capturing ENO schemes for subpixel interpolation, computation and curve evolution*, Graphical Models and Image Processing, in press.

[386] J. Sijbers, P. Scheunders, M. Verhoye, A. Van der Linden, D. Van Dyck, E. Raman, *Watershed-based segmentation of 3D MR data for volume quantization*, Magnetic Resonance Imaging, Vol. 15, 679–688, 1997.

[387] W. Snyder, Y.-S. Han, G. Bilbro, R. Whitaker, S. Pizer, *Image relaxation: Restoration and feature extraction*, IEEE Trans. Pattern Anal. Mach. Intell., Vol. 17, 620–624, 1995.

[388] J. Sporring, *The entropy of scale-space*, Proc. 13th Int. Conf. Pattern Recognition (ICPR 13, Vienna, Aug. 25–30, 1996), Vol. A, 900–904, 1996.

[389] J. Sporring, M. Nielsen, L. Florack, P. Johansen (Eds.), *Gaussian scale-space theory*, Kluwer, Dordrecht, 1997.

[390] J. Sporring, J. Weickert, *On generalized entropies and scale-space*, B. ter Haar Romeny, L. Florack, J. Koenderink, M. Viergever (Eds.), Scale-space theory in computer vision, Lecture Notes in Computer Science, Vol. 1252, Springer, Berlin, 53–64, 1997.

[391] R. Sprengel, *Entwurf und Analyse nichtlinearer Diffusionsverfahren für die Bildverarbeitung*, Ph.D. thesis, Dept. of Computer Science, University of Hamburg, Germany, 1995; DISKI 123, Infix Verlag, Sankt Augustin, 1996.

[392] J.L. Stansfield, *Conclusions from the commodity expert project*, A.I. Memo 671, Artificial Intelligence Lab., Massachusetts Inst. of Technology, Cambridge, MA, U.S.A., 1980.

[393] E. Steen, B. Olstad, *Scale-space and boundary detection in ultrasonic imaging using nonlinear signal-adaptive anisotropic diffusion*, M.H. Loew (Ed.), Image processing, SPIE Vol. 2167, 116–127, 1994.

[394] A. Steiner, R. Kimmel, A.M. Bruckstein, *Planar shape enhancement and exaggeration*, Proc. 13th Int. Conf. Pattern Recognition (ICPR 13, Vienna, Aug. 25–30, 1996), Vol. A, 523–527, 1996.

[395] P. Stoll, C.-W. Shu, B.B. Kimia, *Shock-capturing numerical methods for viscosity solutions of certain PDEs in computer vision: The Godunov, Osher–Sethian and ENO schemes*, Technical Report LEMS-132, Division of Engineering, Brown University, Providence, R.I. 02912, U.S.A., 1994.

[396] D.M. Strong, T.F. Chan, *Relation of regularization parameter and scale in total variation based image denoising*, CAM Report 96-7, Dept. of Mathematics, Univ. of California, Los Angeles, CA 90024, U.S.A., 1996.

[397] D.M. Strong, T.F. Chan, *Spatially and scale adaptive total variation based regularization and anisotropic diffusion in image processing*, CAM Report 96-46, Dept. of Mathematics, Univ. of California, Los Angeles, CA 90024, U.S.A., 1996.

[398] S. Teboul, L. Blanc–Féraud, G. Aubert, M. Barlaud, *Variational approach for edge-preserving regularization using coupled PDEs*, IEEE Trans. Image Proc., March 1998, in press.

[399] H. Tek, B.B. Kimia, *Image segmentation by reaction–diffusion bubbles*, Proc. Fifth Int. Conf. on Computer Vision (ICCV '95, Cambridge, June 20–23, 1995), IEEE Computer Society Press, Los Alamitos, 156–162, 1995.

[400] H. Tek, B.B. Kimia, *Volumetric segmentation of medical images by three-dimensional bubbles*, Computer Vision and Image Understanding, Vol. 65, 246–258, 1997.

[401] D. Terzopoulos, A. Witkin, M. Kass, *Constraints on deformable models: Recovering 3D shape and nonrigid motion*, Artif. Intell., Vol. 36, 91–123, 1988.

[402] A. Tikhonov, V. Arsenin, *Solutions of ill-posed problems*, Wiley, New York, 1977.

[403] F. Torkamani–Azar, K.E. Tait, *Image recovery using the anisotropic diffusion equation*, IEEE Trans. Image Proc., Vol. 5, 1573–1578, 1996.

[404] V. Torre, T.A. Poggio, *On edge detection*, IEEE Trans. Pattern Anal. Mach. Intell., Vol. 8, 148–163, 1986.

[405] A.M. Turing, *The chemical basis of morphogenesis*, Philosoph. Trans. Royal Soc. London B, Vol. 237, 37–72, 1952.

[406] G. Turk, *Generating textures on arbitrary surfaces using reaction–diffusion*, Computer Graphics, Vol. 25, No. 4, 289–298, 1991.

[407] R.A. Varga, *Matrix iterative analysis*, Prentice Hall, Englewood Cliffs, 1962.

[408] K.L. Vincken, A.S.E. Koster, M.A. Viergever, *Probabilistic multiscale image segmentation*, IEEE Trans. Pattern Anal. Mach. Intell., Vol. 19, 109–120, 1997.

[409] C.R. Vogel, M.E. Oman, *Iterative methods for total variation denoising*, SIAM J. Sci. Comput., Vol. 17, 227–238, 1996.

[410] C.R. Vogel, M.E. Oman, *Fast numerical methods for total variation minimization in image reconstruction*, F.T. Luk (Ed.), Advanced signal processing algorithms, SPIE Vol. 2563, 359–367, 1995.

[411] W. Walter, *Differential and integral inequalities*, Springer, Berlin, 1970.

[412] W. Walter, *Gewöhnliche Differentialgleichungen*, Springer, Berlin, 1976.

[413] J. Weickert, *Anisotropic diffusion filters for image processing based quality control*, A. Fasano, M. Primicerio (Eds.), Proc. Seventh European Conf. on Mathematics in Industry, Teubner, Stuttgart, 355–362, 1994.

[414] J. Weickert, *Scale-space properties of nonlinear diffusion filtering with a diffusion tensor*, Report No. 110, Laboratory of Technomathematics, University of Kaiserslautern, P.O. Box 3049, 67653 Kaiserslautern, Germany, 1994.

[415] J. Weickert, *Theoretical foundations of anisotropic diffusion in image processing*, Computing, Suppl. 11, 221–236, 1996.

[416] J. Weickert, *Anisotropic diffusion in image processing*, Ph.D. thesis, Dept. of Mathematics, University of Kaiserslautern, P.O. Box 3049, 67653 Kaiserslautern, Germany, 1996.

[417] J. Weickert, *A model for the cloudiness of fabrics*, H. Neunzert (Ed.), Progress in industrial mathematics at ECMI 94, Wiley–Teubner, Chichester, 258–265, 1996.

[418] J. Weickert, *Multiscale texture enhancement*, V. Hlaváč, R. Šára (Eds.), Computer analysis of images and patterns, Lecture Notes in Computer Science, Vol. 970, Springer, Berlin, 230–237, 1995.

[419] J. Weickert, *Foundations and applications of nonlinear anisotropic diffusion filtering*, Z. Angew. Math. Mech., Vol. 76, Suppl. 1, 283–286, 1996.

[420] J. Weickert, *Nonlinear diffusion scale-spaces: From the continuous to the discrete setting*, M.-O. Berger, R. Deriche, I. Herlin, J. Jaffré, J.-M. Morel (Eds.), ICAOS '96: Images, wavelets and PDEs, Lecture Notes in Control and Information Sciences, Vol. 219, Springer, London, 111–118, 1996.

[421] J. Weickert, *Nonlinear scale-spaces*, J. Sporring, M. Nielsen, L. Florack, P. Johansen (Eds.), Gaussian scale-space theory, Kluwer, Dordrecht, 221–234, 1997.

[422] J. Weickert, *Coherence-enhancing diffusion of colour images*, A. Sanfeliu, J.J. Villanueva, J. Vitrià (Eds.), Pattern Recognition and Image Analysis (VII NSPRIA, Barcelona, April 21–25, 1997), Vol. 1, 239–244, 1997.

[423] J. Weickert, *A review of nonlinear diffusion filtering*, B. ter Haar Romeny, L. Florack, J. Koenderink, M. Viergever (Eds.), Scale-space theory in computer vision, Lecture Notes in Computer Science, Vol. 1252, Springer, Berlin, 3–28, 1997.

[424] J. Weickert, *Recursive separable schemes for nonlinear diffusion filters*, B. ter Haar Romeny, L. Florack, J. Koenderink, M. Viergever (Eds.), Scale-space theory in computer vision, Lecture Notes in Computer Science, Vol. 1252, Springer, Berlin, 260–271, 1997.

[425] J. Weickert, B. Benhamouda, *A semidiscrete nonlinear scale-space theory and its relation to the Perona–Malik paradox*, F. Solina, W.G. Kropatsch, R. Klette, R. Bajcsy (Eds.), Theoretical foundations of computer vision (TFCV '96, Dagstuhl, March 18–22, 1996), Springer, Wien, in press.

[426] J. Weickert, S. Ishikawa, A. Imiya, *On the history of Gaussian scale-space axiomatics*, J. Sporring, M. Nielsen, L. Florack, P. Johansen (Eds.), Gaussian scale-space theory, Kluwer, Dordrecht, 45–59, 1997.

[427] J. Weickert, S. Ishikawa, A. Imiya, *Scale-space has been discovered in Japan*, Report DIKU 97/18, Dept. of Computer Science, University of Copenhagen, Universitetsparken 1, 2100 Copenhagen, Denmark, 1997, submitted.

[428] J. Weickert, B.M. ter Haar Romeny, A. Lopez, W.J. van Enk, *Orientation analysis by coherence-enhancing diffusion*, Proc. Symp. Real World Computing (RWC '97, Tokyo, Jan. 29–31, 1997), 96–103, 1997.

[429] J. Weickert, B.M. ter Haar Romeny, M.A. Viergever, *Conservative image transformations with restoration and scale-space properties*, Proc. IEEE Int. Conf. Image Processing (ICIP–96, Lausanne, Sept. 16–19, 1996), Vol. 1, 465–468, 1996.

[430] J. Weickert, B.M. ter Haar Romeny, M.A. Viergever, *Efficient and reliable schemes for nonlinear diffusion filtering*, IEEE Trans. Image Proc., March 1998, to appear.

[431] J. Weickert, K.J. Zuiderveld, B.M. ter Haar Romeny, W.J. Niessen, *Parallel implementations of AOS schemes: A fast way of nonlinear diffusion filtering*, Proc. 1997 IEEE International Conference on Image Processing (ICIP–97, Santa Barbara, Oct. 26–29, 1997), to appear.

[432] H. Werner, H. Arndt, *Gewöhnliche Differentialgleichungen*, Springer, Berlin, 1986.

[433] R.T. Whitaker, *Geometry limited diffusion in the characterization of geometric patches in images*, CVGIP: Image Understanding, Vol. 57, 111–120, 1993.

[434] R.T. Whitaker, *Characterizing first and second-order patches using geometry-limited diffusion*, H.H. Barrett, A.F. Gmitro (Eds.), Information processing in medical imaging, Lecture Notes in Computer Science, Vol. 687, Springer, Berlin, 149–167, 1993.

[435] R.T. Whitaker, *Algorithms for implicit deformable models*, Proc. Fifth Int. Conf. on Computer Vision (ICCV '95, Cambridge, June 20–23, 1995), IEEE Computer Society Press, Los Alamitos, 822–827, 1995.

[436] R.T. Whitaker, D.T. Chen, *Embedded active surfaces for volume visualization*, M.H. Loew (Ed.), Image processing, SPIE Vol. 2167, 340–352, 1994.

[437] R. Whitaker, G. Gerig, *Vector-valued diffusion*, B.M. ter Haar Romeny (Ed.), Geometry-driven diffusion in computer vision, Kluwer, Dordrecht, 93–134, 1994.

[438] R.T. Whitaker, S.M. Pizer, *A multi-scale approach to nonuniform diffusion*, CVGIP: Image Understanding, Vol. 57, 99–110, 1993.

[439] A.P. Witkin, *Scale-space filtering*, Proc. Eighth Int. Joint Conf. on Artificial Intelligence (IJCAI '83, Karlsruhe, Aug. 8–12, 1983), Vol. 2, 1019–1022, 1983.

[440] A. Witkin, M. Kass, *Reaction–diffusion textures*, Computer Graphics, Vol. 25, No. 4, 299–308, 1991.

[441] A. Witkin, D. Terzopoulos, M. Kass, *Signal matching through scale-space*, Int. J. Comput. Vision, Vol. 1, 134–144, 1987.

[442] N.N. Yanenko, *The method of fractional steps: the solution of problems of mathematical physics in several variables*, Springer, New York, 1971.

[443] G.Z. Yang, P. Burger, D.N. Firmin, S.R. Underwood, *Structure adaptive anisotropic filtering*, Image Vision Comput., Vol. 14, 135–145, 1996.

[444] T.S. Yoo, J.M. Coggins, *Using statistical pattern recognition techniques to control variable conductance diffusion*, H.H. Barrett, A.F. Gmitro (Eds.), Information processing in medical imaging, Lecture Notes in Computer Science, Vol. 687, Springer, Berlin, 459–471, 1993.

[445] Y.-L. You, M. Kaveh, *Anisotropic blind image restoration*, Proc. IEEE Int. Conf. Image Processing (ICIP–96, Lausanne, Sept. 16–19, 1996), Vol. 2, 461–464, 1996.

[446] Y.-L. You, W. Xu, A. Tannenbaum, M. Kaveh, *Behavioral analysis of anisotropic diffusion in image processing*, IEEE Trans. Image Proc., Vol. 5, 1539–1553, 1996.

[447] D.M. Young, *Iterative solution of large linear systems*, Academic Press, New York, 1971.

[448] I.T. Young, L.J. van Vliet, *Recursive implementation of the Gaussian filter*, Signal Processing, Vol. 44, 139–151, 1995.

[449] R.A. Young, *The Gaussian derivative model for spatial vision: I. Retinal mechanisms*, Spatial Vision, Vol. 2, 273–293, 1987.

[450] A.L. Yuille, T.A. Poggio, *Scaling theorems for zero crossings*, IEEE Trans. Pattern Anal. Mach. Intell., Vol. 8, 15–25, 1986.

[451] D. Zhao, B. Li, *A new implementation of discrete multiscale filtering*, Proc. IEEE Int. Conf. Image Processing (ICIP–96, Lausanne, Sept. 16–19, 1996), Vol. 1, 383–386, 1996.

[452] S.C. Zhu, A.L. Yuille, *Region competition: unifying snakes, region growing, energy/Bayes/MDL for multi-band image segmentation*, IEEE Trans. Pattern Anal. Mach. Intell., Vol. 18, 884–900, 1996.

[453] S.W. Zucker, A. Dobbins, L. Iverson, B. Kimia, A. Tannenbaum, *From curve detection to shape description: an outline*, A. Basu, X. Li (Eds.), Computer vision: systems, theory and applications, World Scientific, Singapore, 25–39, 1993.

Index

E C M I

Anisotropic Diffusion in Image Processing

Joachim Weickert
University of Copenhagen

Many recent techniques for digital image enhancement and multiscale image representations are based on nonlinear partial differential equations.

This book gives an introduction to the main ideas behind these methods, and it describes in a systematic way their theoretical foundations, numerical aspects, and applications. A large number of references enables the reader to acquire an up-to-date overview of the original literature.

The central emphasis is on anisotropic nonlinear diffusion filters. Their flexibility allows to combine smoothing properties with image enhancement qualities. A general framework is explored covering well-posedness and scale-space results not only for the continuous, but also for the algorithmically important semidiscrete and fully discrete settings. The presented examples range from applications in medical image analysis to problems in computer aided quality control.

B.G. Teubner Stuttgart